STUDIES IN SUPRAMOLECULAR CHEMISTRY: SELF-SORTING SYSTEMS, PARALLEL REACTIONS, AND DIFFERENTIAL SENSING USING CRUCIFORM/HALF-CRUCIFORM FLUOROPHORES

A Dissertation Presented to

the Faculty of the Department of Chemistry

University of Houston

In Partial Fulfillment

of the Requirements for the Degree

Doctor of Philosophy

By

Rio Carlo Manalo Lirag

August 2015

STUDIES IN SUPRAMOLECULAR CHEMISTRY: SELF-SORTING SYSTEMS, PARALLEL REACTIONS, AND DIFFERENTIAL SENSING USING CRUCIFORM/HALF-CRUCIFORM FLUOROPHORES

_____

Rio Carlo Manalo Lirag

APPROVED:

_____

Dr. Ognjen Š. Miljanić, Chairman

_____

Dr. Steven Baldelli

_____

Dr. Chengzhi Cai

_____

Dr. Olafs Daugulis

_____

Dr. Navin Varadarajan

_____

Dean, College of Natural Sciences and Mathematics

Dedicated to my Lola, my

number one fan,

who had always believed in me.

ACKNOWLEDGMENTS

It has been a long and challenging Ph.D. journey but, as they say, I can now see the light at the end of the tunnel. I am not good with words but I would like to express my gratitude, nevertheless, to these people whose support and encouragement have motivated me to reach for my goals.

First, I would like to thank my Ph.D. advisor, Prof. Ognjen Miljanic, for his unwavering support throughout my graduate career at UH. Your commitment in helping your students succeed amazes me. More than chemistry, you have instilled in me strong attention to details and to do things—be it experiments, write-ups, or presentations—the best way possible. In your lab, I've learned to work hard and to party even harder (our group parties are the best!). I also want to express my appreciation to the members of my committee: Dr. Steven Baldelli, Dr. Chengzhi Cai, Dr. Olafs Daugulis, and Dr. Navin Varadarajan for taking the time to review my dissertation. Your questions have directed me to better understanding of my work.

I would like to thank Dr. Charles Anderson for teaching me the basics on maintaining an NMR Facility and for helping me get my first job in the United States. I was about to say that I would miss our occasional lunches together, but then again I'll be in Clear Lake, so I'll just go visit you for dinner sometimes.

To the people that I had the pleasure of working with on certain projects: Dr. Karolina Osowska, Dr. Jaebum Lim, Ha Le, and Andrew Eisterhold, thank you. Karolina, you are the most hardworking, most productive and prettiest postdoc I know (#distractinglysexy). I can still remember our parties and camping like it was yesterday.

Jaebum, I admit you were intimidating at first, but over time, I learned to appreciate the discipline and work ethics that you showed in the lab. Ha, we constantly annoy each other, but hey, we did finish a project together! Please do not forget that "deal" we agreed on. Special thanks to the members of Miljanić group who tolerated my eccentricity, numerous request for favors, and my occasional "concerts" in the lab (you're welcome): Nadia, Chia-Wei, J-Star, Qing, and Mohammed.

I would like to thank Dr. Mary Jane Felipe and Mr. Ronald Cambel for helping me with almost everything. The list of the things that you have done, and I am grateful for, can fill as much as pages as this whole dissertation so I'll just summarize it in one sentence: one of you can cook better than the other.

My batch mates at UH: Siheng, Dewey, Inch, Phong, Thien, and Ha Do for the "tutorial" sessions and the occasional "favors" that I ask. To my kababayan: Ate Cel, Kata, Enrico, Noemi & Jack, Gino, Marlon, Sean, John, Mau, Kim, Arthur, Greggy, Marj & Joonhee, Radz & Mike, Pabs, and Roger, and travel buddies: Ronald, Minel, Joel, Jossana, and Kat, thank you for the company and for providing me with an escape from the toxic Ph.D. life.

I would like to thank my previous advisors: Dr. Charita Kwan, Dr. Ofelia Giron, Dr. Leni Quirit, and Dr. Irene Villaseñor. Working under your supervision has equipped me with the necessary lab skills and techniques to survive grad school.

Finally, I would like to thank my family, especially my Lola Nelly and Ate Resa. It is because of your hard work and sacrifices that I was able to finish my studies, and eventually, achieve my goal of becoming a Doctor. This achievement is for both of you.

STUDIES IN SUPRAMOLECULAR CHEMISTRY: SELF-SORTING SYSTEMS, PARALLEL REACTIONS, AND DIFFERENTIAL SENSING USING CRUCIFORM/HALF-CRUCIFORM FLUOROPHORES

An Abstract of Dissertation Presented to

the Faculty of the Department of Chemistry

University of Houston

In Partial Fulfillment

of the Requirements for the Degree

Doctor of Philosophy

By

Rio Carlo Manalo Lirag

August 2015

ABSTRACT

This dissertation presents different studies in supramolecular chemistry—the first three chapters deal with self-sorting of dynamic covalent libraries and one-pot parallel reactions, while the final two chapters describe the use of cruciform fluorophores in the construction of differential sensing arrays and the synthesis and characterization of "half-cruciform" fluorophores.

Chapter One. This chapter introduces the broad field of supramolecular chemistry with an emphasis on dynamic covalent chemistry (DCC). Notable applications of DCC and simplification of dynamic covalent libraries via self-sorting induced by chemical and physical stimuli is reviewed.

Chapter Two. Kinetic self-sorting of dynamic imine libraries, constructed from aromatic aldehydes and substituted anilines, was achieved through selective precipitation. The selectivity of the process is caused by the solubility differences among possible imines in the ethanol-water solvent mixtures used in precipitation.

Chapter Three. Parallel reactions are introduced and self-sorting event is extended to include several competing reversible reactions. Four simultaneous dehydration reactions: imine formation, acetal formation, ester formation, and tertiary alcohol dehydration, were shown to proceed simultaneously in one pot using *para*-toluenesulfonic acid as the catalyst.

Chapter Four. This chapter describes a protocol for discriminating structurally-related analytes using a differential sensing array constructed from 1,4-distyryl-2,5-bis(arylethynyl)benzene cruciform, benzobisoxazole cruciform, and benzobisoxazole-boronic acid hybrid sensors. This method relies on the differences of the emission colors of the cruciform solutions before and after analyte addition. Ten carboxylic acids, nine organoboronic acids, and twelve organic amines, and ureas were differentiated from each other using this procedure.

Chapter Five. Nine "half-cruciform" fluorophores containing benzimidazole core were synthesized in two steps: oxidative condensation of 3-bromo-*o*-phenylenediamine with three commercially-available aromatic aldehydes, which installs the horizontal axis, followed by Sonogashira coupling with aryl alkynes, which installs the vertical axis. Computational studies show that donor/acceptor substituted half-cruciform can localize their frontier molecular orbitals. These compounds were found to be viable fluorescent sensors, as they showed significant changes in their UV/Vis absorbance and fluorescence properties upon addition of bases, acids, and small anions.

TABLE OF CONTENTS

Chapter One Simplification of Dynamic Covalent Libraries through Self-sorting Induced by Physical and Chemical Stimuli

1.1 Introduction....1

1.2 Self-sorting Systems....13

1.3 The Dynamic Nature of Imines....20

1.4 Self-sorting of Dynamic Imine Libraries....23

1.4.1 Self-sorting of Dynamic Imine Libraries via Slow Irreversible Oxidation....23

1.4.2 Self-sorting of Dynamic Imine Libraries through Distillation....26

1.4.3 Self-sorting of Dynamic Imine Libraries through Silica Gel Adsorption....28

1.5 Conclusion....31

Chapter Two Kinetic Self-Sorting of Imines by Selective Precipitation

2.1 Introduction....33

2.2 Results and Discussion....36

2.3 Conclusions and Outlook....48

2.4 Experimental Section....50

2.4.1 General Experimental Methods....50

2.4.2 Experimental Protocols for Selective Precipitation of Imines....51

2.4.2.1 Selective Precipitation of *N*-(2,4-dinitro-benzylidene)-2,4-

dimethoxyaniline (**31**) and *N*-benzylideneaniline (**23**) 51

2.4.2.2 Selective Precipitation of *N*-(2,4-dinitro-benzylidene)-2,4-dimethoxyaniline (**31**) and 4-Methoxy-*N*-(4-nitrobenzylidene)aniline (**21**).....53

2.4.2.3 Precipitation-Driven Imine Transmutation 56

2.4.2.4 Selective Precipitation of *N*-benzylideneaniline (**2**), *N*-(2,4-dinitro-benzylidene)-2,4-dimethoxyaniline (**31**), and 4-methoxy-*N*-(4-nitrobenzylidene) aniline (**21**) 57

2.4.2.5 Selective Precipitation of *N*-(2,4-dinitro-benzylidene)-2,4-dimethoxyaniline (**31**), *N*-([1,1'-biphenyl]-4-ylmethylene)-4-methoxyaniline (**60**), and *N*-(4-nitrobenzylidene)-[1,1'-biphenyl]-3-amine (**61**) 59

Chapter Three Self-sorting in Parallel Reactions: Four Acid-Catalyzed Dehydration Reactions Proceed Without Interference

3.1 Introduction.....62

3.2 Results and Discussion 68

3.2.1 Parallel Dehydration Reactions to Form Imine, Boronate Ester, Ester, and Alkene (I) 70

3.2.2 Parallel Dehydration Reactions to Form Imine, Acetal, Ester, and Alkene (II).....71

3.2.3 Effect of Competing Diols in the Parallel Dehydration Reactions (III) 74

3.3 Conclusions and Outlook.....76

3.4 Experimental Section.....77

3.4.1 General Experimental Methods 77

3.4.2 Structures and Chemical Shifts of Possible Dehydration Products 78

3.4.2.1 Possible Imine Products and Their Signature ^{1}H NMR Signals 78

3.4.2.2 Possible Acetal Products and Their Signature ^{1}H NMR Signals 79

3.4.2.3 Possible Alkene and Boronate Ester Products and Their Signature ^{1}H NMR Signals 80

3.4.2.4 Possible Ester/Diester Products and Their Signature ^{1}H NMR Signals 80

3.4.3 Experimental Protocols for Parallel Dehydration Reactions 81

3.4.3.1 Parallel Reaction #1 (Reaction Set I, Entry 1) 81

3.4.3.2 Parallel Reaction #2 (Reaction Set I, Entry 2) 84

3.4.3.3 Parallel Reaction #3 (Reaction Set II, Entry 1) 86

3.4.3.4 Parallel Reaction #4 (Reaction Set II, Entry 2) 89

3.4.3.5 Parallel Reaction #5 (Reaction Set II, Entry 3) 91

3.4.3.6 Parallel Reaction #6 (Reaction Set II, Entry 4) 93

3.4.3.7 Parallel Reaction #7 (Reaction Set II, Entry 5) 95

3.4.3.8 Parallel Reaction #8 (Reaction Set II, Entry 6) 97

3.4.3.9 Parallel Reaction #9 (Reaction Set II, Entry 7) 99

3.4.3.10 Parallel Reaction #10 (Reaction Set II, Entry 8) 101

3.4.3.11 Parallel Reaction #11 (Reaction Set II, Entry 9) 103

3.4.3.12 Parallel Reaction #12 (Reaction Set II, Entry 10) 105

3.4.3.13 Parallel Reaction #13 (Reaction Set II, Entry 11) 107

3.4.3.14 Parallel Reaction #14 (Reaction Set II, Entry 12).....109

3.4.3.15 Parallel Reaction #15 (Reaction Set II, Entry 13).....111

3.4.3.16 Parallel Reaction #16 (Reaction Set III, Entry 1) 113

3.4.3.17 Parallel Reaction #17 (Reaction Set III, Entry 2) 116

3.4.4 Synthesis of Other Plausible Dehydration Products 118

Chapter Four Cruciforms as Supramolecular Sensors for Qualitative Identification of Carboxylic Acids, Boronic Acids, and Amines

4.1 Introduction.....122

4.1.1 Supramolecular Analytical Chemistry.....122

4.1.2 Indicator Displacement Assay (IDA) and Differential Sensing 124

4.1.3 Supramolecular Sensing Arrays Using Cruciform Fluorophores 132

4.2 Results and Discussion 137

4.2.1 Detection of Carboxylic Acids Using 1,4-Distyryl-2,5-bis(arylethynyl) benzene Cruciforms 138

4.2.2 Detection of Boronic Acids Using Benzobisoxazole Cruciforms 139

4.2.3 Detection of Amines and Ureas Using a Hybrid Benzobisoxazole Cruciform.....141

4.3 Conclusions and Outlook.....144

4.4 Experimental Section.....147

4.4.1 General Experimental Methods 147

4.4.2 Experimental Protocol for the Detection of Carboxylic Acids Using

Distyrylbis(arylethynyl)benzene Cruciforms.....147
4.4.3 Experimental Protocol for the Detection of Boronic Acids Using Benzobisoxazole Cruciforms.....148
4.4.4 Experimental Protocol for the Detection of Amine Analytes Using Benzobisoxazole Cruciform/Boronic Acids Hybrid Sensing System.....149
4.4.5 Image Processing and Numeric Analyte Discrimination.....150

Chapter Five L-shaped Benzimidazole Fluorophores: Synthesis, Characterization, and Optical Response to Bases, Acids and Small Anions

5.1 Introduction.....151
5.2 Results and Discussion.....155
5.2.1 Synthesis.....155
5.2.2 Computational Studies.....156
5.2.3 Optical Properties.....158
5.2.4 Response of Fluorophores **162** and **167** to Acids, Bases, and Anions.....161
5.3 Conclusions and Outlook.....166
5.4 Experimental Section.....168
5.4.1 General Experimental Sections.....168
5.4.2 Synthesis of 7-Bromo-2-phenyl-1*H*-benzo[*d*]imidazole (**159**).....169
5.4.3 Synthesis of 4-(7-Bromo-1*H*-benzo[*d*]imidazol-2-yl)-*N*,*N*-dimethyl benzenamine (**160**).....170
5.4.4 Synthesis of 7-bromo-2-(pyridine-4-yl)-1*H*-benzo[*d*]imidazole (**161**).....171

5.4.5 Synthesis of Half-Cruciform **162**.....172

5.4.6 Synthesis of Half-Cruciform **163**.....173

5.4.7 Synthesis of Half-Cruciform **164**.....175

5.4.8 Synthesis of Half-Cruciform **165**.....176

5.4.9 Synthesis of Half-Cruciform **166**.....177

5.4.10 Synthesis of Half-Cruciform **167**.....179

5.4.11 Synthesis of Half-Cruciform **168**.....180

5.4.12 Synthesis of Half-Cruciform **169**.....181

5.4.13 Synthesis of Half-Cruciform **170**.....182

5.4.14 UV/Vis Absorption and Fluorescence Emission Spectra for the Titration of Half-Cruciforms **162**–**170** with TFA and *n*-Bu_4OH.....183

References.....189

LIST OF ABBREVIATIONS AND ACRONYMS

AN	acetonitrile
ANN	artificial neural network
APCI	atmospheric pressure chemical ionization
ATR	attenuated total reflectance
CB	chlorobenzene
CB[*n*]	cucurbit[*n*]uril
CDC	constitutional dynamic chemistry
CF	chloroform
CH	cyclohexane
CI	chemical ionization
CSI	coldspray ionization
DCC	dynamic covalent chemistry
DCL	dynamic combinatorial/covalent library
DCM	dichloromethane
DFT	density functional theory

DMF	*N*,*N*-dimethylformamide
DMSO	*N*,*N*-dimethyl sulfoxide
DNA	deoxyribonucleic acid
DNCC	dynamic non-covalent chemistry
DOSY	diffusion nuclear magnetic resonance spectroscopy
EA	ethyl acetate
ESI	electrospray ionization
Et_3N	triethylamine
Et_2O	ether
FIA	flow injection analysis
FMOs	frontier molecular orbitals
HCA	hierarchical clustering analysis
Hex	hexane
H_2O	water
HOMO	highest occupied molecular orbital
HRMS	high resolution mass spectrometry
IDA	indicator displacement assay

i-Pr_2NH	diisopropylamine
*i*PrOH	isopropanol
IR	infrared
LDA	linear discriminant analysis
LRMS	low resolution mass spectrometry
LUMO	lowest unoccupied molecular orbital
Me_2CO	acetone
MeOH	methanol
NMR	nuclear magnetic resonance
OLEDs	organic light-emitting diodes
OPEs	oligo(phenylene ethynelenes)
OPVs	oligo(phenylene vinylenes)
PCA	principal component analysis
PhMe	toluene
RCHO	aldehyde
$RB(OH)_2$	boronic acid
RGB	red/green/blue

ROH	alcohol
RCOOH	carboxylic acid
RNH_2	amine
TBA	tetrabutylammonium
TBAOH	tetrabutylammonium hydroxide
TCB	1,2,4-trichlorobenzene
TFA	trifluoroacetic acid
THF	tetrahydrofuran
*p*TSA	*para*-toluenesulfonic acid
UV/Vis	ultraviolet/visible
VOCs	volatile organic compounds
ZIFs	zeolitic imidazolate frameworks

Chapter One

Simplification of Dynamic Covalent Libraries: Self-sorting Induced by Physical and Chemical Stimuli

1.1 Introduction

Supramolecular chemistry has been defined as the study of systems involving aggregates of molecules or ions held together by non-covalent interactions, such as electrostatic interactions, hydrogen bonding, π–π stacking, dispersion interactions, and hydrophobic or solvophobic effects.[1] Whereas molecular chemistry is concerned with building molecules by stepwise formation and breakage of covalent bonds, supramolecular ensembles are built by linking molecules with intermolecular forces.[2] Historically, this field can be traced back to the discovery of zeolites or "boiling stones" by Axel Cronstedt in 1756 and the preparation of clathrate hydrates or "anomalous ice" by Joseph Priestly in 1778.[3] Development of macrocylic ligands for metal cations, in the late 1960s and early 1970s, spurred the growth of this field which culminated to the awarding of the Nobel Prize in Chemistry in 1987 to Donald J. Cram, Jean-Marie Lehn, and Charles J. Pedersen for their development and use of molecules with structure-specific interactions of high selectivity.[4] Supramolecular chemistry is a multidisciplinary field that resides on the interface of several traditional areas of chemistry such as analytical, organic, inorganic, physical, and computational chemistry, and finds significant impact in the fields of biology, chemistry, and material science.

Recognizing that molecular chemistry is also endowed with similar dynamic features, Lehn has introduced the term Constitutional Dynamic Chemistry (CDC).[5,6] CDC brings together the Dynamic Non-Covalent Chemistry (DNCC) at the supramolecular level with Dynamic Covalent Chemistry (DCC) at the molecular level. DCC is concerned with molecular entities containing covalent bonds that can form and break reversibly. The dynamic reactions allow continuous change in constitution by reorganization and exchange of building blocks to generate a library of interconverting species, called the dynamic combinatorial library (DCL). This DCL may be characterized by three main parameters: (*a*) *conversion*: the total amount of the dynamic members of the library with respect to the free building blocks, (*b*) *composition*: the distribution of the library members which also represents the selectivity of the system, and (*c*) *expression* of a given member as a consequence of product conversion and selectivity. This is a unique property of DCL—exposing it to external stimuli leads to adaptation of the system to the new environmental conditions.

Different physicochemical stimuli have been shown to influence the distribution of DCL members, including variation of temperature and pH,[7] introduction of electric field modulation,[8] and irradiation with different wavelengths of light.[9] Hafezi and Lehn have also demonstrated that expression of a particular member(s) from the DCL can be achieved upon phase separation of an initially homogenous mixture.[10,11] Using a mixture of imines (**1**–**4**) dissolved in an acetonitrile/water mixture (3:2, v/v), they reported that phase separation induced by physical stimulus (heat) or addition of chemical effector (inorganic salt, sugar, organic solvent) led to uneven distribution of imine building

blocks. This event resulted in a complete change in the composition of the mixture—from an initial random distribution of all four imines to the selective expression of imine **1** in the aqueous phase, and imine **3** in the organic phase (Figure 1.1).

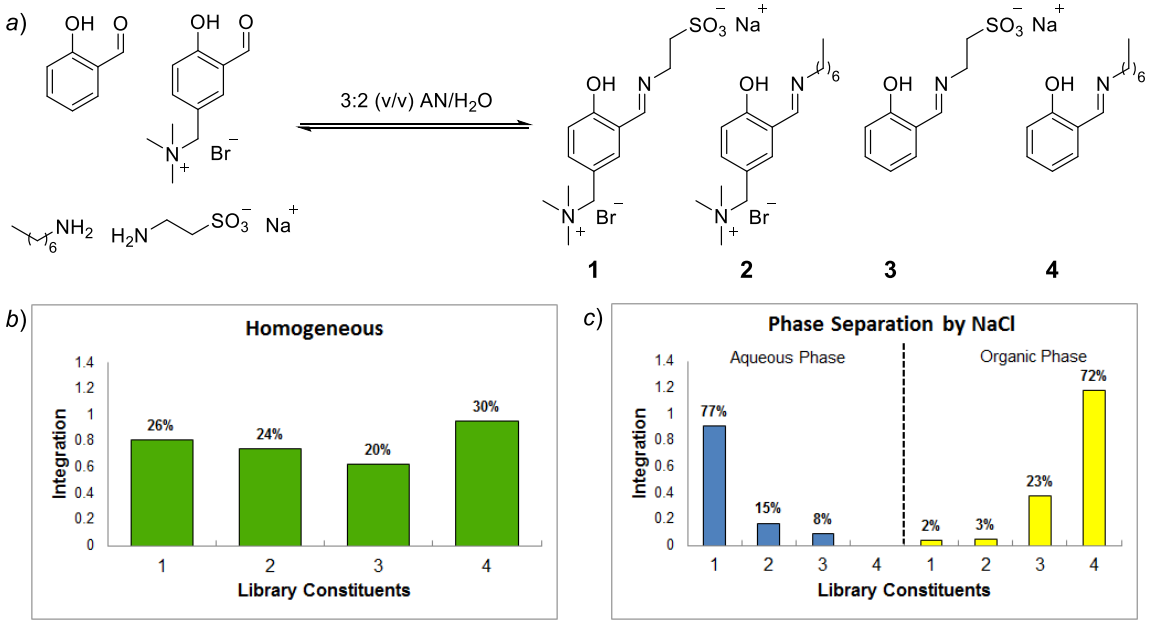

Figure 1.1 (*a*) Formation of a dynamic covalent library of imines **1**–**4**, (*b*) their distribution in a homogenous mixture of AN and H_2O, and (*c*) after phase separation.[11] Phase separation was achieved by addition of NaCl.

Addition of an external "template" molecule can also influence the distribution of the members of the DCL. As the added template interacts with certain library member, *e.g.* through noncovalent interaction such as complementary hydrogen bonding, that member becomes stabilized. The equilibrium will shift, normally resulting in the increase in the concentration (also called amplification) of the selected library member.[12] Moreover, an external template can serve several purposes: (*a*) direct the formation of

product, (*b*) select DCL members that can act as hosts or receptors (for the template molecule), and (*c*) identify new guests or ligands, which is particularly useful in the discovery of new ligands for biomolecules and for fragment-based lead discovery for potential new drugs.[13] In some cases, the library members can form stabilizing intra- and intermolecular noncovalent interactions with each other, and achieve amplification on their own. This internal templating gives rise to perhaps the most fascinating property of DCL—self replication, which is of interest in the studies of the chemical origin of life.[14]

Studies in DCC require searching for reversible reactions or finding catalysts that allow forming and breaking of covalent bonds, preferably under mild conditions. A number of reversible reactions are currently used for studies in dynamic covalent chemistry and these reactions are listed in Table 1.1.

Dynamic C–S Bond	
Thioacetal Exchange	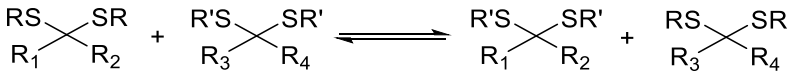
Thiazolidine Exchange	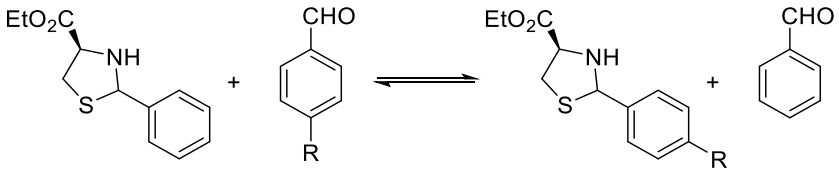
Thia-Michael Reaction	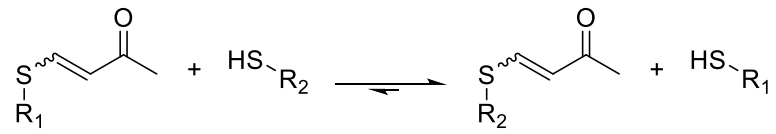

Table 1.1 Summary of reversible reactions reported for studies in dynamic covalent chemistry.[12,15,16]

Dynamic C–N Bond	
Imine Formation/ Exchange	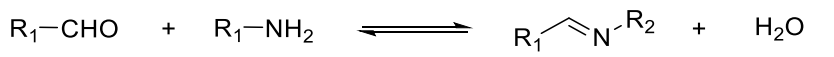
	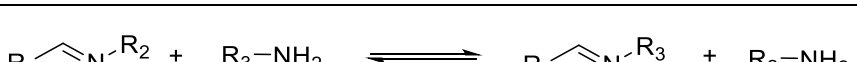
	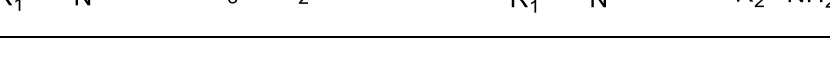
Hydrazone Exchange	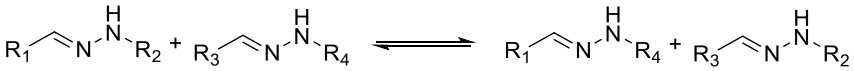
Oxime Exchange	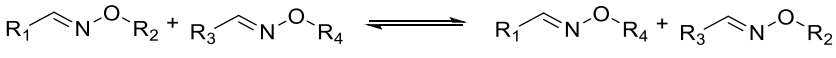
Nitrone Exchange	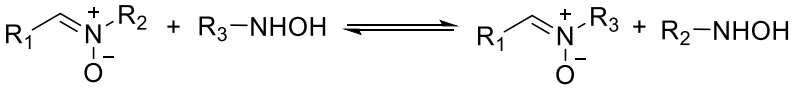
Aminal Formation	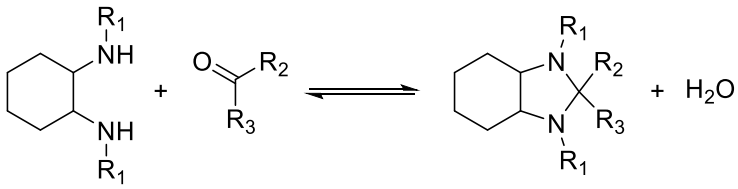
Amide Formation/ Exchange	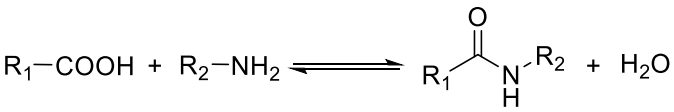
	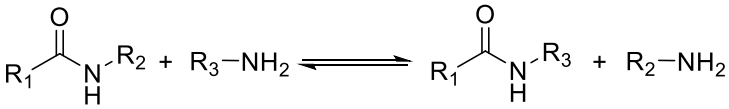
	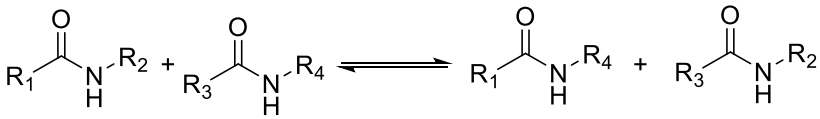

Table 1.1 Summary of reversible reactions reported for studies in dynamic covalent chemistry.[12,15,16]

Dynamic C–C Bond	
Diels-Alder/ retro-Diels-Alder Reaction	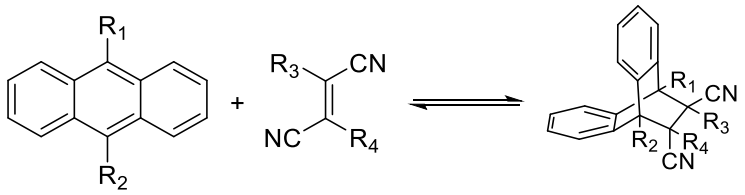
Phenol/Aldehyde Condensation	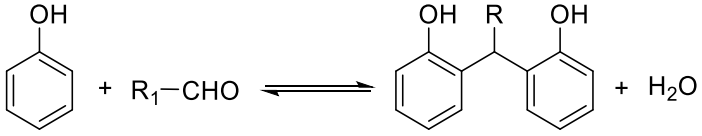
Aldol Reaction	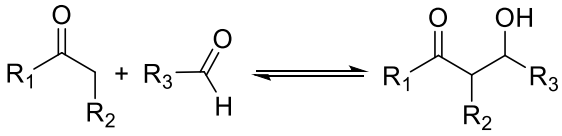
Carbene Coupling	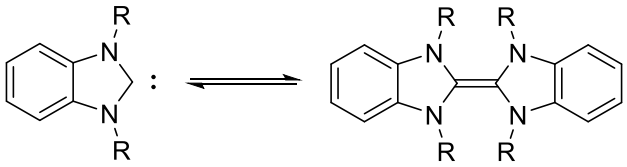
Strecker Reaction	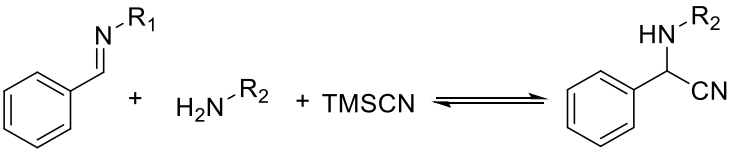
Olefin Metathesis	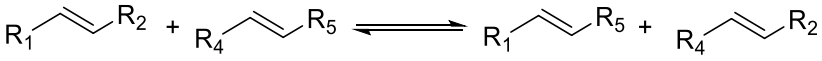
Alkyne Metathesis	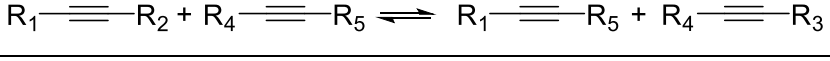

Table 1.1 Summary of reversible reactions reported for studies in dynamic covalent chemistry.[12,15,16]

Dynamic C–C Bond	
[2+1] Cycloaddition	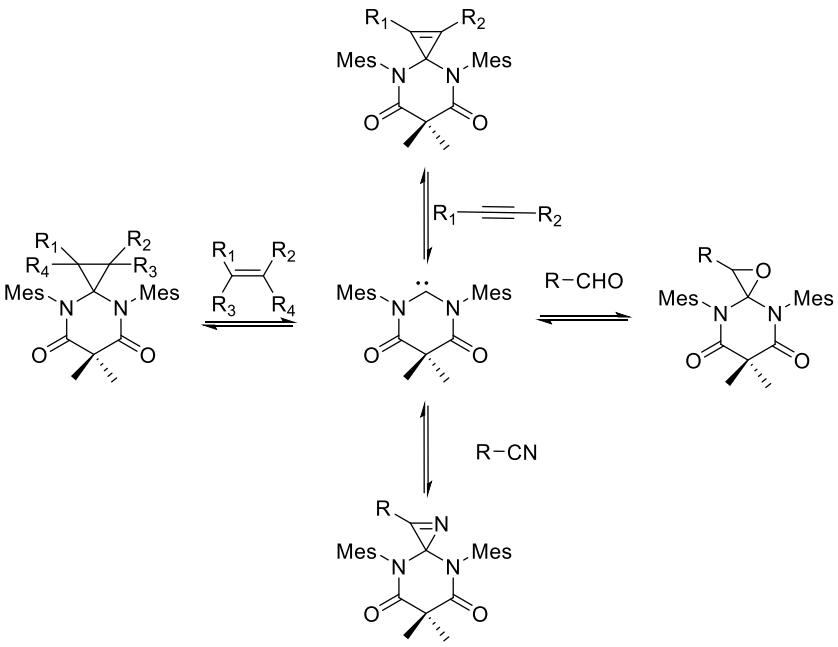
Resorcinol and 1,4-Butanedial Condensation	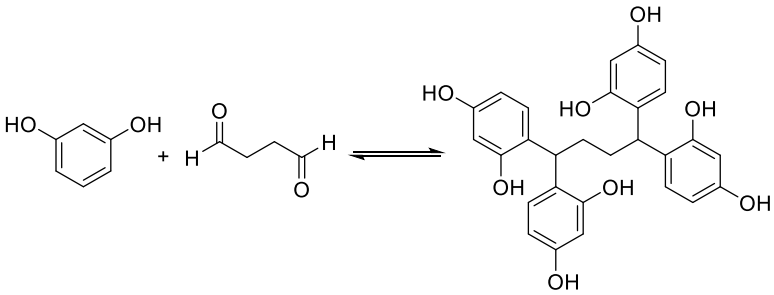
Dynamic S–S Bond	
Disulfide Exchange	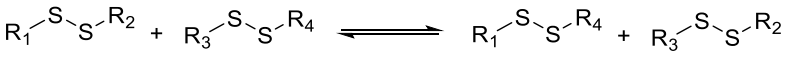

Table 1.1 Summary of reversible reactions reported for studies in dynamic covalent chemistry.[12,15,16]

Dynamic C–O Bond	
Ester Formation	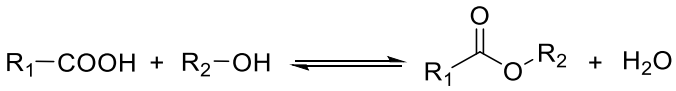
Ester Exchange	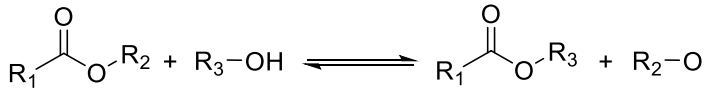
	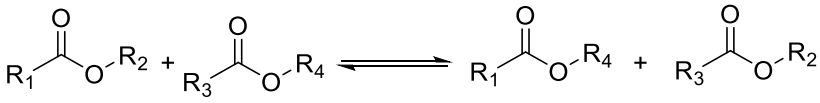
Acetal Formation	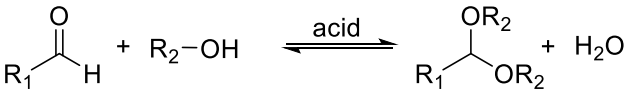
Acetal Exchange	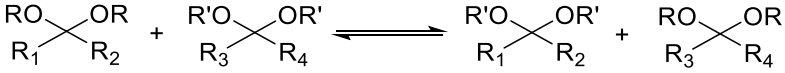
Nicholas Ether-Exchange	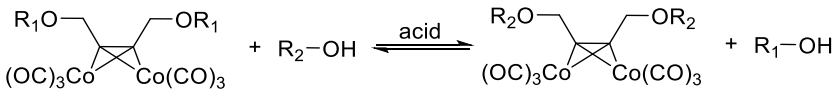
Hemiaminal Ether Exchange	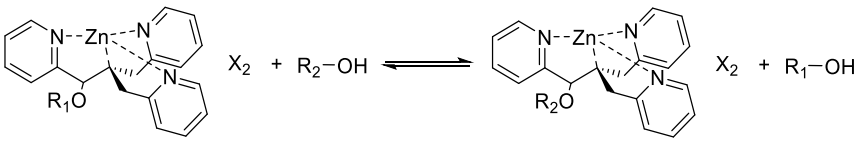
Alkoxyamine Exchange	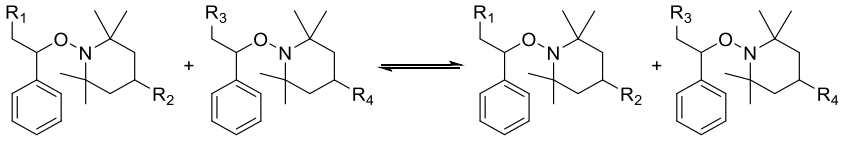

Table 1.1 Summary of reversible reactions reported for studies in dynamic covalent chemistry.[12,15,16]

Dynamic B–O Bond	
Boronic Acid Condensation and Exchange	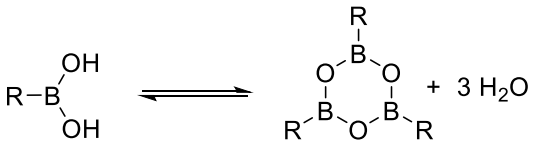
	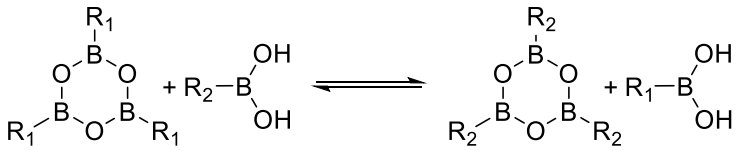
Boronic Acid Exchange	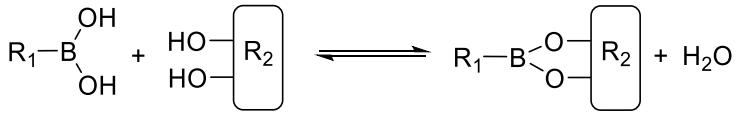
Transboroxoaromatic Esterification	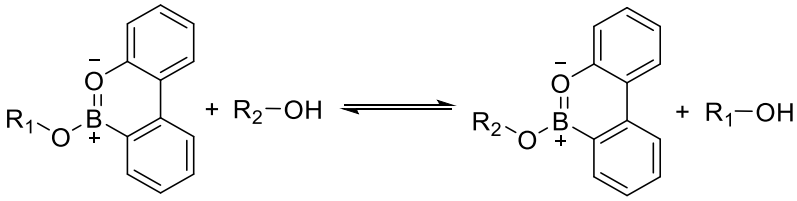

Table 1.1 Summary of reversible reactions reported for studies in dynamic covalent chemistry.[12,15,16]

The strength of DCC lies in its ability to exchange the molecular components and therefore form a multitude of combinations from a given set of building blocks, with a minimal investment of synthetic effort. For example, Otto's group has reported a dynamic disulfide library, constructed from eight different dithiol building blocks, that is capable of generating at least 9,000 unique cyclic trimers and tetramers![17] From this highly diverse library, screening for new molecules or supramolecular assemblies that have unexpected properties can be conveniently done. This is exemplified by the

discovery of acetylcholine-binding 2-catenane from an equilibrating library of dipeptide hydrazones by Sanders group (Figure 1.2).[18]

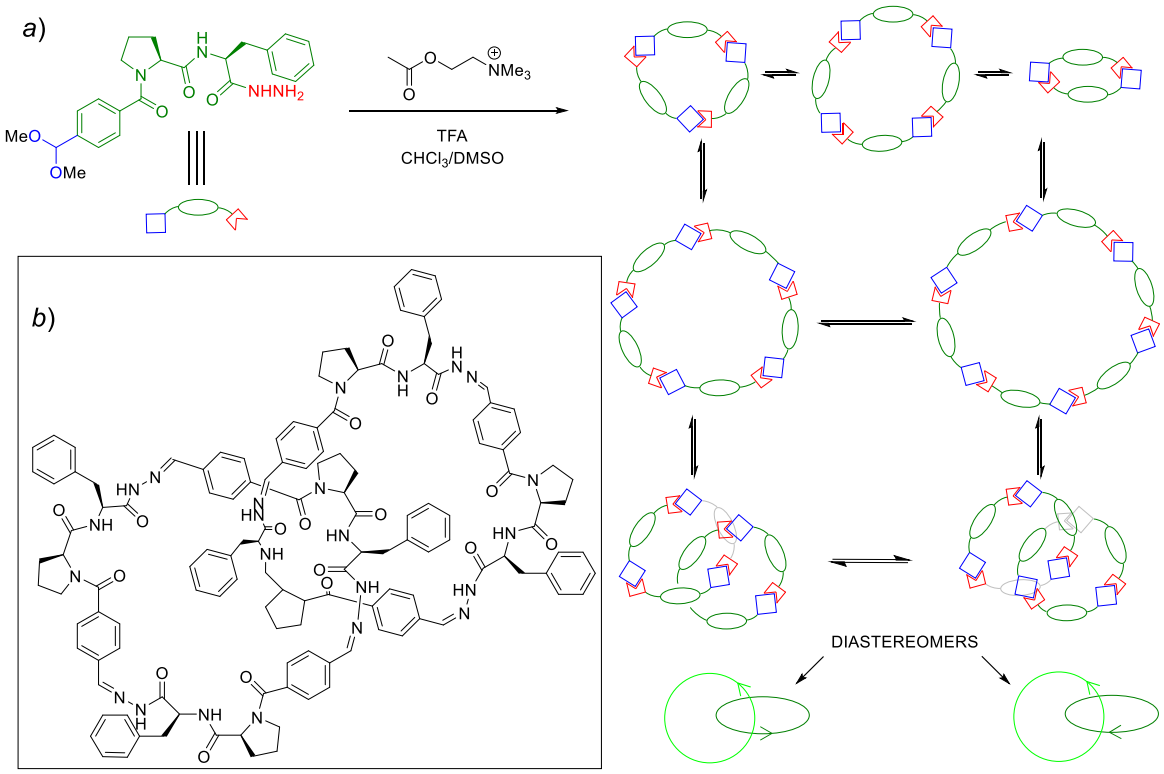

Figure 1.2 (*a*) Generation of a dynamic library from a small peptide-hydrazone building blocks upon addition of acetylcholine: the blue end represents the de-protected aldehyde functional group, the red end stands for the hydrazide functional group, and the green part represents the structural backbone of the peptide. (*b*) Structure of [2]catenane expressed by the library in the presence of 2.0 equivalents of acetylcholine.

Under acidic conditions, the DCC system underwent hydrazone exchange to form cyclic oligomers. At equilibrium, the combinatorial library is composed of cyclic dimers, trimers, tetramers, pentamers, and hexamers as determined by mass spectrometry. Upon

addition of 200 mM acetylcholine, formation of an elaborate [2]catenane (Figure 1.2b) made up of two interlocked macrocyclic trimers was observed within 25 minutes; the catenane became the most abundant species after 44 days. The catenane receptor exhibits high affinity for the target (100 nM) and could be isolated in 65% yield.

In addition to discovery of synthetic receptors[19] for various analytes in different media, DCC has also played an important role in the development of assorted molecular containers or cages[20] that can be used for catalysis[21] and can demonstrate complex host-guest behavior. For example, Rebek's group reported a self-assembled cylindrical capsule[22] that exhibits sequence-specific kinetics in terms of exchange of several *n*-alkane guests. When the capsule is exposed to a mixture of six *n*-alkanes (nonane–tetradecane), the capsule is predominantly occupied by nonane initially. During the first 100 minutes, nonane is gradually replaced by decane, while decane is displaced very slowly by undecane in approximately 3 months. Encapsulation of dodecane, tridecane, and tetradecane was only detected at very low concentrations.[23]

Molecular containers have also been reported to be capable of stabilizing highly reactive compounds. In 2009, Nitschke's group reported a tetrahedral cage **5** constructed by the combination of reversible imine formation between 2-pyridinecarboxaldehyde and 4,4'-diamino-2,2'-biphenyldisulfonic acid, and the coordination of the resultant ligands around an Fe^{2+} metal template (Figure 1.3). The self-assembled molecular container possesses a hydrophobic core with a volume big enough to accommodate one tetrahedral white phosphorus molecule. White phosphorus is an extremely pyrophoric material because the P–P bonds have low activation barrier to oxidation. However, when

incorporated inside the molecular container, the P_4 molecules are rendered air- and water-stable because addition of oxygen atoms to P_4 would result in the formation of oxidized species that would be too large to fit into the containers.[24] Controlled release of P_4 from its cage can be done by adding benzene, a competing guest that can displace P_4 from inside the cage.

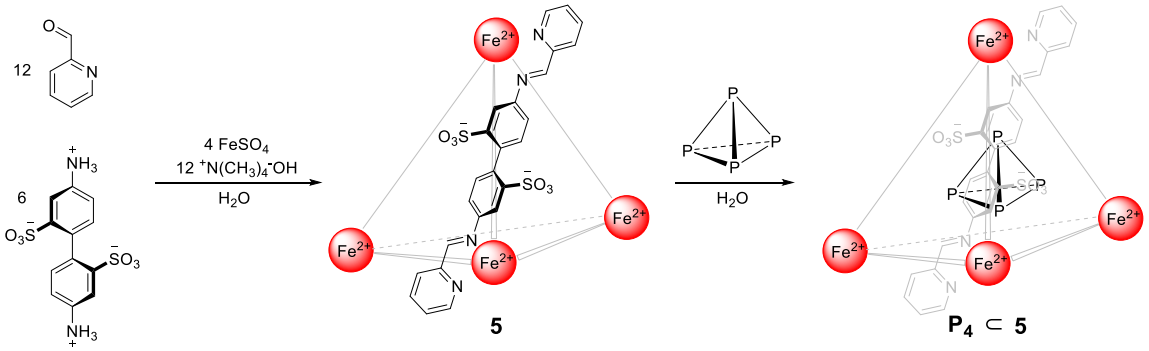

Figure 1.3 Synthesis of tetrahedral cage **5** and encapsulation of white phosphorus (P_4) inside the hydrophobic cavity of the cage.[24]

Molecular containers can also impose spatial segregation between incompatible reaction components and chemical reactions, allowing the construction of a self-organizing chemical assembly line. Using the same tetrahedral cage, Nitschke's group created a molecular assembly line, capable of one-pot sequential transformation of furan to fumaraldehydic acid, without the need for intermediate purification procedure.[24,25]

Self-assembly and self-sorting played an important role in the formation of these molecular containers and cages. According to Isaacs,[26] though these two concepts may be related, they are not the same. Self-assembly is the spontaneous high-fidelity synthesis of

higher order structure from a single set of components. On the other hand, self-sorting is the spontaneous high-fidelity synthesis of systems of higher order structures within complex multicomponent mixtures. These self-sorting systems can exhibit characteristics that cannot be expressed by its components in isolation. Alongside the development of dynamic covalent chemistry and identification of new reversible reactions, studies involving self-sorting systems have also advanced.

1.2 Self-sorting Systems

Self-sorting represents the spontaneous transformation of a low-order multicomponent system into several high-order subsystems with fewer components.[27] This phenomenon is commonly observed in nature. For example, the formation of DNA double helix structure, where the four bases: adenine (A), thymine (T), guanine (G), and cytosine (C) sort into two base pairs A–T and G–C, is an important consequence of self-sorting.[28] Even the common occurrence of separation of oil and water into two distinct layers is an expression of self-sorting.

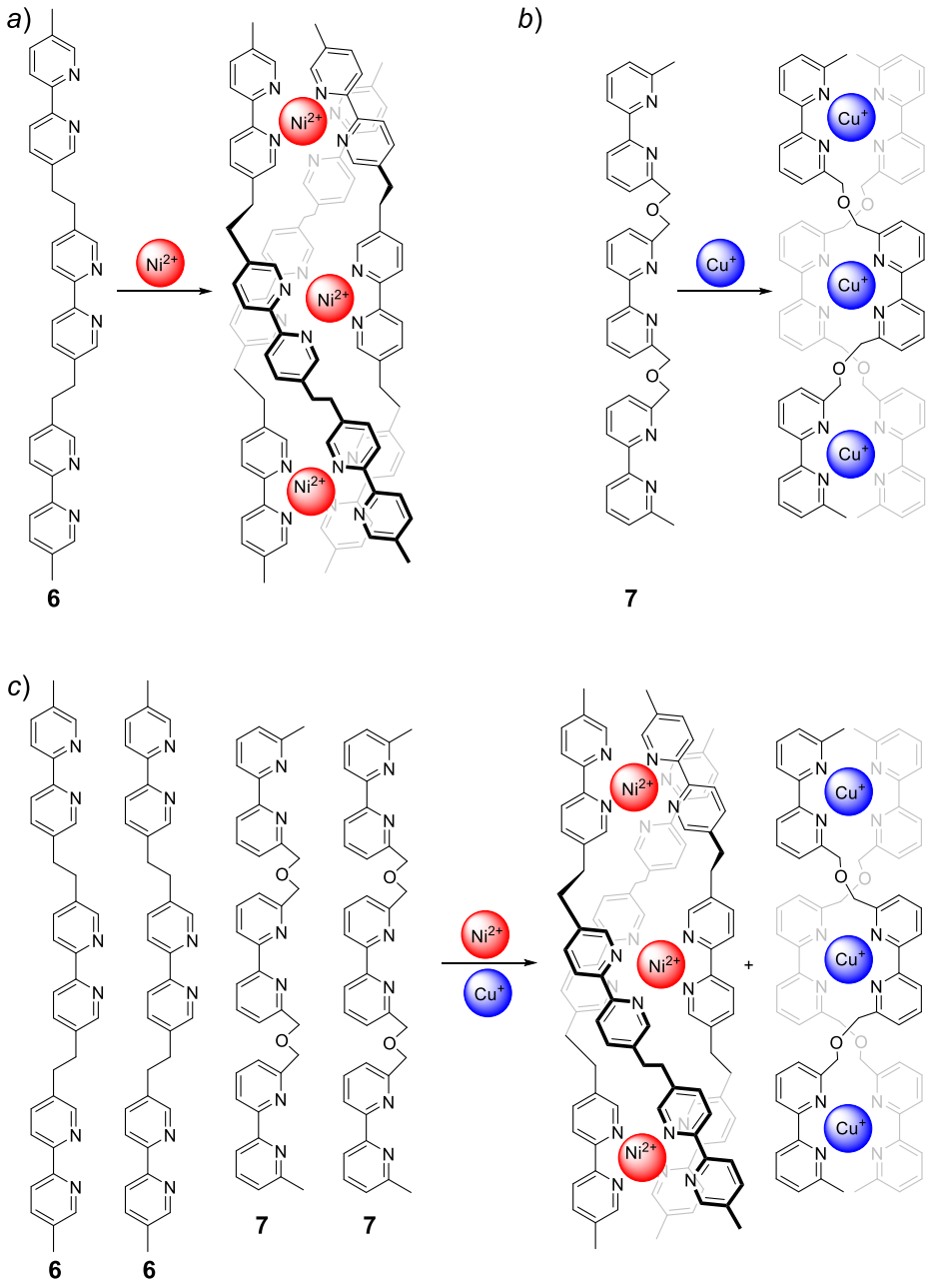

Figure 1.4 Self-assembly of (*a*) triple helicate from oligobipyridine strand **6** and Ni^{2+} ions (*b*) double helicate from oligobipyridine **7** and Cu^{+} ions, and (*c*) self-recognition in the self-assembly of double helicate and triple helicate structures from a complex mixture of oligobipyridines **6** and **7** with Ni^{2+} and Cu^{+} ions.

One of the earliest synthetic self-sorting systems was reported by Lehn *et al.*, where they described the propensity of a mixture of tris-bipyridine ligands with Ni^{2+} and Cu^{+} ions, to undergo self-recognition and self-assembly, forming double and triple helicates with no crossover products (Figure 1.4). The success of these experiments involves the interplay of structural and thermodynamic factors. These includes coordination geometry of the metal ions (Cu^{+} dictates tetrahedral geometry while Ni^{2+} has octahedral geometry), the position and nature of the spacers in the oligobipyridine ligands, and the energy-related principle of "maximal site occupancy" that dictates that the most stable state of the system must have the highest occupancy of the binding sites available on both the ligand and the metal ions.[11]

A number of studies in self-sorting systems have been published since then, involving different species, such as cucurbit[*n*]urils from Isaacs' group,[29] calix[4]arenes from Desreux's group,[30] various metal-ligand pairs from Stang's,[31] Schmittel's,[32] and Nitschke's groups,[33] crown ethers and ammonium ions from Schalley's group,[34] rotaxanes from Stoddart's group,[35] and imines and ester mixtures from Miljanić group,[27,36] to name a few.

Different authors have come up with several ways of classifying self-sorting systems. For example, Isaacs *et al.* used the terms *social* and *narcissistic* self-sorting.[37] The former describes high affinity between two different molecules forming a heteromeric aggregation, while the latter is for molecules that display high affinity for themselves creating a homomeric aggregation. On the other hand, Schalley *et al.* came forth with the terms *integrative* and *non-integrative*[38] self-sorting. *Integrative* self-sorting

incorporates all building blocks to form one complex assembly, where the different subunits are bound in two or more recognition events with positional control. *Non-integrative* self-sorting on the other hand, leads to a smaller than possible set of discrete complexes (Figure 1.5).

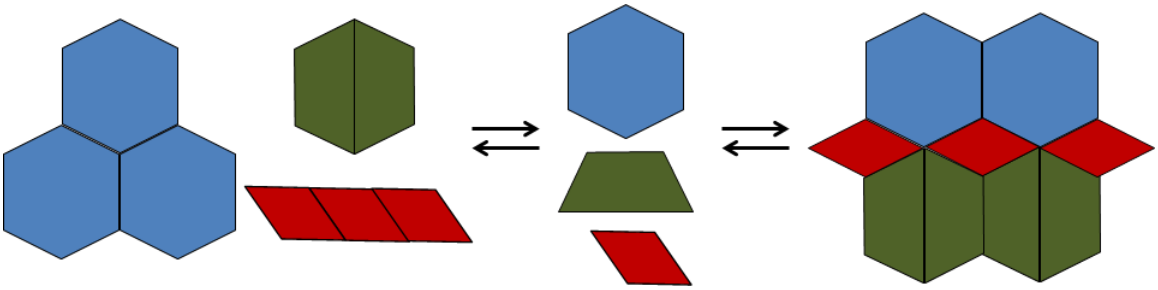

Figure 1.5 Schematic representation of *non-integrative* and *narcissistic* self-sorting (left) and *integrative* and *social* self-sorting (right) behaviors.

Another way of classifying self-sorting is based on the analysis of the kinetics and thermodynamics of a dynamic covalent library (DCL) as it approaches its self-sorted state.[39–41] A system is said to undergo *thermodynamic* self-sorting if the product distribution is directly related to the relative stabilities of the products, *i.e.* the system is at its most stable when sorted. Thermodynamic control of the DCL can be achieved by the use of high temperature or equilibration catalyst, since these conditions facilitate the system's travel across the energy landscape. By contrast, kinetic self-sorting generates products in ratios that are correlated to the relative rates of corresponding products' formation, which are in turn dictated by the relative activation energies. Kinetic control can be achieved by the use of low temperature and highly reactive reagents that disfavor reverse reactions.[40]

Switching between thermodynamic and kinetic control on one dynamic library of starting materials has been demonstrated by Patchell *et al.*[42] using cucurbit[6]uril, cucurbit[7]uril, and a spermine derivative (Figure 1.6).

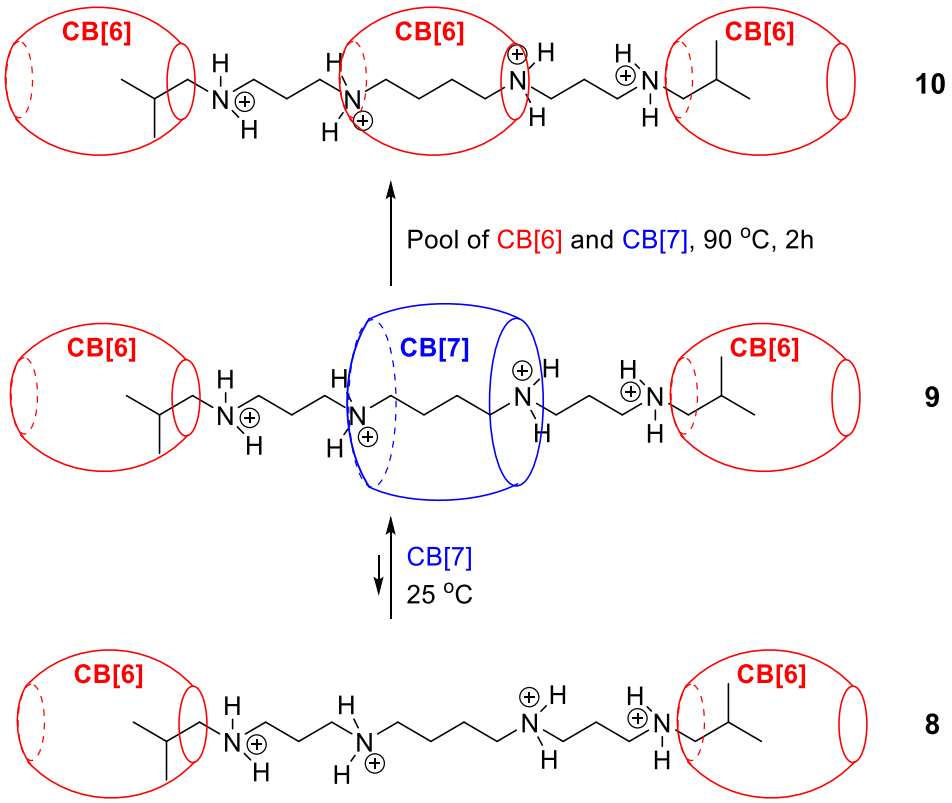

Figure 1.6 Thermodynamic (top) and kinetic (middle) self-sorted products from a dynamic pool of spermine derivative, cucurbit[6]uril, and cucurbit[7]uril.

Cucurbit[*n*]urils (CB[*n*]s) are pumpkin-shaped molecules that contain a hydrophobic core and two carbonyl-laced hydrophilic portals. CB[*n*]s have strong binding affinity to alkylammonium ions. The rigid inner cavities of CB[*n*]s stabilize the hydrocarbon backbone of the guest through van der Waals interactions, while the positively-charged nitrogen atoms are fixed at the portals through Coulombic interactions

and hydrogen bonding.[43] Affinities are even greater when the size of the guest matches well the dimensions of the cavity of the CB[*n*] host. At 25 °C, the kinetic product from the dynamic library is [4]pseudorotaxane **9**. Due to the bigger cavity of CB[7], it can easily get past the bulky isobutyl ammonium groups at the terminals to coordinate with the 1,4-diammonium cation at the center, albeit weakly, and the terminals are capped with the smaller and stronger binding CB[6]. Heating the same library produced the thermodynamic product [4]pseudorotaxane **10**, where the weakly binding CB[7] has been replaced by the smaller but stronger binding CB[6].

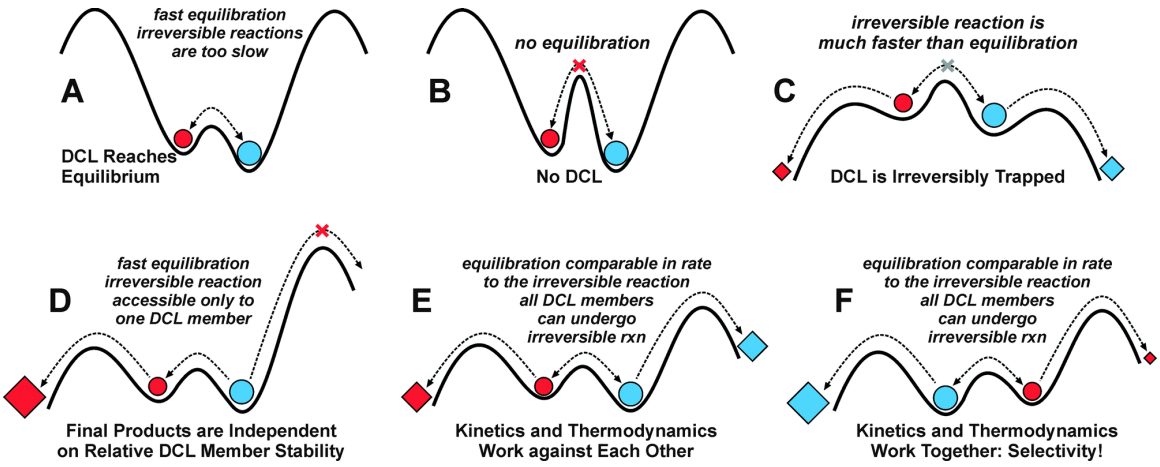

Figure 1.7 Different combinations of kinetic and thermodynamic parameters and their corresponding DCL product distributions. Circles represent dynamic compounds that are in equilibrium, blue signifies more stable species. Squares represent irreversible reaction products derived from the circles of the same color.[40]

Dominant kinetic and thermodynamic control represents the two extremes of reactivity for a dynamic library of equilibrating members. In between these two extremes,

we can anticipate mixed kinetic and thermodynamic control on the expressed self-sorted products. The theoretical energy profiles for these different combinations are summarized in Figure 1.7.

The second energy profile, **B**, corresponds to a non-dynamic system since there exist a high internal barrier preventing interconversion between states. Lowering this internal barrier allows facile interconversion between the DCL members (**A**). This energy profile represents "classical" DCC, where the most thermodynamically stable product is expressed by the DCL. If all members of the DCL are allowed to undergo irreversible reactions that are faster than their equilibration rate (**C**), then the DCL is essentially "frozen" and the distribution of the irreversibly formed products corresponds to the original distribution of their precursors from the DCL. This is a common technique used in studying DCC systems. The use of irreversible reactions, for example reduction of imines, converts the dynamic members (imines) into stable molecules (secondary amines) that can be separated and analyzed. However, if only one DCL component can irreversibly react (**D**), then high selectivity in the irreversible reaction is expected regardless of the stability and equilibrium concentration of its substrate. The reactive substrate simply "waits" for the equilibration to produce more of it (a consequence of Le Châtelier principle). Even minor components of the library can be quantitatively expressed from the DCL through this irreversible "escape route".

Profiles **E** and **F** highlight how the interplay of kinetics and thermodynamics can work for, or against, selectivity in self-sorting systems. If one DCL member reacts quickly but the other is dominant in equilibrium (**E**), the irreversible reaction is not

expected to proceed selectively. In contrast, if the more stable member also undergoes irreversible reaction quickly (**F**), then there is synergy between the reaction's thermodynamics and kinetics. Selectivity is enhanced and the amount of product produced from the irreversible reaction is higher than what can be expected from the equilibrium concentration of its precursor.

Early studies in DCC have concentrated on forming DCLs that are equilibrated. Research involving DCL's that is coupled with kinetically controlled chemical or physical steps has recently been the subject of much scrutiny, since these out-of-equilibrium systems are capable of creating emergent structures with functions that mimics those found in living systems.[44]

Generation of a dynamic combinatorial library suitable for self-sorting studies requires that: (*a*) the reaction must be reversible on a reasonable timescale (seconds to hours), (*b*) it generates library members which are close to being isoenergetic to avoid strong bias towards certain library member(s), and (*c*) it should be possible to "turn-off" the reversible reaction to allow isolation of selected library members without the complication of further exchange.[12,16] Reversible imine formation/exchange satisfies these basic requirements and has been a popular testing ground for DCC self-sorting studies.

1.3 The Dynamic Nature of Imines

Imines, anils, or azomethines, all refer to compounds that are formed between the condensation reaction between an amine and an aldehyde or ketone. This reaction was

first reported in 1864 by Hugo Schiff at the University of Florence.[45–50] In his honor, imines formed from aromatic aldehydes and amines (either aliphatic or aromatic) are also called Schiff bases.[45,46]

Imine formation is achieved by heating carbonyl compound and amine to reflux, usually with the use of an azeotroping agent. By removing the water by-product, the equilibrium is pushed towards the formation of imine (Figure 1.8). Water is normally removed by using a Dean–Stark apparatus or by adding a drying agent such as anhydrous magnesium sulfate, or 4 Å molecular sieves. Imine formation can also be catalyzed by acid.

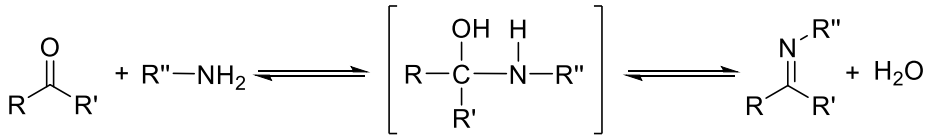

Figure 1.8 Imine formation.

Mechanistic studies suggest that acids protonate the carbonyl group, forming a carbonium ion, to which the amine quickly adds. The rate determining step is the deprotonation to give the unstable intermediate carbinolamine which rapidly eliminates a water molecule to give the final imine product.[51] Using benzaldehyde, aniline, and acid catalyst in benzene containing tributylamine, Remizov *et al.* established that the reaction is first order with respect to the aldehyde, amine, and catalyst.[50] They also reported that anilines with electron-donating groups in the *para*-position increase the reaction rate while the opposite is true for similarly *para*-substituted benzaldehydes. Aromatic aldehydes are good substrates for imine formation, which can give quantitative yields

even at room temperature. On the other hand, aliphatic aldehydes containing α-hydrogen may give polymeric materials with amine, instead of imine, due to subsequent aldol condensation.[51]

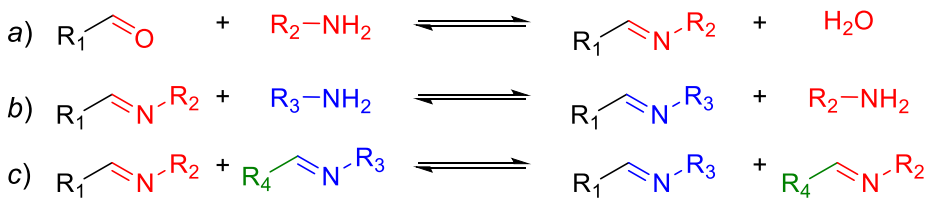

Figure 1.9 The reversible reactions of imine: (*a*) imine condensation and hydrolysis, (*b*) imine exchange, and (*c*) imine metathesis.

As shown in Figure 1.9, imines undergo several reversible reactions[47] such as (*a*) hydrolysis: where the condensation reaction to form imine and water can be reversed to give the aldehyde and amine precursors, (*b*) exchange: where a preformed imine reacts with a free amine and undergoes transimination, exchanging amine components, and (*c*) metathesis: where two imines swap their aldehyde and amine components.

Our group has reported several ways of achieving kinetic self-sorting of imine DCLs by combining reversible dynamic exchange reactions with irreversible sequestration of "favored" species via chemical (oxidation) and physical (distillation and adsorption on silica gel) means. These experiments expressed "*self-sorted*" products based on Curtin-Hammett principle—that is, the species with the lowest standard Gibbs free energy of transition state ($\Delta G^{\ddagger}$) is the one produced.[52–54]

1.4 Self-sorting of Dynamic Imine Libraries

1.4.1 Self-sorting of Dynamic Imine Libraries via Slow Irreversible Oxidation[53]

Using slow oxidation as the stimulus to induce self-sorting, a dynamic mixture of oxidizable imines was prepared from *o*-hydroxy- and *o*-aminoanilines with aromatic aldehydes of different electronic characters. These substrates were chosen because: (*a*) the imines formed can undergo imine exchange to form all possible amine-aldehyde combinations, (*b*) the oxidation step to benzimidazole or benzoxazole is irreversible and will convert the dynamic DCL members to stable species that can be separated, and (*c*) the rates of oxidation to form the cyclized products are sufficiently different and can be further modulated by substitution where the most electron-rich imine is expected to be oxidized the fastest, while the opposite is true for the most electron poor one.

A [2×2] imine mixture was prepared by heating equimolar amounts of *o*-phenylenediamine, *o*-aminophenol, 2,4-dimethoxybenzaldehyde, and 4-nitrobenzaldehyde in toluene at 65 °C for twelve hours (Figure 1.10). Analysis of the aliquot showed that all four possible imines **11**–**14** were formed and they were easily identified using their signature N═C–*H* ^{1}H NMR chemical shifts. Slow oxidation was achieved by adding one equivalent of iodine in toluene solution to the mixture using a syringe pump over the course of eight hours. The limited availability of the weak oxidant in the mixture ensures that only the most electron-rich imine **11** will be oxidized and will slowly be removed from the equilibrating mixture. This experimental design ensures that the oxidation step is slower than imine exchange.

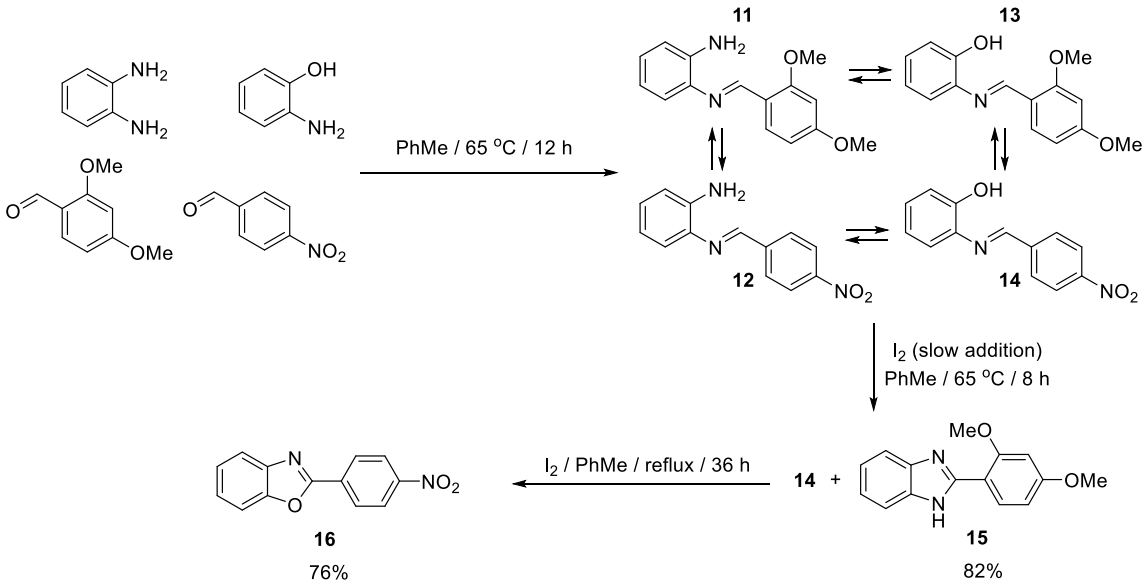

Figure 1.10 A representative example of kinetic self-sorting of a [2×2] imine library using slow oxidation.

As benzimidazole **15** precipitates out of the solution, imines **12** and **13** undergo imine metathesis to form more imine **11** as a consequence of Le Châtelier principle, until all the supply of its building blocks *o*-phenylenediamine and 2,4-dimethoxybenzaldehyde is exhausted. Since imine **14** is a relatively electron-poor imine, its oxidation is accomplished by adding another equivalent of iodine solution and by heating the mixture to reflux for thirty six hours. Oxidized products **15** and **16** were recovered in good yields (82% and 76 %, respectively).

Encouraged by this efficient self-sorting system, a bigger [3×3] imine library was constructed from *o*-phenylenediamine, *o*-aminophenol, 4-methoxyaniline, 2,4-dimethoxybenzaldehyde, 4-nitrobenzaldehyde, and 4-methylbenzaldehyde, forming an equilibrating mixture of nine imines: **11**–**14**, and **17**–**21** (Figure 1.11).

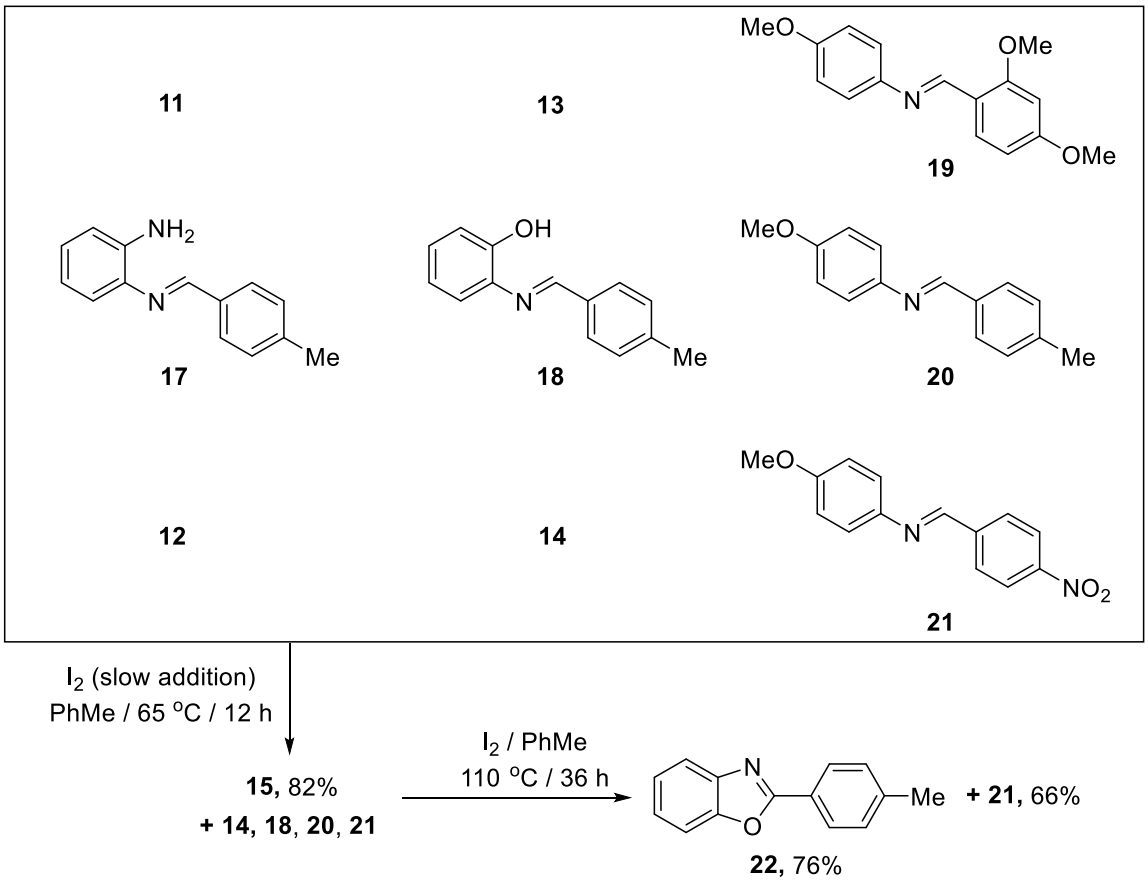

Figure 1.11 A representative example of kinetic self-sorting of a [3×3] imine library using slow oxidation.

Adding one equivalent of iodine solution to the imine mixture, over the course of twelve hours, led to the slow and irreversible formation of benzimidazole **15**, with 82 % yield, removing the supply of *o*-phenylenediamine and 2,4-dimethoxybenzaldehyde from the mixture. This process essentially simplified the [3×3] library into a smaller [2×2] mixture of imines. Imine **18** became the most electron-rich species in the smaller library and addition of a second equivalent of oxidizing agent led to oxidative cyclization of **18** forming benzoxazole **22** in 76% yield. Imine **21** was recovered at the end of the reaction,

in 65% yield, since it is non-oxidizable and it does not share any components with the imines that were oxidized.

1.4.2 Self-sorting of Dynamic Imine Libraries through Distillation[55]

The dynamic nature of the resulting DCL presents a significant challenge during separation and analyses of the self-sorted products since the dynamic species might decompose or interconvert when attempts for isolation are carried out. To circumvent this problem, Osowska and Miljanić coupled imine metathesis with a physical separation technique to produce multiple self-sorted imine products that are not only of high purity, but also mechanically separated.

Distillation is a physical separation process used for separating mixtures based on the differences in the volatilities of the components.[56] The boiling point of a compound is dependent on several factors such as strength of intermolecular attractions and the molecular weight of the compound. These factors can be manipulated by varying the substitution on the starting aromatic amines and aromatic aldehydes. To achieve kinetic self-sorting, using selective distillation as the driving force, starting materials was chosen to ensure that the resulting library will have members with sufficiently different boiling points. If the distillation is carried out slowly, then imine exchange will allow the members of the library to re-equilibrate and generate more of the compound that is being distilled, resulting in high selectivity of the self-sorting process.

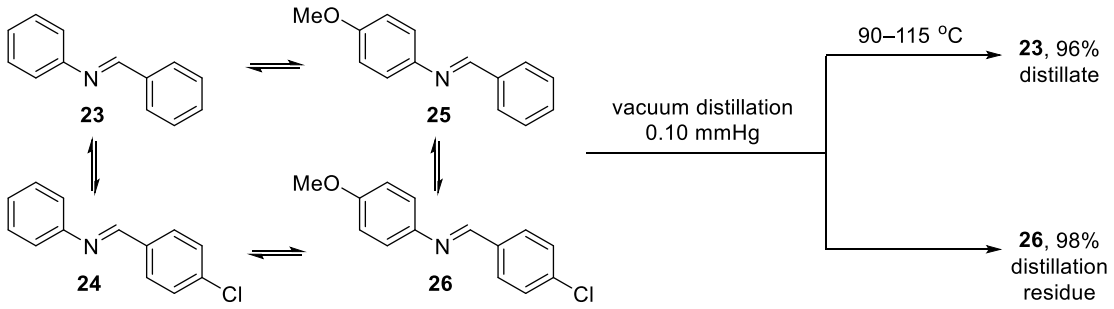

Figure 1.12 Kinetic self-sorting of a [2×2] imine library by distillation.

For example, a [2×2] imine library produced from 4-methoxyaniline, aniline, benzaldehyde, and 4-chlorobenzaldehyde gave four different imines **23**–**26**, with different molecular weights. Careful heating of this mixture at 90 °C under vacuum resulted to the selective distillation of the lightest and most volatile imine **23** (Figure 1.12). As aniline and benzaldehyde is consumed during the distillation of **23,** the imine library is reduced in complexity until the only remaining building blocks are 4-methoxyaniline and 4-chlorobenzaldehyde. Imine **26** is collected as the distillation residue with 98% yield and 99% NMR purity.

This self-sorting scheme could be translated to bigger imine libraries, such as [3×3], [4×4] (shown in Figure 1.13), and even [5×5], allowing one-pot simultaneous synthesis of up to five different imines, in high yields and high purity.

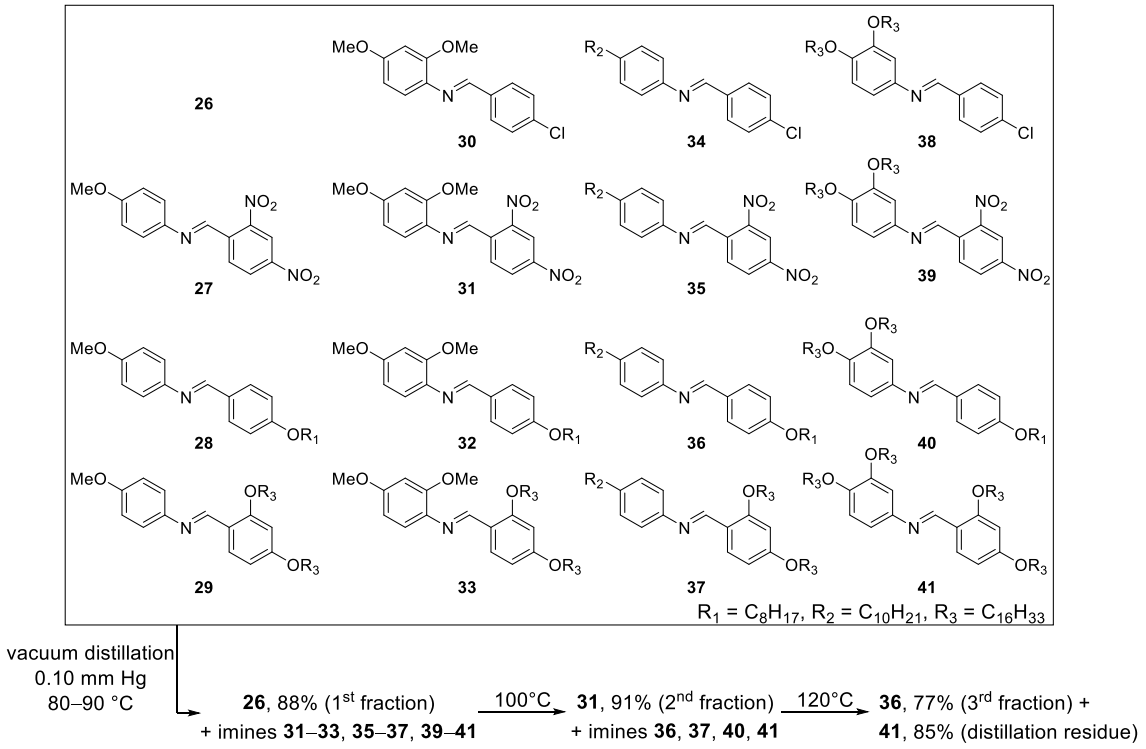

Figure 1.13 Kinetic self-sorting of a [4×4] imine library by distillation.

1.4.3 Self-sorting of Dynamic Imine Libraries through Silica Gel Adsorption[57]

Another common technique that is used to purify compounds in an organic laboratory is column chromatography.[58] With this procedure, a *stationary phase* such as silica gel (SiO_2) or alumina (Al_2O_3) is loaded on a column. The compound to be purified is then placed on top of the column. An organic solvent, or a mixture of solvents called the *mobile phase*, is allowed to pass through the column either due to gravity or positive air pressure. Based on the compounds' structure, they will either have stronger affinity to the stationary phase or the mobile phase. For example, a polar compound such as amine will tend to stay on the surface of the more polar silica gel rather than be eluted by a less

polar solvent like hexane. The difference in the strength of interactions among the compound being eluted, the stationary phase, and the mobile phase is the basis for how column chromatography can separate the different compounds in a mixture.

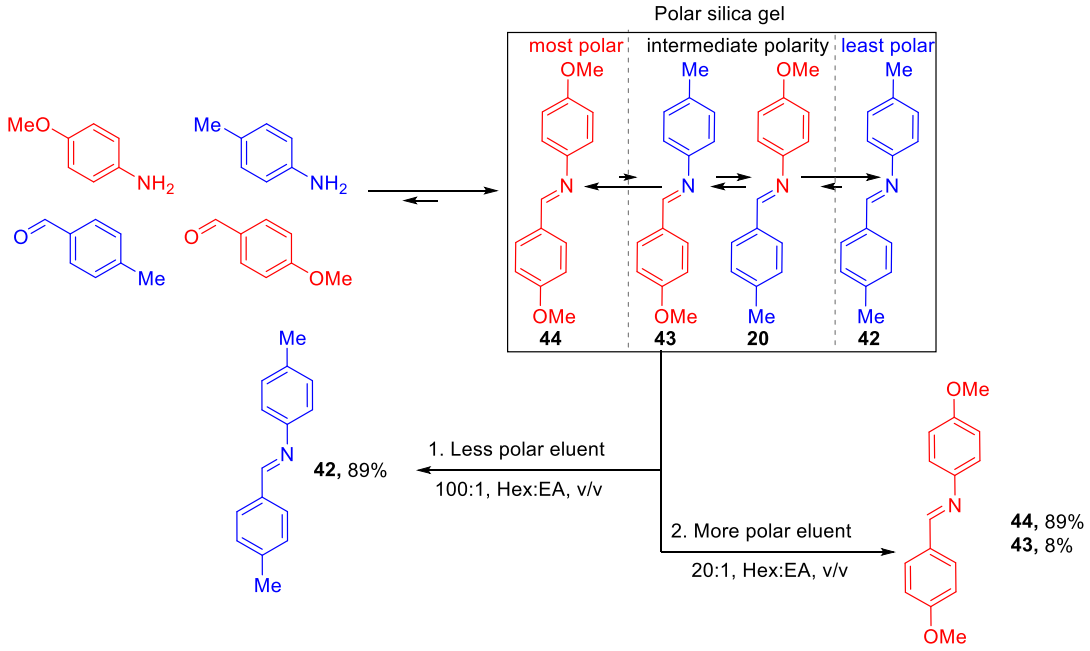

Figure 1.14 An illustration of how a [2×2] imine library undergoes self-sorting as it passes through the polar silica gel column. Using a relatively non-polar mobile phase elutes the least polar imine **42**. The self-sorting process is completed by flushing the column with a more polar mobile phase, removing the most polar imine **44** from the silica gel column.

By combining this separation technique with the dynamic nature of imine library, Hsu and Miljanić have shown that certain imines can be amplified based on their partition coefficients between the mobile and the stationary phase during the course of column chromatography. An imine library consisting of **42**, **20**, **43**, and **44** with an initial ratio of 1.00:0.65:0.66:0.99 was dry-loaded on top of the silica gel column. By passing a non-

polar mobile phase (100:1, Hex:EA, v/v), the least polar imine, **42**, was eluted out of the column, while the more polar imine species is retained in the column due to their stronger association with the polar surface of the silica gel (Figure 1.14). The fast elution of **42** disturbed the equilibrium of the initial library, resulting in the rearrangement of the building blocks from **20** and **43**. As imine **42** and its components are depleted, only **44** is left in the column and elution of this compound was achieved by passing a more polar mobile phase (20:1, Hex: EA, v/v). Compound **42** was collected from the first fraction at 89±1% yield, while the second fraction contains **44** at 89±1% yield with a small amount of **43** at 8±0.2% yield.

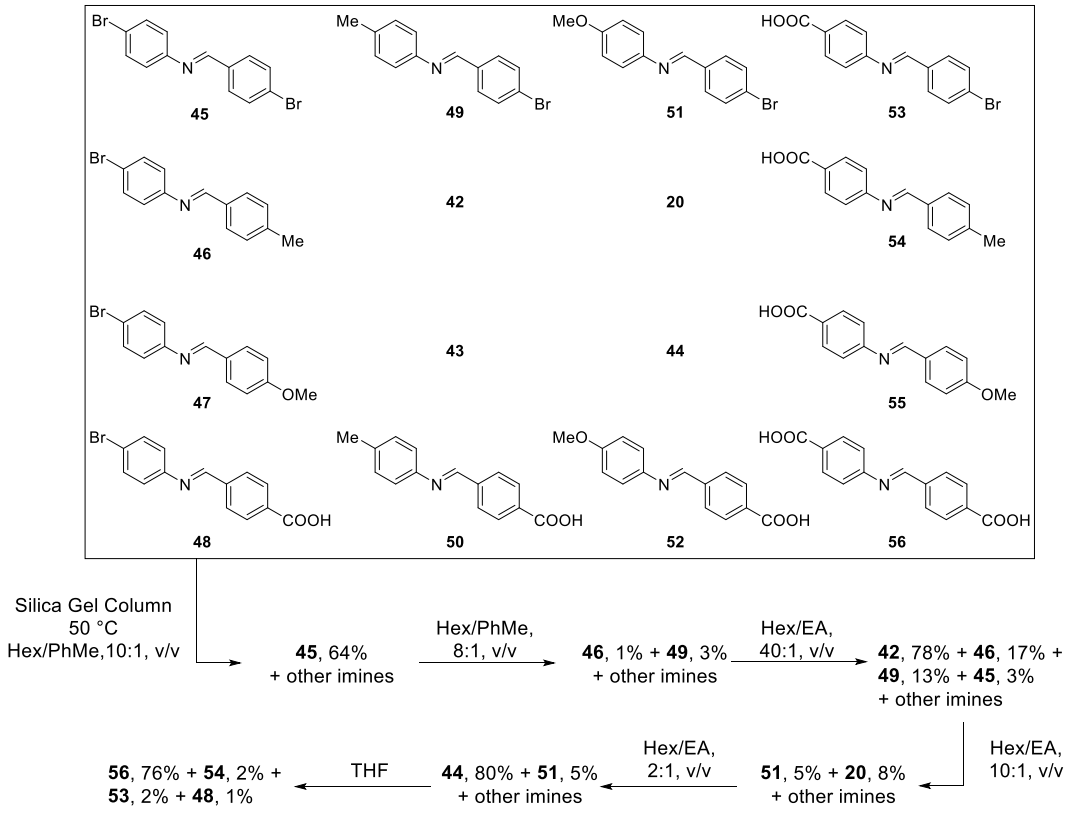

Figure 1.15. Adsorption-driven self-sorting of a [4×4] imine library.

Although this protocol can be translated to bigger [3×3] and [4×4] libraries (shown in Figure 1.15), larger libraries lose fidelity in the selectivity, and the collected fractions show overlaps between eluted imines. This can be explained by the similar polarity of the resulting imine species, *e.g.* **20** and **43**, which results in almost identical rates of elution with a given mobile phase. However, this procedure offers a possibility for multi-dimensional simplification of complex libraries, if for example, the chromatographic separation is done on a column impregnated with a catalyst.[57]

1.5 Conclusion

This chapter gives a brief overview of the development of supramolecular chemistry and how it ushered a paradigm shift from the traditional static chemistry to one that embraces dynamic, diverse and complex systems: Dynamic Covalent Chemistry.

The reversible reactions employed by DCC generate a dynamic combinatorial library of equilibrating species which can rearrange, exchange, and incorporate components through reversible bond breaking and bond forming processes to form all possible combinations of the building blocks. The resulting adaptive DCL can then be exposed to external stimuli, and the corresponding change in the distribution of the members, as well as the ensuing intra- and inter-molecular associations of and between the library members, has been used in the discovery of new receptors, and creation of exotic molecular structures and molecular cages.

Self-sorting or the ability of the complex dynamic combinatorial library to simplify and express only some members upon exposure to irreversible chemical or physical transformations, at the expense of "non-selected" ones, was also presented. Selectivity in these systems depends on the interplay between the thermodynamics and kinetics of the systems.

Finally, various ways of achieving kinetic self-sorting in a dynamic imine library reported by the Miljanić group were reviewed. Irreversible oxidation, distillation, and adsorption on silica gel surface have been shown to allow removal of certain member from the dynamic library. The irreversible removal of their components simplifies the library allowing the self-sorting process to produce multiple products, in high yields and purities, in one-pot. Chapter 2 of this dissertation will present another approach in achieving self-sorting of a dynamic imine library—via selective precipitation. In Chapter 3, the self-sorting process will be extended to involve parallel, multiple reversible reactions that share common building blocks while Chapters 4 and 5 will discuss the emerging field of supramolecular analytical chemistry and fluorescent sensing using cruciform/half-cruciform motifs.

Chapter Two

Kinetic Self-sorting of Imines by Selective Precipitation[59]

2.1 Introduction

As introduced in Chapter 1, freely equilibrating dynamic imine libraries can be compelled to undergo self-sorting during the course of an irreversible oxidation reaction,[53] or a physical transformation such as distillation[55] or adsorption.[57] However, these methods require substrates that can be easily oxidized, evaporated, or have significant differences in polarities. In this chapter, our efforts to effect self-sorting of imines via selective precipitation are presented. Precipitation should present a much broader route to self-sorting, as virtually any imine can be precipitated, or dissolved, provided that conditions are appropriately adjusted.

Precipitation and crystallization are terms that are often used interchangeably—while both refer to the generation of solid from a supersaturated solution, the distinction is often made on the basis of the speed of the process and the size of the particles produced. Precipitation is generally described as the rapid crystallization of sparingly soluble materials, usually as a result of an irreversible chemical reaction or physical changes in the solution.[60] The formation of precipitates, like in crystallization processes,[61] occurs in three basic steps: (*a*) the creation of supersaturation, followed by (*b*) the generation of nuclei and finally, (*c*) the subsequent growth of these nuclei to detectable

[59] Lirag, R. C.; Osowska, K.; Miljanič, O. Š. *Org. Biomol. Chem.* **2012**, *10*, 4847–4850.

size.[62] Once a nucleus of critical size is attained, the non-equilibrium nature of crystallization, and precipitation, means that it is a one-way process in which crystal growth occurs in a run-away fashion until the local supersaturation is depleted.[61]

Precipitation plays an important role in Nature. One such example is the controlled biomineralization, a complex precipitation process, used by mollusk to build its shell.[63,64] Using a biopolymer to control the nucleation event, this species precipitates calcium carbonate (in the form of aragonite) from the surrounding seawater to form layered, microscopic, plate-like, composite structure of aragonite surrounded by sheets of organic matrix. A number of studies also point to the important role that kinetically and thermodynamically induced amplification via crystallization played in prebiotic peptide synthesis[14] and enantiomeric amplification[65–67] processes.

In academic and industrial settings, selective precipitation or crystallization is used to separate a target compound from a complex matrix of starting materials, or from a reaction mixture containing co-products or by-products.[68] Precipitation is normally used in managing laboratory wastes such as in removing various cations—including toxic metal elements cadmium, chromium, and lead, from waste solutions by precipitating the cations as their oxides, hydroxides, carbonates, sulfates or sulfides.[69] In the pharmaceutical industry, selective crystallization is the final step in the manufacture of active pharmaceutical ingredients.[70]

In the field of supramolecular chemistry and DCC, crystallization has played an important role in formation of interlocked Solomon knots,[71] self-assembly of molecular

cages,[72] and in the reversible trapping of carbon dioxide.[73] It has also been demonstrated that crystallization can be used to simplify a complex DCL. In 2007, Nitscke's group[74,75] has reported that a DCL of interconverting diastereomers can be made to express a single pair of enantiomers upon slow crystallization (Figure 2.2).

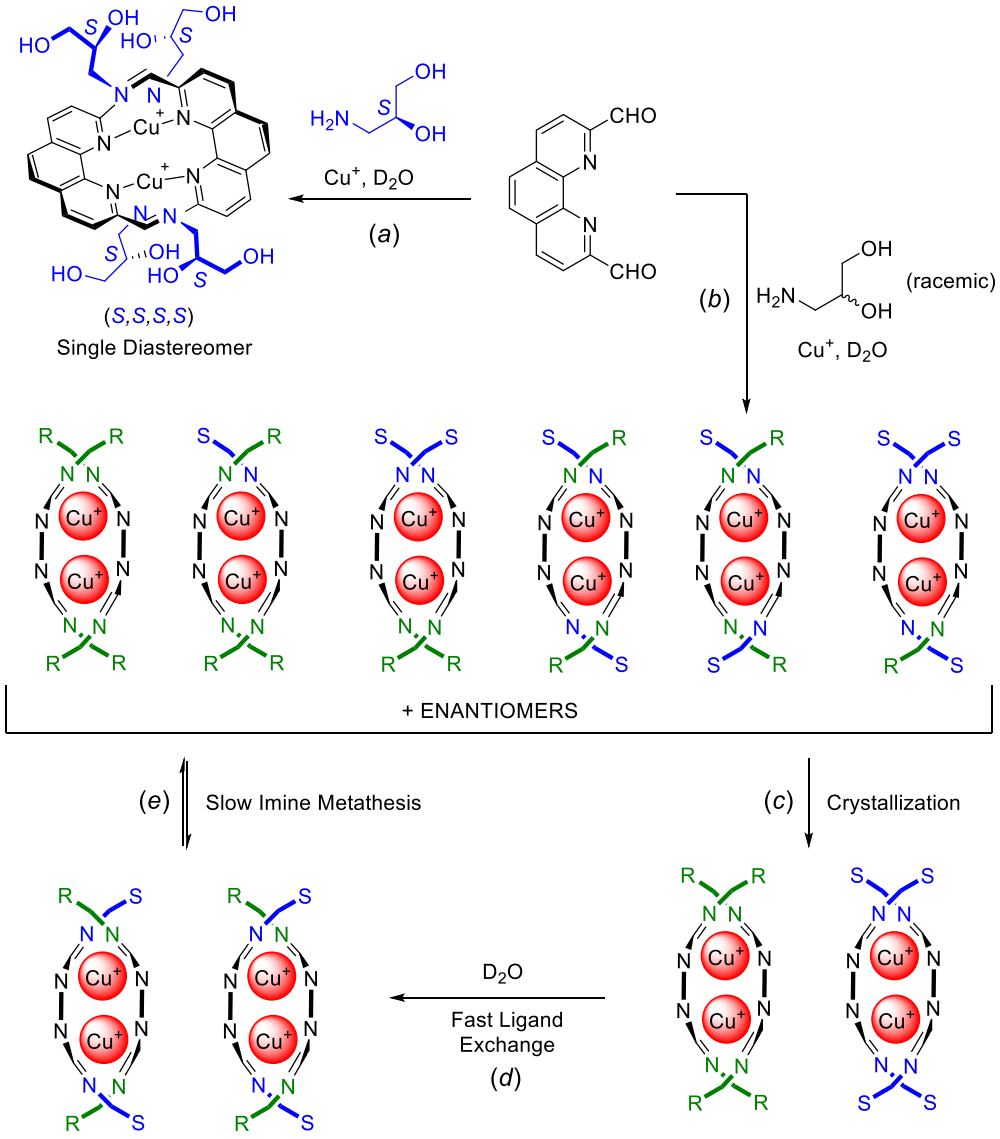

Figure 2.1 Generation of a single pair of enantiomers from a complex DCL through slow crystallization.

As shown in Figure 2.2a, imine formation between an enantiopure (*S*)-(–)-1-amino-2,3-propanediol and 2,9-diformyl-1,10-phenanthroline, followed by coordination with Cu^{+} ions produced a single helical (*S*,*S*,*S*,*S*) diastereomer product. On the other hand, replacing the chiral amine with its racemic mixture generated a dynamic library comprised of six diastereomeric pairs of enantiomers (Figure 2.2b), since either enantiomer can be incorporated at each equivalent location. By allowing the solution to stand for two weeks, crystals were recovered and were determined to be the enantiomeric pair (*S*,*S*,*S*,*S*) and (*R*,*R*,*R*,*R*) diasteromers.

The slow process of crystallization allowed the DCL of diastereomers to interconvert in the solution, through dynamic imine metathesis and ligand exchange, to express only the most insoluble products. The lower solubility of the highly symmetric enantiomeric pair was ascribed to its ability to form a crystalline network with four hydrogen bonds per molecule. As demonstrated in this example, selectivity-through-precipitation protocols simplifys the composition of the DCL solution—often to a single compound that can be isolated in high yield. With our interest in self-sorting processes, we speculated that parallel synthesis of multiple imines could be achieved under precipitative conditions, provided that their low solubilities favor them over the alternative crossover products.

2.2 Results and Discussion

To test our hypothesis, we chose aromatic amines and aromatic aldehydes that have substituents with varying electronic and steric properties, to produce imines that will

have different solubilities. The structures of imines investigated in this study, as well as their "signature" azomethine signals, are presented in Figure 2.2.

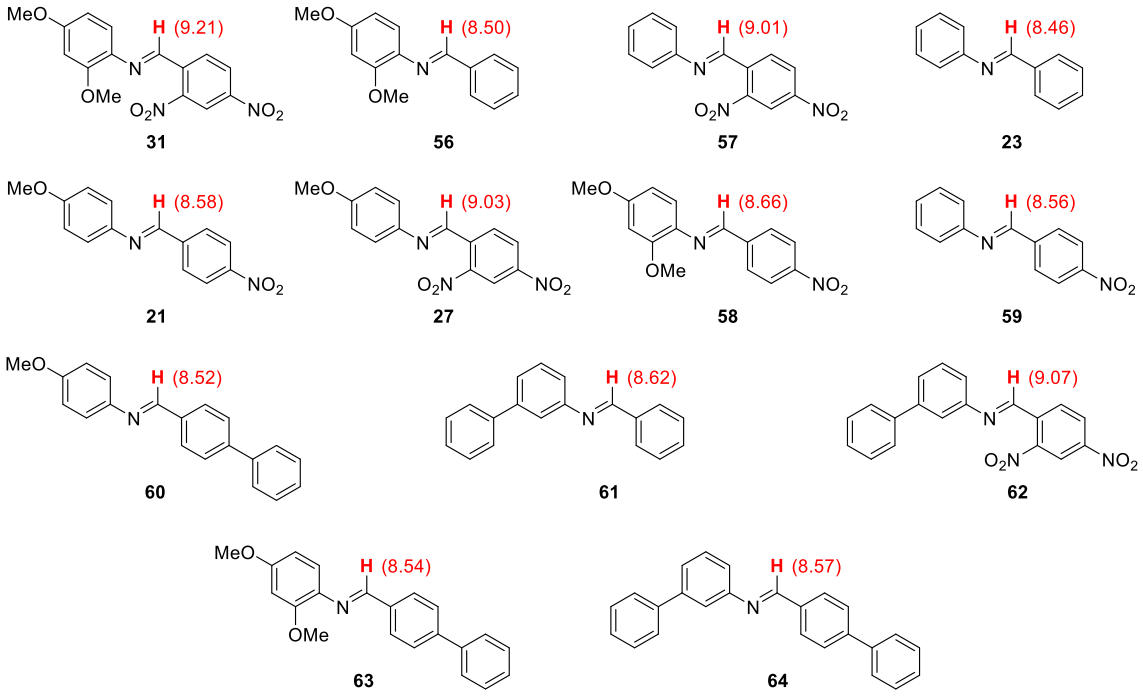

Figure 2.2 Structures and signature chemical shifts of imines investigated in this study.

Our first system consisted of equimolar amounts of aniline, 2,4-dimethoxyaniline, benzaldehyde, and 2,4-dinitrobenzaldehyde dissolved in absolute EtOH to give a 25.5 mM solution with respect to each components (Figure 2.3). The solution was initially clear but quickly turned cloudy, indicating the onset of precipitation of an imine product. Two crops of the resulting orange precipitate were collected and combined, and their analysis revealed virtually pure imine **31**, giving a total yield of 77%. The filtrate was collected, dried in vacuo, and was found to contain imine **23** as the dominant component (82%), together with imines **56** (11%), **57** (7%), and **31** (2%).

These yields were calculated from the overall mass recovery of the mixture and ^{1}H NMR spectra integration data since isolating the individual imines using e.g. column chromatography would likely change the distribution of the products.[57] These results confirmed that self-sorting of an imine library can be achieved through precipitation. Instead of getting a random combination of all four imines (**31**, **56**, **5**, and **23**) from the starting mixture of two aldehydes and two amines, in both the precipitate and the filtrate, we observed the exclusive formation of **31** in the precipitate and **23** in the filtrate—two imine species that do not share the same starting materials.

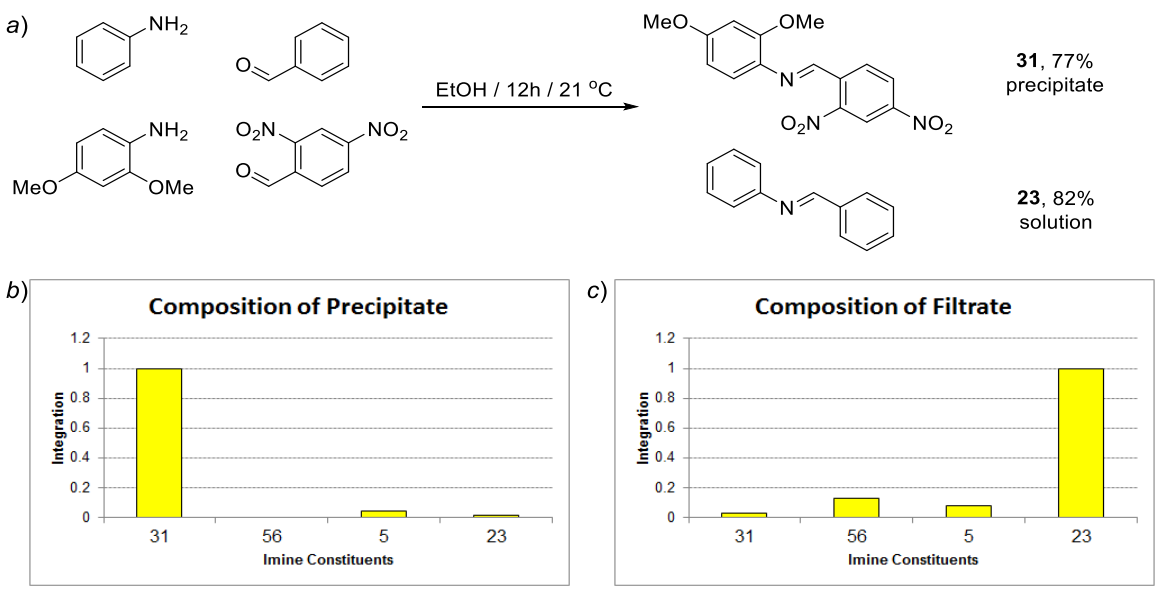

Figure 2.3 *a*) General scheme for the first precipitative self-sorting of an EtOH solution of a [2×2] imine library. Composition of the *b*) precipitate and *c*) filtrate as determined by ^{1}H NMR spectroscopy.

This initial result encouraged us to try a mixture of anilines and aldehydes with smaller structural differences. Upon dissolution of 2,4-dimethoxyaniline, 4-

methoxyaniline, 2,4-dinitrobenzaldehyde, and 4-nitrobenzaldehyde in EtOH, immediate formation of precipitate was also observed. Using ^{1}H NMR spectroscopy, the precipitate was determined to be composed of imines **21** and **31.** While the two imines co-precipitated, there was no trace of the crossover products **27** or **58** in the precipitate. However, analysis of the solution revealed that the precipitation-induced self-sorting event is not yet complete since all imines were still detected even after stirring the solution for 24 h.

To circumvent this problem, we devised a protocol in which H_2O was slowly injected into the EtOH solution during the course of the reaction. The purpose of this modification was to turn EtOH into a poor solvent for imines, but to do so gradually in order to avoid precipitating starting anilines or aldehydes. At the end of H_2O addition, the final H_2O:EtOH volume ratio was 1.33:1. As shown in Figure 2.4, overnight precipitation using this new strategy resulted in a solid that contained **31** (78%) and **21** (84%) as major components, with minor amounts of crossover imines **58** (10%) and **27** (11%). Doing three independent trials confirmed the repeatability of this observed self-sorting, since the variation of the NMR yields was calculated to be less than 2%. More importantly, the addition of H_2O did not lower imine yields. Once precipitated, imines examined in this study appeared stable to hydrolysis on the time scale of the performed experiments.

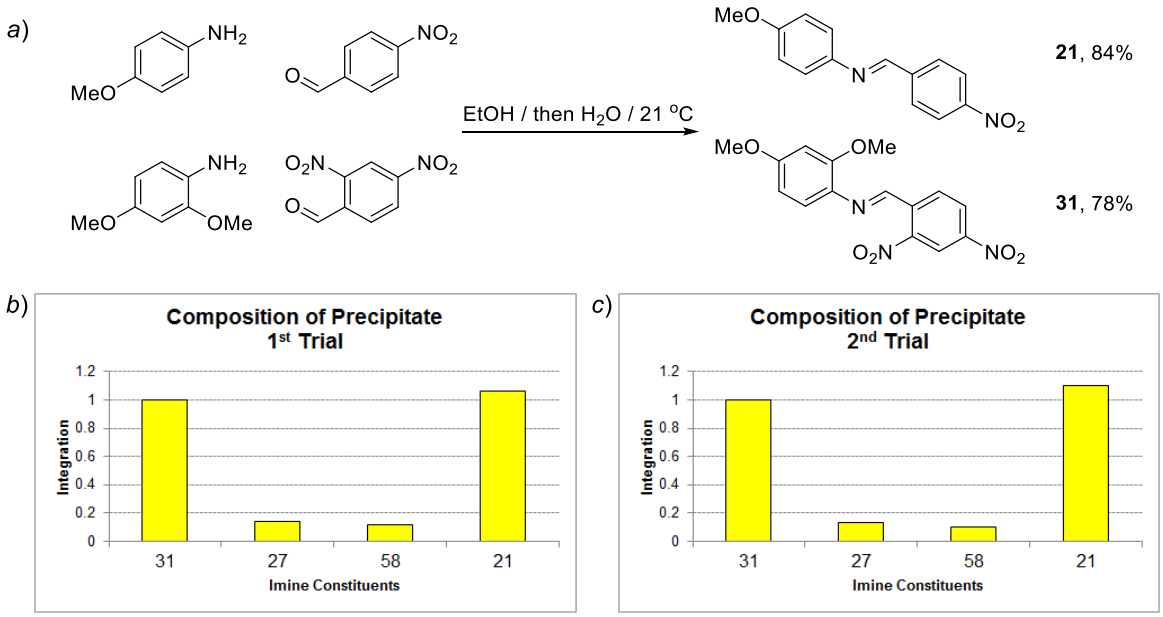

Figure 2.4 *a*) General scheme for the second precipitative self-sorting induced by the slow addition of water to an EtOH solution of a [2×2] imine library. Composition of the precipitate for the *b*) first and *c*) second trials as determined by ^{1}H NMR spectroscopy.

High selectivities observed in these two [2×2] experiments suggested that self-sorting of imines was possible during their precipitation and that it was not limited to a strict fractionation between a solution and a precipitate, *i.e.* selectivity can be achieved even during co-precipitation. Low solubility of precipitated imines appears to control the selectivities of these reactions. This assumption was confirmed by the transmutation experiment in which pure imines **56** and **23** were dissolved in EtOH and subjected to the slow addition of H_2O. After overnight stirring, imine **31** precipitated as a virtually pure compound, reaching 90% yield, while the solution contained chiefly **23**, which could be isolated in 75% yield (Figure 2.5).

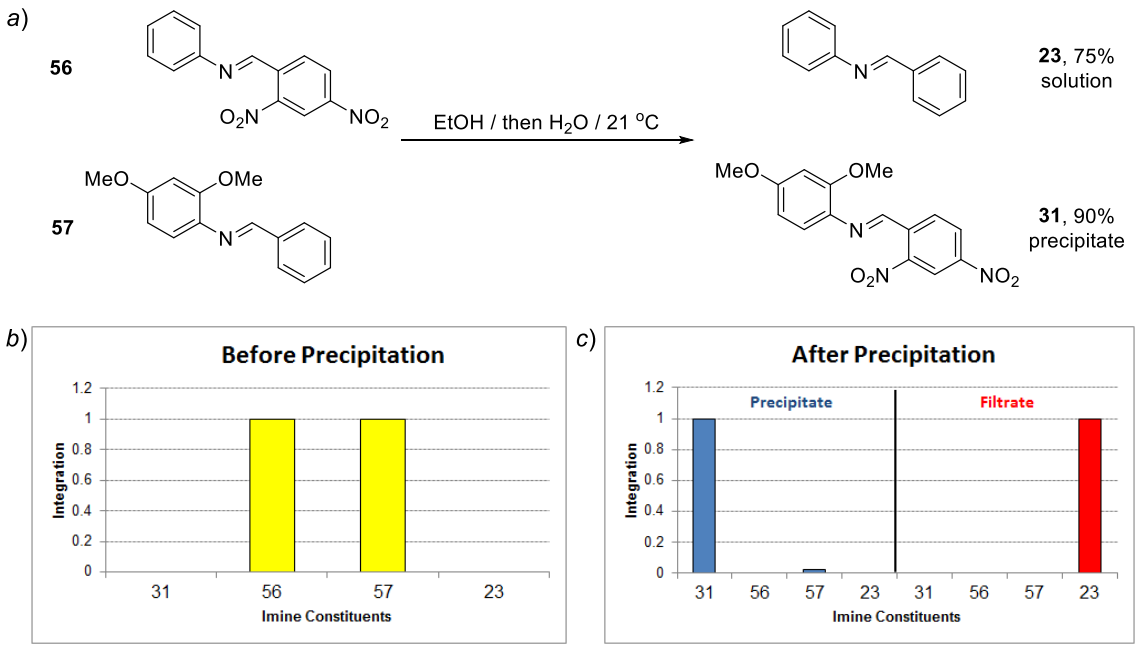

Figure 2.5 *a*) General scheme for the imine transmutation experiment between imines **56** and **57**. ^{1}H NMR analysis of the collected *b*) precipitate showed exclusive formation of imine **31** while the *c*) filtrate showed exclusive formation of imine **23**.

After demonstrating the successful self-sorting of [2×2] mixtures of anilines and aldehydes, we decided to increase the complexity of the dynamic imine library by adding one more aldehyde/amine pair. First we combined aniline, 4-methoxyaniline, and 2,4-dimethoxyaniline with benzaldehyde, 4-nitrobenzaldehyde, and 2,4-dinitrobenzaldehyde in EtOH and subjected the mixture to slow addition of H_2O (Figure 2.6).

Again, orange solid was isolated after overnight precipitation. Its spectroscopic analysis revealed a mixture dominated by imines **31** (77%) and **21** (79%). Varying amounts of five additional imines, with NMR yields ranging from 1–15%, could be identified from the crude ^{1}H NMR spectrum of the collected precipitate. The filtrate, on

the other hand, showed the presence of all nine possible imine combinations—with **23** as the main component (81%) and the eight remaining imines in low amounts (0.2–9%).

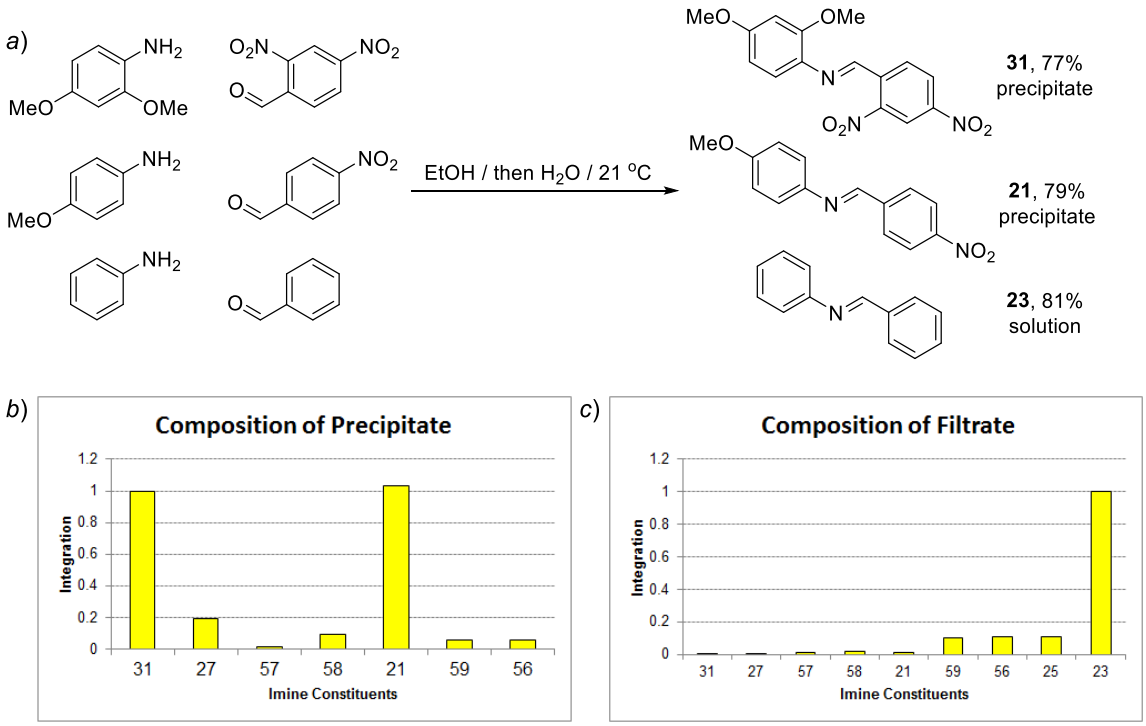

Figure 2.6 *a*) General scheme for the first precipitative self-sorting induced by the slow addition of water to an EtOH solution of a [3×3] imine library. ^{1}H NMR analysis of the collected *b*) precipitate showed preference for the formation of both imines **21** and **31** while the *c*) filtrate showed preference for the formation of imine **23**.

For our final [3×3] experiment, we replaced benzaldehyde with 4-phenylbenzaldehyde, and aniline with 3-phenylaniline, while keeping 4-nitobenzaldehyde, 2,4-dinitrobenzaldehyde, 4-methoxyaniline, and 2,4-dimethoxyaniline as the components of the mixture (Figure 2.7). We also slightly modified our procedure—after slow H_2O addition, the mixture was stirred in an open flask for seven

days, and then dried by exposing it to a gentle stream of nitrogen for three days. This modification further ensured that the irreversible formation of insoluble precipitate is slower than imine metathesis, increasing the fidelity of the self-sorting event. The collected precipitate was analyzed and found to contain imines **31** (73%), **60** (82%), and **61** (84%) as the major components. Considering our previous experiments, we were surprised that neither **21** nor **64** were detected. This precipitation protocol was also repeated three times to ensure reproducibility, and only minor variations in yields were observed—up to 6% for **31**, 4% for **60**, and 2% for **61**.

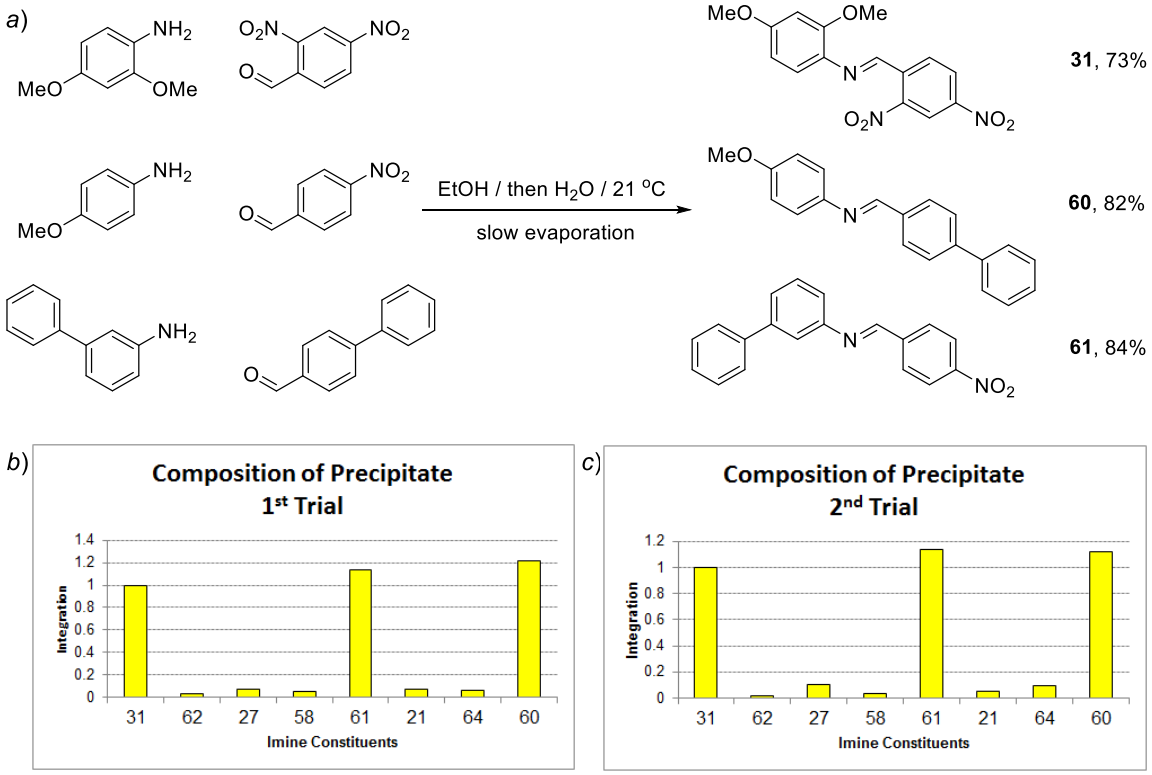

Figure 2.7 *a*) General scheme for the second precipitative self-sorting induced by the slow addition of water to an EtOH solution of a [3×3] imine library. Composition of the precipitate for the *b*) first and *c*) second trials as determined by ^{1}H NMR spectroscopy.

Imine	Solubility [mmol/L]	
	EtOH	EtOH–H_2O (1:2.4, v/v)
31	0.6	<0.1
23	>36.8	13.3
56	>27.6	>16.6
57	11.1	1.5
21	10.9	0.2
58	>23.3	2.8
27	5.2	0.3
25	>31.6	8.5
59	29.5	3.5
60	2.3	1.7
61	12.1	1.0
64	7.4	0.3
63	8.7	1.6
62	8.6	2.9

Table 2.1 Individual imine solubilities measured at 22 °C. Imine **23** is the only liquid among the studied imines. Imines are listed in the order in which they appear in the discussion.

To better understand the observed self-sorting of the different imine libraries studied, we determined the individual solubilities of all possible members of the dynamic

imine libraries in absolute EtOH and in EtOH–H_2O mixture. These solubilities are summarized in Table 2.1.

Successful self-sorting observed in the first [2×2] experiment is readily explained after examination of the solubility data presented in Table 2.1. Imine **31** is clearly the compound with the lowest molar solubility: ~18 times less soluble than **57**, and >40 times less soluble than either **23** or **56**. Thus, its precipitation is "uncontested" and essentially complete in pure EtOH, removing all 2,4-dimethoxyaniline and 2,4-dinitrobenzaldehyde from the solution. With these two components sequestered in the precipitate, remaining aniline and benzaldehyde have no choice but to form **23** as the solution-phase second product.

Examination of the relative solubilities of possible imines in the second [2×2] self-sorting experiment again suggests **31** as the least soluble compound. However, the differences are not as dramatic as in the previous case: **58** is ~9 times less soluble than **27**, ~18 times less than **21**, and >35 less than **58**. These smaller differences, along with the lower absolute solubility of **21**, explain why **31** could not be precipitated alone, leaving the more soluble imines in the solution. The formation of **21** as the second product is rationalized by the fact that it does not share either the aldehyde or the aniline component with the favored **31**. Thus, precipitative self-sorting can express the more soluble **21**, which does not compete with **31**, rather than the less soluble **27**—which must compete with **31** for a building block—2,4-dinitrobenzaldehyde.

Sorting of the more complex [3×3] aniline–aldehyde mixtures could have potentially generated nine imines, but resulted in the high-yield formation of only three. These findings can also be rationalized using the solubility data. In the first [3×3] study, the possible products are imines **21**, **23**, **25**, **27**, **31**, and **56**–**59**. Among these possible products, imine **31** is ~9 times less soluble than next most-insoluble compound, **27**. Precipitation of **31** will thus be favored, sequestering 2,4-dimethoxyaniline and 2,4-dinitrobenzaldehyde from all other imines that contain them. Within the reduced pool of imines that do not share a component with **31**—that is, compounds **21**, **23**, **25**, and **59**—the only imine that can be precipitated under the examined conditions is **21**. The absolute solubility of **23**, **25**, and **59** is too high for them to effectively compete during the precipitation process. Exclusive precipitation of **21** removes all 4-methoxyaniline and 4-nitrobenzaldehyde from the solution and the soluble **23** must form as the third product. Similar reasoning explains the outcome of the last [3×3] experiment. Introduction of the new aldehyde component 4-phenylbenzaldehyde allows the generation of a highly insoluble imine **60**, which is now the second least-soluble compound, after **31**. Since **31** and **60** do not share constituents, their precipitation can proceed orthogonally and simultaneously, depleting the solution's supply of 2,4-dinitrobenzaldehyde and 4-phenylbenzaldehyde, as well as 4-methoxyaniline and 2,4-dimethoxyaniline. This leaves **61** as the only possible imine in the mother liquor; addition of H_2O ensures its complete precipitation, completing the self-sorting event.

Using the second [2×2] library, we also explored the effects of concentration and solvent on the compositions of final imine libraries. If the concentration of the starting

materials 4-methoxyaniline, 2,4-dimethoxyaniline, 4-nitrobenzaldehyde and 2,4-dinitrobenzaldehyde in EtOH is 4.17 mM, which is ten times more dilute than the concentration used in our studies, incomplete self-sorting is observed even after the addition of water. In this dilute concentration, an orange precipitate was also collected at the end of the overnight water addition. The precipitate still exhibits "sorting" to some extent—imines **21** (45%) and **31** (19%) are still the major components with **27** (10%) and **58** (1%) as the minor ones. However, the solution contains appreciable amounts of all four imines: **31** (42%), **21** (27%), **58** (28%), and **27** (17%). Switching the solvent to AN made all imines soluble in the solution but gave random mixtures of four or nine components in all [2×2] and [3×3] experiments. These two control experiments virtually exclude the possibility that self-sorting was caused by electronic factors alone, and highlights the importance of slow precipitation in the selective expression of some members of the library.

On the other hand, concentrations of all components can be increased threefold, up to 125 mM, without a large loss in the fidelity of self-sorting (83% **31**, 74% **21**). However, at component concentrations of 209 mM (5× more concentrated), we started to observe the formation of 4-nitrobenzaldehyde diethyl acetal, formed from 4-nitrobenzaldehyde and the solvent. The formation of this species lessens the available concentration of 4-nitrobenzaldehyde in the library which led to a dramatic deterioration in fidelity of self-sorting: **31** is formed in 51% yield, **27** in 42% yield, and **21** in 34% yield.

Imines	25.5 mM	83.4 mM	125 mM	209 mM
31	78%	77%	83%	51%
21	84%	77%	73%	34%
58	10%	9%	5%	4%
27	11%	18%	12%	42%
4-nitrobenzaldehyde diethyl acetal	NA	NA	NA	29%

Table 2.2 Yields from precipitative self-sorting experiments of a [2×2] imine mixture at increasing concentrations of starting materials. The reported experiments were performed using 25.5 mM of aniline and aldehyde components.

2.3 Conclusions and Outlook

The results presented in this chapter suggest that self-sorting of imine DCLs can proceed under precipitative conditions. During precipitation, some imine libraries sorted into segregated solution/solid or solid/solid ensembles, while others produced co-precipitated mixtures, but all reactions proceeded with high selectivities. The precipitated imines exhibit a certain degree of kinetic stability—they resist hydrolysis in the aqueous solvent, and the precipitated imines can be dissolved in acetonitrile without changing

their observed imine distribution. A random distribution of all possible imine species in the DCL can only be generated upon heating the acetonitrile solution at reflux for 24 h.

These experiments illustrate an important concept in the study of self-sorting systems—collective properties take precedence over the properties of individual components studied in isolation. This switch is not absolute: dominant members of the potential imine pool, such as **31** in all our examples, will invariably occur in the self-sorted state because of their extreme individual insolubility. On the other hand, library members with higher individual solubilities are forced to compete with each other for their aldehyde and aniline building blocks. In those cases, the influence of the remainder of the mixture can be crucial, as a library member (*e.g.* **27**) can be strongly disfavored if it competes for a resource with a dominant member (**31**). Conversely, a library member can be favored beyond its individual "merit", if its composition is orthogonal to the dominant member, while that of its less soluble competitors is not. This primitive form of internal regulation of a synthetic process appears to be a general feature of self-sorting systems.

So far, we have presented several ways of compelling a dynamic library of imines to undergo kinetic self-sorting and produce some members of the library in high yields and high purities. Future work in this area will involve investigation of a DCL formed from a combination of different reversible reactions to see if kinetic self-sorting will allow the system to express multiple products, containing different functional groups, based on the different reaction rates. Kinetic self-sorting involving non-reversible

reactions, *e.g.* amide formation, can also be explored to determine if preferential formation of certain short oligopeptides can be achieved.

2.4 Experimental Section

2.4.1 General Experimental Methods

All reactions were performed at 21 °C in oven-dried glassware. Reagents and solvents were purchased from commercial suppliers and used without further purification.

Mass spectral measurements were performed by the Mass Spectrometry Facility of the Department of Chemistry and Biochemistry at the University of Texas at Austin. NMR spectra were obtained on JEOL ECX-400 and ECA-500 spectrometers, with working frequencies (for ^{1}H nuclei) of 400 and 500 MHz, respectively. All ^{13}C NMR spectra were recorded with simultaneous decoupling of ^{1}H nuclei. ^{1}H NMR chemical shifts are reported in ppm units relative to the residual signal of the solvent ($CDCl_3$: 7.25 ppm). All NMR spectra were recorded at 21 °C in $CDCl_3$. Infrared spectra were recorded on a Perkin-Elmer Spectrum 100 FT-IR spectrophotometer using Pike MIRacle Micrometer pressure clamp. Microanalyses were conducted by Intertek USA, Inc. Melting points measurements were performed in open capillary tubes using Mel-Temp Thermo Scientific apparatus, and are uncorrected.

Five new imines (**58**, **61**–**64**) were synthesized for comparison purposes using the following general procedure: aldehyde (0.50 mmol) and aniline (0.50 mmol) were dissolved in PhMe (8 mL), and 4 Å molecular sieves were added to remove H_2O. These mixtures were stirred for 12–24 h at 80 °C. Reaction completion was monitored by ^1H NMR spectroscopy.

Imine solubilities quoted in this chapter were measured in the following fashion. An imine sample (20 mg) was suspended in either EtOH (3 mL) or EtOH/H_2O mixture (1:2.4 v/v, 5 mL). The suspension was sonicated for 2 h at 21 °C and filtered. The residual solid, if any, was dried and weighed. The solubility of a corresponding imine was obtained by subtracting the weight of the precipitate from the original 20 mg sample. For imines that were fully soluble, only the lower limit of solubility was established.

2.4.2 Experimental Protocols for Selective Precipitation of Imines

2.4.2.1 Selective Precipitation of *N*-(2,4-dinitro-benzylidene)-2,4-dimethoxyaniline (**31**) and *N*-benzylideneaniline (**23**)

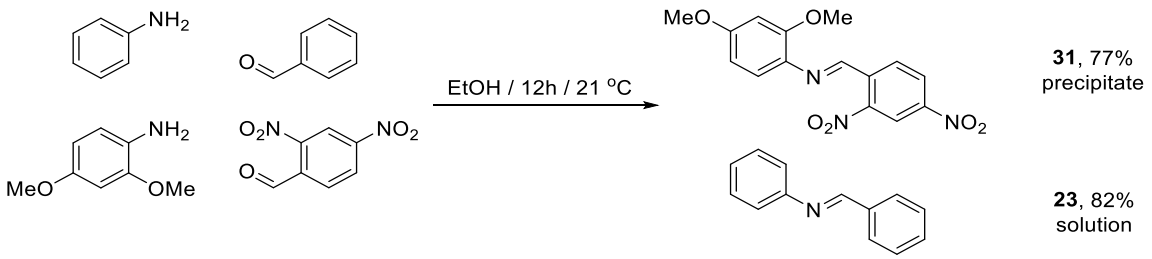

Benzaldehyde (130 µL, 1.25 mmol) and 2,4-dinitrobenzaldehyde (250 mg, 1.25 mmol) were dissolved in absolute EtOH (50 mL) with sonication. Then, aniline (115 µL, 1.25 mmol) and 2,4-dimethoxyaniline (195 mg, 1.25 mmol) were added into the solution.

The mixture became cloudy. After overnight stirring, orange precipitate was filtered and dried. ^{1}H NMR spectroscopic analysis of the precipitate indicated formation of pure *N*-(2,4-dinitro-benzylidene)-2,4-dimethoxyaniline (**31**, 80 mg, 19%). The filtrate was clear at the beginning but forms orange precipitate within minutes. Solvent was removed from the filtrate using a rotary evaporator, and absolute EtOH (50 mL) was added to the orange solid. The mixture was stirred for 2 h and the formed precipitate was filtered using Whatman 40 filter paper. The precipitate was dried in vacuo (3 mmHg) at 21 °C for 1 h, resulting in 248 mg of an orange solid, while the filtrate was evaporated to dryness, resulting in 249 mg of an orange solid.

^{1}H NMR spectroscopic analysis of the second precipitate shows the presence of **31** (58%), **57** (2%), and **23** (1%). Analogous analysis of the filtrate revealed the presence of **23** (82%), **56** (11%), **57** (7%), and **31** (2%).

23: ^{1}H NMR ($CDCl_3$, 400 MHz): δ 8.46 (s, 1H), 7.93–7.91 (m, 2H), 7.50–7.47 (m, 3H), 7.43–7.39 (m, 2H), 7.27–7.22 (m, 3H). ^{13}C NMR ($CDCl_3$, 100 MHz): δ 160.5, 152.2, 136.3, 131.5, 129.3, 128.9, 128.9, 126.1, 121.0. Spectral data agree with a previous literature report.[76]

31: ^{1}H NMR ($CDCl_3$, 500 MHz): δ 9.21 (s, 1H), 8.87 (d, *J*=2.3 Hz, 1H), 8.61 (d, *J*=8.6 Hz, 1H), 8.48 (dd, *J*= 8.6, 2.3 Hz, 1H), 7.25-7.23 (m, 1H), 6.55-6.53 (m, 2H), 3.91 (s, 3H), 3.85 (s, 3H). ^{13}C NMR ($CDCl_3$, 125 MHz): δ 161.2, 154.9, 150.9, 148.9, 148.1, 137.0, 132.3, 131.2, 127.3, 123.9, 120.4, 105.0, 99.6, 60.0, 55.7. Spectral data agree with a previous literature report.[53]

56: ^{1}H NMR ($CDCl_3$, 500 MHz): δ 8.52 (s, 1H), 7.93 (s, 2H), 7.45 (s, 3H), 7.03 (d, *J*=8.2 Hz, 1H) 6.65–6.35 (m, 2H), 3.88 (s, 3H), 3.82 (s, 3H). ^{13}C NMR ($CDCl_3$, 125 MHz): δ 159.6, 159.2, 153.9, 136.8, 135.1, 131.1, 129.9, 128.8, 120.6, 104.5, 99.6, 56.0, 55.6. Spectral data agree with a previous literature report.[77]

57: ^{1}H NMR ($CDCl_3$, 500 MHz): δ 9.01 (s, 1H), 8.92 (d, *J*=2.2 Hz, 1H), 8.60 (d, *J*=8.7 Hz, 1H), 8.55 (dd, *J*=8.6, 2.0 Hz, 1H), 7.46 (t, *J*=7.8 Hz, 2H), 7.32–7.36 (m, 3H) ppm. ^{13}C NMR ($CDCl_3$, 125 MHz): δ 153.3, 150.2, 149.2, 148.6, 136.1, 131.6, 129.6, 128.2, 127.6, 121.5, 120.4. Spectral data agree with a previous literature report.[78]

2.4.2.2 Selective Precipitation of *N*-(2,4-dinitro-benzylidene)-2,4-dimethoxyaniline (**31**) and 4-Methoxy-*N*-(4-nitrobenzylidene)aniline (**21**)

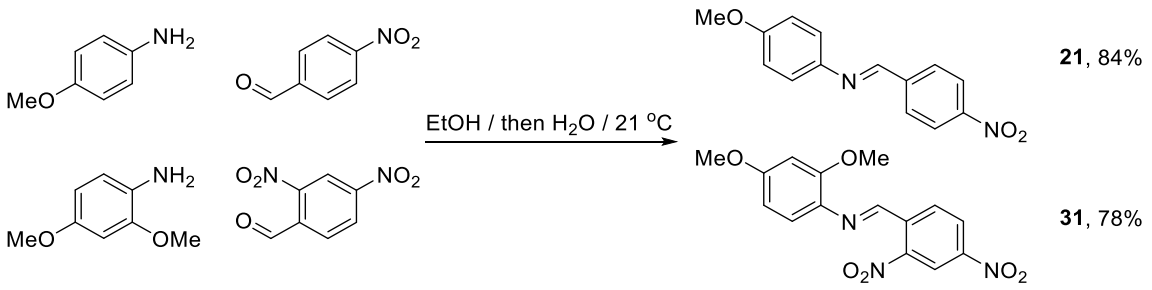

Compounds 2,4-dinitrobenzaldehyde (150 mg, 0.75 mmol) and 4-nitrobenzaldehyde (114 mg, 0.75 mmol) were dissolved in absolute EtOH (18 mL) with sonication. Once dissolved, 2,4-dimethoxyaniline (117 mg, 0.75 mmol) and 4-methoxyaniline (93 mg, 0.75 mmol) were added into the solution. The mixture was stirred for 4 h and the formation of precipitate was observed after 1 h of stirring. After 4 h, H_2O (24 mL) was injected via a syringe pump at a rate of 3 mL/h. The orange

precipitate was vacuum filtered using Whatman 40 filter paper and dried in vacuo (3 mmHg) at 21 °C overnight, resulting in 400 mg of orange solid.

^{1}H NMR analysis of the precipitate showed the formation of imines **21** (84%), **31** (78%), **27** (11%), and **58** (10%).

The same procedure was repeated twice giving similar yields for all four imines: in the second trial, the yields were 78% for **31**, 10% of **27**, 8% of **58**, and 86% of **21**. In the third trial, the yields were 77% for **31**, 15% for **27**, 10% for **58**, and 83% for **21**.

This experiment was performed at both higher and lower concentrations of starting materials. Running the experiment at ten times lower concentration (4.17 mM) still resulted in the formation of an orange precipitate by the end of H_2O addition consisting of imines **21** (39%), **31** (17%), **27** (9%), and **58** (3%), while the filtrate is a mixture of imines **21** (28%), **31** (45%), **27** (18%), and **58** (30%). No precipitation occurred prior to H_2O addition.

Increasing the concentration of the starting materials resulted to faster formation of precipitate (within 5 min), composed primarily of imines **31** and **21**. At two times higher concentration (83.4 mM) the yields were **31** (77%), **21** (77%), **58** (9%), and **27** (18%). At three times more concentrated conditions (125 mM) the yields were **31** (83%), **21** (73%), **58** (5%) and **27** (12%). At five times more concentrated conditions (209 mM) the yields were **31** (51%), **21** (34%), **58** (4%), and **27** (42%). The formation of 4-nitrobenzaldehyde diethyl acetal (singlet at δ=5.57 ppm), was detected at this concentration.

21: ^{1}H NMR ($CDCl_3$, 500 MHz): δ 8.57 (s, 1H), 8.30 (d, *J*=8.7 Hz, 2H), 8.05 (d, *J*=8.7 Hz, 2H), 7.30 (d, *J*=8.7 Hz, 2H), 6.95 (d, *J*=8.7 Hz, 2H), 3.84 (s, 3H). ^{13}C NMR ($CDCl_3$, 125 MHz): δ 159.3, 154.9, 149.1, 143.7, 142.0, 129.2, 124.1, 122.7, 114.6, 55.6 ppm. Spectral data agree with a previous literature report.[79]

58: brown powder, mp 96 °C. IR (neat): 3002, 1602, 1584, 1516, 1342, 1308, 1295, 848, 831, 795 cm^{-1}. ^{1}H NMR ($CDCl_3$, 400 MHz): δ 8.66 (s, 1H), 8.27 (d, *J*=8.7 Hz, 1H), 8.03 (d, *J*=8.7 Hz, 1H), 7.11 (d, *J*=8.2 Hz, 1H), 6.55–6.50 (m, 2H), 3.89 (s, 3H), 3.83 (s, 3H) ppm. ^{13}C NMR ($CDCl_3$, 100 MHz): δ 160.2, 155.9, 154.4, 149.0, 142.4, 133.5, 129.2, 124.0, 121.7, 104.7, 99.6, 50.0, 55.7 ppm. HRMS (ESI): Calcd for $C_{15}H_{15}N_2O_4^+$: 287.1026. Found: 287.1026. Anal. calcd for $C_{19}H_{13}N_3O_4$: C, 62.93; H, 4.93; N, 9.79. Found: C, 62.14; H, 4.56; N, 9.87.

27: ^{1}H NMR ($CDCl_3$, 400 MHz): δ 9.02 (s, 1H), 8.89 (d, *J*=2.2 Hz, 1H), 8.61 (*J*=8.7Hz, 2H), 8.51 (ddd, *J*=8.5, 2.2, 0.9 Hz, 2H), 7.37 (d, *J*=9.0 Hz, 3H), 6.97 (d, *J*=9.0 Hz, 2H), 3.86 (s, 3H) ppm. ^{13}C NMR ($CDCl_3$, 100 MHz): δ 160.2, 150.0, 149.0, 148.3, 142.9, 136.4, 131.2, 127.4, 123.5, 120.5, 114.8, 55.7 ppm. Spectral data agree with a previous literature report.[53]

2.4.2.3 Precipitation-Driven Imine Transmutation

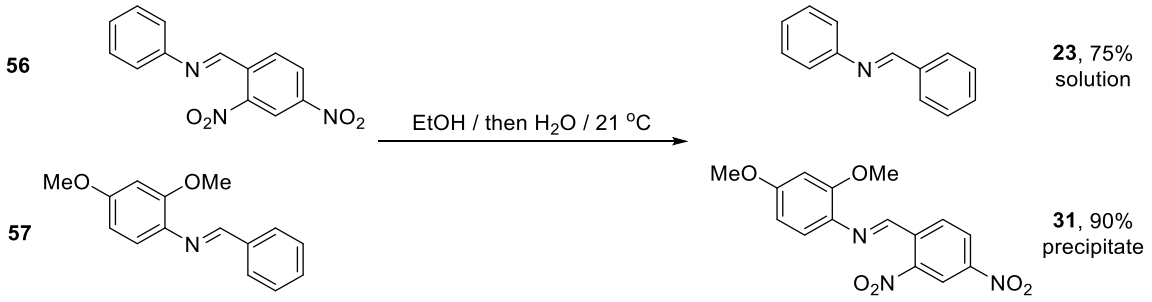

Compounds *N*-(2,4-dinitrobenzylidene)aniline (**57**, 89 mg, 0.37 mmol) and *N*-benzylidene-2,4-dimethoxyaniline (**56**, 100 mg, 0.37 mmol) were completely dissolved in absolute EtOH (50 mL). Precipitation started after overnight stirring. Then, H_2O (96 mL) was added via a syringe pump at a rate of 1 mL h^{-1}. The orange precipitate was filtered out and identified as *N*-(2,4-dinitrobenzylidene)-2.4-dimethoxyaniline, **31** (112 mg, 90%), with only a minor amount of starting imine **57** left. Water fraction was extracted with DCM and filtered through 5 cm silica gel plug. After solvent removal, off-white solid was obtained and identified as pure *N*-benzylideneaniline, **23** (50 mg, 75%).

2.4.2.4 Selective Precipitation of *N*-benzylideneaniline (**2**), *N*-(2,4-dinitro-benzylidene)-2,4-dimethoxyaniline (**31**), and 4-methoxy-*N*-(4-nitrobenzylidene)aniline (**21**)

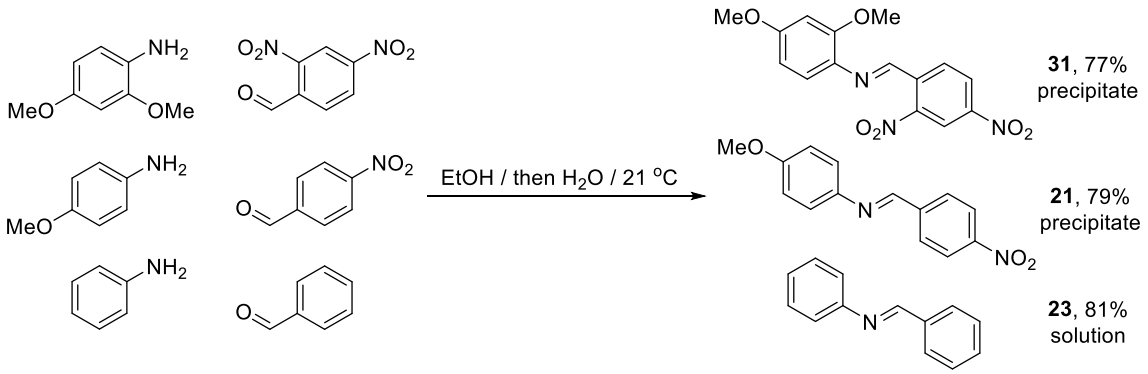

Benzaldehyde (130 µL, 1.25 mmol), 2,4-dinitrobenzaldehyde (250 mg, 1.25 mmol), and 4-nitrobenzaldehyde (190 mg, 1.25 mmol) were dissolved in absolute EtOH (50 mL) with sonication. Once dissolved, aniline (115 µL, 1.25 mmol), 2,4-dimethoxyaniline (195 mg, 1.25 mmol), and 4-methoxyaniline (155 mg, 1.25 mmol) were added into the solution. The mixture was stirred for 4 h. After 4 h, H_2O (120 mL) was injected via a syringe pump, at a rate of 5 mL h^{-1}. After H_2O addition was complete, mixture was left to stir for 2 h, and the orange precipitate was then filtered using Whatman 40 filter paper. The precipitate was dried in vacuo (3 mmHg) at 21 °C overnight, to give 679 mg of an orange precipitate. The yellow filtrate was collected and extracted with 170 mL of CH_2Cl_2. After solvent evaporation, 270 mg of a red-orange oil was obtained.

^{1}H NMR analysis of the precipitate showed the formation of imines **21** (79%), **31** (77%), **27**(15%), **58** (7%), **59** (4%), **56** (4%), and **57** (1%). Analogous analysis of the filtrate revealed the presence of **23** (81%), **56** (9%), **25** (9%), **59** (8%), **58** (1%), **21** (1%), **57** (0.8%), **31**(0.3%), and **27** (0.2%).

25: ^{1}H NMR ($CDCl_3$, 500 MHz): δ 8.48 (s, 1H), 7.90–7.88 (m, 2H), 7.47–7.46 (m, 3H), 7.24 (d, *J*=8.5 Hz, 2H), 6.94 (d, *J*=8.5 Hz, 2H), 3.84 (s, 3H) ppm. ^{13}C NMR ($CDCl_3$, 125 MHz): δ 158.5, 158.4, 145.0, 136.5, 131.1, 128.8, 128.7, 122.3, 114.8, 55.6 ppm. Spectral data agree with a previous literature report.[80]

59: ^{1}H NMR ($CDCl_3$, 400 MHz): δ 8.55 (s, 1H), 8.32 (d, *J*=8.8 Hz, 2H) 8.07 (d, *J*=8.9 Hz, 2H), 7.43 (t, *J*=7.6 Hz, 2H), 7.32–7.24 (m, 3H) ppm. ^{13}C NMR ($CDCl_3$, 100 MHz): δ 157.5, 151.0, 141.7, 129.5, 129.4, 127.2, 124.1, 121.1, 115.2 ppm. Spectral data agree with a previous literature report.[81]

2.4.2.5 Selective Precipitation of *N*-(2,4-dinitro-benzylidene)-2,4-dimethoxyaniline (**31**), *N*-([1,1'-biphenyl]-4-ylmethylene)-4-methoxyaniline (**60**), and *N*-(4-nitrobenzylidene)-[1,1'-biphenyl]-3-amine (**61**)

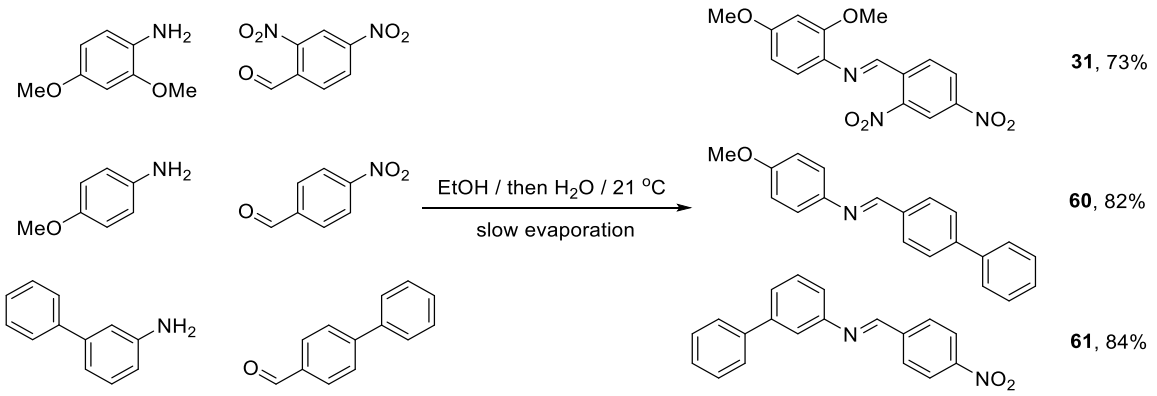

Compounds 2,4-dinitrobenzaldehyde (50 mg, 0.25 mmol), 4-nitrobenzaldehyde (38 mg, 0.25 mmol), and 4-phenylbenzaldehyde (46 mg, 0.25 mmol), were dissolved in absolute EtOH (35 mL), with sonication. Once dissolved, 2,4-dimethoxyaniline (39 mg, 0.25 mmol), 4-methoxyaniline (31 mg, 0.25 mmol), and 3-aminobiphenyl (43 mg, 0.25 mmol) were added into the solution. The mixture was stirred for 12 h, during which time the formation of a bright yellow precipitate was observed. After 12 h, H_2O (40 mL) was injected via a syringe pump, at a rate of 1 mL h^{-1}. The yellow precipitate gradually changed into orange. After water addition was complete, the mixture was stirred for 7 d in an open flask. The solution was then exposed to a low pressure N_2 stream for 3 d to remove the solvent, resulting in 200 mg of an orange solid.

^{1}H NMR analysis of the solid, orange residue indicated the dominant formation of imines **31** (72%), **60** (88%), and **61** (82%), with only traces of imines **27** (5%), **21** (5%),

64 (5%), **58** (3%), and **62** (2%). Two additional trials were performed which confirmed the same preferences. The yields for the second trial were **31** (67%), **60** (84%), **61** (81%), **62** (2%), **27** (9%), **58** (7%), **21** (6%), and **64** (7%). The yields for the third trial were **31** (73%), **60** (82%), **61** (84%), **62** (1%), **27** (7%), **58** (2%), **21** (4%), and **64** (7%), confirming the repeatability of the observed self-sorting processes.

A 30 mg aliquot of this imine mixture was dissolved in AN (20 mL) and stirred at 21 °C for 7 d. ^{1}H NMR spectroscopic analysis of the solution during this period showed that the ratio of the imines to each other remained the same. However, heating the solution to reflux for 24 h caused the system to form all possible imines.

60: ^{1}H NMR ($CDCl_3$, 400 MHz): δ 8.52 (s, 1H), 7.96 (d, *J*=8.2 Hz, 2H), 7.70 (d, *J*=8.2 Hz, 2H), 7.65 (d, *J*=7.3 Hz, 2H), 7.47 (t, *J*=7.3 Hz, 2H), 7.38 (t, *J*=7.3 Hz, 1H), 7.26 (d, *J*=8.5 Hz, 2H), 6.94 (d, *J*=8.5 Hz, 2H), 3.84 (s, 3H) ppm. ^{13}C NMR ($CDCl_3$, 100 MHz): δ 158.4, 158.0, 145.0, 143.8, 140.4, 135.5, 129.1, 129.0, 127.9, 127.5, 127.3, 122.3, 114.5, 55.6. Spectral data agree with a previous literature report.[82]

61: yellow-green powder, mp 112 °C. IR (neat): 1595, 1517, 1476, 1347, 1315, 917, 891, 872, 857, 841, 794, 760, 702 cm^{-1}. ^{1}H NMR ($CDCl_3$, 400 MHz): δ 8.62 (s, 1H), 8.34 (d, *J*=8.7 Hz, 2H), 8.10 (d, *J*=8.7 Hz, 2H), 7.65–7.63 (m, 2H), 7.54–7.44 (m, 5H), 7.39–7.35 (m, 1H), 7.25–7.23 (m, 1H) ppm. ^{13}C NMR ($CDCl_3$, 100 MHz): δ 157.8, 151.5, 149.4, 142.6, 141.6, 140.6, 129.8, 129.6, 129.0, 127.8, 127.3, 125.9, 124.1, 120.0, 119.7 ppm. HRMS (ESI): Calcd for $C_{19}H_{15}N_2O_2^+$: 303.1128. Found: 303.1128. Anal. calcd for $C_{19}H_{14}N_2O_2$: C,75.48; H, 4.67; N, 9.27. Found: C, 74.58; H, 4.20; N, 9.08.

64: yellow powder, mp 127 °C. IR (neat): 1627, 1593, 1475, 1408, 1176, 1007, 890, 763, 699 cm^{-1}. ^{1}H NMR ($CDCl_3$, 500 MHz): δ 8.57 (s, 1H), 8.00 (d, *J*=8.2 Hz, 2H), 7.73 (d, *J*=8.7 Hz, 2H), 7.68–7.64 (m, 4H), 7.50–7.44 (m, 7H), 7.42–7.35 (m, 2H), 7.24–7.21 (m, 1H) ppm. ^{13}C NMR ($CDCl_3$, 125 MHz): δ 160.3, 152.7, 144.2, 142.4, 141.0, 140.3, 135.2, 129.7, 129.4, 129.0, 128.9, 128.0, 127.6, 127.3, 124.9, 119.9, 119.7 ppm. HRMS (CI): Calcd for $C_{25}H_{21}N^{2+}$: 335.1674. Found: 335.1670. Anal. calcd for $C_{25}H_{19}N$: C, 90.05; H, 5.74; N, 4.20. Found: C, 89.25; H, 5.23; N, 4.16.

63: yellow-green powder, mp 124 °C. IR (neat): 3026, 1623, 1605, 1593, 1307, 1206, 1031, 828, 767 cm^{-1}. ^{1}H NMR ($CDCl_3$, 400 MHz): δ 8.54 (s, 1H), 7.97 (d, *J*=8.2 Hz, 2H), 7.68 (d, *J*=8.2 Hz, 2H), 7.65–7.62 (m, 2H), 7.48–7.44 (m, 2H), 7.39–7.35 (m, 1H), 7.02 (d, *J*=8.2 Hz, 2H), 6.55 (d, *J*=2.7 Hz, 1H), 6.50 (dd, *J*=8.2 Hz, 2.7 Hz, 1H) ppm. ^{13}C NMR ($CDCl_3$, 100 MHz): δ 159.2, 159.1, 153.9, 143.7, 140.5, 135.7, 135.2, 129.3, 129.0, 127.9, 127.4, 127.3, 120.5, 104.4, 99.6, 56.1, 55.6 ppm. HRMS (ESI): Calcd for $C_{21}H_{20}NO_2^{+}$: 318.1488. Found: 318.1487. Anal. calcd for $C_{21}H_{19}NO_2$: C, 79.45; H, 6.03.; N, 4.41. Found: C, 78.21; H, 5.69; N, 4.26.

62: light-brown powder, mp 118 °C. IR (neat): 1597, 1523, 1476, 1343, 1147, 1059, 906, 833, 762, 697 cm^{-1}. ^{1}H NMR ($CDCl_3$, 400 MHz): δ 9.07 (s, 1H), 8.92 (d, *J*=2.3 Hz, 1H), 8.62–8.54 (m, 2H), 7.64–7.45 (m, 7H), 7.40–7.29 (m, 2H) ppm. ^{13}C NMR ($CDCl_3$, 100 MHz): δ 153.6, 150.7, 149.2, 148.7, 142.8, 140.4, 136.1, 131.6, 130.0, 129.0, 127.9, 127.7, 127.3, 126.9, 120.5, 120.4, 120.0 ppm. HRMS (CI): Calcd for $C_{19}H_{14}N_3O_4^{+}$: 348.0984. Found: 348.0980.

Chapter Three

Self-sorting in Parallel Reactions: Four Acid-catalyzed Dehydration Reactions Proceed Without Interference[83]

3.1 Introduction

Dynamic combinatorial libraries that are based on one dynamic reaction can be constructed and regulated relatively easily since the reaction conditions dictate the constraints of the overall system.[84] For example, an imine DCL can be made dynamic under acidic conditions, and static at basic pH, and can be analysed after exposing the library to an irreversible reaction (such as reduction or Ugi reaction)[85] that preserves the equilibrium concentration of the library members. A more challenging task is combining multiple dynamic reactions since the independent chemistries must be carefully considered to ensure that the reactions will not interfere with each other. One-pot multiple parallel reactions are of interest for several reasons: (*a*) they can create more complex libraries since one building block can react in several ways, (*b*) orthogonal reversible processes offers a higher degree of control over the library composition and its organization in the interaction with a prospective target,[86,87] and (*c*) they present a potentially practical way of doing synthesis since multiple value-added products could be produced simultaneously in a single reactor.

One of the hallmarks of living systems is the ability to synthesize multiple well-

[83] Lirag, R. C.; Miljanič, O. Š. *Chem. Commun.* **2014**, *50*, 9401–9404.

defined products from complex, "messy", mixtures of starting materials. Although we have not achieved the same level of extraordinary control in synthetic systems yet, several multilevel dynamic reactions have been reported, most notably from Lehn's,[86,87] Otto's,[88–90] and Severin's[91,92] research groups. Simultaneously, Otera's[93–99] research group has been active in the area of parallel reactions and "shotgun" processes.

Two or more reversible reactions can be combined to produce multilevel dynamic libraries that can have "orthogonal" DCLs where the reversible reactions operate independently and can be activated under different conditions.[87,100] Early reports on orthogonal DCLs involved pairing imine formation with other reversible reactions such as metal-ion coordination,[86,87,101] boronate ester formation,[91,92] and alkene/alkyne metathesis.[102,103] One-pot syntheses of various macrocycles have been accomplished using this approach (Figure 3.1). Zhang *et al*. prepared shape-persistent two- and three-dimensional macrocyles by combining imine formation and olefin metathesis using second generation Hoveyda-Grubbs catalyst, while Severin *et al.*[92] reported a mechanochemical synthesis involving imine condensation and boronate ester formation to produce nanometer-size macrocycle—a process that involved formation of 18 covalent bonds between 11 building blocks. In a recent review, Matile *et al*.[104] have made a comprehensive list of functional systems that operate using orthogonal dynamic bonds. The most common pair of orthogonal dynamic reactions reported is dynamic disulfide exchange and hydrazone exchange which has been used for various applications including: (*a*) construction of molecular components that can move along a molecular track in one direction (molecular walkers),[105] (*b*) synthesis of dynamic hydrogels that

displays adaptive self-healing ability,[106] and (*c*) development of double channel photosystem, with anti-parallel redox gradients, attached on the surface of indium tin oxide (ITO) via surface-initiated disulfide-exchange polymerization.[107]

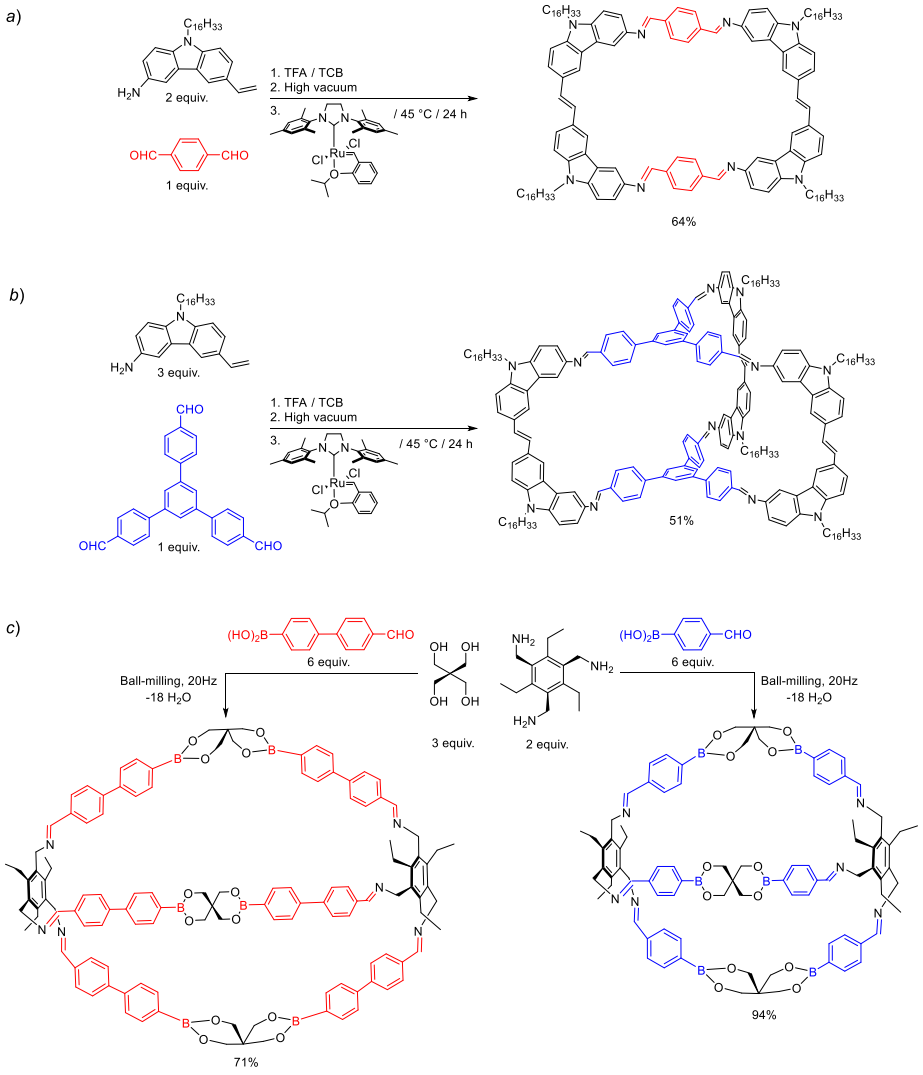

Figure 3.1 One-pot synthesis of (*a*) two-dimensional and (*b*) three-dimensional macrocyles using orthogonal imine formation and alkene metathesis.[102] Mechanochemical synthesis of (*c*) a macrocycle containing imine and boronate ester covalent bonds.[92]

Other reported pairs of orthogonal reversible reactions are Cope rearrangement and boronate ester exchange used to synthesize a polyphenol sensor based on a bullvalene core,[108] and disulfide exchange and boronate ester exchange used to create molecular structures that can be utilized as gene delivery vectors.[109]

On the other hand, when the DCL is generated by reversible reactions that can cross-over, *i.e.* the cases in which the same building block can take part in two or more reversible reactions, the multilevel dynamic libraries are said to be "communicating".[88–90] A good example is the simultaneous exchange of disulfide and thioester linkages reported by Sanders group,[88] using a single starting material that contains two exchangeable units; a thiol and a thioester functional groups. In the absence of oxygen, the only operational dynamic reaction is the thiol-thioester exchange that converts **65** to **66** and **67** (Figure 3.2).

Upon exposure of the library consisting of these three species to air, thiol oxidation and disulfide exchange became operational along with thioester exchange. This created a dynamic library that can interconvert between open oligomers—that had both disulfide and thioester linkages—and closed cyclic structures linked via disulfide bonds. The much slower rate of oxidation of thiols, as compared to the rate of exchange of the thioesters, allowed the generation of a double-level communicating library that can be activated and studied simultaneously, or sequentially.

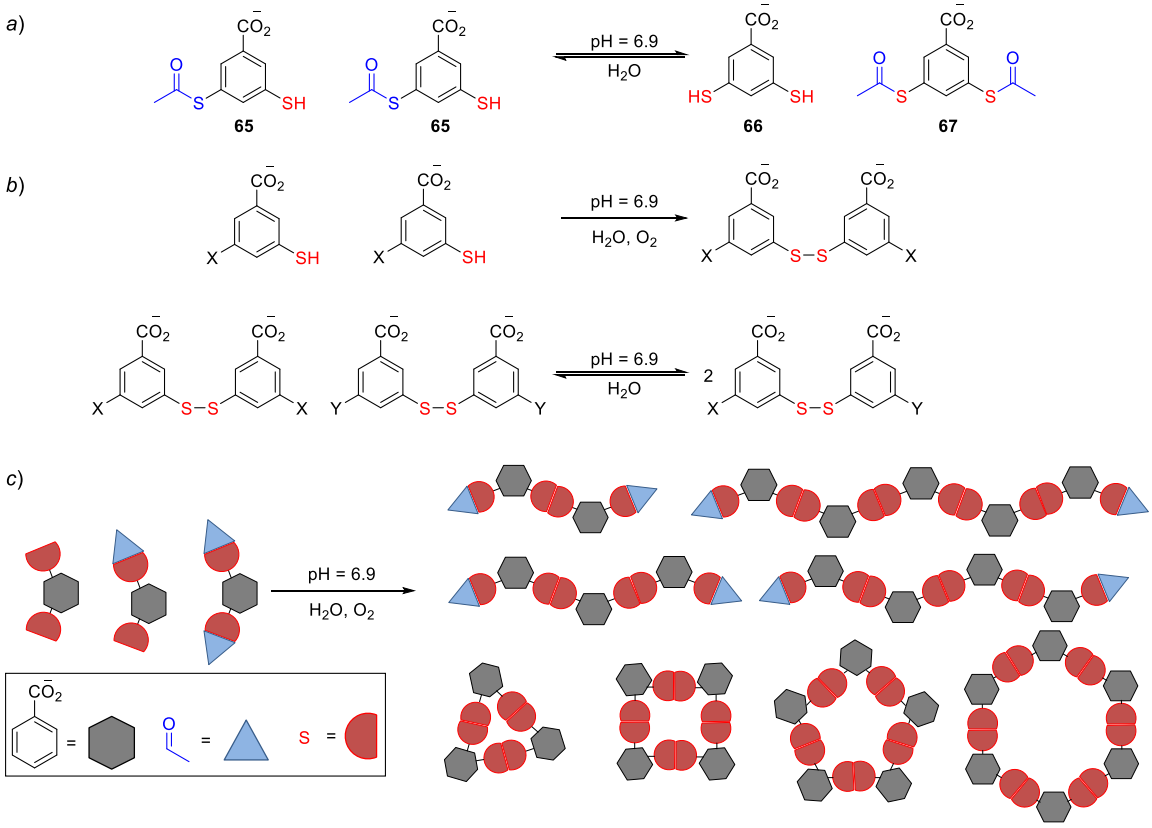

Figure 3.2 (*a*) Thioester exchange to produce **66** and **67** from a single building block **65**. (*b*) Exposure to oxygen activates disulfide exchange. (*c*) A library of linear oligomers and cyclic structures was formed by simultaneous thioester and disulfide exchanges.[88]

Otera's group has also taken advantage of the different rates of reactions to achieve simultaneous chemical transformations, on various sites within the same molecule, without the need for additional protection–deprotection steps. They have coined the terms *parallel recognition*[97–99] for non-interfering parallel reactions which occur at sites that react completely and independently from each other, and *shotgun process*[93–96] for reactions that occur at rates sufficiently different to allow them to proceed in a single flask without interference. They have reported several combinations

of chemical reactions that are compatible and can engage in parallel recognition and shotgun processes: aldehyde allylation and aldol reaction,[96] multiple Diels-Alder reactions,[95] and a combination of Diels-Alder reaction, alcohol acetylation, and aldehyde allylation.[93] Combining multiple reactions makes synthesis more practical—shortening reaction time and minimizing the use of chemical reagents. The expeditious synthesis of 9,11-dodecadien-1-yl acetate[94] (female sex-pheromone of the red-bollworm moth *Oiparopsis castanea*) from ω-hydroxy dodecanal demonstrates the practical aspect of this concept (Figure 3.3).

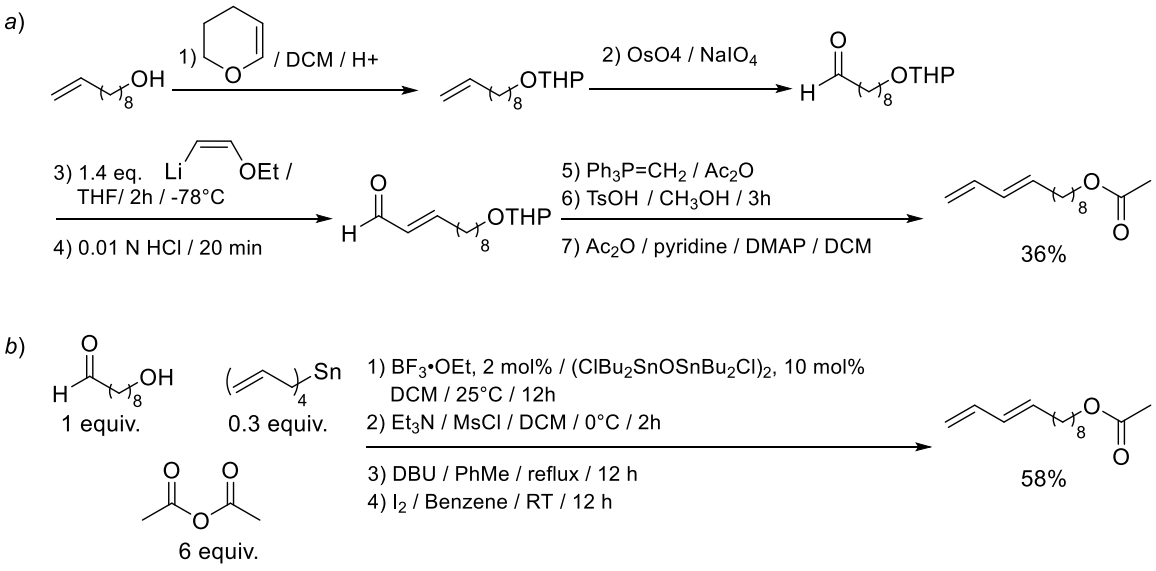

Scheme 3.1 Synthesis of 9,11-dodecadien-1-yl acetate using (*a*) conventional synthetic strategy, with protection–deprotection schemes,[110] and (*b*) parallel synthesis.[94]

Our group has shown that libraries of as many as 25 equilibrating members can self-sort into a handful of pure products through iterative application of an irreversible chemical[53] or physical stimulus.[36,55,57,59] In this chapter, we examine the question of

whether similar reduction of complexity is possible in a system where chemical functionalities of reacting species are different and multiple reactions are involved.

3.2 Results and Discussion

As the model system, we chose a set of five reactions, all of which are catalyzed by Brønsted acids: (*1*) imine formation from aldehydes and primary amines, (*2*) acetalization of aldehydes and alcohols, (*3*) boronic ester formation from alcohols and boronic acids, (*4*) esterification of carboxylic acids with alcohols, and (*5*) alkene formation through intramolecular dehydration of alcohols. We chose starting materials that are different in terms of their electronic and steric properties to see how these factors will affect the tendency of a substrate to undergo one reaction or the other (Figure 3.4).

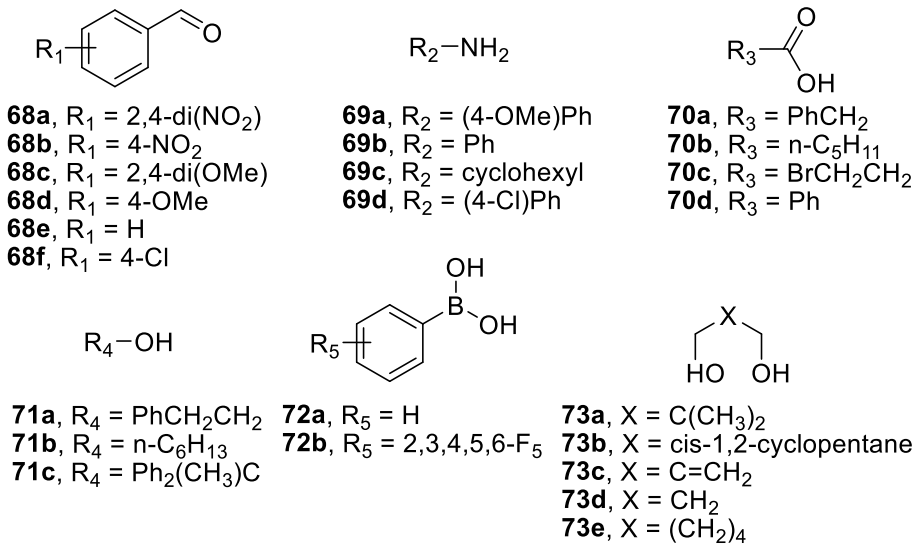

Figure 3.3 Starting materials used for the parallel dehydration reactions.

All of these dehydration reactions are in principle reversible, but equilibria can be forced toward the dehydrated products by H_2O removal via a Dean-Stark trap. In

addition, compounds like aldehydes, alcohols, and diols can engage in reactions with multiple partners. For example, an alcohol can form an ester with a carboxylic acid, a boronic ester with a boronic acid, an acetal with an aldehyde or dehydrates to form an alkene. This fact allowed the exploration of situations wherein multiple species can compete for a reaction partner. We examined the behaviour of various libraries of starting materials which we divided into three sets of reactions (Figure 3.5). The first set of reaction (**I**) examined parallel dehydration to form imine, boronate ester, ester, and alkene, the second set (**II**) replaced boronate ester formation with acetal formation, while the third set (**III**) investigated the effect of competing diols in the preference for acetal and ester formation.

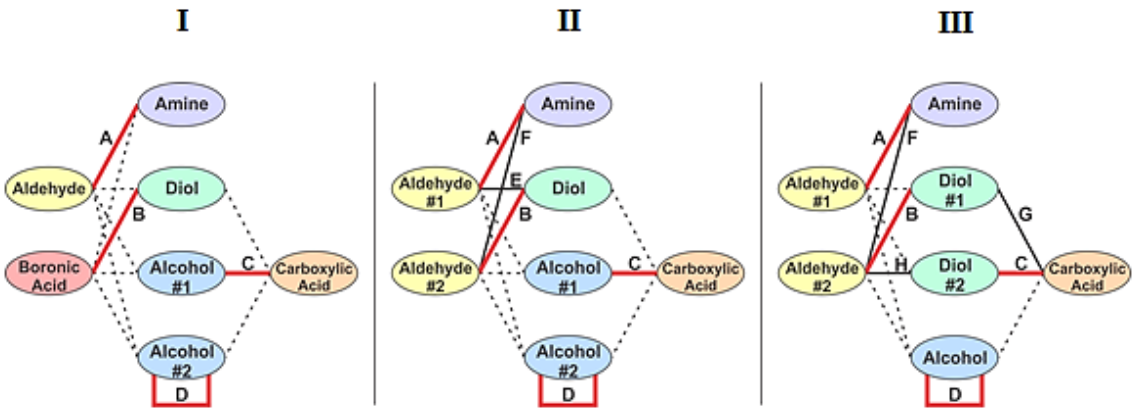

Figure 3.4 Three sets of reactions probed in this study. The solid red line represents the observed dominant dehydration pathways and full black lines for minor pathways. Pathways that were theoretically possible—but were not observed—are shown in dashed black lines. The different dehydration pathways are designated with letters (**A**–**H**) to differentiate the yields obtained from each pathway.

3.2.1 Parallel Dehydration Reactions to Form Imine, Boronate Ester, Ester, and Alkene (I)

In the first set of parallel reactions (Table 3.1, entries 1 and 2), we combined imine formation, boronate ester formation, ester formation, and dehydration of a tertiary alcohol by using equimolar amounts of 2,4-dinitrobenzaldehyde (**68a**), phenylboronic acid (**72a**) or pentafluorophenylboronic acid (**72b**), 4-methoxyaniline (**69a**), 2,2-dimethyl-1,3-propanediol (**73a**), phenylacetic acid (**70a**), and 1,1-diphenylethanol (**71c**), along with a threefold excess of 2-phenylethanol (**71a**). An excess of **71a** was used to ensure complete conversion of the carboxylic acid to ester and still have enough primary alcohol to compete with **73a** in forming acetal with **68a**, or boronate ester with **72a**/**72b**. Catalytic amount of *p*-toluenesulfonic acid was added and the solution was heated at reflux for two days with H_2O removal. Within such a library of starting materials, many possible products could have formed: one imine, four acetals, four boronic esters, four esters, and two alkenes, and possibly other dehydration products such as amides or boroxines. However, only four discrete products were observed: one imine from **68a** and **69a** (pathway **A**), one boronic ester from **72a**/**72b** and **73a** (pathway **B**), one ester from **70a** and **71a** (pathway **C**), and one alkene from **71c** (pathway **D**). These dehydration products were formed in yields that typically exceeded 90% as determined by ^{1}H NMR spectroscopy using 1,3,5-trimethoxybenzene as the internal standard.

Entry	RCHO #1	$RB(OH)_2$	RNH_2	Diol	ROH #1	ROH #2	RCOOH	NMR Yields (%)			
								A	**B**	**C**	**D**
1	**68a**	**72a**	**69a**	**73a**	**71a**	**71c**	**70a**	93	99	99	98
2	**68a**	**72b**	**69a**	**73a**	**71a**	**71c**	**70a**	97	74	99	99

Table 3.1 Yields for the dehydration reactions in the first set (**I**) of parallel reaction.

The formation of a boronate ester between **73a** and **72a**/**72b** occurred quickly, since the diol is predisposed to form a favorable six-membered ring boronate ester.[111] In addition, **69a** is a stronger nucleophile than **73a**—imine formation between electron-rich amine **69a** and electron-deficient aldehyde **68a** is faster than acetal formation between **73a** and **68a**. The two orthogonal reactions, imine and acetal formation, were able to proceed independently giving good yields. Dehydration of tertiary alcohol **71c** under acidic conditions was quick, leaving the primary alcohol **71a** to form ester with the only remaining starting material, **70a**.

3.2.2 Parallel Dehydration Reactions to Form Imine, Acetal, Ester, and Alkene (II)

In the second set of thirteen experiments (Table 3.2, entries 1–13), boronic acid was replaced with a second aldehyde, setting up a competition between the two aldehydes—as each could form either an imine or an acetal, or both. In total, at least 16 products could be formed: two imines, eight acetals, four esters, and four alkenes.

Entry	RCHO #1	RCHO #2	RNH_2	Diol	ROH #1	ROH #2	RCOOH	NMR Yields (%)					
								A	**B**	**C**	**D**	**E**	**F**
1	**68a**	**68e**	**69a**	**73a**	**71a**	**71c**	**70a**	84	77	96	99	0.4	9
2	**68a**	**68c**	**69a**	**73a**	**71a**	**71c**	**70a**	92	79	98	99	1	5
3	**68b**	**68d**	**69a**	**73a**	**71a**	**71c**	**70a**	75	72	59	99	—	5
4	**68b**	**68f**	**69a**	**73a**	**71a**	**71c**	**70a**	52	52	99	99	48	43
5	**68a**	**68c**	**69b**	**73a**	**71a**	**71c**	**70a**	86	80	98	99	—	—
6	**68a**	**68c**	**69c**	**73a**	**71a**	**71c**	**70a**	72	95	43	99	—	—
7	**68a**	**68c**	**69d**	**73a**	**71a**	**71c**	**70a**	83	74	99	99	—	—
8	**68a**	**68d**	**69a**	**73b**	**71a**	**71c**	**70a**	98	94*	99	99	—	1
9	**68a**	**68d**	**69a**	**73c**	**71a**	**71c**	**70a**	86	64	93	99	—	1
10	**68a**	**68c**	**69a**	**73d**	**71a**	**71c**	**70a**	96	92	91	99	—	4
11	**68a**	**68c**	**69a**	**73a**	**71b**	**71c**	**70b**	79	76	75	99	1	12
12	**68a**	**68c**	**69a**	**73a**	**71a**	**71c**	**70c**	85	84	99	99	4	13
13	**68a**	**68c**	**69a**	**73a**	**71a**	**71c**	**70d**	90	78	11	98	1	10

Table 3.2 Yields for the dehydration reactions in the second set (**II**) of parallel reaction. *Acetal formation gave a mixture of two diasteromers.

In the benchmark reaction (Table 3.2, entry 1), we chose a pair of aldehydes with very different electronic characters: an electron-rich 2,4-dimethoxybenzaldehyde (**68c**), and the electron-poor **68a**. Results showed that **68a** reacted with **69a** to form an imine (pathway **A**, 84%) and with **73a** to give a miniscule amount of acetal (pathway **E**, 0.4%). Aldehyde **68c** was dominantly converted into an acetal with **73a** (pathway **B**, 77%), but a minor imine product (with **69a**, pathway **F**, 9%) was also observed. As in the previous set of experiments, **70a** and **71a** formed an ester (pathway **C**, 96%) and **71c** exclusively dehydrated into an alkene (pathway **D**, 99%). We have rationalized the observed

preference of the starting materials to undergo a particular dehydration reaction as follows. Donor-acceptor imines are both more stable and form faster than their donor-donor counterparts. Although significant formation of imine between **68c** and **69a** was initially observed (as determined by ^{1}H NMR analysis of an aliquot of the reaction mixture after the first hour of heating), imine metathesis allowed the exchange of components between the two imines, which led to the exclusive expression of the more stable imine from aldehyde **68a** at the end of the two-day reaction. Aldehyde **68c** can only form an acetal and it has a choice between diol **73a,** or 2 equivalents of mono-ol **71a**. Aldehyde **68c** and **73a** exclusively formed the acetal due to entropy consideration and Thorpe-Ingold effect.[112] Unimolecular dehydration of tertiary alcohol **71c** into an alkene was quick, leaving **71a** with no choice but to slowly, in a bimolecular reaction, form an ester with **70a**.

The observed sorting between a pair of aldehydes, where the electron-poor aldehyde forms imine and the electron-rich aldehyde gives acetal, was observed when there is a sufficient difference in the electronic characters of the pair (Table 3.2, entries 1–3). When two electron-deficient aldehydes—such as 4-nitrobenzaldehyde and 4-chlorobenzaldehyde—were used (Table 3.2, entry 4), the selectivity was lost and all possible imine and acetal products were formed. We also found that we can vary the amine without affecting the imine–acetal selectivity (Table 3.2, entries 5–7), although more nucleophilic alkyl amines can lower the yield of the ester formed due to formation of an amide side product with the carboxylic acid. As shown in Table 3.2, entries 8–10, diols can be varied freely without affecting the preference for either acetal or ester

formation. The same statement applies for the carboxylic acid and mono-ol components (Table 3.2, entries 11–13), although esterification of benzoic acid proceeded only to 11% conversion. This low yield is expected for esterification of aromatic carboxylic acid.[113]

3.2.3 Effect of Competing Diols in the Parallel Dehydration Reactions (III)

The final set of experiments (**III**) examined what happens when one of the mono-ols is replaced with a diol—thus setting up a competition between two aldehydes and two diols, removing the entropy-consideration in the formation of acetals. Thirteen products: two imines, four acetals, five esters, and two alkenes could be formed from these mixtures.

Entry	RCHO #1	RCHO #2	RNH_2	Diol #1	Diol #2	ROH	RCOOH	NMR Yields (%)						
								A	**B**	**C**	**D**	**F**	**G**	**H**
1	**68a**	**68e**	**69a**	**73a**	**73a**	**71c**	**70a**	98	54	95	98	—	5	46
2	**68a**	**68c**	**69a**	**73a**	**73a**	**71c**	**70a**	78	77	99*	99	1	—	—

Table 3.3 Yields for the dehydration reactions in the third set (III) of parallel reactions. *Yield for both the monoester and diester products.

In the first experiment (Table 3.3, entry 1), the two diols used—2,2-dimethyl-1,3-propanediol (**73a**), and 1,3-propanediol (**73d**), were of the same length, and were both capable of forming a 6-membered cyclic acetal with the aldehyde. As observed in the previous reactions, **68a** formed the major imine product with **69a**. Aldehyde **68e** had the option to either react with **73a** or **73d**; however, since both diols are capable of forming a favourable six-membered cyclic acetal, **68e** did not show selectivity (reaction with **73a**,

pathway **B**: 54% and reaction with **73b**, pathway **H**: 46%). Carboxylic acid then reacted with the excess of **73d** to produce an ester (pathway **C**, 95%). The second experiment replaced **73d** with the longer 1,6-hexanediol (**73e**). Since **73e** is not capable of forming a favourable cyclic acetal structure, **73d** was exclusively used for acetal formation. The original selectivity was restored and only four products from pathways **A**–**D** were observed.

The observed reaction preferences, in the three sets of dehydration reactions, appear to be kinetic in character. By focusing on entry 1, Table 3.2, and observing its progress by ^{1}H NMR spectroscopy, we were able to estimate rates of formation of dehydrated products as following the trend: alkene ≈ imine > acetal > ester. We then independently prepared the crossover imine and acetal species not observed in the actual reaction: imine formed from **68c** and **69a** and acetal from **68a** and **73a**. When these two "wrong" products were heated in anhydrous PhMe at reflux in the presence of *p*-toluenesulfonic acid, no equilibration was observed even after 4 d—suggesting that the mixture composition more likely corresponds to the kinetic distribution of the products. No equilibration was observed in a similar experiment where "wrong" ester and acetal partners were heated for 2 d in the presence of acid catalyst.

3.3 Conclusions and Outlook

In conclusion, we have demonstrated that dehydration reactions yielding imine, acetal/boronate ester, ester, and alkene products may be accomplished in one pot with a common simple acid catalyst. A single set of dehydrated products stems from different mechanisms for the participant reactions and electronic properties of starting materials, which together translate into sufficiently different rates of competing reactions. This system is modular, but within limits. While individual components can be swapped, examples of aldehydes with similar electronic properties and diols of similar chain lengths showed that selectivity quickly erodes when substrates are offered a "confusing" choice of reagents.

Future work will focus on the application of these simultaneous dehydration reactions. For example, a single polyfunctional building block can be synthesized—where the functional groups differ in electronic character due to inductive or resonance effect of the adjacent side groups (Figure 3.6). This molecule may be used to construct discrete, multifunctional, molecular architectures. Alternatively, construction of multi-level DCLs from these polyfunctional building blocks using simultaneous imine, acetal, and ester formation can be further explored.

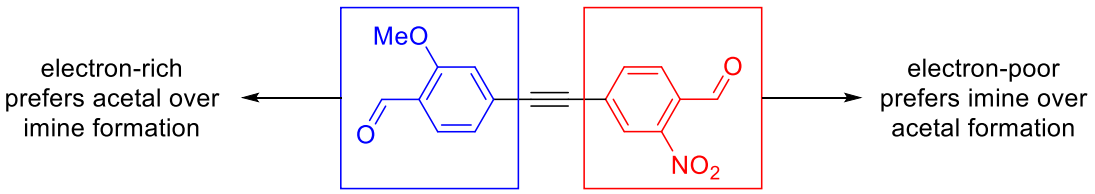

Figure 3.5 Sample oligofunctional building block.

3.4 Experimental Section

3.4.1 General Experimental Methods

All reactions were performed under nitrogen atmosphere in oven-dried glassware. Reagents were purchased from commercial suppliers and used without further purification. Solvents were dried by adding activated 4 Å molecular sieves. Microwave-assisted reactions were performed in a Biotage Initiator 2.0 microwave reactor, producing monochromatic microwave radiation with the frequency of 2.45 GHz. Mass spectral measurements were performed by the Mass Spectrometry Facilities of the Department of Chemistry, University of Houston and the Department of Chemistry at the University of Texas at Austin. NMR spectra were obtained on JEOL ECA-500 MHz spectrometer, with working frequency (for ^{1}H nuclei) of 500 MHz. All ^{13}C-NMR spectra were recorded with simultaneous decoupling of ^{1}H nuclei. ^{1}H NMR chemical shifts are reported in ppm units relative to the residual signal of the solvent ($CDCl_3$: 7.25 ppm) and were recorded at 25 °C. NMR yields were calculated by adding approx. 1.0 equivalent of 1,3,5-trimethoxybenzene (Alfa Aesar, 99%) as the internal standard to the crude reaction mixture. Infrared spectra were recorded on a Nicolet iS10 FT-IR spectrometer equipped with a Thermo Scientific iTR for multi-purpose ATR sampling. Melting points were measured in open capillary tubes using Mel-Temp Thermo Scientific apparatus, and are uncorrected. Short column chromatography for purification was performed using basic alumina Act 1 (Sorbent Technologies), 50–200 μm. Analytical TLC was performed on JT Baker alumina oxide IB-F plates.

3.4.2 Structures and Chemical Shifts of Possible Dehydration Products

3.4.2.1 Possible Imine Products and Their Signature ^{1}H NMR Signals

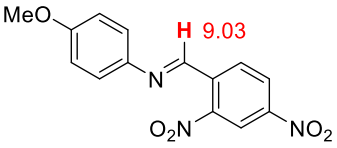

27

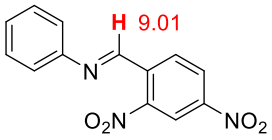

57

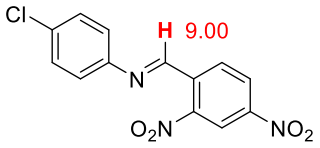

74

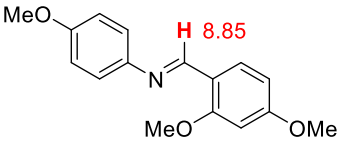

19

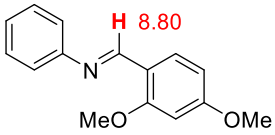

75

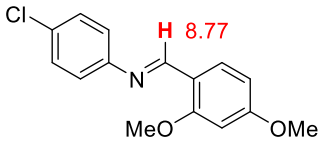

76

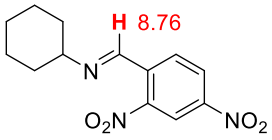

77

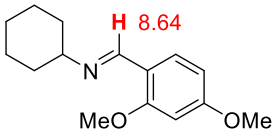

78

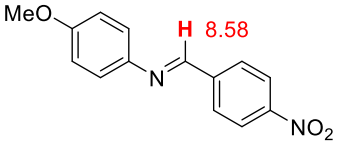

21

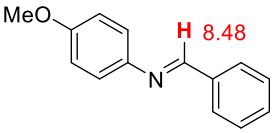

25

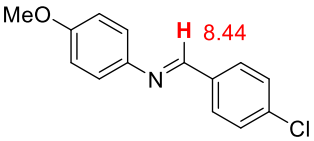

26

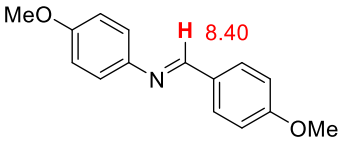

44

3.4.2.2 Possible Acetal Products and Their Signature ^{1}H NMR Signals

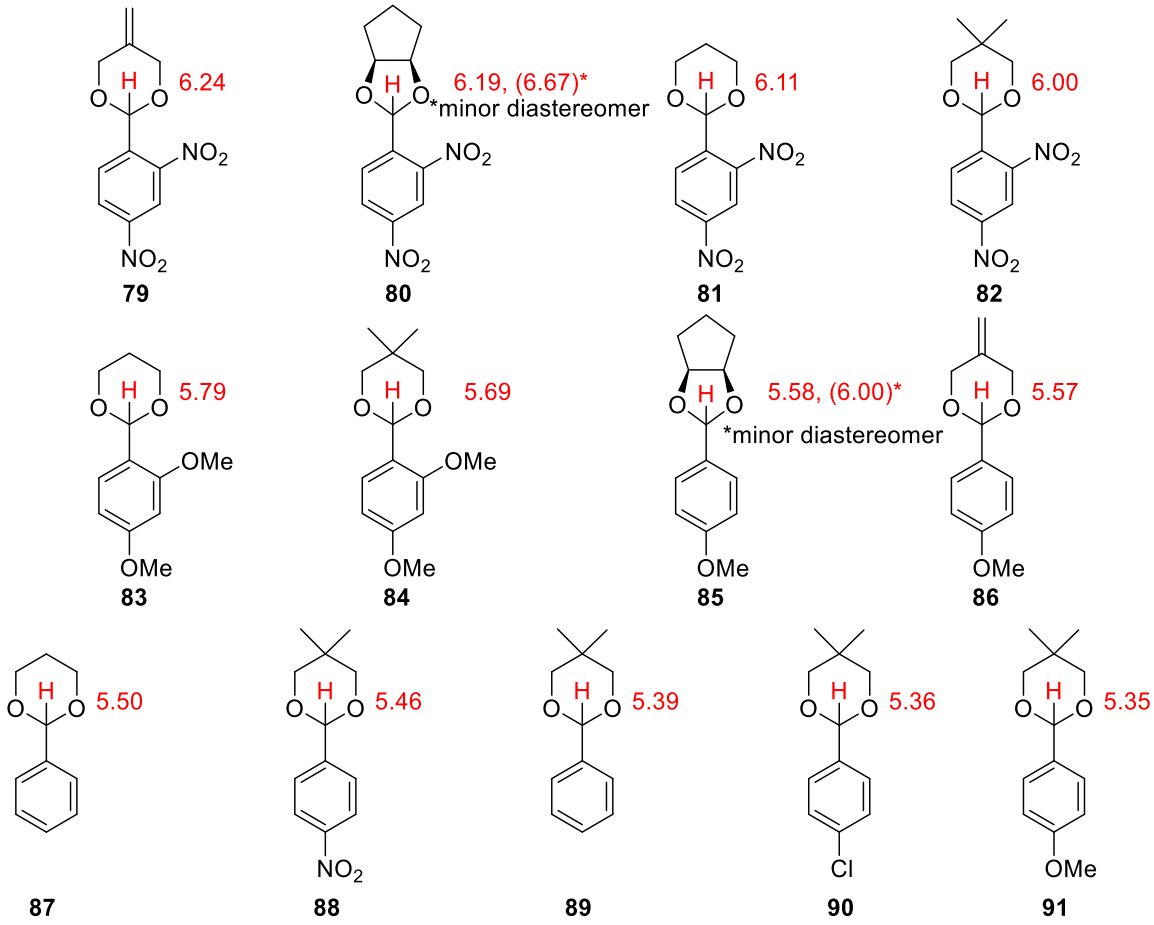

3.4.2.3 Possible Alkene and Boronate Ester Products and Their Signature ^{1}H NMR Signals

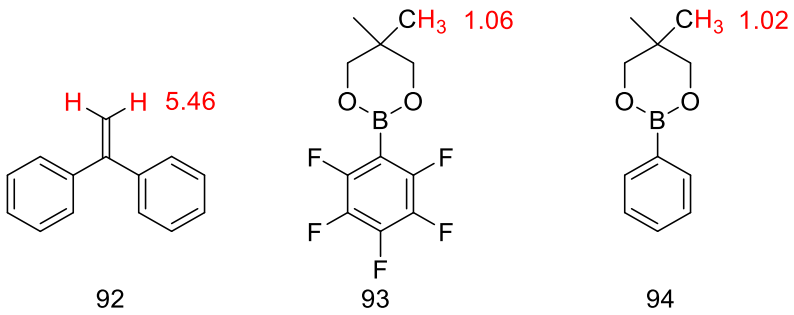

92 93 94

3.4.2.4 Possible Ester/Diester Products and Their Signature ^{1}H NMR Signals

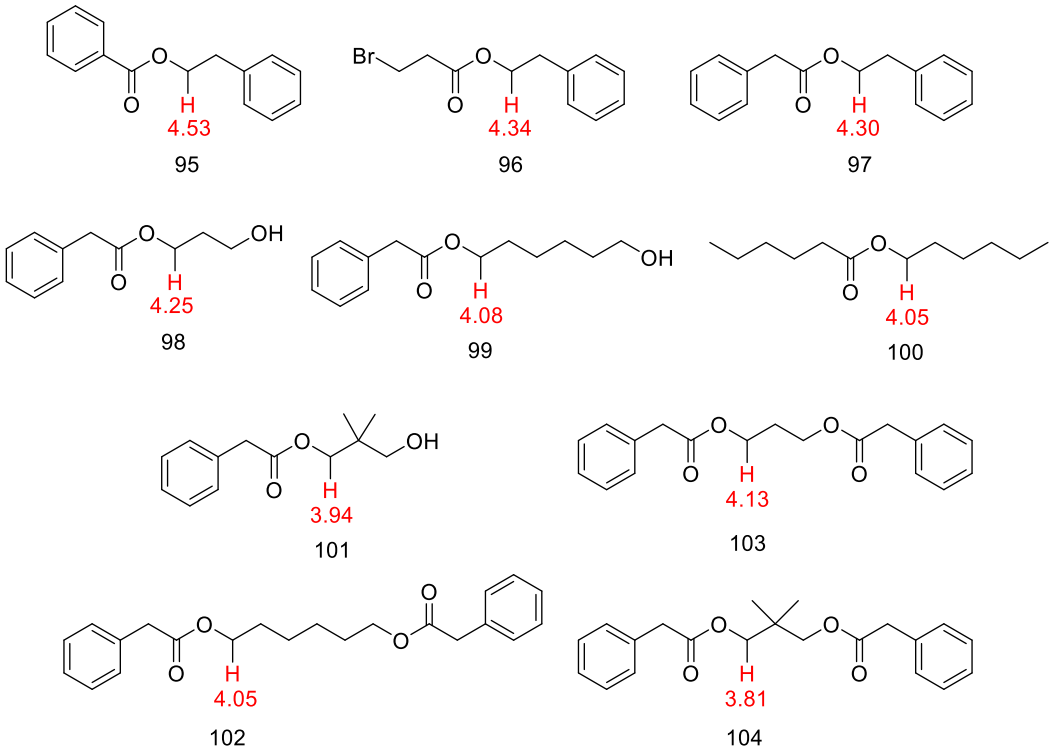

95 96 97 98 99 100 101 102 103 104

3.4.3 Experimental Protocols for Parallel Dehydration Reactions

3.4.3.1 Parallel Reaction #1 (Reaction Set I, Entry 1)

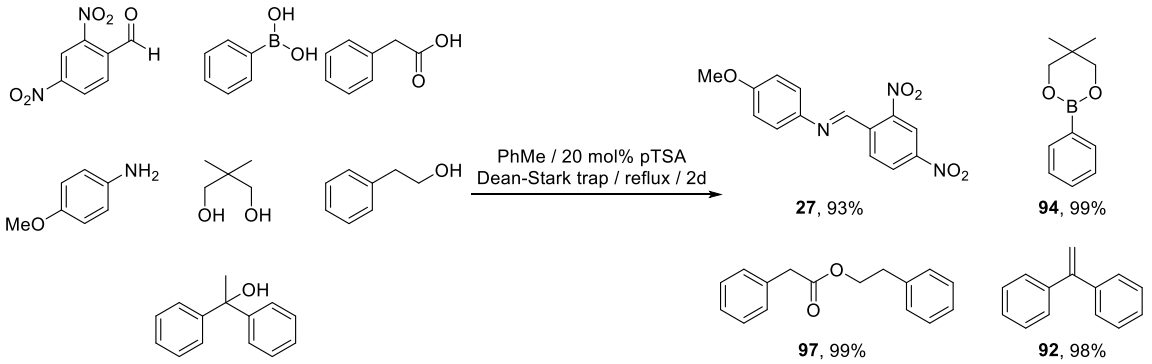

In a round-bottom flask fitted with a reflux condenser and a Dean-Stark adapter, compounds 2,4-dinitrobenzaldehyde (**68a**, 62.8 mg, 0.32 mmol), phenylboronic acid (**72a**, 39.0 mg, 0.32 mmol), phenylacetic acid (**70a**, 43.6 mg, 0.32 mmol), *p*-anisidine (**69a**, 39.4 mg, 0.32 mmol), 2,2-dimethyl-1,3-propanediol (**73a**, 33.3 mg, 0.32 mmol), 1,1-diphenylethanol (**71c**, 63.4 mg, 0.32 mmol), 2-phenylethanol (**71a**, 115 µL, 0.96 mmol), and *p*-toluenesulfonic acid monohydrate (12.2 mg, 0.064 mmol) were dissolved in PhMe (60 mL). The solution was heated to reflux. After 2 d, a 1.0 mL aliquot was taken (temperature of the solution: 85 °C), dried in vacuo and analyzed using ^{1}H NMR spectroscopy with an internal standard (Figure 3.7).

27: ^{1}H NMR ($CDCl_3$, 500 MHz,): δ 9.03 (s, 1H), 8.90 (d, *J*=2.3 Hz, 1H), 8.61 (d, *J*=8.6 Hz, 1H), 8.51 (dd, *J*=8.9, 2.3 Hz, 1H), 7.38 (d, *J*=8.6 Hz, 2H), 6.97 (d, *J*=9.2 Hz, 2H), 3.86 (s, 9H) ppm. Spectral data agree with a previous literature report.[59]

94: ^{1}H NMR ($CDCl_3$, 500 MHz): δ 7.80 (d, J=6.9 Hz, 2H), 7.43 (t, J=7.5 Hz, 1H), 7.35 (t, J=7.4 Hz, 2H), 3.77 (s, 4H), 1.03 (s, 6H) ppm. Spectral data agree with a previous literature report.[114]

97: ^{1}H NMR ($CDCl_3$, 500 MHz): δ 7.14–7.33 (m, 10H), 4.31 (t, J=7.1 Hz, 2H), 3.60 (s, 2H), 2.92 (t, J=7.1 Hz, 2H) ppm. Spectral data agree with a previous literature report.[115]

92: ^{1}H NMR ($CDCl_3$, 500 MHz): δ 7.31–7.34 (m, 10H), 5.46 (s, 2H) ppm. Spectral data agree with a previous literature report.[116]

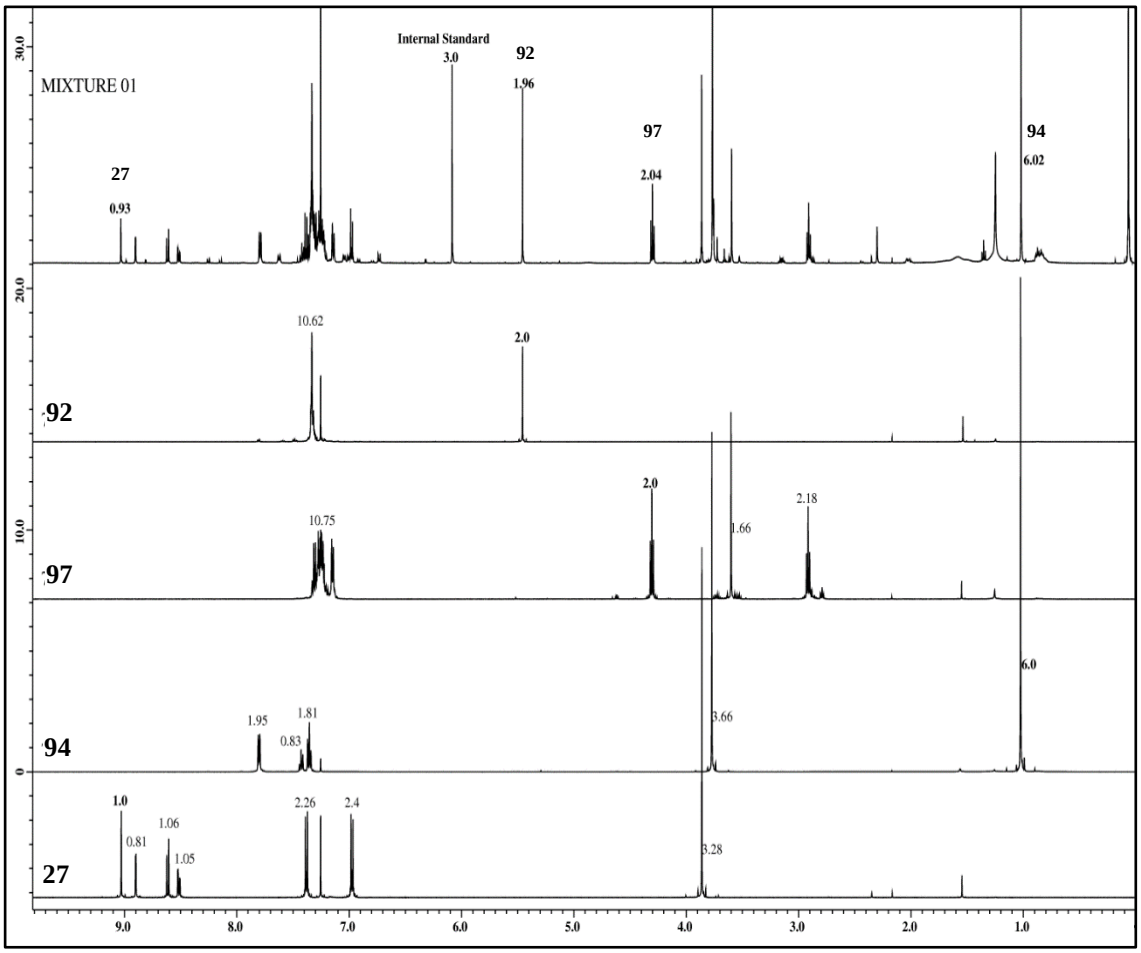

Figure 3.7 ^{1}H NMR spectra of the individual dehydration products and crude reaction mixture #1. For clarity, only the integration of the signature peaks of the observed products is shown in the ^{1}H NMR spectrum of the crude mixture (top).

3.4.3.2 Parallel Reaction #2 (Reaction Set I, Entry 2)

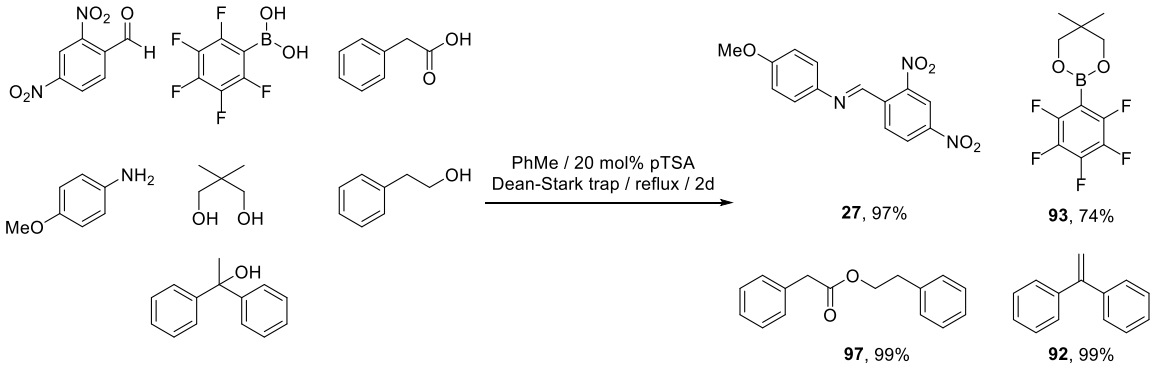

In a round-bottom flask fitted with a reflux condenser and a Dean-Stark adapter, compounds **68a** (62.8 mg, 0.32 mmol), pentafluorophenylboronic acid (**72b**, 67.8 mg, 0.32 mmol), **70a** (43.6 mg, 0.32 mmol), **69a** (39.4 mg, 0.32 mmol), **73a** (33.3 mg, 0.32 mmol), **71c** (63.4 mg, 0.32 mmol), **71a** (115 µL, 0.96 mmol), and *p*-toluenesulfonic acid monohydrate (12.2 mg, 0.064 mmol) were dissolved in PhMe (60 mL). The solution was heated to reflux. After 2 days, a 1.0 mL aliquot was taken (temperature of the solution: 85 °C), dried in vacuo and analyzed using ^{1}H NMR spectroscopy with an internal standard (Figure 3.8).

To synthesize 5,5-dimethyl-2-(perfluorophenyl)-1,3,2-dioxaborinane (**93**), **72b** (211.9 mg, 1.0 mmol) and **73a** (104.15 mg, 1.0 mmol) were dissolved in PhMe (10 mL) and stirred under nitrogen for 12 h at 80 °C. The solution was dried in vacuo to give **93** as white crystalline solid in quantitative yield.

93: mp 73–75 °C. IR (neat): 2962, 1386, 1325, 1255, 1205, 1143, 1122, 666 cm^{-1}. ^{1}H NMR ($CDCl_3$, 500 MHz): δ 3.81 (s, 3H), 1.06 (s, 6H) ppm. ^{13}C NMR ($CDCl_3$, 125

MHz): δ 149.5, 147.6, 143.2, 141.2, 138.2, 136.2, 72.9, 32.0, 21.9 ppm. ^{19}F NMR ($CDCl_3$, 470 MHz): −131.78 to −131.85 (m, 2F), −151.72 to −151.82 (m, 1F), −162.03 to −162.14 (m, 2F) ppm. HRMS (CI): Calcd for $C_{11}H_{11}BF_5O_2^+$: 281.0772. Found: 281.0760.

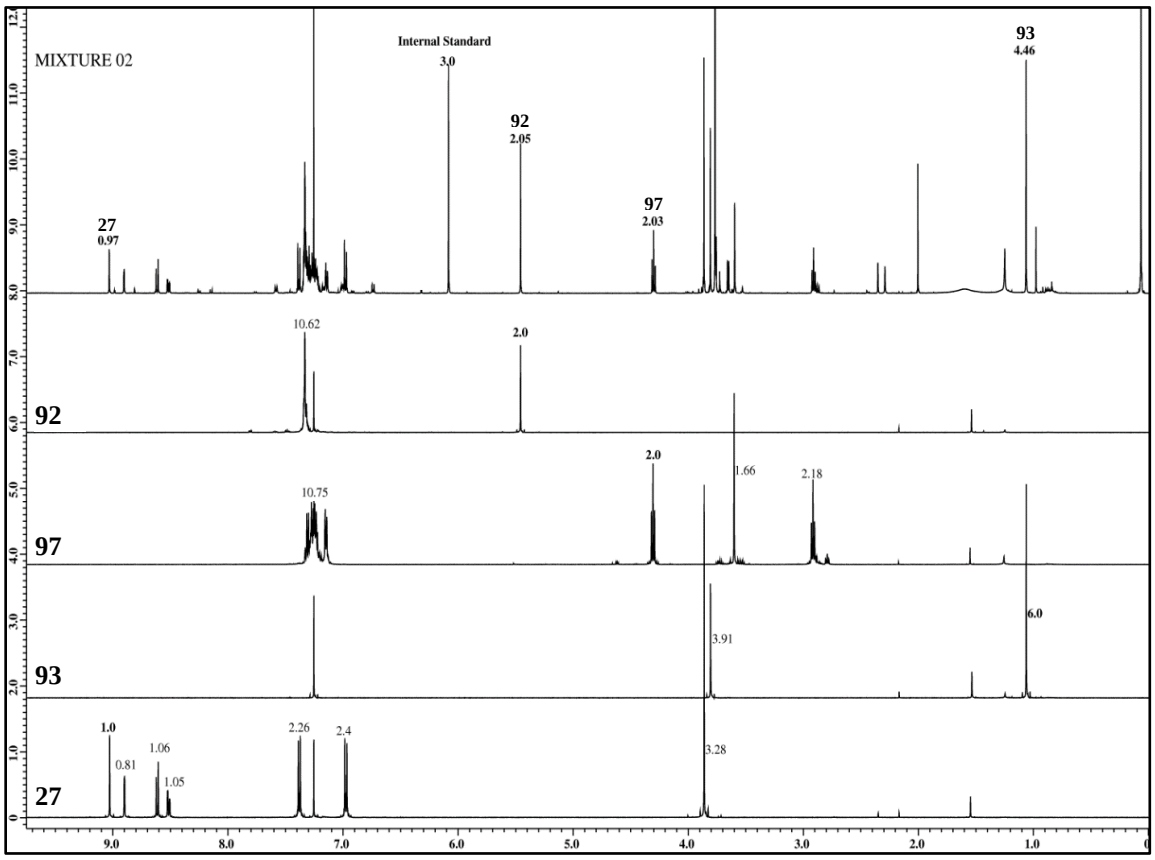

Figure 3.8 ^{1}H NMR spectra of the individual dehydration products and crude reaction mixture #2. For clarity, only the integration of the signature peaks of the observed products is shown in the ^{1}H NMR spectrum of the crude mixture (top).

3.4.3.3 Parallel Reaction #3 (Reaction Set II, Entry 1)

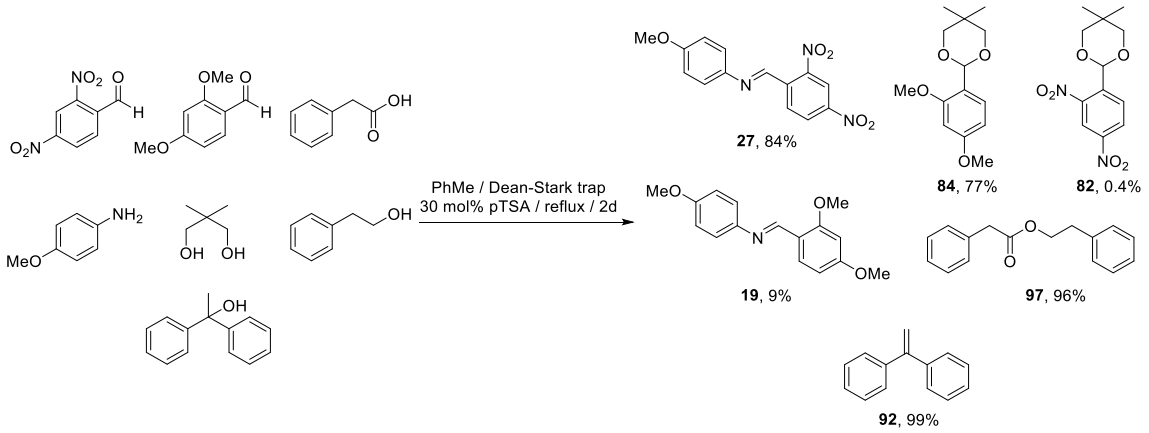

In a round-bottom flask fitted with a reflux condenser and a Dean-Stark adapter, compounds **68a** (62.8 mg, 0.32 mmol), 2,4-dimethoxybenzaldehyde (**68c**, 53.2 mg, 0.32 mmol), **70a** (43.6 mg, 0.32 mmol), **69a** (39.4 mg, 0.32 mmol), **73a** (33.3 mg, 0.32 mmol), **71c** (63.4 mg, 0.32 mmol), **71a** (115 µL, 0.96 mmol), and *p*-toluenesulfonic acid monohydrate (18.3 mg, 0.096 mmol) were dissolved in PhMe (60 mL). The solution was heated to reflux. After 2 d, a 1.0 mL aliquot was taken (temperature of the solution: 85 °C), dried in vacuo, and analyzed using ^{1}H NMR spectroscopy with an internal standard (Figure 3.9).

To synthesize 2-(2,4-dimethoxyphenyl)-5,5-dimethyl-1,3-dioxane (**84)**, **68c** (166.17 mg, 1.0 mmol), **73a** (104 mg, 1.0 mmol), and *p*-toluenesulfonic acid monohydrate (10 mg) were dissolved in PhMe (10 mL). Anhydrous $MgSO_4$ was added to the solution, which was then stirred under nitrogen for 12 h at 80 °C. The solution was cooled to room temperature, washed twice with saturated $NaHCO_3$ (2×15 mL), followed by brine and dried over anhydrous $MgSO_4$. The solvent was removed in vacuo and

passed through a short basic alumina column eluted by hexane, 5% EA in hexane, then 10% EA in hexane to give **84** as white crystalline solid (145mg, 57%).

84: mp 71.5–72.5 °C. IR (neat): 2953, 2829, 1397, 1350, 1284, 1095, 1031, 824 cm^{-1}. ^{1}H NMR ($CDCl_3$, 500 MHz): δ 7.56 (d, *J*=8.4 Hz, 1H), 6.51 (dd, *J*=8.6, 2.4 Hz, 1H), 6.42 (d, *J*=2.3 Hz, 1H), 5.69 (s, 1H), 3.80 (s, 3H), 3.79 (s, 3H), 3.73 (d, *J*=11.0 Hz, 2H), 3.65 (d, *J*=11.0 Hz, 2H), 1.31 (s, 3H), 0.76 (s, 3H) ppm. ^{13}C NMR ($CDCl_3$, 125 MHz): δ 161.4, 157.7, 128.1, 119.8, 104.7, 98.4, 97.0, 78.0, 55.7, 55.5, 30.3, 23.2, 22.0 ppm. LRMS (ESI): Calcd for $C_{14}H_{21}O_4^+$: 253.14. Found: 252.98.

To synthesize 2-(2,4-dinitrophenyl)-5,5-dimethyl-1,3-dioxane (**82**), **68a** (196.12 mg, 1.0 mmol), **73a** (104 mg, 1.0 mmol), and *p*-toluenesulfonic acid monohydrate (10 mg) were dissolved in PhMe (10 mL) and stirred under nitrogen for 12 h at 80 °C. The solution was cooled to room temperature, washed twice with saturated $NaHCO_3$ (2×15 mL), followed by brine and dried over anhydrous $MgSO_4$. The solvent was removed in vacuo and passed through a short basic alumina column eluted by hexane, then 10% EA in hexane to give **82** as off-white solid (180 mg, 64%).

82: mp 94–96 °C. IR (neat): 2962, 2825, 1531, 1381, 1348, 1312, 1029, 719 cm^{-1}. ^{1}H NMR ($CDCl_3$, 500 MHz): δ 8.66 (d, *J*=2.3 Hz, 1H), 8.44 (dd, *J*=8.6, 2.3 Hz, 1H), 8.14 (d, *J*=8.6 Hz, 1H), 6.00 (s, 1H), 3.76 (d, *J*=11.4 Hz, 2H), 3.68 (d, *J*=11.4 Hz, 2H), 1.21 (s, 3H), 0.80 (s, 3H) ppm. ^{13}C NMR ($CDCl_3$, 125 MHz): δ 148.6, 147.9, 138.4, 129.6, 126.9, 119.6, 96.3, 78.0, 30.4, 23.1, 21.8 ppm. LRMS (APCI): Calcd for $C_{12}H_{13}N_2O_6^-$: 281.08. Found: 281.98.

19: ^{1}H NMR ($CDCl_3$, 500 MHz): δ 8.82 (s, 1H), 8.08 (d, J=8.6 Hz, 1H), 7.20 (d, J=9.1 Hz, 2H), 6.90 (d, J=9.1 Hz, 2H), 6.57 (dd, J=8.8, 2.3 Hz, 1H), 6.46 (d, J=2.5 Hz, 1H), 3.86 (s, 3H), 3.85 (s, 3H), 3.82 (s, 3H) ppm. Spectral data agree with a previous literature report.[117]

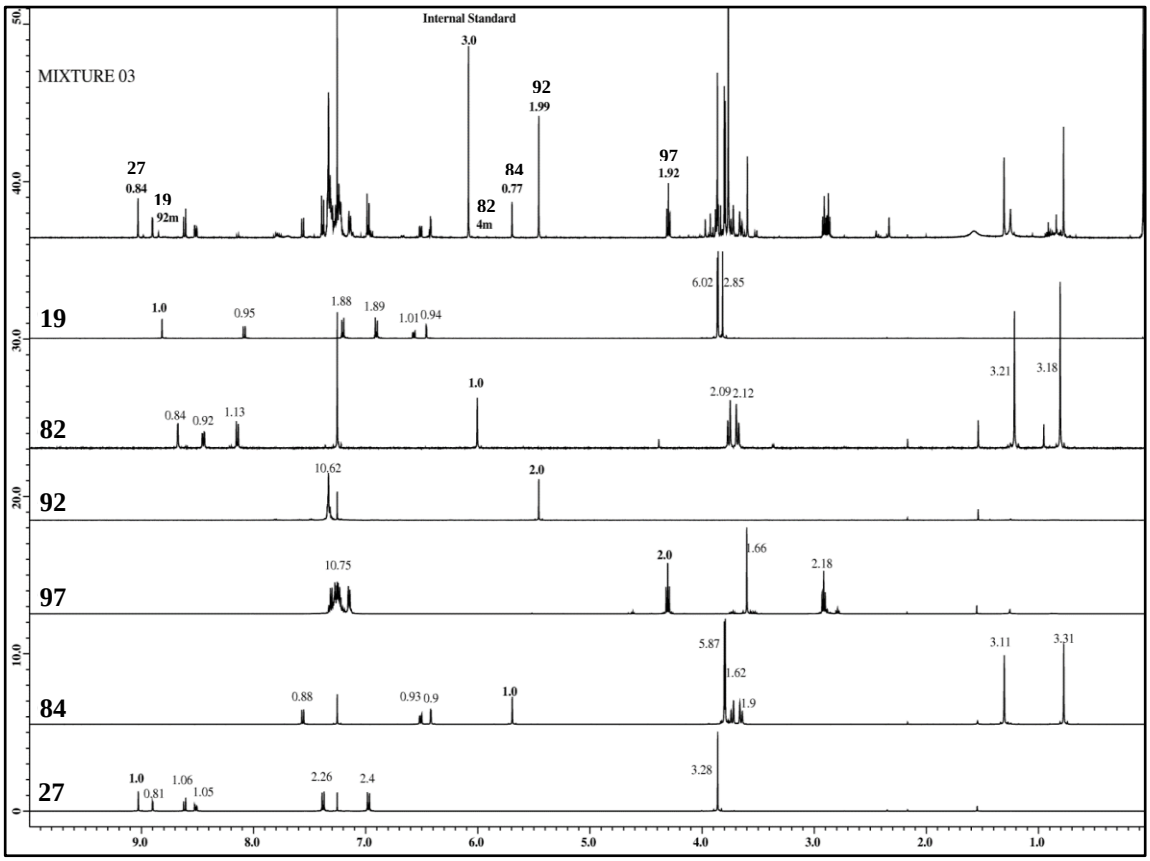

Figure 3.9 ^{1}H NMR spectra of the individual dehydration products and crude reaction mixture #3. For clarity, only the integration of the signature peaks of the observed products is shown in the ^{1}H NMR spectrum of the crude mixture (top).

3.4.3.4 Parallel Reaction #4 (Reaction Set II, Entry 2)

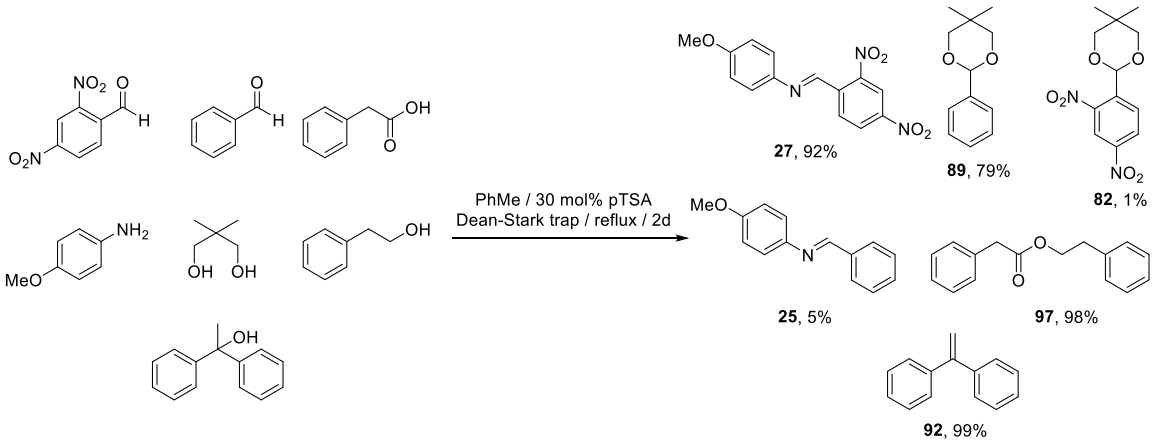

In a round-bottom flask fitted with a reflux condenser and a Dean-Stark adapter, compounds **68a** (62.8 mg, 0.32 mmol), benzaldehyde (**68e**, 32.5 µL, 0.32 mmol), **71a** (43.6 mg, 0.32 mmol), **69a** (39.4 mg, 0.32 mmol), **73a** (33.3 mg, 0.32 mmol), **71c** (63.4 mg, 0.32 mmol), **71a** (115 µL, 0.96 mmol), and *p*-toluenesulfonic acid monohydrate (18.3 mg, 0.096 mmol) were dissolved in PhMe (60 mL). The solution was heated to reflux. After 2 d, a 1.0 mL aliquot was taken (temperature of the solution: 85 °C), dried in vacuo and analyzed using ^{1}H NMR spectroscopy with an internal standard (Figure 3.10).

89: ^{1}H NMR ($CDCl_3$, 500 MHz): δ 7.51 (d, *J*=7.0 Hz, 2H), 7.33–7.39 (m, 3H), 5.40 (s, 1H), 3.78 (d, *J*=11.1 Hz, 2H), 3.66 (d, *J*=11.1 Hz, 2H), 1.31 (s, 3H), 0.80 (s, 3H) ppm. Spectral data agree with a previous literature report.[118]

25: ^{1}H NMR ($CDCl_3$, 500 MHz): δ 8.48 (s, 1H), 7.89 (dd, *J*=7.5, 2.7 Hz, 2H), 7.46 (t, *J*=3.1 Hz, 3H), 7.24 (d, *J*=9.1 Hz, 2H), 6.93 (d, *J*=9.1 Hz, 2H), 3.83 (s, 3H) ppm. Spectral data agree with a previous literature report.[119]

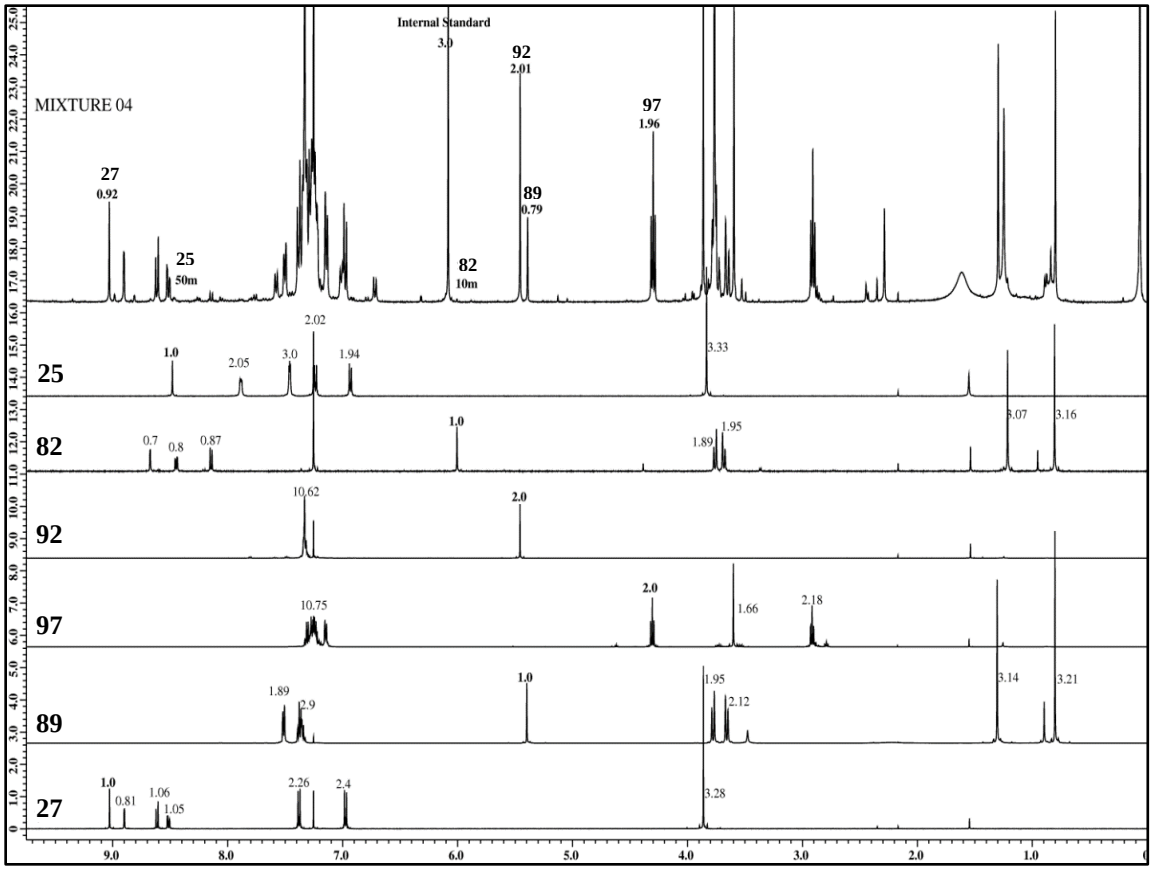

Figure 3.10 ^{1}H NMR spectra of the individual dehydration products and crude reaction mixture #4. For clarity, only the integration of the signature peaks of the observed products is shown in the ^{1}H NMR spectrum of the crude mixture (top).

3.4.3.5 Parallel Reaction #5 (Reaction Set II, Entry 3)

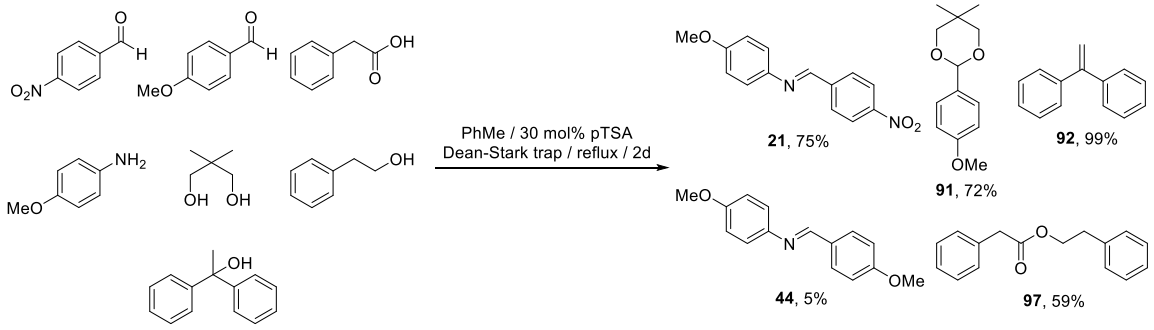

In a round-bottom flask fitted with a reflux condenser and a Dean-Stark adapter, compounds 4-nitrobenzaldehyde (**68b**, 48.4 mg, 0.32 mmol), *p*-anisaldehyde (**68d**, 38.9 µL, 0.32 mmol), **70a** (43.6 mg, 0.32 mmol), **69a** (39.4 mg, 0.32 mmol), **73a** (33.3 mg, 0.32 mmol), **71c** (63.4 mg, 0.32 mmol), **71a** (115 µL, 0.96 mmol), and *p*-toluenesulfonic acid monohydrate (18.3 mg, 0.096 mmol) were dissolved in PhMe (60 mL). The solution was heated to reflux with. After 2 d, a 1.0 mL aliquot was taken (temperature of the solution: 85 °C), dried in vacuo and analyzed using ^{1}H NMR with an internal standard (Figure 3.11).

21: ^{1}H NMR ($CDCl_3$, 500 MHz): δ 8.58 (s, 1H), 8.31 (d, J=8.7 Hz, 2H), 8.06 (d, J=8.6 Hz, 2H), 7.31 (d, J=8.6 Hz, 2H), 6.96 (d, J=8.6 Hz, 2H), 3.85 (s, 3H) ppm. Spectral data agree with a previous literature report.[120]

91: ^{1}H NMR ($CDCl_3$, 500 MHz): δ 7.43 (d, J=8.6 Hz, 2H), 6.89 (d, J=8.6 Hz, 2H), 5.35 (s, 1H), 3.79 (s, 3H), 3.75 (d, J=11.0 Hz, 2H), 3.63 (d, J=11.0 Hz, 2H), 1.29 (s, 3H), 0.79 (s, 3H) ppm. Spectral data agree with a previous literature report.[118]

44: ^{1}H NMR ($CDCl_3$, 500 MHz): δ 8.40 (s, 1H), 7.83 (d, *J*=8.6 Hz, 2H), 7.20 (d, *J*=8.6 Hz, 2H), 6.97 (d, *J*=8.6 Hz, 2H), 6.92 (d, *J*=9.0 Hz, 2H), 3.86 (s, 3H), 3.82 (s, 3H) ppm. Spectral data agree with a previous literature report.[119]

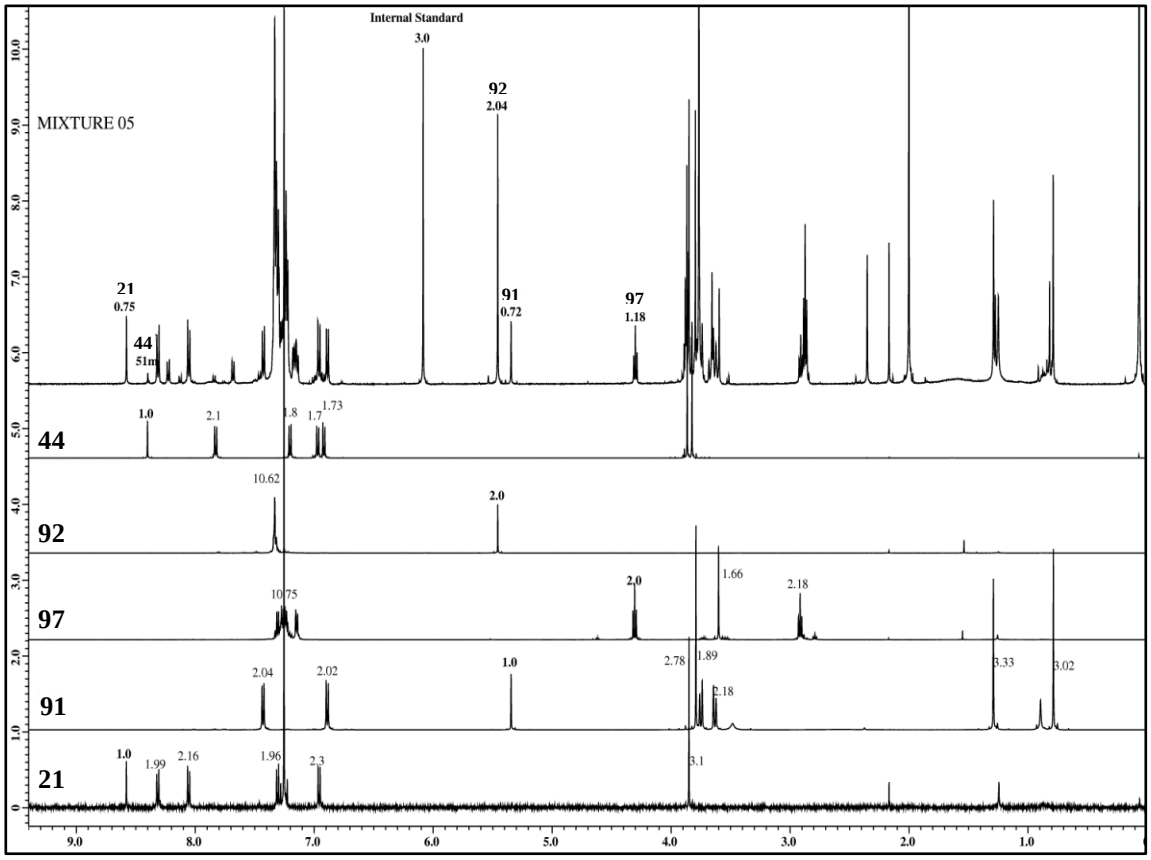

Figure 3.11 ^{1}H NMR spectra of the individual dehydration products and crude reaction mixture #5. For clarity, only the integration of the signature peaks of the observed products is shown in the ^{1}H NMR spectrum of the crude mixture (top).

3.4.3.6 Parallel Reaction #6 (Reaction Set II, Entry 4)

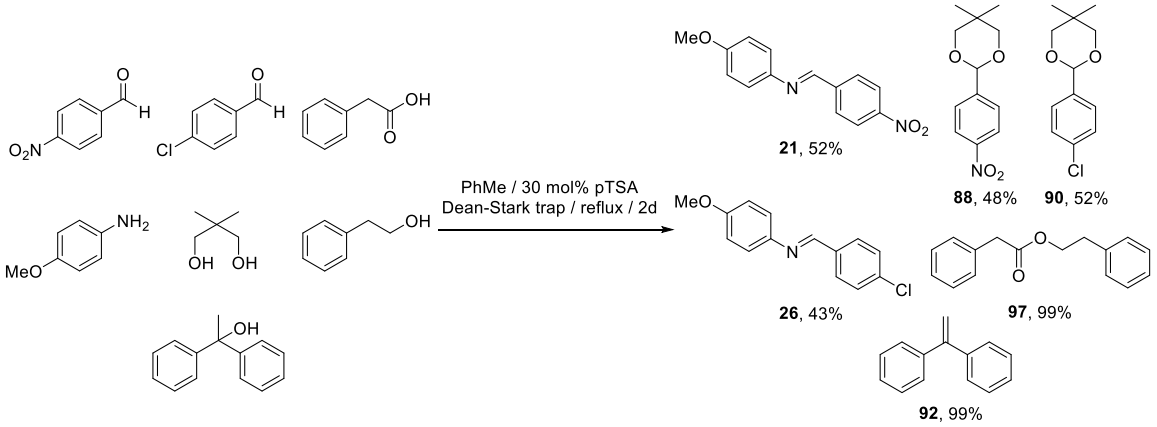

In a round-bottom flask fitted with a reflux condenser and a Dean-Stark adapter, compounds **68b** (48.4 mg, 0.32 mmol), **68f** (45.0 mg, 0.32 mmol), **70a** (43.6 mg, 0.32 mmol), **69a** (39.4 mg, 0.32 mmol), **73a** (33.3 mg, 0.32 mmol), **71c** (63.4 mg, 0.32 mmol), **71a** (115 µL, 0.96 mmol), and *p*-toluenesulfonic acid monohydrate (18.3 mg, 0.096 mmol) were dissolved in PhMe (60 mL). The solution was heated to reflux. After 2 d, a 1.0 mL aliquot was taken (temperature of the solution: 85 °C), dried in vacuo and analyzed using ^{1}H NMR with an internal standard (Figure 3.12).

90: ^{1}H NMR ($CDCl_3$, 500 MHz): δ 7.44 (d, *J*=8.5 Hz, 2H), 7.33 (d, *J*=8.5 Hz, 2H), 5.36 (s, 1H), 3.76 (d, *J*=11.1 Hz, 2H), 3.63 (d, *J*=11.1 Hz, 2H), 1.27 (s, 3H), 0.79 (s, 3H) ppm. Spectral data agree with a previous literature report.[121]

88: ^{1}H NMR ($CDCl_3$, 500 MHz): δ 8.22 (d, *J*=8.7 Hz, 2H), 7.68 (d, *J*=8.7 Hz, 2H), 5.46 (s, 1H), 3.79 (d, *J*=11.3 Hz, 2H), 3.67 (d, *J*=11.3 Hz, 2H), 1.27 (s, 3H), 0.82 (s, 3H) ppm. Spectral data agree with a previous literature report.[118]

26: ^{1}H NMR ($CDCl_3$, 500 MHz): δ 8.43 (s, 1H), 7.82 (d, J=8.3 Hz, 2H), 7.43 (d, J=8.4 Hz, 2H), 7.23 (d, J=8.7 Hz, 2H), 6.93 (d, J=8.7 Hz, 2H), 3.83 (s, 3H) ppm. Spectral data agree with a previous literature report.[55]

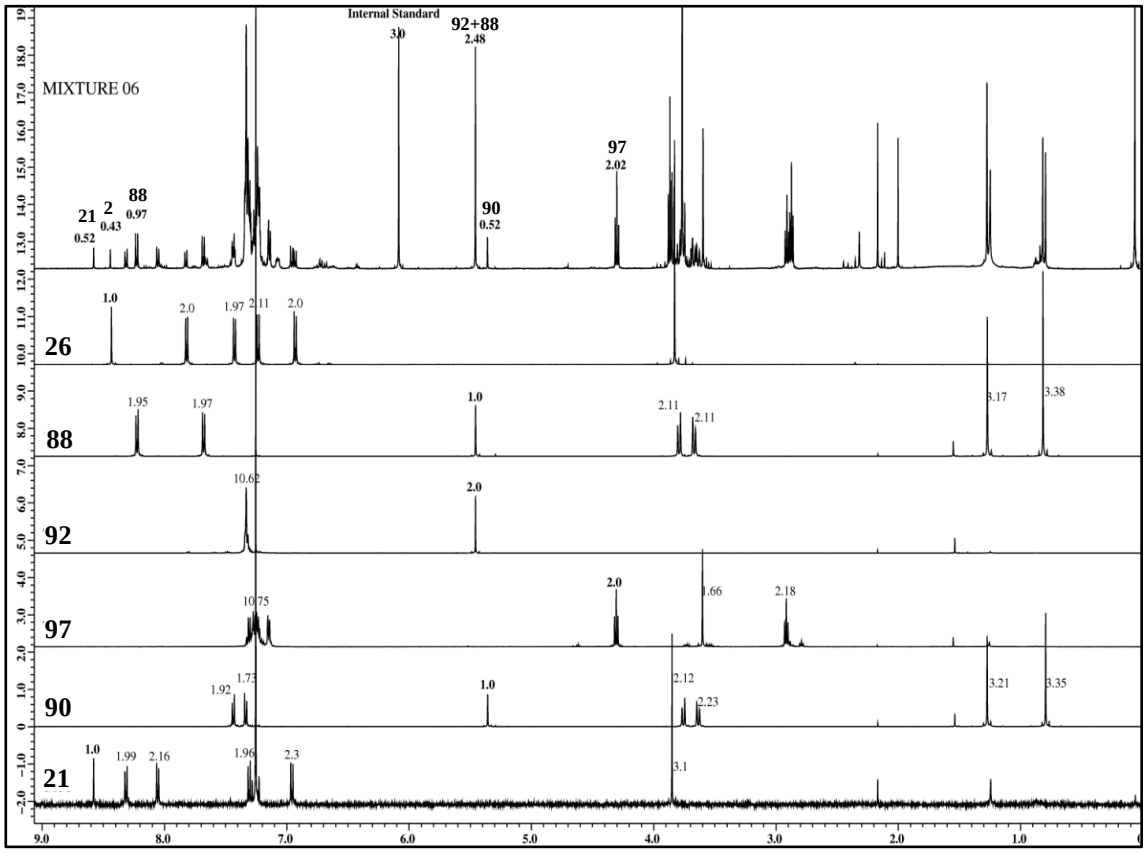

Figure 3.12 ^{1}H NMR spectra of the individual dehydration products and crude reaction mixture #6. For clarity, only the integration of the signature peaks of the observed products is shown in the ^{1}H NMR spectrum of the crude mixture (top).

3.4.3.7 Parallel Reaction #7 (Reaction Set II, Entry 5)

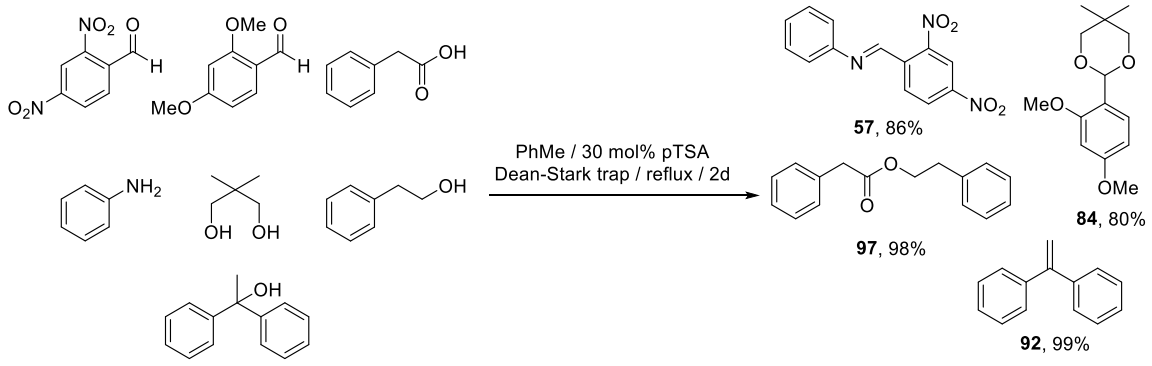

In a round-bottom flask fitted with a reflux condenser and a Dean-Stark adapter, compounds **68a** (62.8 mg, 0.32 mmol), **68c** (53.2 mg, 0.32 mmol), **70a** (43.6 mg, 0.32 mmol), **69b** (29.2 µL, 0.32 mmol), **73a** (33.3 mg, 0.32 mmol), **71c** (63.4 mg, 0.32 mmol), **71a** (115 µL, 0.96 mmol), and *p*-toluenesulfonic acid monohydrate (18.3 mg, 0.096 mmol) were dissolved in PhMe (60 mL). The solution was heated to reflux. After 2 d, a 1.0 mL aliquot was taken (temperature of the solution: 85 °C), dried in vacuo and analyzed using ^{1}H NMR with an internal standard (Figure 3.13).

57: ^{1}H NMR ($CDCl_3$, 500 MHz): δ 9.01 (s, 1H), 8.92 (d, *J*=2.2 Hz, 1H), 8.60 (d, *J*=8.7 Hz, 1H), 8.55 (dd, *J*=8.6, 2.0 Hz, 1H), 7.46 (t, *J*=7.8 Hz, 2H), 7.32–7.36 (m, 3H) ppm. Spectral data agree with a previous literature report.[59]

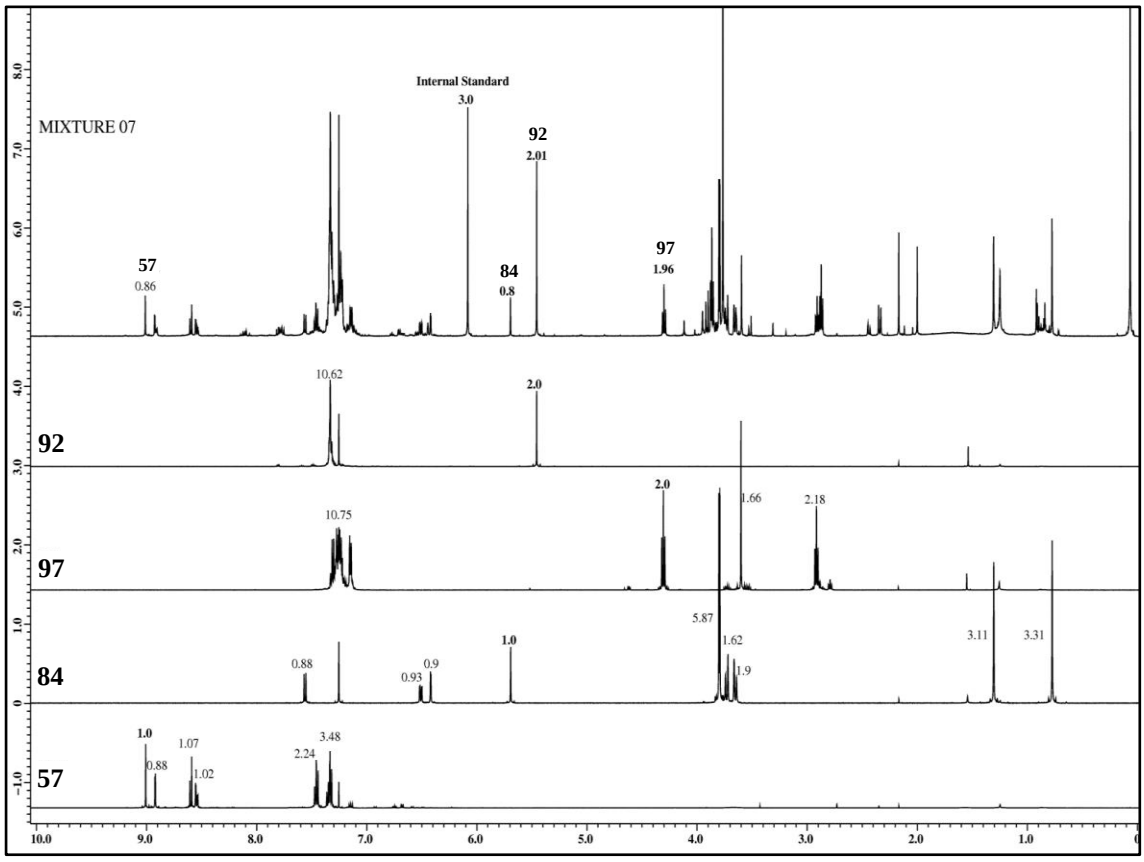

Figure 3.13 ^{1}H NMR spectra of the individual dehydration products and crude reaction mixture #7. For clarity, only the integration of the signature peaks of the observed products is shown in the ^{1}H NMR spectrum of the crude mixture (top).

3.4.3.8 Parallel Reaction #8 (Reaction Set II, Entry 6)

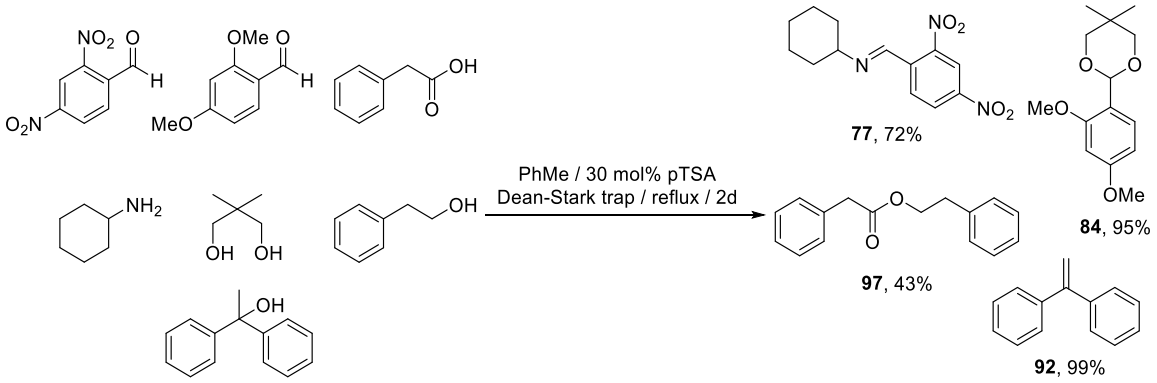

In a round-bottom flask fitted with a reflux condenser and a Dean-Stark adapter, compounds **68a** (62.8 mg, 0.32 mmol), **68b** (53.2 mg, 0.32 mmol), **70a** (43.6 mg, 0.32 mmol), cyclohexylamine (**69c**, 36.6 µL, 0.32 mmol), **73a** (33.3 mg, 0.32 mmol), **71c** (63.4 mg, 0.32 mmol), **71a** (115 µL, 0.96 mmol), and *p*-toluenesulfonic acid monohydrate (18.3 mg, 0.096 mmol) were dissolved in PhMe (60 mL). The solution was heated to reflux. After 2 d, a 1.0 mL aliquot was taken (temperature of the solution: 85 °C), dried in vacuo and analyzed using ^{1}H NMR with an internal standard (Figure 3.14).

To synthesize *N*-(2,4-dinitrobenzylidene)cyclohexanamine (**77**), **68a** (196 mg, 1.0 mmol) and **69c** (99 mg, 114 µL, 1.0 mmol) were dissolved in PhMe (10 mL) and the solution was stirred under nitrogen for 12 h at 80 °C. The solvent was removed in vacuo to give **77** as yellow-orange solid in quantitative yield.

77: mp 74.6–76 °C. IR (neat): 3089, 2928, 1634, 1594, 1528, 1384, 1343, 904 cm^{-1}. ^{1}H NMR ($CDCl_3$, 500 MHz): δ 8.84 (d, *J*=2.3 Hz, 1H), 8.75 (s, 1H), 8.45 (dd, *J*=8.7, 2.3 Hz, 1H), 8.32 (d, *J*=8.7 Hz, 1H), 3.39 (m, 1H), 1.81 (dt, *J*=13.5, 3.8 Hz, 2H), 1.78 (dd,

J=13.2, 3.5 Hz, 2H), 1.69 (dt, *J*=12.7, 3.8 Hz, 1H), 1.59 (qd, *J*=12.2, 3.4 Hz, 2H), 1.39 (qt, *J*=12.1, 3.0 Hz, 2H), 1.28 (qt, *J*=12.3, 3.5 Hz, 1H) ppm. ^{13}C NMR ($CDCl_3$, 125 MHz): δ 152.8, 148.7, 148.3, 136.6, 131.7, 127.4, 120.1, 70.3, 34.0, 25.6, 24.5 ppm. HRMS (CI): Calcd for $C_{13}H_{16}N_3O_4^+$:278.1141. Found: 278.1135.

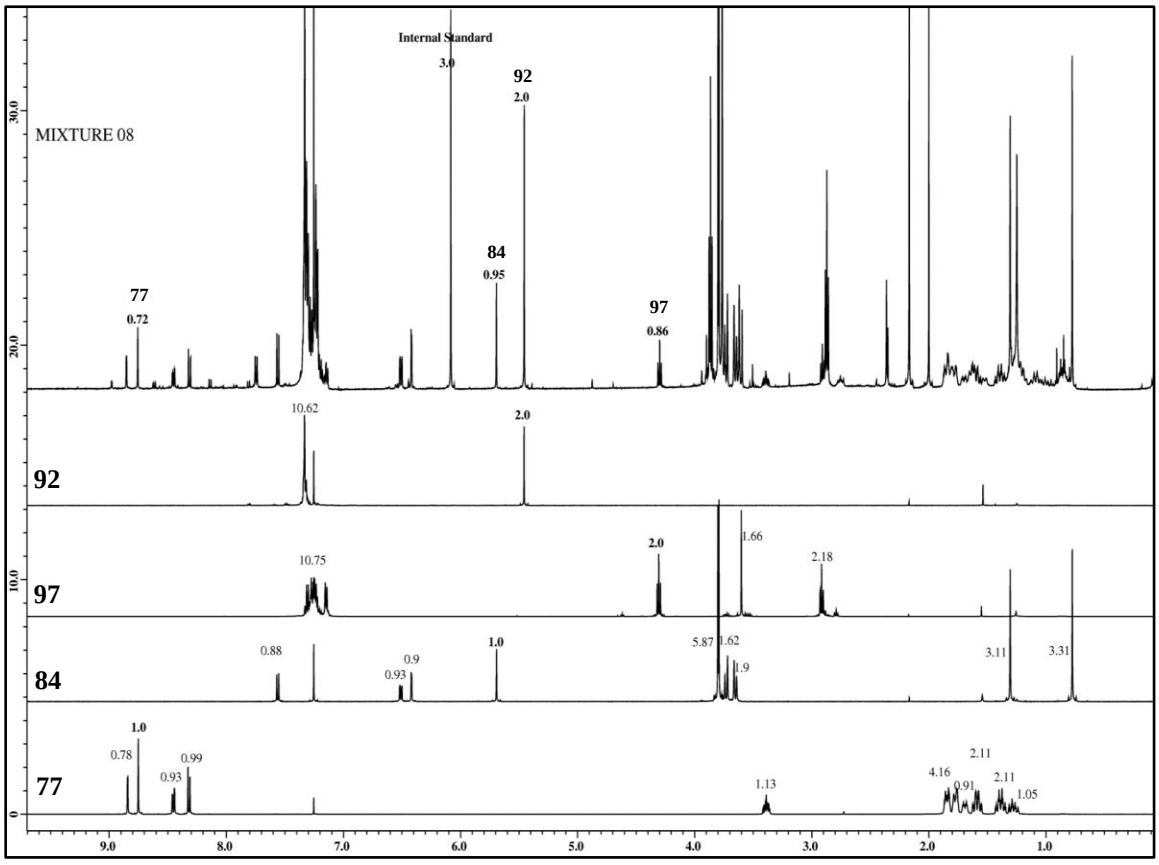

Figure 3.14 ^1H NMR spectra of the individual dehydration products and crude reaction mixture #8. For clarity, only the integration of the signature peaks of the observed products is shown in the ^1H NMR spectrum of the crude mixture (top).

3.4.3.9 Parallel Reaction #9 (Reaction Set II, Entry 7)

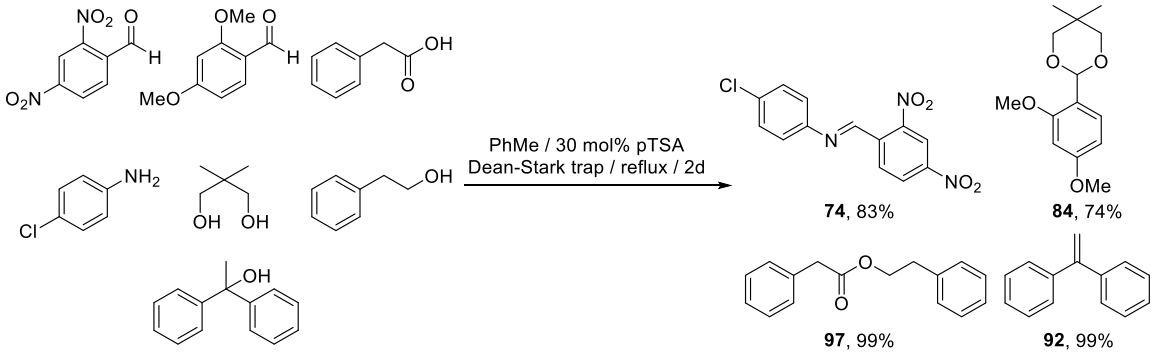

In a round-bottom flask fitted with a reflux condenser and a Dean-Stark adapter, compounds **68a** (62.8 mg, 0.32 mmol), **68c** (53.2 mg, 0.32 mmol), **70a** (43.6 mg, 0.32 mmol), 4-chloroaniline (**69d**, 40.8 mg, 0.32 mmol), **73a** (33.3 mg, 0.32 mmol), **71c** (63.4 mg, 0.32 mmol), **71a** (115 µL, 0.96 mmol), and *p*-toluenesulfonic acid monohydrate (18.3 mg, 0.096 mmol) were dissolved in PhMe (60 mL). The solution was heated to reflux. After 2 d, a 1.0 mL aliquot was taken (temperature of the solution: 85 °C), dried in vacuo and analyzed using ^{1}H NMR with an internal standard (Figure 3.15).

To synthesize 4-chloro-*N*-(2,4-dinitrobenzylidene)aniline (**74**), **68a** (196 mg, 1.0 mmol) and **69d** (128 mg, 1.0 mmol) were dissolved in PhMe (10 mL) and the solution was stirred under nitrogen for 12 h at 80 °C. The solvent was removed in vacuo to give **74** as a red-orange solid in quantitative yield.

74: mp 160.8–163 °C. IR (neat): 3107, 1594, 1522, 1395, 1337, 1090, 835 cm^{-1}. ^{1}H NMR ($CDCl_3$, 500 MHz): δ 8.99 (s, 1H), 8.93 (s, 1H), 8.56 (d, J=8.3 Hz, 1H), 8.55 (dd, J=8.5, 2.3 Hz, 2H), 7.42 (d, J=8.7 Hz, 2H), 7.27 (d, J=8.7 Hz, 2H) ppm. ^{13}C NMR ($CDCl_3$, 125 MHz): δ 153.6, 149.2, 148.8, 148.5, 135.8, 134.0, 131.5, 129.7, 127.7, 122.9, 120.5 ppm. HRMS (CI): Calcd for $C_{13}H_9ClN_3O_4^+$: 306.0282. Found: 306.0281.

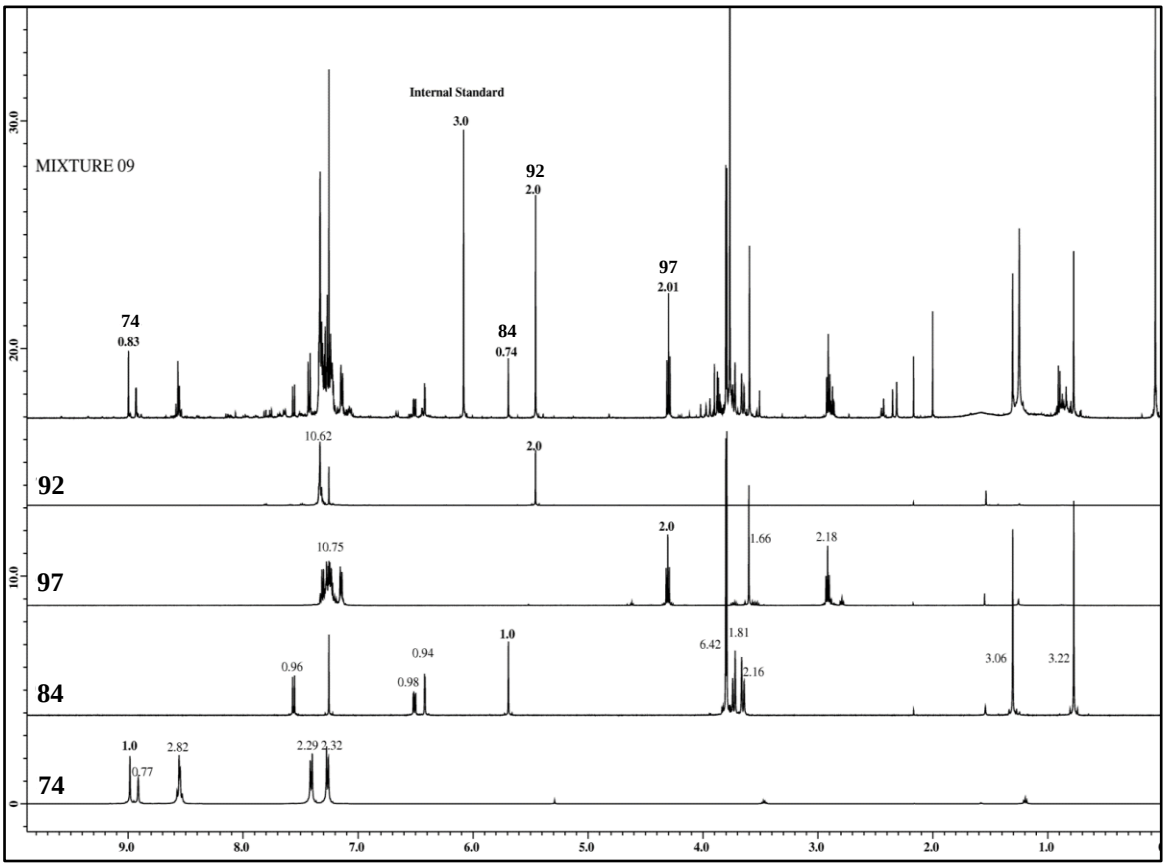

Figure 3.15 ^{1}H NMR spectra of the individual dehydration products and crude reaction mixture #9. For clarity, only the integration of the signature peaks of the observed products is shown in the ^{1}H NMR spectrum of the crude mixture (top).

3.4.3.10 Parallel Reaction #10 (Reaction Set II, Entry 8)

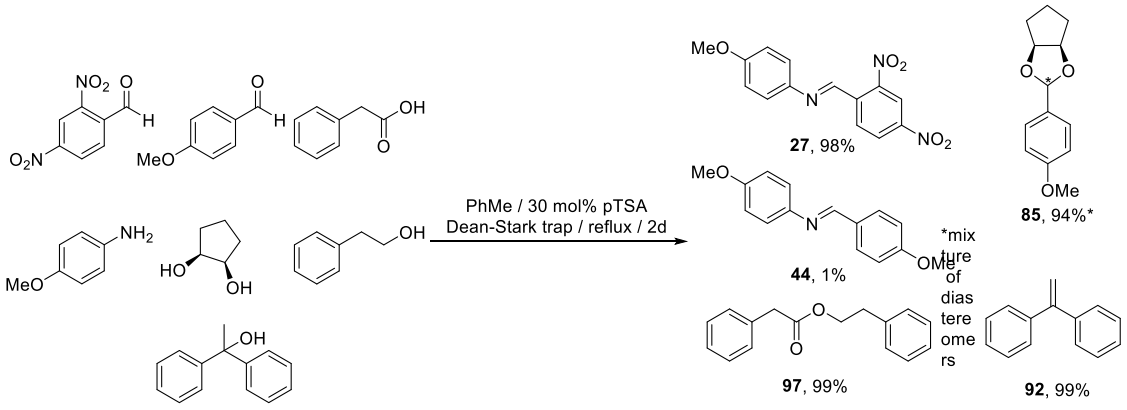

In a round-bottom flask fitted with a reflux condenser and a Dean-Stark adapter, compounds **68a** (62.8 mg, 0.32 mmol), **68d** (38.9 µL, 0.32 mmol), **70a** (43.6 mg, 0.32 mmol), **69a** (39.4 mg, 0.32 mmol), *cis*-1,2-cyclopentanediol (**73b**, 32.7 mg, 0.32 mmol), **71c** (63.4 mg, 0.32 mmol), **71a** (115 µL, 0.96 mmol), and *p*-toluenesulfonic acid monohydrate (18.3 mg, 0.096 mmol) were dissolved in PhMe (60 mL). The solution was heated to reflux. After 2 d, a 1.0 mL aliquot was taken (temperature of the solution: 85 °C), dried in vacuo and analyzed using ^{1}H NMR with an internal standard (Figure 3.16).

85* (*major diastereomer*): ^{1}H NMR ($CDCl_3$, 500 MHz): δ 7.43 (d, *J*=8.6 Hz, 2H), 6.89 (d, *J*=8.6 Hz, 2H), 5.58 (s, 1H), 4.65 (d, *J*=4.4 Hz, 2H), 3.80 (s, 3H), 2.05 (dd, *J*=13.9, 6.4 Hz, 2H), 1.90 (m, 1H), 1.64 (m, 1H), 1.48 (m, 2H) ppm. Spectral data agree with a previous literature report.[122]

85** (*minor diastereomer*): ^{1}H NMR ($CDCl_3$, 500 MHz): δ 7.37 (d, *J*=8.6 Hz, 2H), 6.88 (d, *J*=8.6 Hz, 2H), 6.00 (s, 1H), 4.67 (d, *J*=4.3 Hz, 2H), 3.80 (s, 3H), 1.96 (dd, *J*=13.0,

6.2 Hz, 2H), 1.80 (m, 1H), 1.64 (m, 1H), 1.45 (m, 2H) ppm. Spectral data agree with a previous literature report.[122]

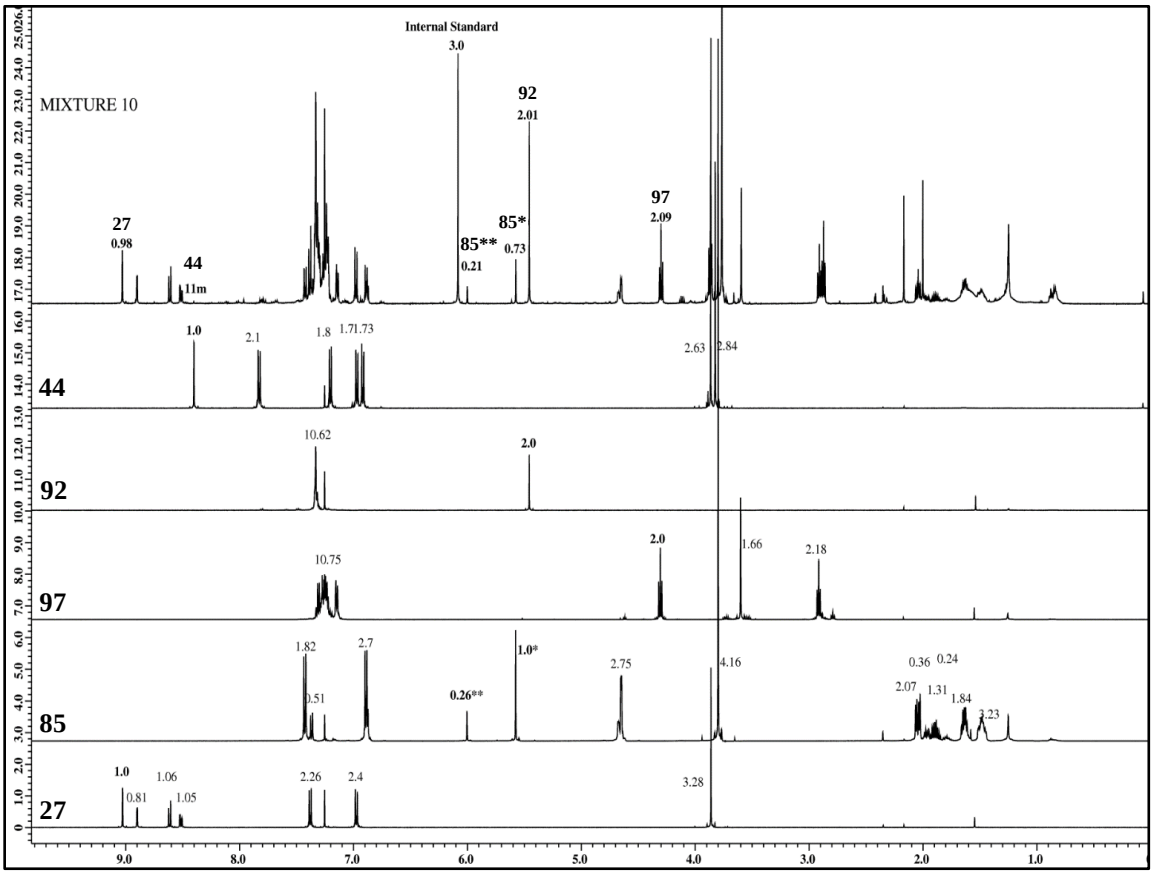

Figure 3.16 ^{1}H NMR spectra of the individual dehydration products and crude reaction mixture #10. For clarity, only the integration of the signature peaks of the observed products is shown in the ^{1}H NMR spectrum of the crude mixture (top).

3.4.3.11 Parallel Reaction #11 (Reaction Set II, Entry 9)

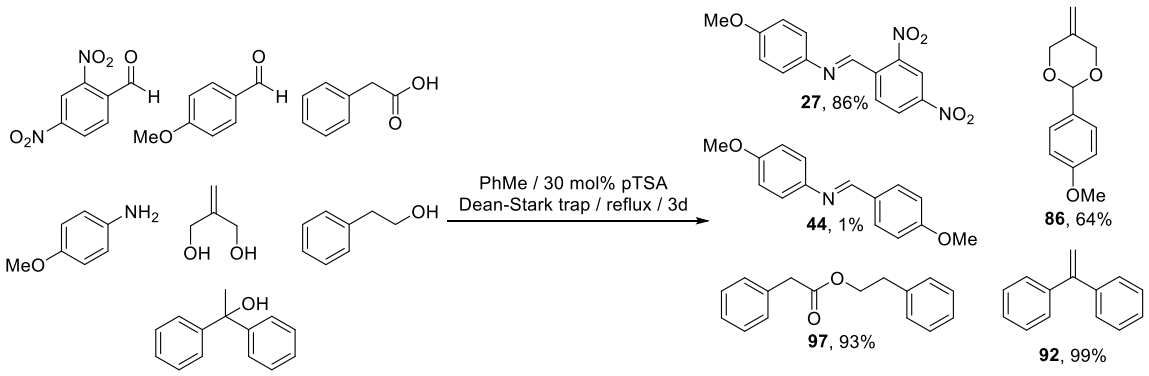

In a round-bottom flask fitted with a reflux condenser and a Dean-Stark adapter, compounds **68a** (62.8 mg, 0.32 mmol), **68d** (38.9 µL, 0.32 mmol), **71a** (43.6 mg, 0.32 mmol), **69a** (39.4 mg, 0.32 mmol), 2-methylene-1,3-propanediol (**73c**, 26.1 µL, 0.32 mmol), **71c** (63.4 mg, 0.32 mmol), **71a** (115 µL, 0.96 mmol) and *p*-toluenesulfonic acid monohydrate (18.3 mg, 0.096 mmol) were dissolved in PhMe (60 mL). The solution was heated to reflux. After 3 d, a 1.0 mL aliquot was taken (temperature of the solution: 85 °C), dried in vacuo and analyzed using ^{1}H NMR with an internal standard (Figure 3.17).

86: ^{1}H NMR ($CDCl_3$, 500 MHz): δ 7.41 (d, J=8.8 Hz, 2H), 6.88 (d, J=8.8 Hz, 2H), 5.57 (s, 1H), 4.99 (s, 2H), 4.50 (d, J=4.8 Hz, 4H), 3.80 (s, 3H) ppm. Spectral data agree with a previous literature report.[123]

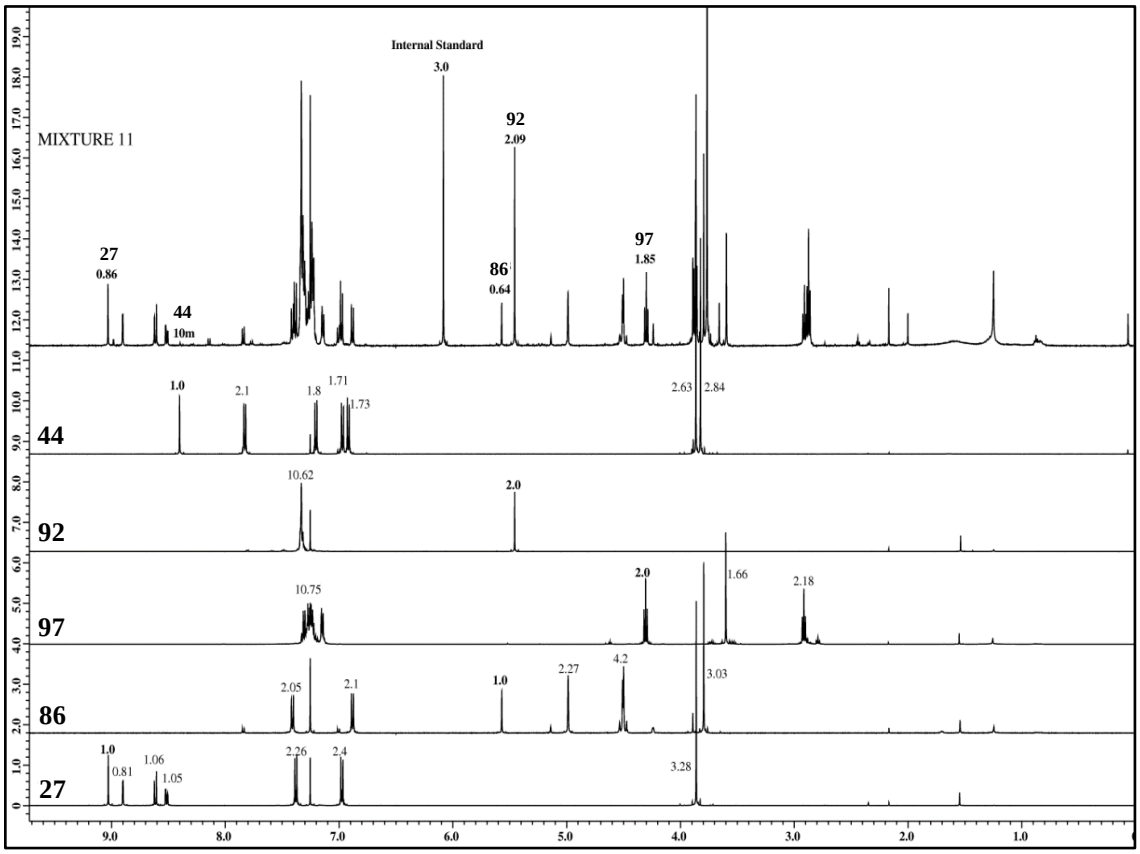

Figure 3.17 ^{1}H NMR spectra of the individual dehydration products and crude reaction mixture #11. For clarity, only the integration of the signature peaks of the observed products is shown in the ^{1}H NMR spectrum of the crude mixture (top).

3.4.3.12 Parallel Reaction #12 (Reaction Set II, Entry 10)

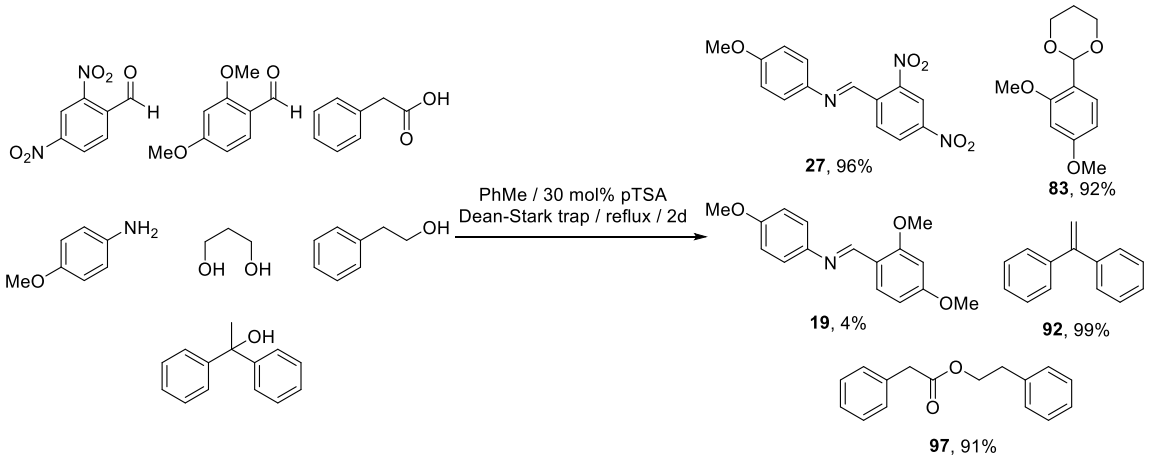

In a round-bottom flask fitted with a reflux condenser and a Dean-Stark adapter, compounds **68a** (62.8 mg, 0.32 mmol), **68c** (53.2 mg, 0.32 mmol), **70a** (43.6 mg, 0.32 mmol), **69a** (39.4 mg, 0.32 mmol), 1,3-propanediol (**73d**, 23.0 µL, 0.32 mmol), **71c** (63.4 mg, 0.32 mmol), **71a** (115 µL, 0.96 mmol), and *p*-toluenesulfonic acid monohydrate (18.3 mg, 0.096 mmol) were dissolved in PhMe (60 mL). The solution was heated to reflux. After 2 d, a 1.0 mL aliquot was taken (temperature of the solution: 85 °C), dried in vacuo and analyzed using ^{1}H NMR with an internal standard (Figure 3.18).

To synthesize 2-(2,4-dimethoxyphenyl)-1,3-dioxane (**83**), **68c** (166 mg, 1.0 mmol), **73d** (91 mg, 86.7 µL, 1.2 mmol), and *p*-toluenesulfonic acid monohydrate (10 mg) were dissolved in PhMe (10 mL). Anhydrous $MgSO_4$ is added to the solution then stirred under nitrogen for 12 h at 80 °C. The solution was cooled to room temperature, washed twice with saturated $NaHCO_3$ (2×15 mL), followed by brine and dried over anhydrous $MgSO_4$. The solution was dried in vacuo and the crude product was passed

thru a short basic alumina column eluted by hexane then 10% EA in hexane to give **83** as a clear oil (95 mg, 42%).

83: IR (neat): 2957, 2842, 1615, 1511, 1266, 1124, 1095, 1033, 982 cm^{-1}. ^{1}H NMR ($CDCl_3$, 500 MHz): δ 7.52 (d, J=8.5 Hz, 1H), 6.50 (dd, J=8.5, 2.5 Hz, 1H), 6.42 (d, J=2.5 Hz, 1H), 5.79 (s, 1H), 4.23 (ddd, J=11.4, 5.3, 1.0 Hz, 2H), 3.98 (td, J=12.0, 2.5 Hz, 2H), 3.80 (s, 3H), 3.78 (s, 3H), 2.21 (m, 1H), 1.40 (dt, J=13.0, 1.0 Hz, 1H) ppm. ^{13}C NMR ($CDCl_3$, 125 MHz): δ 161.3, 157.5, 128.0, 120.0, 104.6, 98.3, 97.0, 67.7, 55.7, 55.5, 26.0 ppm. LRMS (ESI): Calcd for $C_{12}H_{17}O_4^+$: 225.11. Found: 225.00.

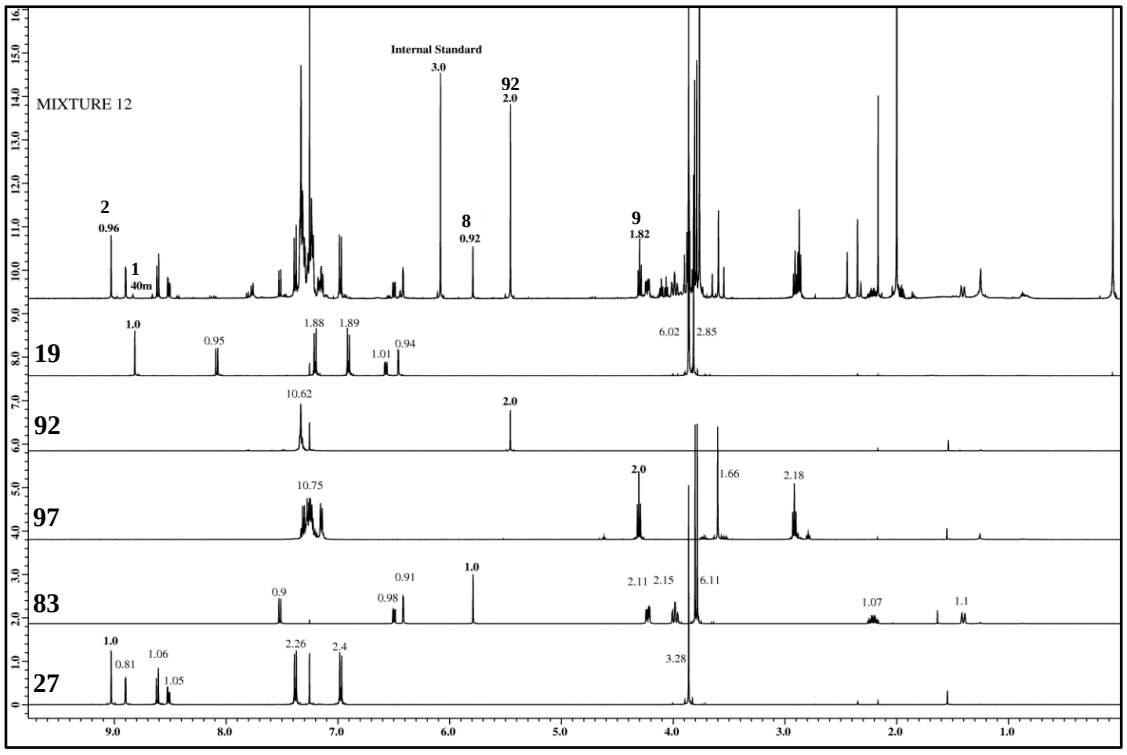

Figure 3.18 ^{1}H NMR spectra of the individual dehydration products and crude reaction mixture #12. For clarity, only the integration of the signature peaks of the observed products is shown in the ^{1}H NMR spectrum of the crude mixture (top).

3.4.3.13 Parallel Reaction #13 (Reaction Set II, Entry 11)

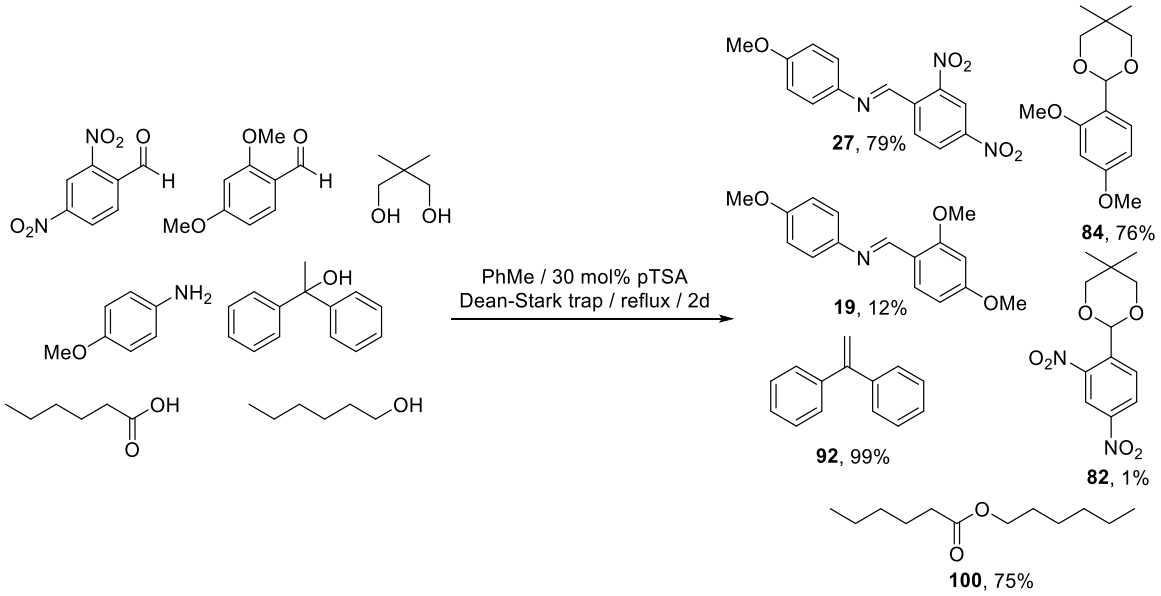

In a round-bottom flask fitted with a reflux condenser and a Dean-Stark adapter, compounds **68a** (62.8 mg, 0.32 mmol), **68c** (53.2 mg, 0.32 mmol), hexanoic acid (**70b**, 40.1 µL, 0.32 mmol), **69a** (39.4 mg, 0.32 mmol), **73a** (33.3 mg, 0.32 mmol), **71c** (63.4 mg, 0.32 mmol), 1-hexanol (**71b**, 120.5 µL, 0.96 mmol), and *p*-toluenesulfonic acid monohydrate (18.3 mg, 0.096 mmol) were dissolved in PhMe (60 mL). The solution was heated to reflux. After 2 d, a 1.0 mL aliquot was taken (temperature of the solution: 85 °C), dried in vacuo and analyzed using ^{1}H NMR with an internal standard (Figure 3.19).

100: ^{1}H NMR ($CDCl_3$, 500 MHz): δ 4.04 (t, J=7.0 Hz, 2H), 2.27 (t, J=7.3 Hz, 2H), 1.57–1.63 (m, 4H), 1.29 (m, 10H), 0.86–0.89 (m, 6H) ppm. Spectral data agree with a previous literature report.[124]

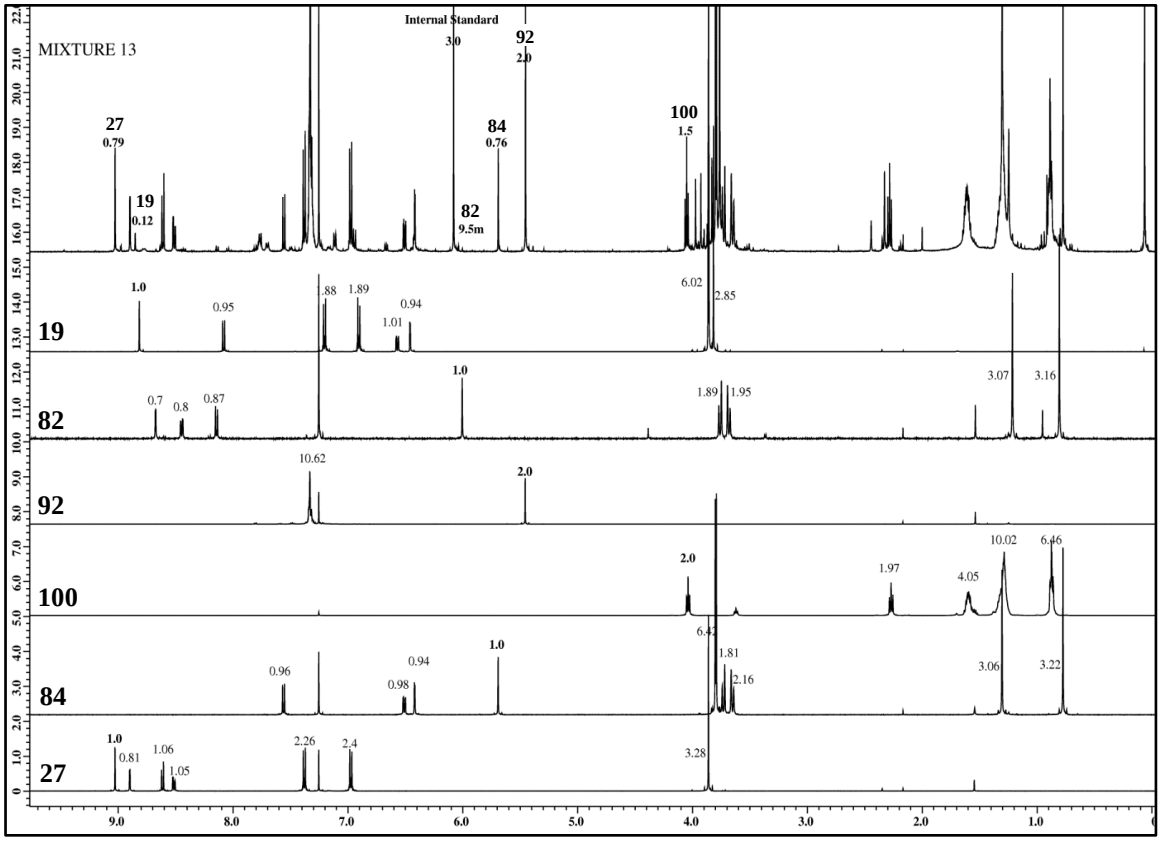

Figure 3.19 ^{1}H NMR spectra of the individual dehydration products and crude reaction mixture #13. For clarity, only the integration of the signature peaks of the observed products is shown in the ^{1}H NMR spectrum of the crude mixture (top).

3.4.3.14 Parallel Reaction #14 (Reaction Set II, Entry 12)

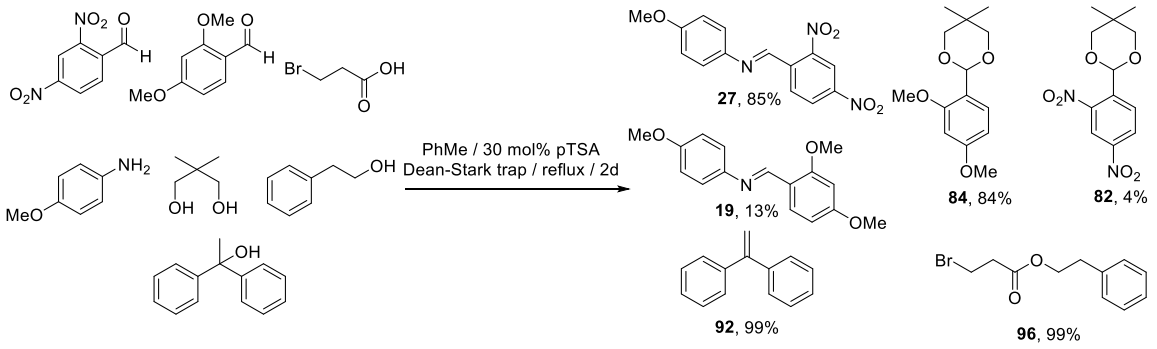

In a round-bottom flask fitted with a reflux condenser and a Dean-Stark adapter, compounds **68a** (62.8 mg, 0.32 mmol), **68c** (53.2 mg, 0.32 mmol), 3-bromopropionic acid (**70c**, 49.0 mg, 0.32 mmol), **69a** (39.4 mg, 0.32 mmol), **73a** (33.3 mg, 0.32 mmol), **71c** (63.4 mg, 0.32 mmol), **71a** (115 µL, 0.96 mmol), and *p*-toluenesulfonic acid monohydrate (18.3 mg, 0.096 mmol) were dissolved in PhMe (60 mL). The solution was heated to reflux. After 2 d, a 1.0 mL aliquot was taken (temperature of the solution: 85 °C), dried in vacuo and analyzed using ^{1}H NMR with an internal standard (Figure 3.20).

To synthesize phenethyl-3-bromopropanoate (**96**), **70c** (153 mg, 1.0 mmol), **71a** (122 mg, 120 µL, 1.0 mmol) and *p*-toluenesulfonic acid monohydrate (10 mg) were dissolved in PhMe (10 mL), and heated at reflux under nitrogen with Dean-Stark trap for 24 h. The solution was dried in vacuo to give the crude product **96**, as pale yellow oil (154 mg, 60%). This compound readily loses HBr upon work-up and thus was analyzed as crude.

96: IR (neat): 2957, 1733, 1232, 1173, 1131, 748, 699 cm^{-1}. ^{1}H NMR ($CDCl_3$, 500 MHz): δ 7.21–7.32 (m, 5H), 4.35 (t, *J*=7.0 Hz, 2H), 3.54 (t, *J*=7.0 Hz, 2H), 2.96 (t, *J*=7.0

Hz, 2H), 2.90 (t, *J*=7.0 Hz, 2H) ppm. ^{13}C NMR ($CDCl_3$, 125 MHz): δ 170.6, 137.6, 129.0, 128.6, 126.7, 65.6, 37.8, 35.1, 25.9 ppm. HRMS (CI): Calcd for $C_{11}H_{14}BrO_2^+$: 257.0177. Found: 257.0178.

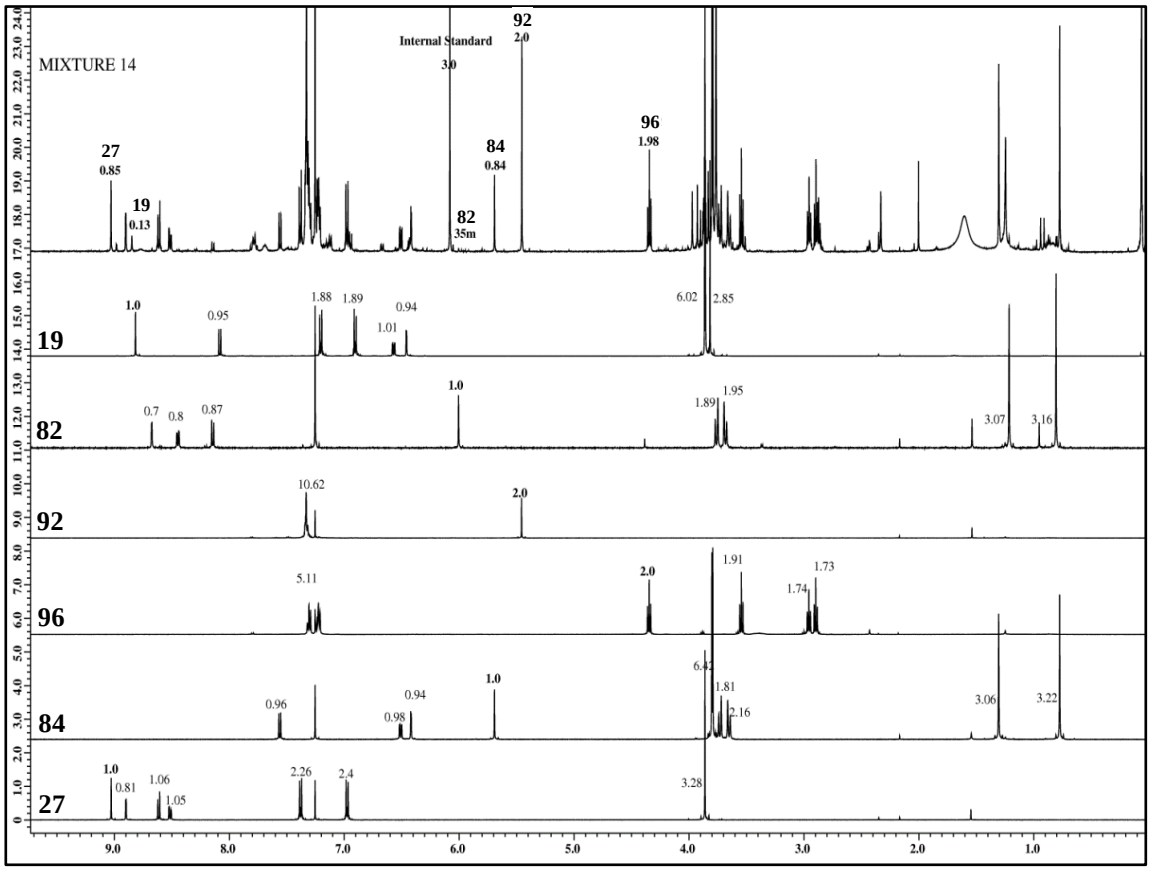

Figure 3.20 ^{1}H NMR spectra of the individual dehydration products and crude reaction mixture #14. For clarity, only the integration of the signature peaks of the observed products is shown in the ^{1}H NMR spectrum of the crude mixture (top).

3.4.3.15 Parallel Reaction #15 (Reaction Set II, Entry 13)

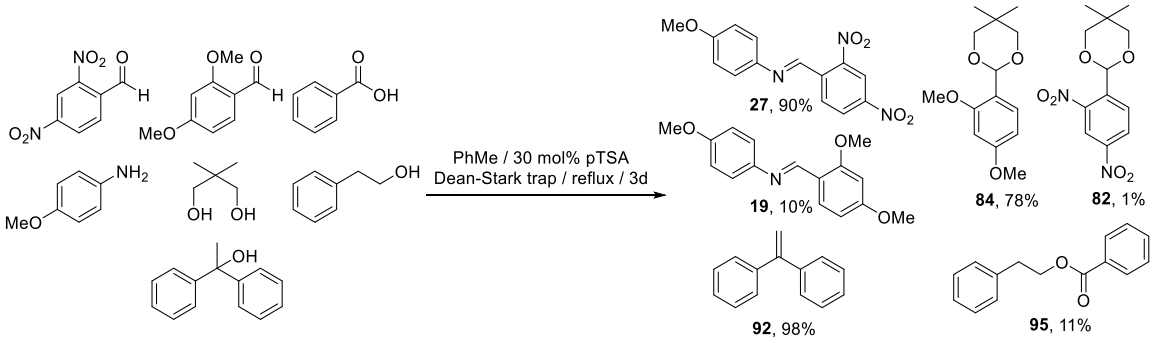

In a round-bottom flask fitted with a reflux condenser and a Dean-Stark adapter, compounds **68a** (62.8 mg, 0.32 mmol), **68c** (53.2 mg, 0.32 mmol), benzoic acid (**70d**, 39.1 mg, 0.32 mmol), **69a** (39.4 mg, 0.32 mmol), **73a** (33.3 mg, 0.32 mmol), **71c** (63.4 mg, 0.32 mmol), **71a** (115 µL, 0.96 mmol), and *p*-toluenesulfonic acid monohydrate (18.3 mg, 0.096 mmol) were dissolved in PhMe (60 mL). The solution was heated to reflux. After 3 d, a 1.0 mL aliquot was taken (temperature of the solution: 85 °C), dried in vacuo and analyzed using ^{1}H NMR with an internal standard (Figure 3.21).

95: ^{1}H NMR ($CDCl_3$, 500 MHz): δ 8.10 (d, J=7.6 Hz, 2H), 7.59 (t, J=7.6 Hz, 1H), 7.47 (t, J=7.6 Hz, 2H), 7.26–7.38 (m, 5H), 4.59 (t, J=7.0 Hz, 2H), 3.13 (t, J=7.0 Hz, 2H) ppm. Spectral data agree with a previous literature report.[125]

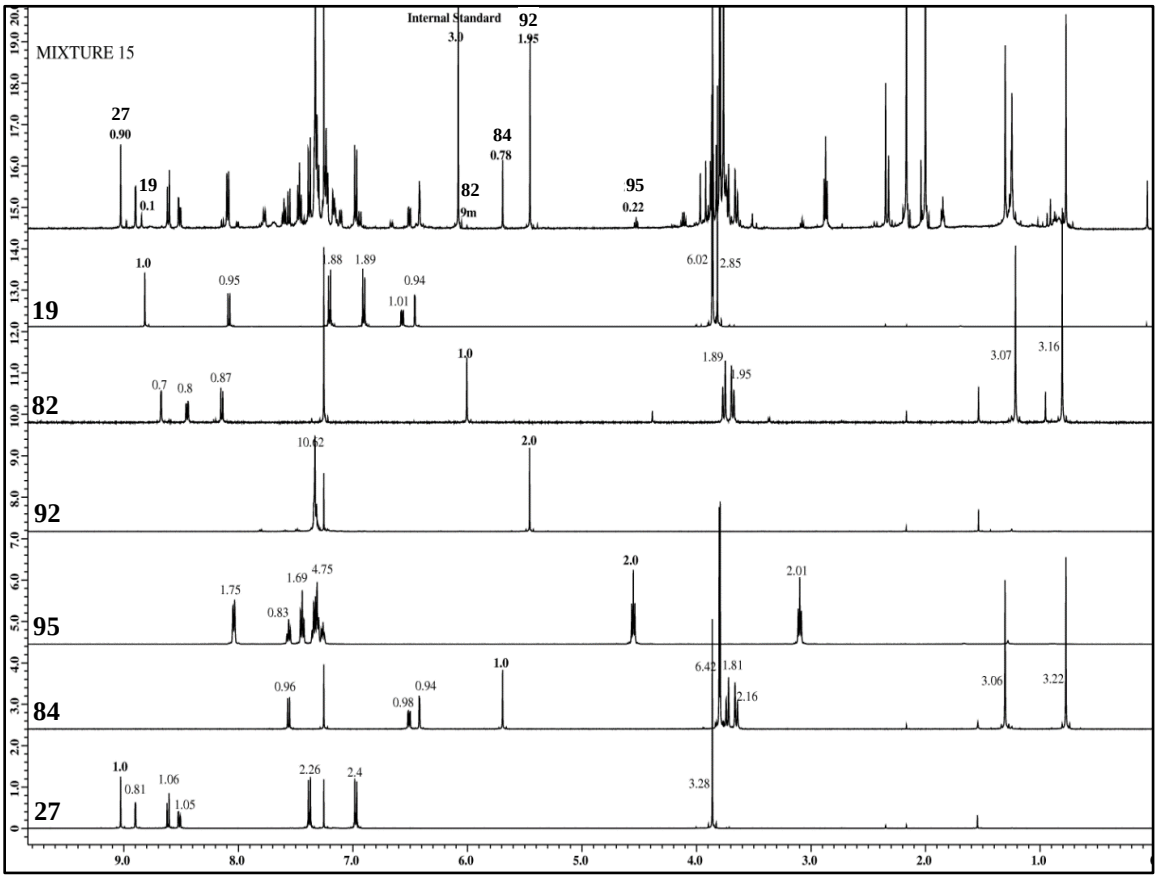

Figure 3.21 ^{1}H NMR spectra of the individual dehydration products and crude reaction mixture #15. For clarity, only the integration of the signature peaks of the observed products is shown in the ^{1}H NMR spectrum of the crude mixture (top).

3.4.3.16 Parallel Reaction #16 (Reaction Set III, Entry 1)

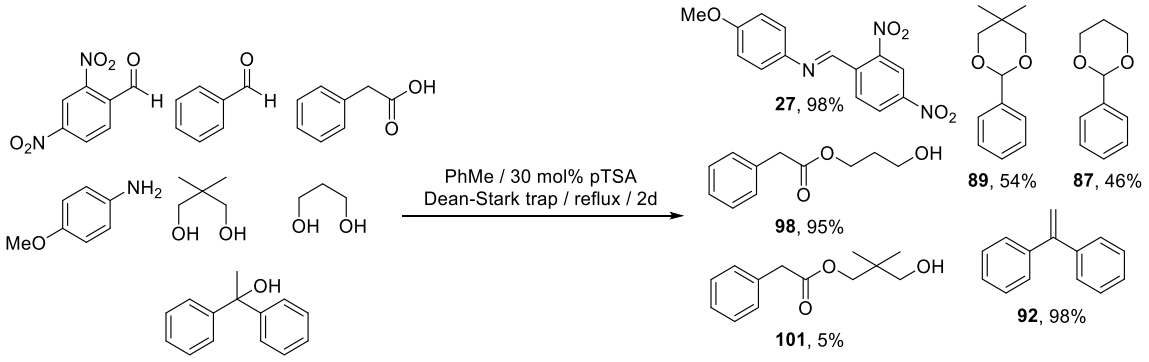

In a round-bottom flask fitted with a reflux condenser and a Dean-Stark adapter, compounds **68a** (62.8 mg, 0.32 mmol), **68e** (32.5 µL, 0.32 mmol), **70a** (43.6 mg, 0.32 mmol), **69a** (39.4 mg, 0.32 mmol), **73a** (33.3 mg, 0.32 mmol), **71c** (63.4 mg, 0.32 mmol), **73d** (69.4 µL, 0.96 mmol), and *p*-toluenesulfonic acid monohydrate (18.3 mg, 0.096 mmol) were dissolved in PhMe (60 mL). The solution was heated to reflux. After 2 d, a 1.0 mL aliquot was taken (temperature of the solution: 85 °C), dried in vacuo and analyzed using ^{1}H NMR with an internal standard (Figure 3.22).

87: ^{1}H NMR ($CDCl_3$, 500 MHz): δ 7.49 (dd, *J*=8.1, 1.4 Hz, 2H), 7.33–7.39 (m, 3H), 5.51 (s, 1H), 4.27 (ddd, *J*=11.5, 5.2, 1.2 Hz, 2H), 3.99 (td, *J*=12.6, 2.3 Hz, 2H), 2.19–2.27 (m, 1H), 1.44 (m, 1H) ppm. Spectral data agree with a previous literature report.[111]

98: ^{1}H NMR ($CDCl_3$, 500 MHz): δ 7.27–7.34 (m, 5H), 4.25 (t, *J*=6.0 Hz, 2H), 3.63 (s, 2H), 3.62 (q, *J*=5.9 Hz, 1H), 2.17 (s, 1H), 1.85 (quin, *J*=5.9 Hz, 2H), 1.67 (t, *J*=5.9 Hz, 1H) ppm. Spectral data agree with a previous literature report.[126]

To synthesize 3-hydroxy-2,2-dimethylpropyl-2-phenylacetate (**101**), **70a** (136.15 mg, 1 mmol), **73a** (417 mg, 4.0 mmol), and *p*-toluenesulfonic acid monohydrate (10 mg) were placed in a thick-walled microwave pressure vial and dissolved in PhMe (10mL). Molecular sieves (4 Å) were added and the resulting mixture was sealed and exposed to microwave irradiation for 1 h at 170 °C. After cooling, the solution was washed twice with saturated $NaHCO_3$ (2×15 mL), followed by brine and dried over anhydrous $MgSO_4$. The solvent was removed in vacuo and passed thru a short basic alumina column eluted by hexane then 10% EA in hexane to give **101** as clear oil (120 mg, 54%).

101: IR (neat): 3436, 2961, 2875, 1729, 1371, 1255, 1006, 696 cm^{-1}. ^1H NMR ($CDCl_3$, 500 MHz): δ 7.25–7.34 (m, 5H), 3.94 (s, 1H), 3.65 (s, 1H), 3.19 (d, J=7.0 Hz, 1H), 0.85 (s, 6H) ppm. ^{13}C NMR (125 MHz, $CDCl_3$): δ 172.4, 134.0, 129.3, 128.7, 127.3, 69.9, 68.3, 41.6, 36.6, 21.5 ppm. LRMS (ESI): Calcd for $C_{13}H_{19}O_3^+$: 223.13. Found: 222.86.

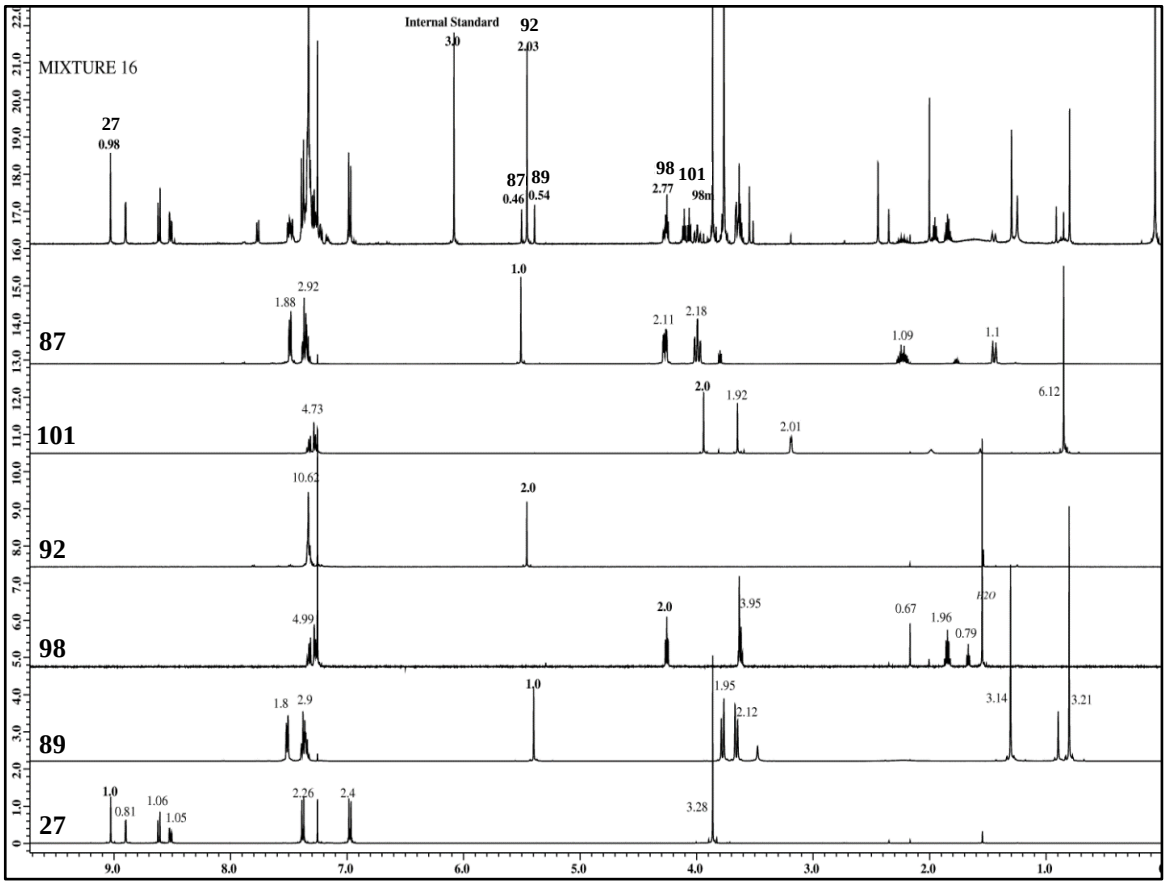

Figure 3.22 ^{1}H NMR spectra of the individual dehydration products and crude reaction mixture #16. For clarity, only the integration of the signature peaks of the observed products is shown in the ^{1}H NMR spectrum of the crude mixture (top).

3.4.3.17 Parallel Reaction #17 (Reaction Set III, Entry 2)

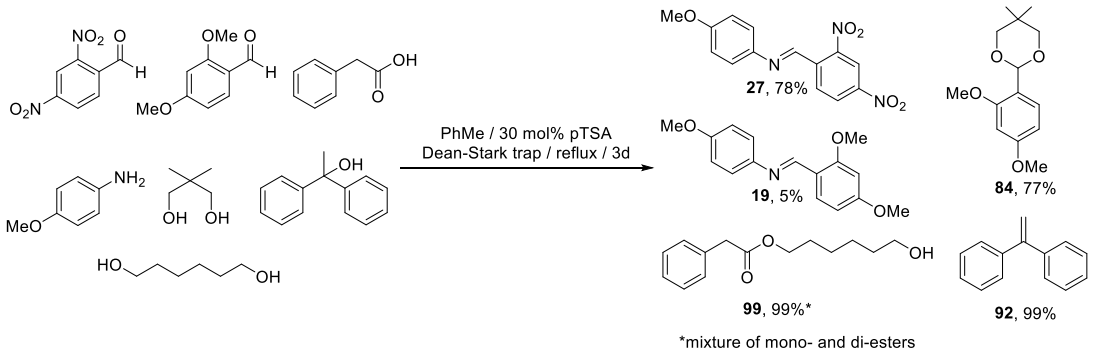

In a round-bottom flask fitted with a reflux condenser and a Dean-Stark adapter, compounds **68a** (62.8 mg, 0.32 mmol), **68c** (53.2 mg, 0.32 mmol), **70a** (43.6 mg, 0.32 mmol), **69a** (39.4 mg, 0.32 mmol), **73a** (33.3 mg, 0.32 mmol), **71c** (63.4 mg, 0.32 mmol), 1,6-hexanediol (**71b**, 113.4 mg, 0.96 mmol), and *p*-toluenesulfonic acid monohydrate (18.3 mg, 0.096 mmol) were dissolved in PhMe (60 mL). The solution was heated to reflux. After 3 d, a 1.0 mL aliquot was taken (temperature of the solution: 85 °C), dried in vacuo and analyzed using ^{1}H NMR with an internal standard (Figure 3.23)

99: ^{1}H NMR ($CDCl_3$, 500 MHz): δ 7.27–7.33 (m, 5H), 4.08 (t, *J*=6.8 Hz, 2H), 3.62 (t, *J*=6.8 Hz, 2H), 3.61 (s, 2H), 1.59–1.65 (m, 2H), 1.51–1.57 (m, 2H), 1.33–1.34 (m, 4H), 1.22 (t, *J*=5.4 Hz, 1H) ppm. Spectral data agree with a previous literature report.[112]

102: ^{1}H NMR ($CDCl_3$, 500 MHz): δ 7.24–7.33 (m, 10H), 4.06 (t, *J*=6.8 Hz, 4H), 3.61 (s, 4H), 1.55–1.61 (m, 4H), 1.27–1.30 (m, 4H) ppm. Spectral data agree with a previous literature report.[112]

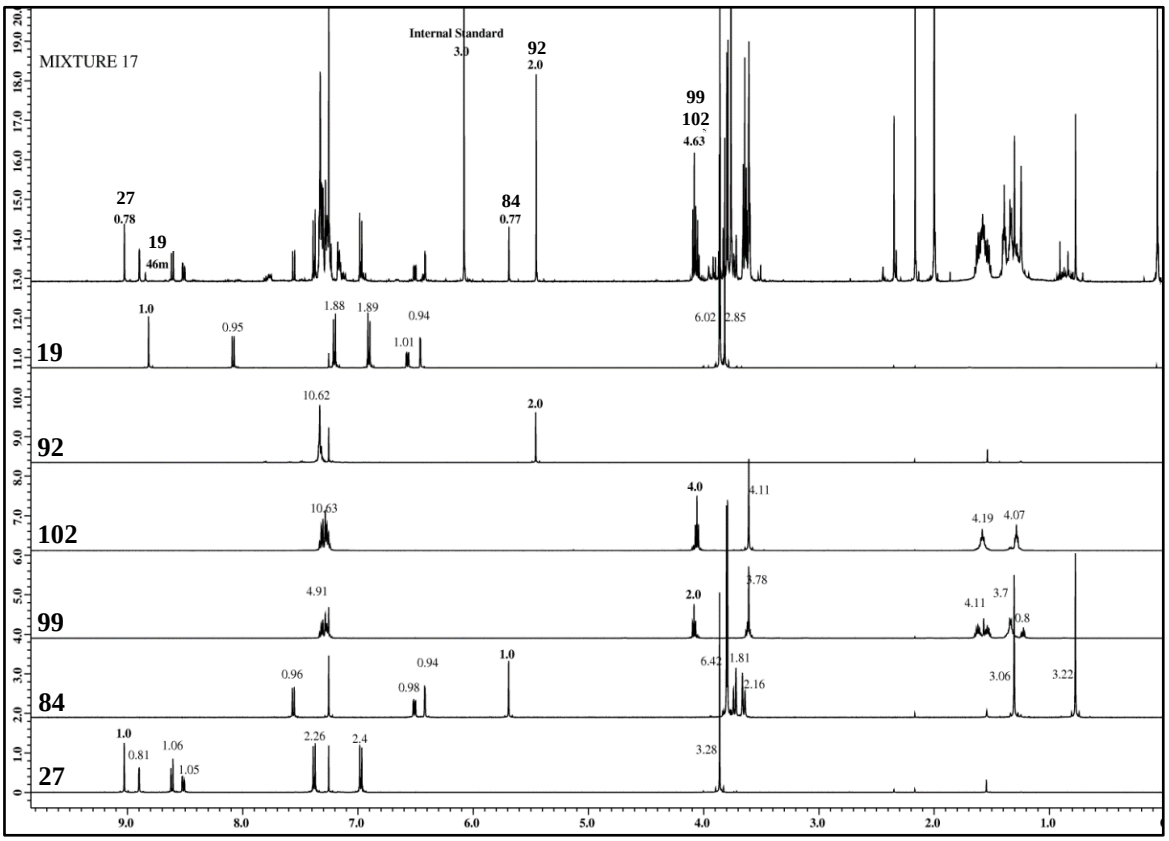

Figure 3.23 ^{1}H NMR spectra of the individual dehydration products and crude reaction mixture #17. For clarity, only the integration of the signature peaks of the observed products is shown in the ^{1}H NMR spectrum of the crude mixture (top).

3.4.4 Synthesis of Other Plausible Dehydration Products

4-Chloro-*N*-(2,4-dimethoxybenzylidene)aniline (76). Synthesized by dissolving **68c** (166.17 mg, 1.0 mmol) and **69d** (127.6mg, 1.0 mmol) in PhMe (10 mL). The solution was stirred under nitrogen for 12 h at 80 °C. The solvent was removed in vacuo to give **76** as a white solid in quantitative yield.

76: mp: 73.5–74.5 °C. IR (neat): 2947, 1608, 1583, 1291, 1275, 1159, 1029, 819 cm^{-1}. ^{1}H NMR ($CDCl_3$, 500 MHz): δ 8.77 (s, 1H), 8.08 (d, *J*=8.6 Hz, 1H), 7.31 (d, *J*=8.7 Hz, 2H), 7.13, (d, *J*=8.6 Hz, 2H), 6.58 (dd, *J*=8.7, 2.3 Hz, 1H), 6.46 (d, *J*=2.2 Hz, 1H), 3.87 (s, 3H), 3.86 (s, 3H) ppm. ^{13}C NMR ($CDCl_3$, 125 MHz): δ 164.0, 161.1, 156.4, 151.6, 130.8, 129.1, 129.0, 122.5, 118.0, 105.8, 98.1, 55.6 ppm. LRMS (ESI): Calcd for $C_{15}H_{15}ClNO_2^+$: 276.08. Found: 276.17.

2-(2,4-dinitrophenyl)-5-methylene-1,3-dioxane (79). Synthesized by dissolving **68a** (196.12 mg, 1.0 mmol), **73c** (88.11 mg, 81.5 µL, 1.0 mmol), and *p*-toluenesulfonic acid monohydrate (10 mg) in PhMe (10 mL). The solution was stirred under nitrogen for 12–24 h at 80 °C. The solution was cooled to room temperature, washed twice with saturated $NaHCO_3$ (2×15 mL), followed by brine and dried over anhydrous $MgSO_4$. The solution was dried in vacuo and passed through a short basic alumina column eluted by 100% hexane, then 10% EA in hexane to give **79** as a yellow solid (81 mg, 30%).

79: mp: 84–86 °C. IR (neat): 2922, 2852, 1533, 1450, 1387, 1345, 1020, 828, 726 cm^{-1}. ^{1}H NMR ($CDCl_3$, 500 MHz): δ 8.69 (d, *J*=2.3 Hz, 1H), 8.44 (dd, *J*=8.6, 2.3 Hz, 1H), 8.11 (d, *J*=8.6 Hz, 1H), 6.24 (s, 1H), 5.03 (s, 2H), 4.56 (d, *J*=13.0 Hz, 2H) 4.50 (d, *J*=13.0 Hz,

2H) ppm. ^{13}C NMR ($CDCl_3$, 125 MHz): δ 148.5, 148.0, 138.0, 137.3, 129.6, 126.9, 119.8, 112.1, 95.8, 71.6 ppm. LRMS (APCI): Calcd for $C_{11}H_9N_2O_6^-$: 265.05. Found: 265.96.

2-(2,4-dinitrophenyl)tetrahydro-3H-cyclopenta[1,3]dioxole (80). Synthesized by dissolving **68a** (196.12 mg, 1.0 mmol), **73b** (102.13 mg, 1.0 mmol), and *p*-toluenesulfonic acid monohydrate (10 mg) in PhMe (10 mL). The solution was stirred under nitrogen for 12–24 h at 80 °C. The solution was cooled to room temperature, washed twice with saturated $NaHCO_3$ (2×15 mL), followed by brine and dried over anhydrous $MgSO_4$. The solvent was removed in vacuo and passed through a short basic alumina column eluted by 100% hexane, 5% EA in hexane, then 10% EA in hexane to give **80** as light-yellow solid (107 mg, 38%).

80: mp: 89–91 °C. IR (neat): 2962, 1530, 1381, 1347, 1328, 1019, 726, 704 cm^{-1}. ^{1}H NMR ($CDCl_3$, 500 MHz): δ 8.73 (d, *J*=2.3 Hz, 1H), 8.46 (dd, *J*=8.6, 2.3 Hz, 1H), 8.17 (d, *J*=8.6 Hz, 1H), 6.19 (s, 1H), 4.74 (dd, *J*=3.4, 1.2 Hz, 2H) 1.98 (dt, *J*=15.5, 2.8 Hz, 2H), 1.60 (m, 2H), 1.50 (m, 2H) ppm. ^{13}C NMR ($CDCl_3$, 125 MHz): δ 148.9, 148.1, 138.1, 129.8, 127.3, 119.8, 97.5, 82.7, 33.1, 22.5 ppm. LRMS (APCI): Calcd for $C_{12}H_{11}N_2O_6^-$: 279.06. Found: 279.97.

2-(2,4-dinitrophenyl)-1,3-dioxane (81): Synthesized by dissolving **68a** (196.12 mg, 1.0 mmol), **73d** (91.3 mg, 86.7 µL, 1.2 mmol), and *p*-toluenesulfonic acid monohydrate (10 mg) in PhMe (10 mL). The solution was stirred under nitrogen for 12 h at 80 °C. The solution was cooled to room temperature, washed twice with saturated $NaHCO_3$ (2×15

mL), followed by brine and dried over anhydrous $MgSO_4$. The solvent was removed in vacuo and passed through a short basic alumina column eluted by hexane then 10% EA in hexane to give 81 as a white solid (214 mg, 84%).

81: mp: 78–81 °C. IR (neat): 2870, 1533, 1349, 1094, 1023, 741, 717 cm^{-1}. ^1H NMR ($CDCl_3$, 500 MHz): δ 8.66 (d, *J*=2.3 Hz, 1H), 8.43 (dd, *J*=8.6, 2.3 Hz, 1H), 8.10 (d, *J*=8.6 Hz, 1H), 6.11 (s, 1H), 4.25 (ddd, *J*=11.4, 5.1, 1.1 Hz, 2H), 4.02 (td, *J*=12.6, 2.7 Hz, 2H), 2.19 (m, 1H), 1.48 (d, *J*=13.7 Hz, 1H) ppm. ^{13}C NMR ($CDCl_3$, 125 MHz): δ 148.5, 147.9, 138.6, 129.6, 126.8, 119.7, 96.2, 67.8, 25.5 ppm. LRMS (APCI): Calcd for $C_{10}H_9N_2O_6^-$: 253.05. Found: 253.95.

Propane-1,3-diyl bis(2-phenylacetate) (103). Synthesized by dissolving **70a** (463 mg, 3.4 mmol), **73d** (129.5 mg, 123 µL, 1.7 mmol), and *p*-toluenesulfonic acid monohydrate (65 mg) were dissolved in PhMe (25 mL) and heated at reflux under nitrogen with Dean-Stark trap for 24 h. The solution was cooled to room temperature, washed twice with saturated $NaHCO_3$ (2×25 mL), followed by brine and dried over anhydrous $MgSO_4$. The solution was dried in vacuo and passed thru a short basic alumina column eluted by hexane then 10% EA in hexane to give **103** as clear oil (258 mg, 49%).

103: IR (neat): 2964, 1730, 1455, 1244, 1135, 1042, 695 cm^{-1}. ^1H NMR ($CDCl_3$, 500 MHz): δ 7.25–7.33 (m, 10H), 4.13 (t, *J*=6.3 Hz, 4H), 3.61 (s, 4H), 1.94 (quin, *J*=6.4 Hz, 2H) ppm. ^{13}C NMR ($CDCl_3$, 125 MHz): δ 170.6, 137.6, 129.0, 128.6, 126.7, 65.5, 37.8, 35.1, 25.8 ppm. LRMS (ESI): Calcd for $C_{19}H_{21}O_4^+$: 313.14. Found: 312.84.

2,2-Dimethylpropane-1,3-diyl bis(2-phenylacetate) (104). Synthesized by mixing **70a**

(544.6 mg, 4 mmol), **73a** (104 mg, 1.0 mmol), and *p*-toluenesulfonic acid monohydrate (10 mg) and PhMe (10 mL) into a thick-walled microwave pressure vial. Molecular sieves (4 Å) were added and the resulting mixture was sealed and exposed to microwave irradiation for 1 h at 170 °C. After cooling, the solution was washed twice with saturated $NaHCO_3$ (2×15 mL), followed by brine and dried over anhydrous $MgSO_4$. The solvent was removed in vacuo and passed through a short basic alumina column eluted by hexane then 10% EA in hexane to give **104** as clear oil (102.4 mg, 30%).

104: IR (neat): 2966, 1731, 1372, 1248, 1135, 1005, 695 cm^{-1}. ^{1}H NMR ($CDCl_3$, 500 MHz): δ 7.23–7.32 (m, 10H), 3.81 (s, 4H), 3.60 (s, 4H), 0.83 (s, 6H) ppm. ^{13}C NMR ($CDCl_3$, 125 MHz): δ 171.5, 134.1, 129.3, 128.7, 127.2, 69.4, 41.5, 34.8, 21.7 ppm. LRMS (ESI): Calcd for $C_{21}H_{25}O_4^+$: 341.17. Found: 340.92.

Chapter Four

Cruciforms as Supramolecular Sensors for Qualitative Identification of Carboxylic Acids, Boronic Acids, and Amines[127]

4.1 Introduction

4.1.1 Supramolecular Analytical Chemistry

Analytical chemistry has played an integral part in the development of the field of supramolecular chemistry. The need to analyze complex systems generated from the noncovalent interactions and weak intermolecular bonding drove the exploration for new analytical techniques that can probe the dynamic features of these supramolecular ensembles. Diffusion nuclear magnetic resonance spectroscopy (DOSY) and mass spectrometry employing soft ionization techniques such as electrospray ionization (ESI) and coldspray ionization (CSI) are two important analytical tools used to achieve this purpose. DOSY experiments can provide hydrodynamic dimensions, which are in turn dependent on both the molecular weight and shape, of chemical species in a complex mixture without the need to separate them. With this information available, important thermodynamic parameters for the supramolecular aggregation processes, such as equilibrium constant (K) and the standard state free energy change ($\Delta G°$), can be calculated.[128,2] On the other hand, the ability of mass spectrometry to detect minute differences in mass allows the simultaneous detection of free components, reaction

[127] Schwaebel, T.; Lirag, R. C.; Davey, E. A.; Lim, J.; Bunz, U. H.; Miljanić, O. Š. *J. Vis. Exp.* **2013**, e50858.

intermediates, wrongly assembled structures and final thermodynamic assemblies which is quite useful in monitoring self-assembly and self-sorting processes.[129]

Better understanding of supramolecular interactions, on the other hand, has contributed to the development of analytical sciences in the past two decades particularly in the understanding of molecular aspects of sensor design, synthesis, and determining binding affinities of the analytes.[130] Anslyn used the term supramolecular analytical chemistry to describe this new discipline at the interface of supramolecular and analytical chemistry.[130–132] Supramolecular analytical chemistry explores the molecular recognition and self-assembly of chemical structures using dynamic interactions that create ensembles which result in signal modulations upon addition of analytes.[132] The different interactions that are utilized in building supramolecular sensors are summarized in Figure 4.1.

A chemical sensor is a device that can selectively respond to a chemical substance of interest, through a physical or chemical interaction, and can be used for qualitative or quantitative determination of analytes.[130,133] It has two basic functional units—*receptor* and *transducer*. The *receptor* is a moiety capable of converting the changes in the chemical composition of the molecular environment into a change in physical or chemical property while the *transducer*, or reporter, transforms and amplifies the perturbed properties into an observable analytical signal output such as a change in color or fluorescence for optical chemical sensors.[130,134] Chemical sensors are typically divided according to the chemical or physical feature employed in the recognition mechanism and operating principle of the transducer. Some common classifications are (*a*) optical

sensors—analyte binding is associated with a change in the optical property of sensors *e.g.* absorbance and emission, (*b*) electrochemical—binding of the analyte induces changes in current or potential, and (*c*) electrical—analyte-sensor interaction results in changes in conductivity, resistivity or permittivity.[130,134] This chapter will focus on the discussion on the contribution of supramolecular analytical chemistry on the development of optical chemical sensing.

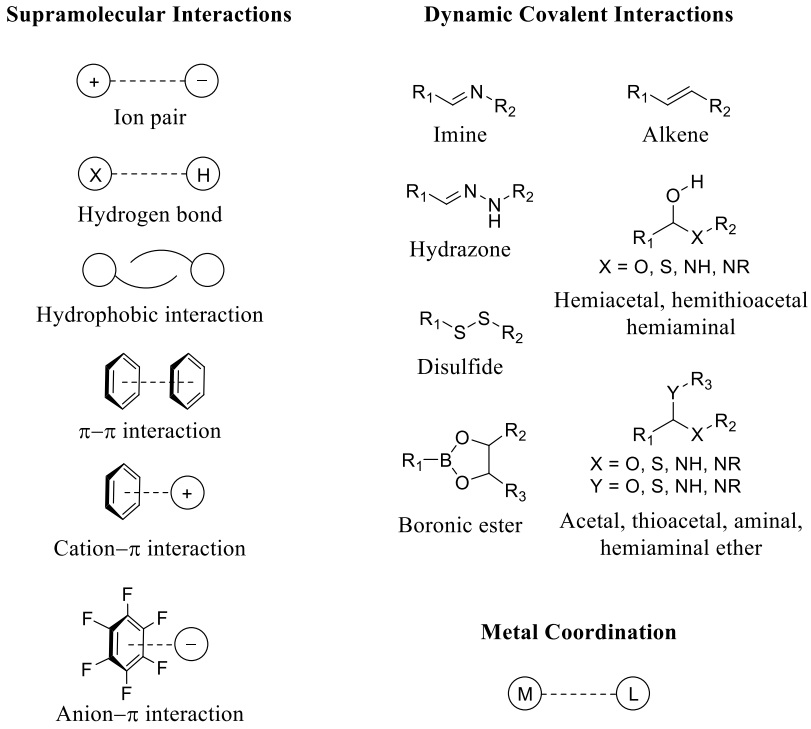

Figure 4.1 Important noncovalent and reversible covalent interactions used in the emerging field of supramolecular analytical chemistry.[132]

4.1.2 Indicator Displacement Assay (IDA) and Differential Sensing

In the conventional design of optical chemical sensors intended for direct sensing of particular analyte(s), the reporter unit can either be (*a*) directly connected to the

receptor unit and the two units are part of the conjugated π system of the chromophore or (*b*) covalently attached to the receptor unit through a short spacer (Figure 4.2). The latter is usually referred to as the receptor–spacer–reporter approach.[132] The selectivity of chemical sensors is achieved by using the "lock-and-key" design, wherein a specific receptor is synthesized in order to strongly and selectively bind the analyte of interest. When the analyte binds to the receptor, a corresponding change in the optical property will be observed—the absorbance or emission intensity of the analyte–sensor complex may increase ("turn-on" sensors) or be quenched ("turn-off" sensors) that signals the binding event. Some examples of "turn-on" and turn-off sensors are shown in Figure 4.2.

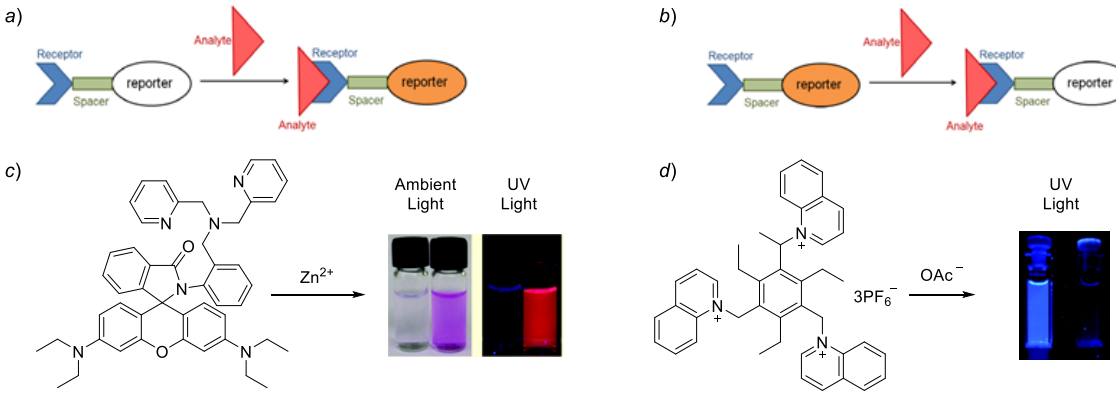

Figure 4.2 Schematic representations for receptor–spacer–reporter structures for "turn-on" (*a*) and "turn-off" (*b*) chemical sensor. (*c*) Turn-on colorimetric and red fluorescent sensor for Zn^{2+} reported by Lippard's group.[135] (*d*) Turn-off fluorescent sensor for acetate from Steed's group.[136] For the pairs of vials—the left vial contains only the sensor and the right vial contains both the sensor and the analyte.

Chemical sensors based on the lock-and-key paradigm are generally designed for specific targets, where every aspect of the receptor is tailored to complement the structure

of the intended analyte. Thus, the first major disadvantage of this approach is the need for a dedicated, and often laborious syntheses.[2] Second, it is difficult to design recognition sites for large analytes, such as peptides or carbohydrates, since the bigger the analyte, the higher the number of degrees of freedom it possesses. Finally, sensors designed for direct sensing of analytes would encounter complications, when used in complex mixtures, arising from competing interactions with species that are structurally similar to its intended analyte. Therefore, single analyte sensor is less effective for the qualitative and quantitative analysis of "real" samples such as food, perfume, or pharmaceutical products.[137] This apparent limitation of direct analyte sensing is complemented by a well-established approach in supramolecular chemistry: the indicator displacement assay (IDA)—a sensing technique that makes use of competitive binding between a series of guests and a host (or receptor).[132]

IDA is based on the competition between an indicator and an analyte for the binding site. An indicator is allowed to bind to a receptor, and then be displaced upon the introduction of an analyte. Normally, the free and bound indicators have different colorimetric or fluorescent properties, causing a signal change upon displacement. The major requirement for an IDA with an acceptable sensitivity is that the binding affinity of the analyte to the receptor is comparable to that of the indicator to the receptor. The interactions between the indicator, analyte, and the receptor can either be covalent or noncovalent. Reversible covalent bonds that have been used for IDA includes boronate ester[138–140] and imine formation.[141] On the other hand, the common noncovalent interactions exploited by IDAs are electrostatic interaction and cation–π interaction,[142]

hydrogen bonding,[143] and metal complexation.[144–146] Some examples of IDAs are presented in Figure 4.3.

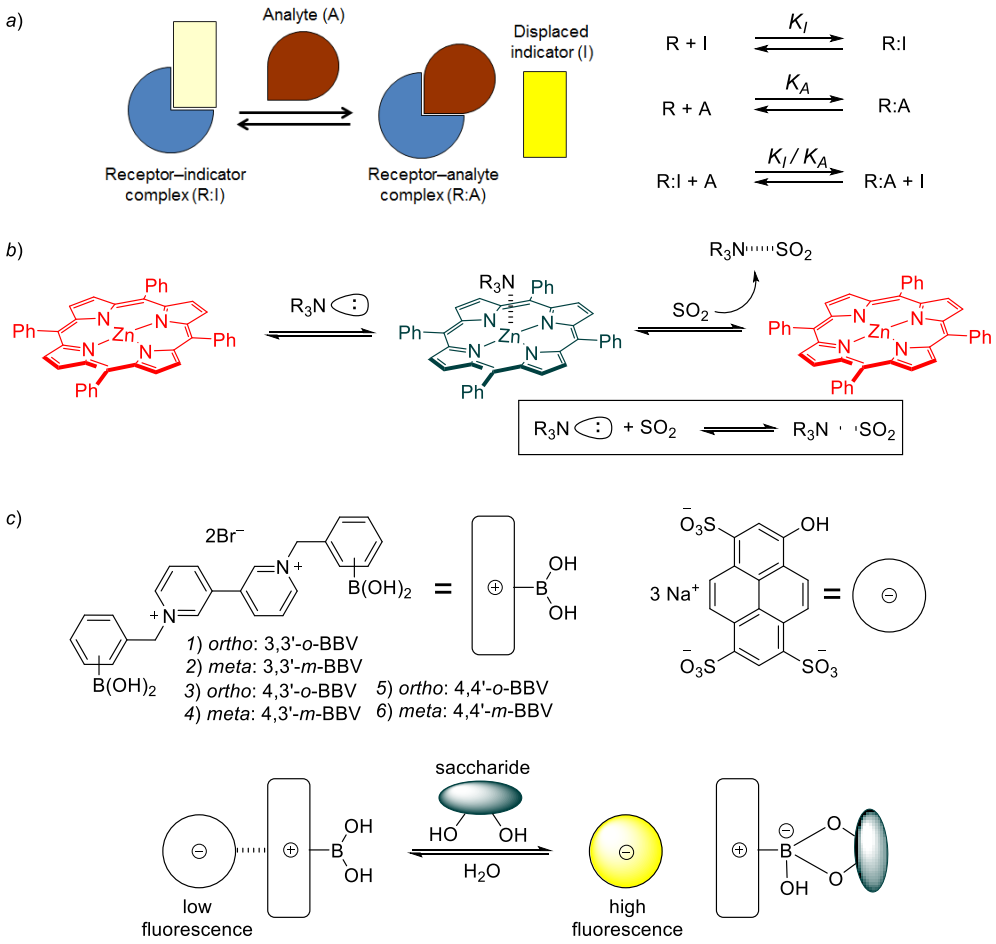

Figure 4.3 (*a*) Schematic representation of IDA. (*b*) IDA based on noncovalent nucleophilic coordination between amines and metallophorphyrin for visual detection of SO_2.[146] (*c*) IDA based on reversible boronate ester formation of an ensemble of six cationic bisboronic acid appended benzyl viologens and an anionic fluorescent dye, for saccharide sensing.[140]

The use of IDA offers several advantages.[2] First, since the indicator is not covalently tethered to the sensor, the need for an elaborate synthesis is eliminated. Second, a broad range of receptor–indicator combinations are (commercially) available; and the best pair that can give the most sensitive and selective assay can be conveniently chosen. Third, IDA can be accomplished in both aqueous and organic media. Thus, the binding constant of the indicator or dye can be appropriately adjusted by modifying the solvent system. Lastly, IDA can be easily coupled with different platforms for quick analysis on a *e.g.* plate reader, flow injection analysis (FIA) or designed to be incorporated in differential sensing arrays.[140]

The most obvious definition of differential sensing comes from the fact that the output signal from each sensor element after analyte application is directly compared to the output of the same element before analyte application. The difference obtained is then used in the processing, evaluation, and analyte identification using pattern recognition protocols[130] such as principal component analysis (PCA) and hierarchical clustering analysis (HCA),[147] linear discriminant analysis (LDA),[148] or the use of artificial neural network (ANN).[149] Additionally, Anslyn[132,150] compared differential sensing to a binding scenario used in the mammalian senses of taste and smell—where the receptors are generalized rather than specialized. Just as a particular smell is recognized by the brain based on a pattern arising from the simultaneous analysis of multiple components of an odorant by potentially thousands of different sensory neurons (olfactory cells), differential (array) sensing discriminates and identifies analytes and complex mixtures from the resulting response patterns of individual receptors with the analytes.

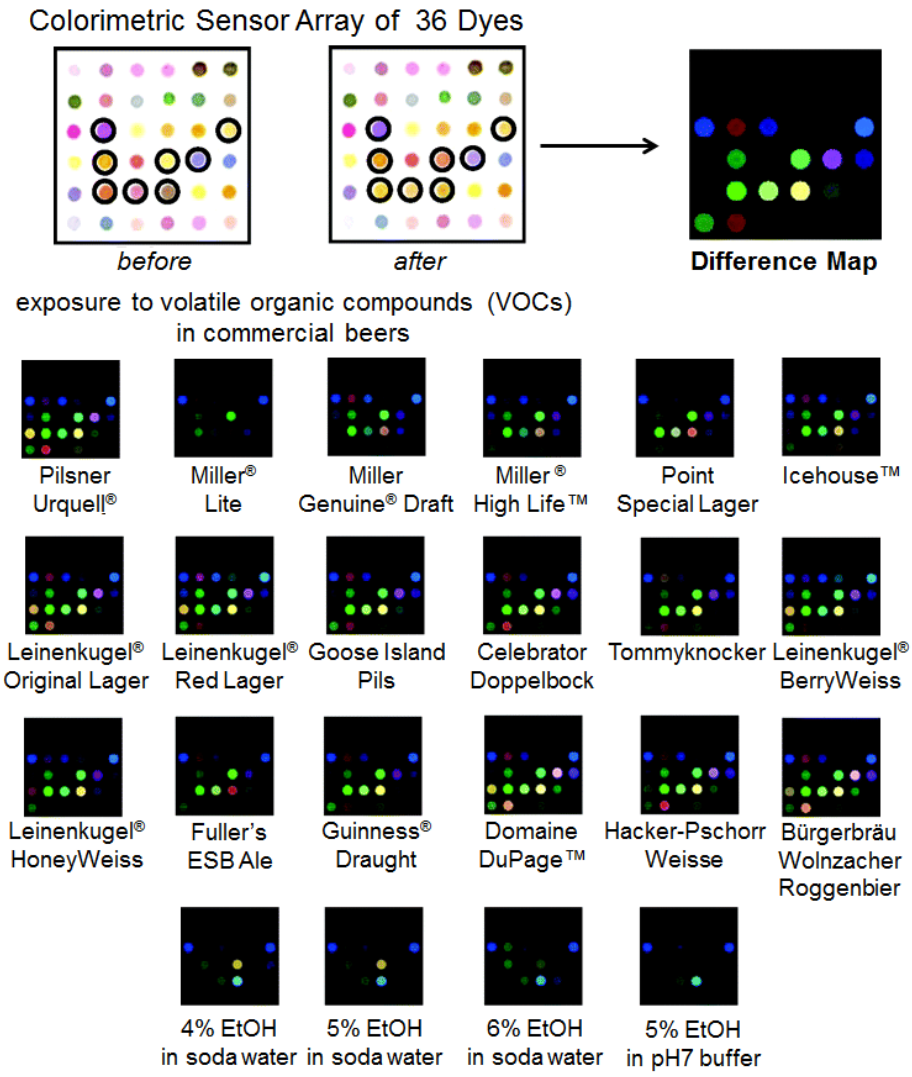

Figure 4.4 The two panels at the top are the images of the gas-phase colorimetric sensor array before and after exposure to head-gas from Goose Island Pils sample. Dyes that undergo significant color change are circled. The color range shown in the difference map has RGB values of 0–255. The 18 panels in the middle show the color change profiles allowing discrimination between 18 commercial beers (lager, ale, and specialty). The bottom 4 panels represent the control.[147]

An interesting example of the practical application of differential sensing array was reported by Suclick *et al.*[147] (Figure 4.4). Their sensing array was constructed from 36 chemically responsive hydrophobic dyes that fall into three classes: (*a*) metal ion containing dyes that change color in response to Lewis basicity *i.e.* electron pair donation and metal ion ligation, (*b*) pH indicators that change color in response to Brønsted acidity/basicity *i.e.* proton acidity and hydrogen bonding, and (*c*) dyes with large permanent dipoles that change color in response to local polarity. These hydrophobic dyes were then dissolved in a polymer film (dibutylphthalate in polystyrene) and deposited on Teflon.[151] Distinct and reproducible patterns were obtained upon exposure of the sensing array to the headspace vapors of beer samples in a sealed chamber. As shown in Figure 4.4, no two panels are exactly the same, thus each panel serves as a "fingerprint" for a particular sample. This excellent discrimination between samples was confirmed using standard chemometric method of hierarchical cluster analysis, with an identification error rates of below 3%.

A large number of dyes and receptors have been utilized in the construction of differential sensing arrays. Recently, cruciform-based sensor arrays have become an attractive means for differentiating structurally related analytes. This is due to the following reasons. First, these cruciforms are extensively conjugated compounds and their dilute solutions are highly emissive. Furthermore, spatially separated frontier molecular orbitals (FMOs) of cruciform molecules allow independent modulation of highest occupied molecular orbital (HOMO) and lowest unoccupied molecular orbital (LUMO) through guest binding, resulting to a hypsochromic and bathochromic (or a

sequence of both) shifts in emission.[132,152] An example of the predicted optical response and actual observed changed in emission upon analyte binding to a cruciform's arm is illustrated in Figure 4.5.

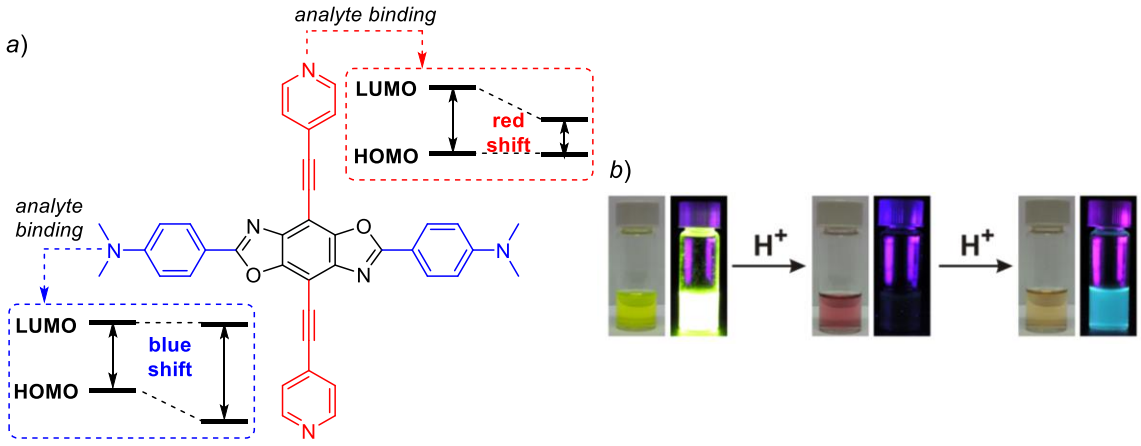

Figure 4.5 (*a*) Analyte binding on the different sites of the cruciform and its anticipated effect to the HOMO–LUMO gap.[152] (*b*) Two step optical response of the cruciform to protonation: a red shift in absorption upon H^+ binding on the vertical axis followed by a blue-shift in absorption and emission upon H^+ binding on the horizontal axis.[152]

This fluorescent response of cruciform sensor upon analyte binding is more sensitive compared to a colorimetric response since the observations are made against a dark background.[153] Second, the emission colors observed when these cruciforms are mixed with analytes are highly sensitive to the details of analyte's structure and, due to the cruciforms' charge-separated excited state, to the solvent in which emission is observed. Thus, a differential sensing array can be conveniently constructed from one or several cruciforms (that possess appropriate binding sites) dissolved in organic solvents of varying polarity. Finally, emission changes upon analyte binding occur instantaneously

and can be recorded through standard digital photography[154,155] using a semi-professional digital camera in a dark room. With minimal graphic manipulation, representative cut-outs of emission color photographs can be arranged into panels which permit quick naked-eye distinction among analytes. If quantification of response is needed, Red/Green/Blue (RGB) values can be extracted from these photographs using free, downloadable software such as Color Contrast Analyser,[156] and the obtained numerical data can be statistically processed.

4.1.3 Supramolecular Sensing Arrays Using Cruciform Fluorophores

Molecular cruciforms are two-dimensional, X-shaped conjugated organic molecules, wherein two or more conjugation currents intersect at a central core.[157,158] The central core is usually an inert conjugated connector that dictates the geometry of the arms of the cruciform, such as in the case of tetrakis(arylethynyl)benzenes,[159] distyrylbis(arylethynyl)benzenes,[158] tetrastyrylbenzenes,[160] and tetrakisalkynylethenes.[161] Recently, cruciforms containing benzobisoxazole[157] and benzobisimidazole[162–164] cores have been reported—these cores present additional molecular recognition sites that are important for sensing purposes. Selected examples of cruciform sensors, with various core motifs, from different research groups are listed in Figures 4.6 and 4.7.

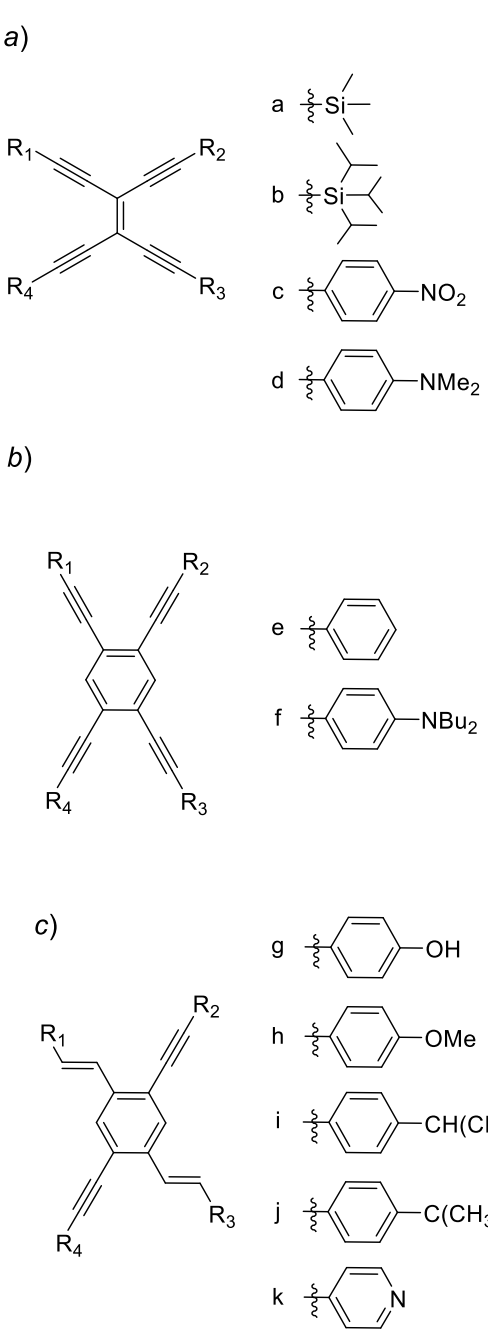

a)	**R_1**	**R_2**	**R_3**	**R_4**
105	a	a	a	a
106	c	b	a	b
107	d	b	a	b
108	c	b	c	b
109	d	d	b	b
110	c	b	d	b
111	c	d	b	b
112	c	c	d	d

b)	**R_1**	**R_2**	**R_3**	**R_4**
113	e	e	e	e
114	f	f	f	f
115	f	c	c	f
116	f	f	c	c
117	f	c	f	c
118	d	d	d	d
119	d	c	c	d
120	d	d	c	c
121	d	c	d	c

c)	**R_1**	**R_2**	**R_3**	**R_4**
122	e	e	e	e
123	g	h	g	h
124	h	g	h	g
125	g	g	g	g
126	i	e	i	e
127	k	j	k	j
128	i	k	i	k
129	f	e	f	e
130	d	k	d	k

Figure 4.6 Selected examples of two-dimensional cruciform fluorophores containing inert core: (*a*) Diederich's tetraethynylethylene cruciforms,[165] (*b*) Haley's tetrakis(arylethynyl)benzene cruciforms,[166–168] and (*c*) Bunz's distyrylbis(arylethynyl)benzene cruciforms.[158,169,170]

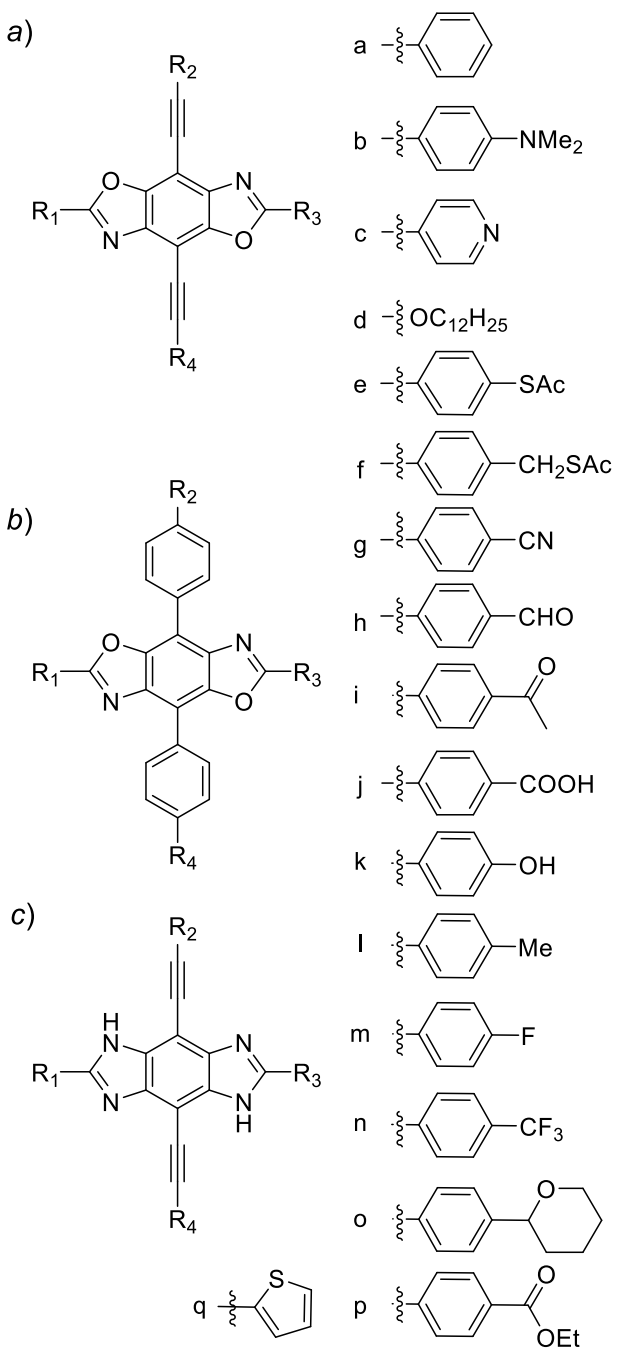

a)	R_1	R_2	R_3	R_4
131	a	a	a	a
132	a	b	a	b
133	a	c	a	c
134	b	a	b	a
135	b	b	b	b
136	b	c	b	c
137	c	a	c	a
138	c	b	c	b
139	c	c	c	c

b)	R_1	R_2	R_3	R_4
140	a	d	a	d
141	e	d	e	d
142	f	d	f	d
143	g	d	g	d
144	h	d	h	d
145	i	d	e	d
146	a	d	j	d

c)	R_1	R_2	R_3	R_4
147	a	a	a	a
148	a	k	a	k
149	a	l	a	l
150	a	m	a	m
151	a	n	a	n
152	a	o	a	o
153	a	p	a	p
154	a	q	a	q
155	a	r	a	r

Figure 4.7 Selected examples of two-dimensional cruciform fluorophores with functionalized cores: benzobisoxazole cruciforms from (*a*) Miljanić's[152] and (*b*) Nuckoll's[171] groups, and (*c*) benzobisimidazole cruciforms from Miljanić's[162] group.

With appropriate substitution, cruciforms allow designed localization of the molecule's FMOs. Computational studies using programs such as Gaussian 09W and Spartan, show that the HOMO density of the molecule is localized on the arm bearing the electron-donating groups while the LUMO density resides on the arm containing the electron-withdrawing groups (Figure 4.8). The spatial isolation of cruciforms' FMOs is essential for their use as sensors since, as shown in Figure 4.5, analyte binding to the cruciform invariably changes its HOMO–LUMO gap and the associated properties.

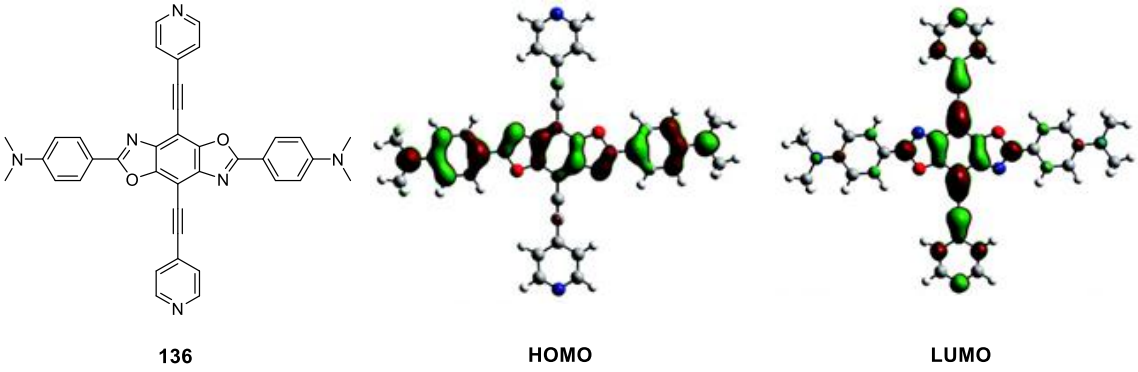

Figure 4.8 HOMO–LUMO localization of cruciform **136** calculated using Gaussian 09W[172] software package. The B3LYP hybrid density functional[173,174] and a standard 3-21G basis set were used for the geometry optimizations.[152]

Using this principle, Miljanić and Bunz groups developed benzobisoxazole[175,176] and 1,4-distyryl-2,5-bis(arylethynyl)benzene cruciforms,[169] respectively, which act as fluorescent sensors for boronic acids, metal ions, and carboxylic acids. However, since these cruciforms contain only basic binding sites, they are limited to sensing acidic analytes. To expand the sensing capability of benzobisoxazole cruciform (**136**), a hybrid

benzobisoxazole–boronic acid sensing ensemble was constructed by Miljanić group to vicariously detect nucleophilic analytes (amines and ureas).[175]

Trisubstituted boron species, *e.g.* organoboronic acids ($R–B(OH)_2$), contain boron atom that has an sp^2 trigonal planar geometry with an empty *p* orbital perpendicular to the plane of the molecule.[177] This feature makes organoboronic acid an excellent sensor for anionic[178] and nucleophilic[179] analytes, most notably, vicinal diols and saccharides[180]—as the Lewis acidic boron center can form coordinate bonds with a variety of heteroatoms such as oxygen, sulfur, phosphorus and nitrogen. A number of colorimetric[180] and fluorescent[181] boronic acid sensors have been reported in literature but one major drawback in this approach is that a fluorophore must be incorporated into the R group of the boronic acid, normally requiring non-trivial synthesis. Alternatively, non-fluorescent boronic acids can be used as sensors through indicator displacement method,[132] wherein the boronic acid transiently binds—and thus quenches—a fluorescent indicator. Upon its displacement by a better binding analyte, the indicator recovers its fluorescence, this methodology often allows simplifications in the synthesis of the sensor, but can be qualitatively limited to the emission responses of the indicator.[175]

In this chapter, a protocol for direct and vicarious sensing methodology to quickly and qualitatively distinguish between structurally related (*a*) carboxylic acids, (*b*) boronic acids, and, vicariously, (*c*) organic amines, is presented. To illustrate the broad applicability of the reported protocols, Bunz's cruciforms (Figure 4.9, cruciforms **129**, **156**, **157**) were used to detect carboxylic acids, while Miljanić's cruciform (Figure 4.9, cruciform **136**) was employed to detect boronic acids, and, through a hybrid sensor, small

organic amines. We presume that these sensors could be readily interchanged without major consequences to the quality of analyte discrimination.

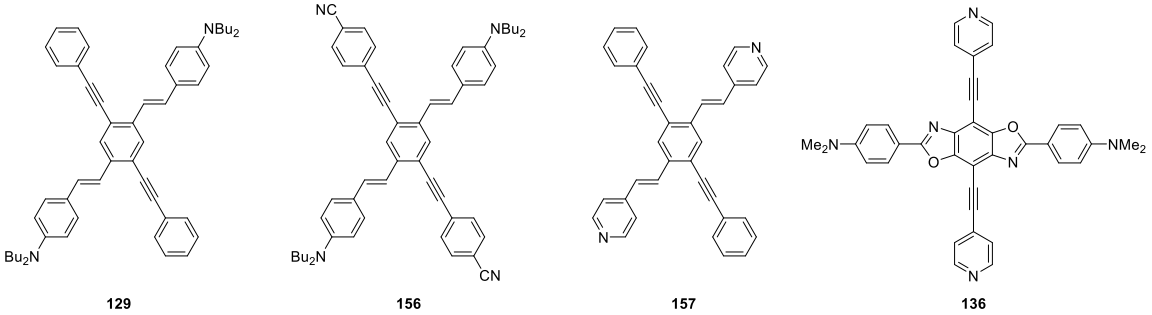

Figure 4.9 Cruciform fluorophores used in the sensing arrays for carboxylic acids, boronic acids and organic amines.

4.2 Results and Discussion

As illustrative of the potential of cruciform fluorophores in sensing and discrimination of closely related analytes, three classes of results are presented. First, 1,4-distyryl-2,5-bis(arylethynyl)benzene cruciforms **129**, **156**, and **157** (Figure 4.9) were used to discriminate among structurally related carboxylic acids **A1–A10** shown in Figure 4.10a. Then, benzobisoxazole-based cruciform **136** (Figure 4.9) has been used to analyze boronic acids **B1**–**B9** (Figure 4.11a). Finally, cruciform **136** in combination with boronic acids **B1** and **B5** were used to analyze amine analytes shown in Figure 4.12a.

4.2.1 Detection of Carboxylic Acids Using 1,4-Distyryl-2,5-bis(arylethynyl)benzene Cruciforms

Using dilute solutions of cruciforms **129**, **156**, and **157** in dichloromethane (DCM), ethyl acetate (EA), acetonitrile (AN), dimethylformamide (DMF), isopropanol (iPrOH), and methanol (MeOH), the fluorescent responses were found to be dependent upon the concentration and the structural identity of a carboxylic acid. Using cruciform **129** and analyte **A2**, it was determined that concentrations above 0.13 M of carboxylic analytes can induce significant change in the cruciforms emission—the fluorescence shifted from green to blue on account of protonation of aniline nitrogens.[169] Since HOMO density lies along this axis, protonation led to stabilization of the cruciform's HOMO, increasing the HOMO–LUMO gap, and is observed as a blue shift in emission. Figure 4.10b shows the digitally recorded emission color of all fluorophore, solvent, and carboxylic acid combinations. As expected, the most acidic analytes **A9** and **A10** showed the greatest change in fluorescence emission.

This sensing array exhibits 18 characteristic emission colors per analyte, which can be used to uniquely characterize an analyte. Using the RGB values of the emission color, a differential autocorrelation plot of the fluorescent response of the sensing array can be constructed (Figure 4.10c). All analytes can be clearly discerned, since the σ values are significantly different upon comparison of all carboxylic acid analytes against each other—the σ values diminish only when identical carboxylic acids are correlated (Figure 4.10c, diagonal series).

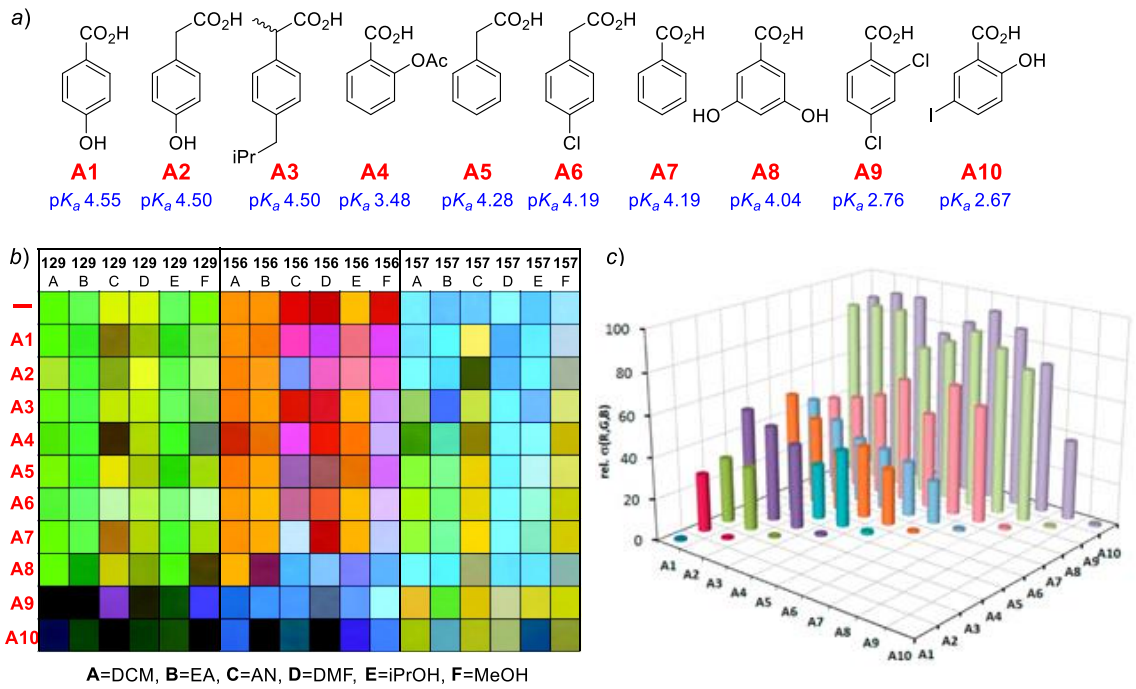

Figure 4.10 (*a*) Structures of different carboxylic acids used in this study. (*b*) Emission color of cruciform **129**, **156**, and **157** before (1st row) and after (2nd–10th rows) exposure to the carboxylic acid analytes in six different organic solvents. For all photographs, λ_{exc} was 365 nm and shutter speed was 0.5 s. (*c*) Correlation diagram showing the standard deviations of **R**/**G**/**B** values for analytes **A1**–**A10**, summed over five solvents, relative to all other analytes. The *z* axis represents the relative standard deviation (σ) of RGB values relative to **A1**.

4.2.2 Detection of Boronic Acids Using Benzobisoxazole Cruciforms

Using a completely analogous procedure, a sensing array was constructed from dilute solutions of cruciform **136** in five different organic solvents—AN, 1,2,4-trichlorobenzene (TCB), DCM, cyclohexane (CH), and chlorobenzene (CB). To balance

the response of sensing array with the solubility of the analytes in the different organic solvents used, it was determined that the optimum concentration is about 16.7 g L^{-1} with respect to each analyte. The array undergoes dramatic changes in fluorescence emission colors upon addition of the analytes, which proved useful in the discrimination of nine different organoboronic acids (Figure 4.11a). The extent of the arrays's ability to differentiate between the boronic acid analytes was quantitatively assessed by extracting the RGB values of the digital photographs using Colour Contrast Analyser for each boronic acid analyte, in five different solvents. The standard deviation (σ) of the compounds' RGB values from the corresponding blank solution was calculated using Microsoft Excel. Similar to the statistical treatment done with carboxylic acid analytes, the relative standard deviation was calculated to determine a non-solvent-specific value that indicates how different one analyte is from the other. The results of the calculation is shown in Figure 4.11c—the graph suggests that all investigated analytes can be differentiated from each other, as well as from that of cruciform **136** alone, since the σ value is only zero when identical boronic acid analytes are correlated (Figure 4.11c, diagonal series).

In the majority of the organoboronic acids studied, the emission colors were red-shifted, suggesting dominant stabilization of the LUMO through a stronger pyridine–boron interaction. While all nine boronic acids can be distinguished from each other, emission of **136**/**B7** combination is not sufficiently different from the emission of pure **136**—presumably because the pyridine moiety of **B7** (which is in excess) replaces the pyridine of **136** in binding to boron.[175] On the other hand, **B9** causes unselective

quenching of fluorescence of **136** in all solvents, possibly due to electron-transfer from the excited state of **136** onto acceptor **B9**.[182]

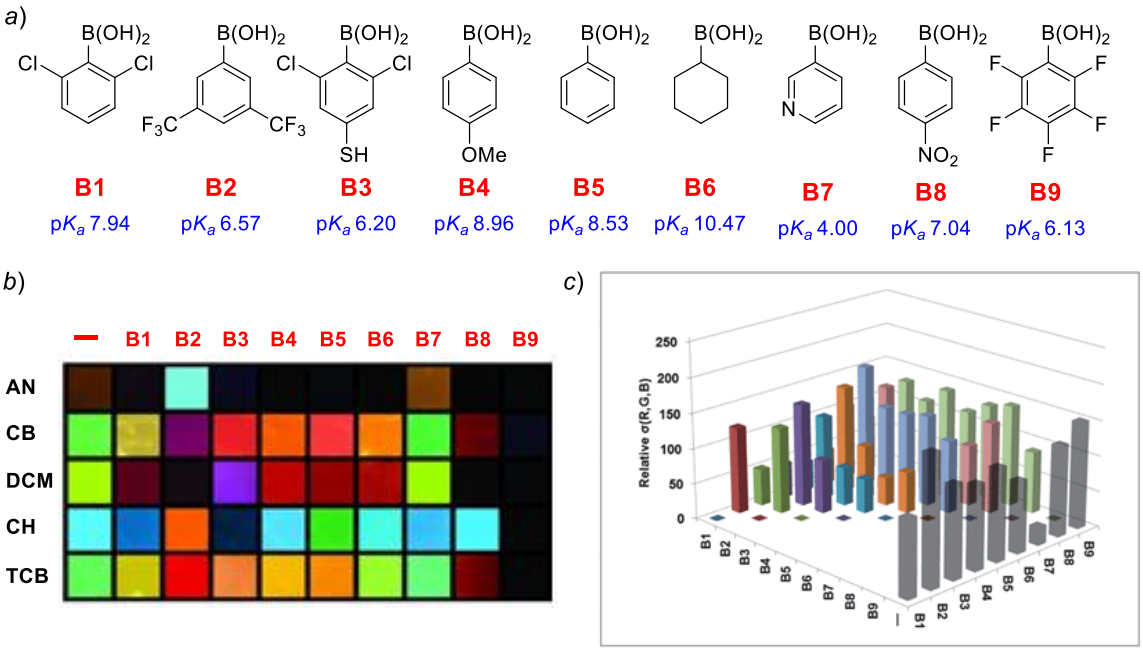

Figure 4.11 (*a*) Structures of the organoboronic acids used in this study. (*b*) Emission color of cruciform **136** before (1st column) and after (2nd–10th columns) exposure to excess amount of organoboronic acid analytes in five different organic solvents. For all photographs, λ_{exc} was 365 nm and shutter speed was 0.5 s. (*c*) Correlation diagram showing the standard deviations of RGB values for analytes **B1**–**B9**, summed over five solvents, relative to all other analytes.

4.2.3 Detection of Amines and Ureas Using a Hybrid Benzobisoxazole Cruciform

The methodology for sensing analytes **N1–N12** operates as follows: cruciform 136 and boronic acid forms a transient complex **136•*n*B1** (or **136•*n*B5**)—the precise

structure of this complex is at present unknown, although they likely involve either coordinative N–B bond (Figure 4.12c) or hydrogen bonding between the boronic acids and the nitrogen atoms in the cruciform—but its fluorescence differs from that of the pure cruciform **136**. If this solution is exposed to Lewis basic analytes, the analytes can replace one or both –OH groups on the boronic acid, thus significantly altering the electronic properties of boron, and in turn, the fluorescence of the entire complex. It is also possible that an analyte can completely break the association between the boronic acid additive and the pyridine moiety of 136 leading to the regeneration of the original emission of **136**.

Using a similar procedure described previously, a sensing array was constructed from dilute solutions of cruciform **136** in five different organic solvents—AN, TCB, DCM, CH, and chloroform (CF). Boronic acid additives **B1** and **B5** were added and the solutions were immediately used to differentiate the amine analytes **N1**–**N12**. Each analyte interacted with 2 different hybrid sensing sytems, which are dissolved in 5 different organic solvents, to give a total of 10 emission colors. This diversity permitted qualitative discrimination between the amine analytes as no two of them had all ten identical emission colors (Figure 4.12b). This is also confirmed by statistical treatment of the extracted RGB values from the photographs (Figure 4.12d).

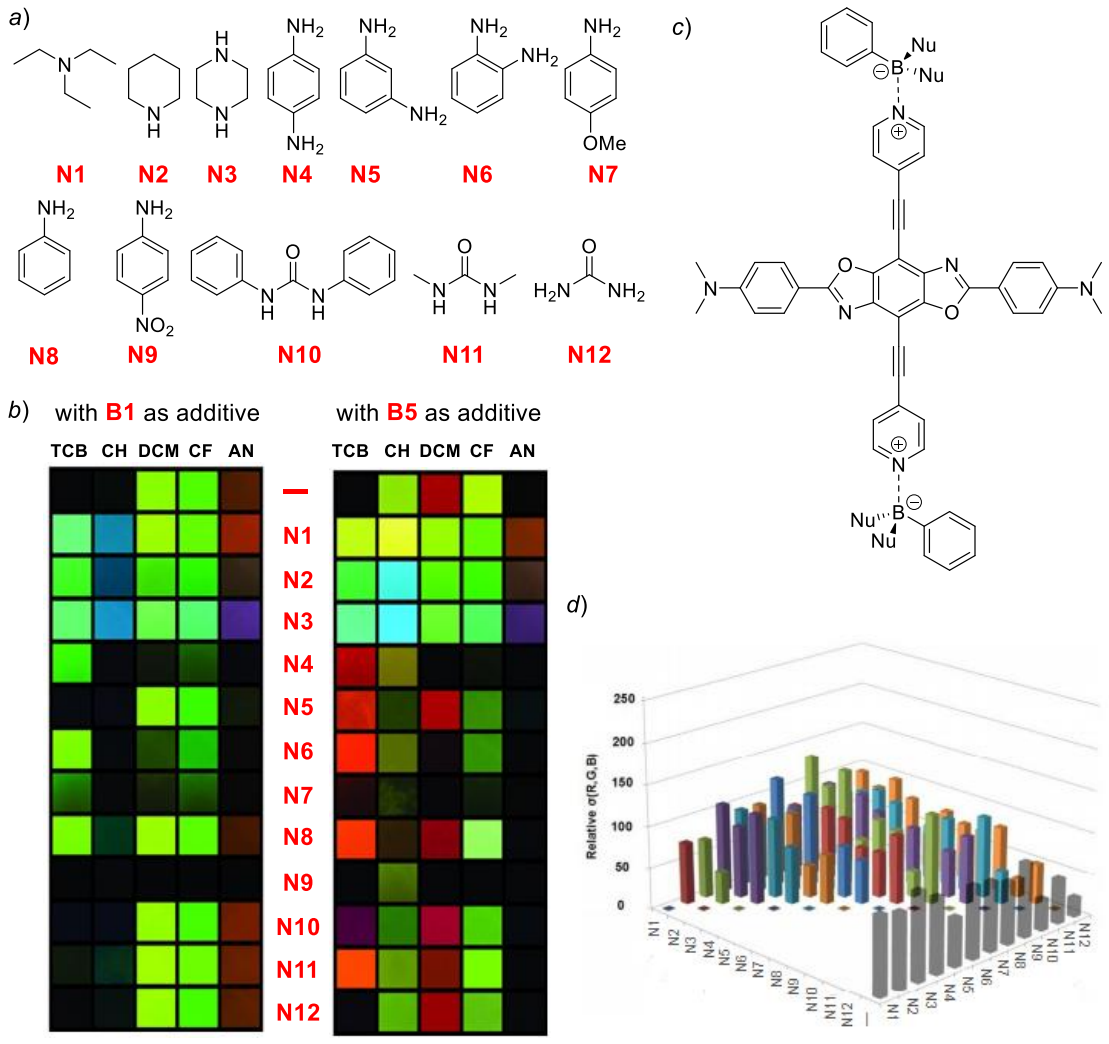

Figure 4.12 (*a*) Structures of the various organic nitrogen compounds differentiated using an ensemble of cruciform **136** and boronic acids (**B1** and **B5**). (*b*) Emission colors of the sensing array before (1st row) and after (2nd–13th rows) adding excess amount of the amine analytes. In all experiments, the molar ratio of cruciform **136** to **B1** and **B5** additives is ~1:20,000. For all photographs, λ_{exc} was 365 nm and shutter speed was 0.5 s. (*c*) Proposed sensing ensemble produced between cruciform **136** and boronic acid additives. (*d*) Correlation diagram showing the standard deviations of RGB values for analytes **N1**–**N12**, summed over five solvents, relative to all other analytes.

As expected, amines more basic than pyridine (analytes **N1**–**N3**, Figure 4.12b) displace cruciform **136** from its complexes with boronic acid additives, thus regenerating the emission colors of pure, uncomplexed cruciform **136** (Figure 4.10b, 1st column). On the other hand, less basic species *i.e.* aniline derivatives and substituted ureas (analytes **N4**–**N12**, Figure 4.11b), appear to bind to the **136**•*n*ArB(OH)$_2$ complex without destroying it and this event results in the modulation of complex's fluorescence emission. Therefore, vicarious sensing methodology is characterized by a leveling effect, wherein analytes above certain threshold of basicity can no longer be discriminated from each other.

4.3 Conclusions and Outlook

The ability of the cruciform-based sensor arrays to discriminate among structurally related analytes is significant, especially since statistically relevant distinction can be obtained without the need to perform exhaustive UV/Vis absorption or fluorescence emission characterization of the optical response of cruciforms to analytes. Instead, simple photographs of emission colors are sufficiently distinct to allow the discrimination among closely related analytes, especially if the photographs are taken in different solvents or using more than one cruciform sensor. Using this quick methodology, dozens of analytes can be quickly analyzed in an afternoon, whereas the same analysis would require weeks if rigorous spectroscopy was employed.

While the presented protocols are highly selective in discerning structural differences among analytes, they are not very sensitive. Typically, analyte concentrations

of several grams per liter are required to modulate cruciforms' emission colors. Thus, these methods are unlikely to play a role in analyses of trace ingredients. However, their strength lies in analyzing species that are available in large quantities but are sensitive to decomposition or counterfeiting: *e.g.* pharmaceuticals, food additives, basic chemicals, or alcoholic beverages.

The protocols for qualitative discrimination described in this chapter can also hold significant potential in routine quality analyses, where even a minimally trained operator could discern the differences in composition, or deviations from a well-defined formula. Practicality of this technique could be further enhanced by using simple cellphone cameras, which—in combination with pattern- and image-recognition software such as Google Goggles—could match the recorded emission colors to the database of known compositions. Simple photography of emission colors is approx. two orders of magnitude faster that the rigorous fluorescence emission spectroscopy analysis, and in many cases can match spectroscopy in its ability to discern among different analytes. These fluorescent cruciforms can also be integrated in the construction of 3D printed lab-on-a-chip devices[183] that can be used as cheap and convenient colorimetric/fluorescent sensors for carboxylic acids and organic amines.

Several modifications could be done to improve the sensitivity of the cruciform sensors—**129**, **136**, **156**, and **157** could in principle be rendered more sensitive by enhancing the binding affinities for analytes. As their pyridine and amine functionalities are basic in nature, the modification of the pyridine ring or the aniline to more specific or alkaline functionalities would be a promising start to decrease the detection limits. For

example, 2-methylpyridine and 2,6-dimethylpyridine are more alkaline than pyridine and therefore the interaction of acidic analytes and fluorophore should improve. Another way to improve the detection limit would be to use a more basic guanidine moiety instead of the alkylated amine. Finally, the sensitivity of the self-assembled **136**/boronic acid sensing system could be improved by switching from boronic acid to a more electrophilic boron source, such as $PhBF_2$, which would increase the complexation constant for the complex.

One caveat exists—the analysis of fluorescent signal recorded with a digital camera is dependent on the color space and shutter speed.[154] Therefore, the RGB values of an emission color differ somewhat, depending on the camera adjustments. Following adjustments can be changed on most cameras: white balance, shutter speed, film sensitivity, focal aperture, data format (RAW files or JPEG files), and color space (*i.e.* sRGB, Adobe RGB, or ProPhotoRGB). The best strategy for ensuring the constancy of the emission color response is to keep the white balance, the film sensitivity, and the focal aperture constant and only vary the shutter speed. Most of the issues are resolved when transforming the RGB values into coordinates of the CIE LUV color space and use only the hue coordinates *u*'*v*' without any brightness information. For this transformation it is important to know the color space of the recorded image. Using brightness-removed color coordinates, the identification of an unknown analyte is greatly improved when having recorded images with different RGB intensities.

4.4 Experimental Section

4.4.1 General Experimental Methods

Carboxylic acids **A1**–**A10**, organoboronic acids **B1**–**B9**, amines, and ureas **N1**–**N12** were purchased from commercial suppliers and used without further purification. ACS reagent grade solvents were used as received. Cruciforms **129**, **136**, **156**, and **157** were prepared according to literature procedures.[152,184]

Photographs of emission colors were taken using a Canon EOS Rebel T3i (objective EFS 18–55 mm zoom lens) digital camera, with a shutter speed of 0.5 s. Alternatively, Fujifilm FinePix S9000 and Canon EOS 30D (objective EFS 18–55 mm zoom lens) can also be used. A handheld UVLS-28 EL series UV lamp (λ_{exc} = 365 nm) was used as the light source. All photographs were taken in a dark windowless room, with a 45 cm distance between the sample cuvettes and the camera lens. Exposure times were varied for each solution to produce images reflecting the color of emission (0.25–15s).

4.4.2 Experimental Protocol for the Detection of Carboxylic Acids Using Distyrylbis(arylethynyl)benzene Cruciforms

1. Prepare a fresh stock solution of cruciforms **129**, **156**, and **157** with a concentration of 1.0×10^{-3} mol L^{-1} in dichloromethane (DCM).

2. Using the fresh stock solutions, prepare 100 mL each of 2.0×10^{-6} M solution of **129**, **156**, and **157** in DCM, ethyl acetate (EA), acetonitrile (AN), *N*,*N*-dimethylformamide (DMF), isopropyl alcohol (*i*PrOH) and methanol (MeOH).

3. Weigh out 0.65 mmol (88.2–124.2 mg) of the analyte carboxylic acid **A1**–**A10** in 5 mL dram vials, add 5 mL of the solutions prepared in step 1 and shake the vial. If heterogeneous, the corresponding solution should be left to settle (filtration is unnecessary). This leads to a total concentration of 0.13 M (31 g L^{-1}) of the carboxylic acid.

4. Capture digital photographs of the fluorescence in a dark room in the absence of ambient light.

4.4.3 Experimental Protocol for the Detection of Boronic Acids Using Benzobisoxazole Cruciforms

1. Prepare a 1.0×10^{-4} M solution of cruciform **136** in DCM.

2. Prepare five individual solutions for each boronic acid analyte, by dissolving 50 mg (0.24–0.41 mmol) of the analyte in 3 mL each of AN, 1,2,4-trichlorobenzene (TCB), DCM, cyclohexane (CH), and chlorobenzene (CB). This should result in approx. 16.7 g L^{-1} solutions with respect to each analyte.

3. Transfer 1.8 mL of each of the analyte solutions into five separate 10×10 mm quartz cuvettes (commonly used for UV/Vis spectroscopy). Then, add 20 μL of the cruciform solution prepared in 2 into each of the five cuvettes, and stir the two solutions to

homogenize. If any precipitation is observed, the corresponding solution should simply be left to settle (filtration is unnecessary).

4. Place all five cuvettes onto a glass plate and irradiate them by a handheld UV lamp (365 nm) from the top. The UV lamp should be positioned in a fashion which ensures equal irradiation to all five vials.

5. Ensure that the room is dark (turn off lights, block windows and other sources of natural and artificial light) and immediately take a digital photograph of the emission colors of the solutions.

4.4.4 Experimental Protocol for the Detection of Amine Analytes Using Benzobisoxazole Cruciform/Boronic Acids Hybrid Sensing System

1. Prepare (at least) 80 mL each of 1.0×10^{-6} M solutions of cruciform **136** in AN, TCB, CH, DCM, and chloroform (CF).

2. Dissolve **B1** (152.6 mg, 0.80 mmol) in 40 mL of each of the solutions prepared in 1.

3. Dissolve **B5** (97.6 mg, 0.80 mmol) in 40 mL of each of the solutions prepared in 1.

4. Immediately use 2 mL of the solutions prepared in 2 and 3 to dissolve the desired amine analyte (40 mg, 0.19–0.47 mmol). For each amine analyte, ten solutions should be prepared: five with **B1** and five with **B5** as additives.

5. For each analyte, transfer aliquots of the ten prepared analyte/boronic acid/cruciform **136** solutions into ten separate quartz cuvettes. Place these two five-cuvette sets (one for **136**/**B1**, one for **136**/**B5**) onto a glass plate and irradiate at 365 nm by a handheld UV

lamp. Capture digital photographs of the fluorescence in a dark room in the absence of ambient light.

4.4.5 Image Processing and Numeric Analyte Discrimination

1. Using Adobe PhotoShop or a similar image-processing program cut out a representative square segment from digital photographs of the emission colors of each photographed vial. Organize these cut-outs into panels similar to those in Figures 4.10b, 4.11b, and 4.12b. These panels in many cases allow rapid naked-eye discrimination among analytes.

2. If quantification of differences in emission color is desired, RGB values can be extracted from panels in 4.1. and then statistically treated. Freely downloadable Colour Contrast Analyser[156] can be used for this purpose. To obtain relative standard deviations of emission colors of one analyte relative to another (e.g. compounds **B1** and **B2**, Figure 4.11c), the following equation is used:

$$\sigma'_{\boldsymbol{B1@B2}} = \sqrt{\frac{\sum_{solv}^{i}(R_{\boldsymbol{B1}} - R_{\boldsymbol{B2}})^2 + (G_{\boldsymbol{B1}} - G_{\boldsymbol{B2}})^2 + (B_{\boldsymbol{B1}} - B_{\boldsymbol{B2}})^2}{3 * i}}$$

3. The equation above is also used to identify unknown carboxylic acid analytes, organic amines, and ureas. Therefore every deviation is determined between the unknown analyte to all substances of the calibration data set. The smallest deviation indicates the corresponding substance.

Chapter Five

L-shaped Benzimidazole Fluorophores: Synthesis, Characterization, and Optical Response to Bases, Acids and Small Anions[185]

5.1 Introduction

Molecular cruciforms, such as those discussed in Chapter 4, showed that cross-conjugated aromatic molecules can be designed to have spatially isolated frontier molecular orbitals (FMOs) by carefully choosing the electronic properties of the functional groups on the cruciforms' arms. The HOMO–LUMO localization on the different axes of the cruciform is important since binding of the analyte to the cruciform will alter the energetic position of either the HOMO or the LUMO which will translate to an observable change in absorption and emission of the molecule.[186] Our group has also demonstrated that the core of the cruciform can be heteroaromatic by incorporating a benzobisoxazole[152] or benzobisimidazole[162] cores. By modifying the core, we can further bias the FMO separation of the molecule and introduce additional binding sites for analytes. Thus, the nature of the core is an important consideration in building cruciform fluorophores.

The amphoteric nature of benzimidazole makes these structures useful for molecular recognition and sensing. The presence of a donor pyridine-like nitrogen atom within the ring presents a binding site for metals and other cations. On the other hand,

[185] Lirag, R. C.; Le, H. T. M.; Miljanić, O. Š. *Chem. Commun.* **2013**, *49*, 4304–4306.

imidazole's N–H moiety can either form hydrogen-bonding or be deprotonated in the presence of anions and bases. Furthermore, the acidity of this N–H proton can be tuned by changing the electronic properties of the benzimidazole substituents.[187] Finally, the conjugation of benzimidazole can be easily extended, for example via Sonogashira[188] or Suzuki[189] cross-coupling reactions, which can lead to its enhanced emission. Some examples of colorimetric and fluorescent benzimidazole-based sensors for various analytes are shown in Figure 5.1.

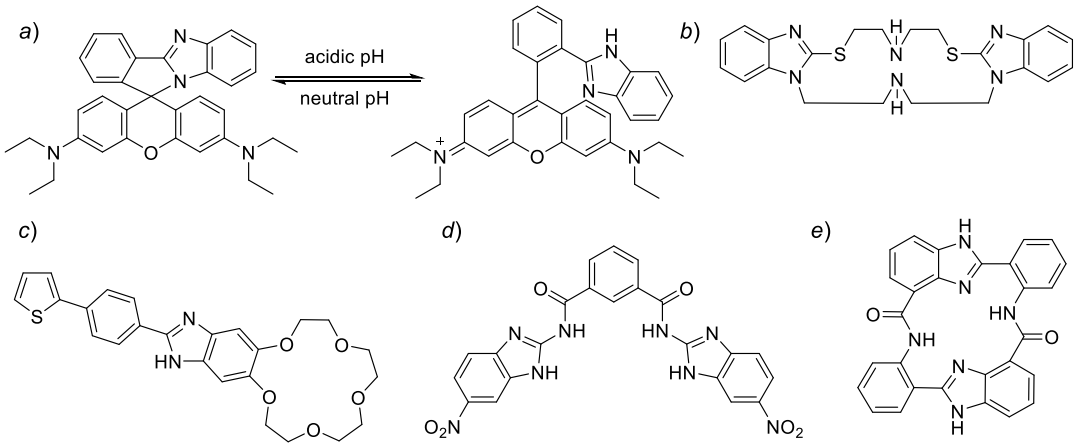

Figure 5.1 Selected examples of benzimidazole-based sensors for different analytes: (*a*) acid,[190] transition metal ions (*b*) Cr^{3+} and Fe^{2+},[191] and (*c*) Cu^{2+} and Pd^{2+},[192] and anions (*d*) F^- and OAc^-,[193] and (*e*) F^-, $H_2PO_4^-$, and benzoate.[194]

The localization of the frontier molecular orbitals in cruciform molecules gives rise to interesting electro-optical properties. For example, the increased localization of the HOMO and LUMO in cruciforms leads to decreased electro-chemical band gap.[195] Upon photonic excitation, an electron from HOMO can be promoted into the LUMO to give a highly polarized state. As a consequence, the intramolecular charge-transfer absorption

and emission is dependent upon solvent polarity, protons, and coordination with metal cations which makes these cruciforms valuable and functional scaffolds for differential sensing arrays.[132,196] In addition to cruciform, FMO localization has also been observed in different π-architectures.[197] Some notable examples of other architectures that have localized FMOs include H-shaped oligo(phenylene ethynelenes) (OPEs) and oligo(phenylene vinylenes) (OPVs),[198] T-shaped polycyclic donor-acceptor systems containing qionoxaline and triphenylamine cores,[199] Y-shaped molecules with imidazole-thiazole core,[200] butterfly-shaped blue emitters based on pyrene,[201] and fluorescent board-shaped qionoxalinophenanthrophenazine dyes[202] (Figure 5.2).

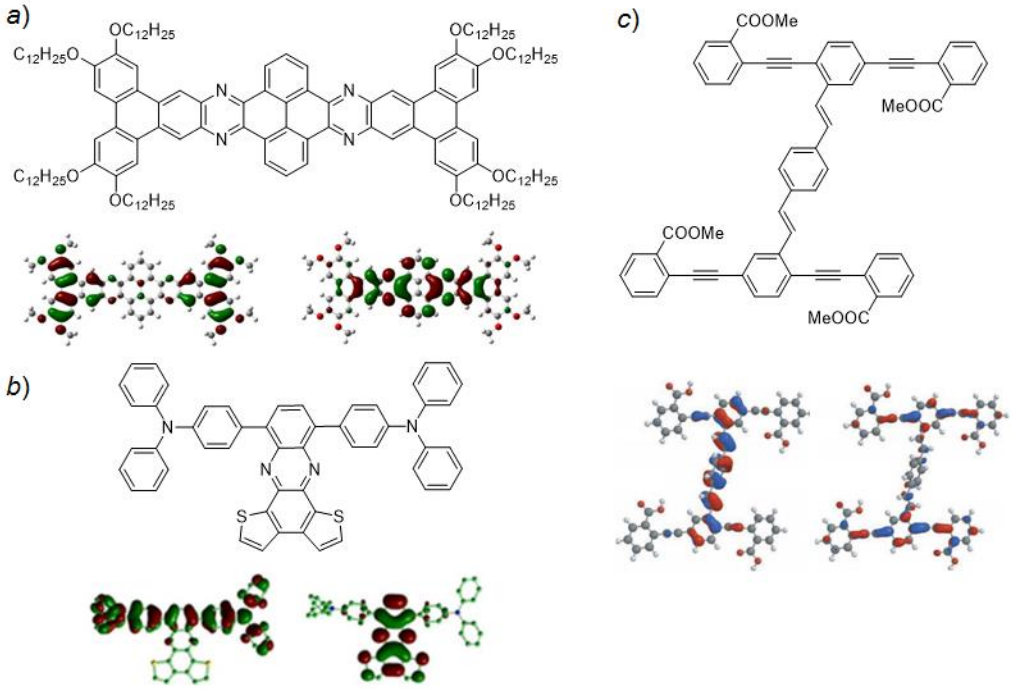

Figure 5.2 Examples of different molecular architectures that have localized FMOs: (*a*) board-shaped,[202] (*b*) T-shaped,[199] and (*c*) H-shaped.[198] Position of the HOMO (*left*) and LUMO (*right*) densities as predicted by Gaussian calculations.

The key in achieving the localization of HOMO and LUMO among these diverse architectures is the strategic placement, within the molecule, of electron-donating and electron-withdrawing moieties that are linked by a π-conjugated bridge. The π-conjugated bridge can also help increase the fluorescence rate of the molecule if it can impose rigidity to the structure (*e.g.* ethynyl group) which can prevent non-radiative relaxation mechanisms arising from the smaller HOMO–LUMO gaps of donor–acceptor systems.[203]

In this chapter, the syntheses and optical properties of L-shaped compounds—cruciforms that are "cut in half" (Figure 5.2), is reported. This study aims to find a minimal system that can still preserve spatially isolated FMOs. We also introduced benzimidazole functional group into the core to evaluate its effect on the HOMO–LUMO separation of the molecule and to enable our sensor to respond to cationic, anionic, and basic analytes.

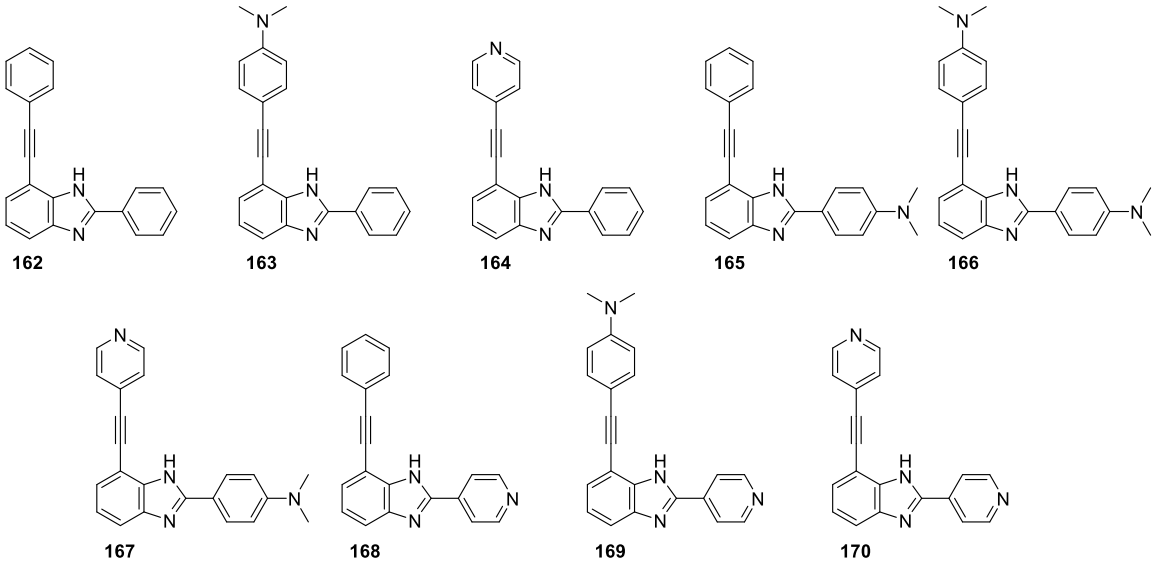

Figure 5.3 L-shaped benzimidazole fluorophores **162**–**170**.

5.2 Results and Discussion

5.2.1 Synthesis

Half-cruciforms **162–170** were synthesized using the protocol presented in Scheme 5.1. The oxidative condensation reaction between 3-bromo-*o*-phenylenediamine (**158**) and three commercially available aldehydes, using iodine as the oxidant, produced brominated benzimidazoles **159–161**. The second step is accomplished by doing the Sonogashira couplings with either phenylacetylene, 4-ethynylpyridine, or 4-ethynyl-*N*,*N*-dimethylaniline, in a microwave reactor, to give the final desired products in moderate yields. Fluorophores **159–161** were isolated as off-white, yellow, and light green powders, following chromatography and/or recrystallization. For the rest of this chapter, the arm containing the benzimidazole group is designated as the *x*-axis while the arm with the arylethynyl group is referred to as the *y*-axis.

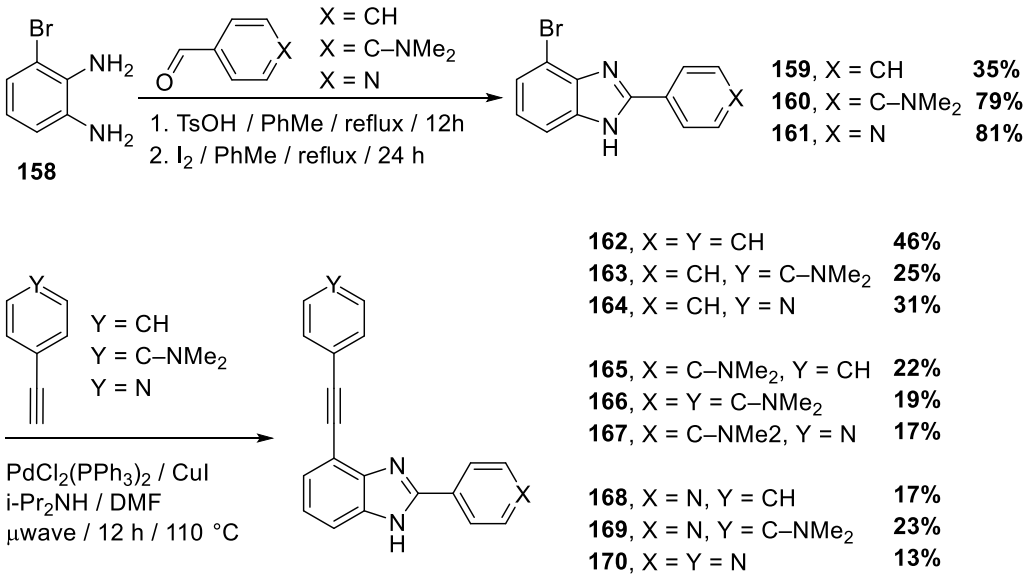

Scheme 5.1 Synthesis of half-cruciforms **162–170**.

5.2.2 Computational Studies

To determine the extent of localization of the FMOs of fluorophores **162–170,** we performed molecular orbital calculations using Gaussian 09W[172] software package and its accompanying graphical interface program GaussView 5.0, at the B3LYP/6-31G^{++} level of theory.

In the absence of any functional groups on the aromatic rings, neutral fluorophore **162** has a LUMO density that is delocalized all over the molecule while the HOMO is localized on the y-axis (Figure 5.4). The overlapping HOMO and LUMO densities at the aromatic core where the two axes intersect and the predisposition of the half-cruciform to localize HOMO on the axis containing the aryl-ethynylbenzimidazole skeleton, is comparable to that reported for a non-functionalized benzobisoxazole cruciform.[152]

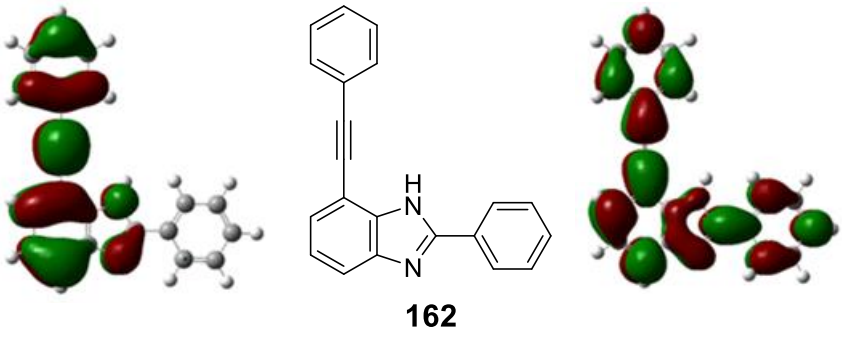

Figure 5.4 FMOs for the unsubstituted half-cruciform **162**.

Next, we examined the effect of introducing electron-rich 4-(*N*,*N*-dimethylamino)phenyl and electron-poor 4-pyridine groups on the spatial separation of the molecule's FMOs.

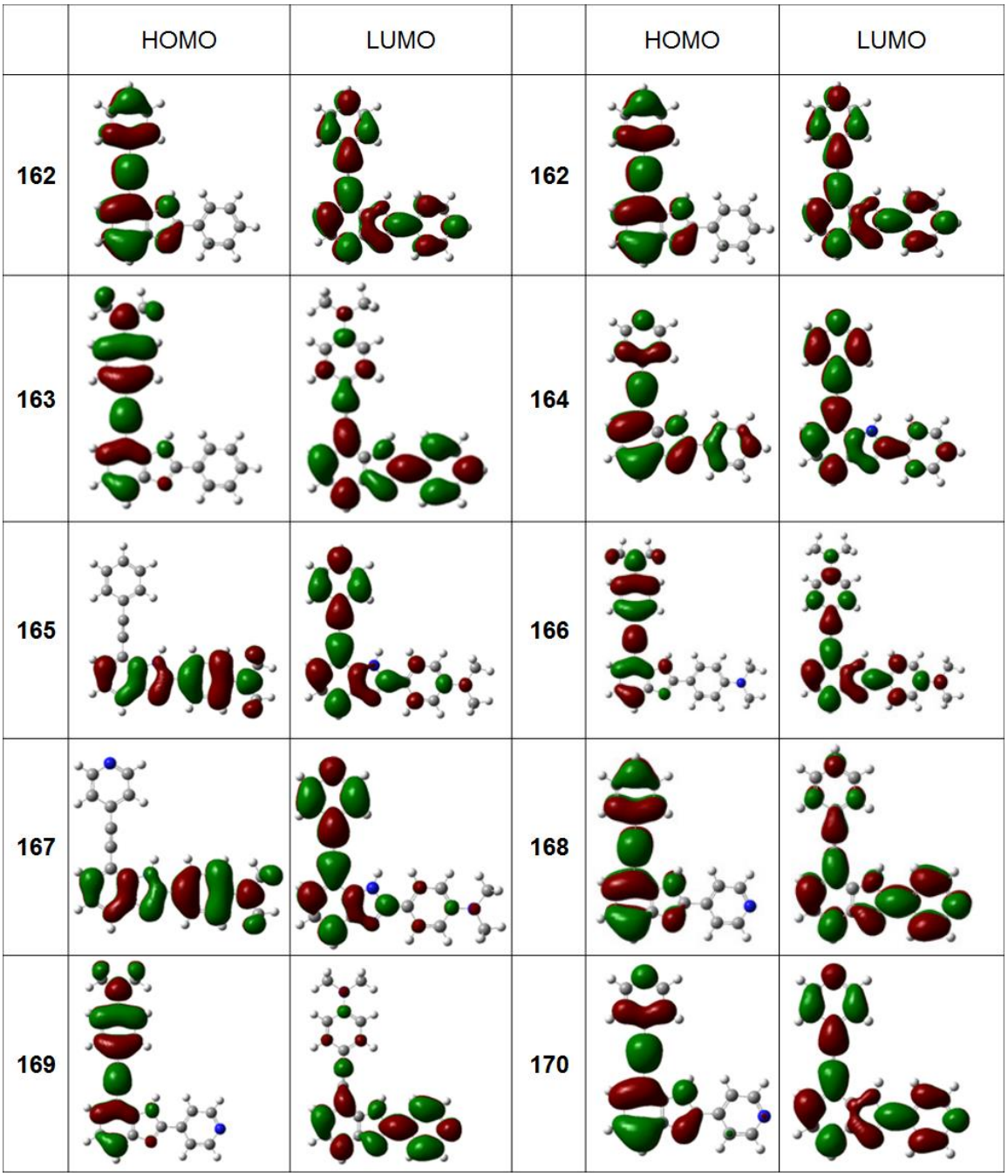

Figure 5.5 Frontier molecular orbitals of L-shaped benzimidazole molecules (**162–170**) calculated using Gaussian 09W software package at B3LYP/6-31G^{++} level of theory.

Based on the results of the Gaussian calculations (Figure 5.5), HOMO tends to be more localized compared to the LUMO. L-shaped fluorophores **163**, **166**, **168**, and **170** have their HOMO density localized on the *y*-axis similar to that observed in **162**. However, when the electron-rich 4-(*N*,*N*-dimethylamino)phenyl is introduced on the *x*-axis, HOMO density switched to this axis. Only fluorophore **164** has a delocalized HOMO which is the result of introducing electron-poor 4-pyridine group on the *y*-axis. On the other hand, LUMO density is delocalized on the majority of the fluorophores. Slight localization of LUMO on the less electron-rich phenyl arm is observed in **165**, which becomes more localized on the electron-poor pyridine-bearing arm of the electron donor–acceptor systems **167** and **169**. This result is consistent with those reported on previous studies[152,158,203] where the LUMO predominantly resides along the electron-poor axis of the molecule while HOMO is localized on the electron rich axis.

5.2.3 Optical Properties

To test the effect of FMO localization on the optical properties of the fluorophores, we prepared 1×10^{-5} M solution of the neutral fluorophore **162** that has delocalized HOMO and LUMO densities and compared its fluorescence emission, when placed under a hand-held UV lamp (λ_{exc}=365 nm), with that of the acceptor-donor systems **167** and **169** (Figure 5.6). In the case of **167** and **169**, their fluorescence emission is highly solvent-dependent, with **167** exhibiting a solvatochromic red shift as the solvent is varied from a nonpolar hexane to polar acetonitrile. This indicates that **167** underwent a significant increase in its permanent dipole moment upon excitation, which is then stabilized by the dipole–dipole interaction between the polar solvent molecules and the

excited state of **167**.[204–206] This phenomenon is not observed for the other fluorophores, especially for the "neutral" diphenyl substituted compound **162** which displayed very weak fluorescence that is independent of the solvent.

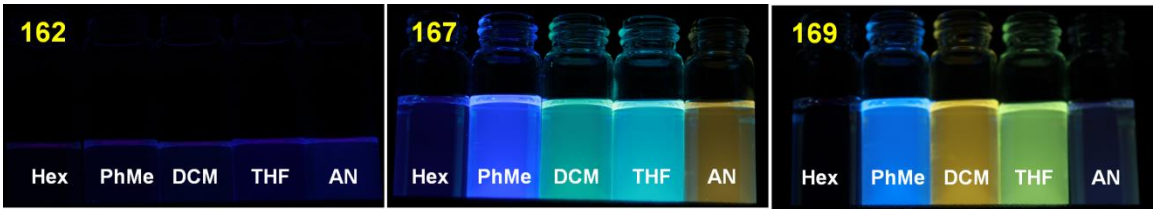

Figure 5.6 Emission colors of fluorophores **162**, **167**, and **169** in five different organic solvents: hexane (Hex), toluene (PhMe), dichloromethane (DCM), tetrahydrofuran (THF), and acetonitrile (AN). Excitation was achieved using a handheld UV lamp, λ_{exc}=365 nm.

Next, we prepared dilute solutions of all nine fluorophores and analyzed their UV-Vis absorption and fluorescence emission. The normalized absorption and emission spectra are shown in Figure 5.7 and summarized in Table 5.1. L-shaped fluorophores that do not have significant FMO localization (**162**, **164**, **168**, and **170**) have almost superimposable UV/Vis absorption spectra with the maximum absorption between 317–325 nm. All four fluorophores showed emission that is bathochromically shifted by 60 nm. On the other hand, fluorophores **163** and **169** showed similar features in their UV/Vis absorption spectra with a maximum absorption at 316 nm and 314 nm, respectively, and an additional band at around 350 nm. Their emission is also "red-shifted"—with **163** showing more significant Stoke's shift (128 nm) compared to **169** (64 nm) that has electron-accepting group on the *x*-axis and electron-donating group on the *y*-axis. Finally,

fluorophores **165**, **166**, and **167** containing the electron-rich 4-(*N*,*N*-dimethylamino)phenyl group on their *x*-axis are grouped together due to their absorption spectra that is characterized by two major absorption bands: the higher energy absorption band appearing around 300 nm and the lower energy absorption around 350 nm.

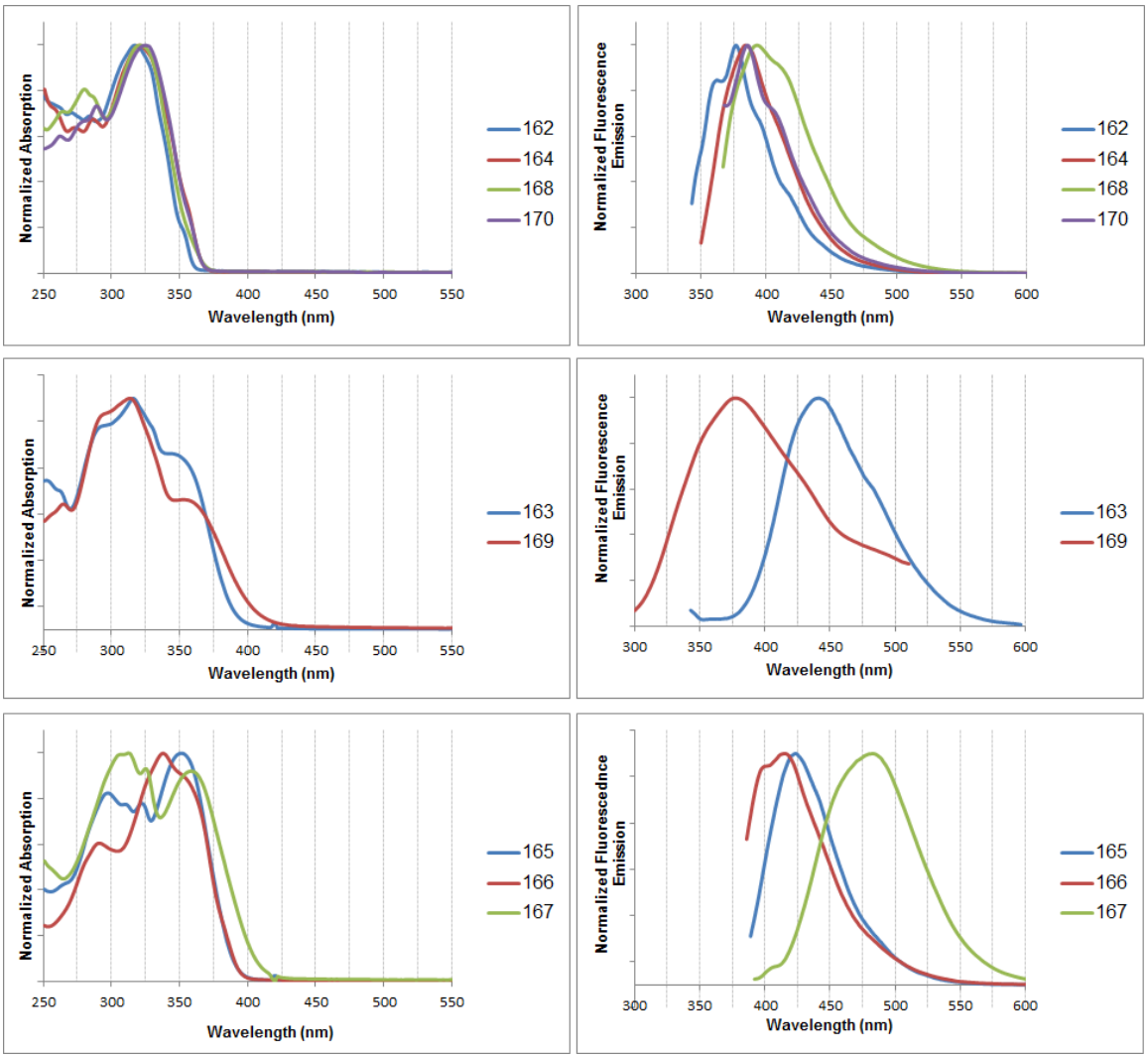

Figure 5.7 UV-Vis absorption (left) and emission (right) spectra of L-shaped fluorophores **162**–**170** in THF. Excitation wavelengths used were 313 (**162** and **163**), 344 (**164**), 359 (**165**), 356 (**166**), 362 (**167**), 337 (**168**), 317 (**169**), 338 (**170**) nm.

Compound	λ_{max} absorption in THF (nm)	λ_{max} emission in THF (nm)	Stoke's shift (nm)	Calcd HOMO–LUMO gap (eV, nm)
162	317	377	60	4.04, 307
163	316	444	128	3.52, 353
164	321	384	63	4.02, 308
165	351	424	73	3.64, 341
166	338	415	77	3.75, 331
167	313	483	170	3.30, 375
168	322	389	67	3.87, 320
169	314	378	64	3.21, 386
170	325	386	61	3.99, 311

Table 5.1 Optical properties and calculated HOMO–LUMO gaps for L-shaped fluorophores **162**–**170**.

In contrast to **169**, the donor–acceptor system **167** showed the greatest Stokes shift (170 nm) that is indicative of strong charge-transfer in the excited state. This observation highlights the significant effect of the position of the functional groups along the fluorophores backbone to the optical properties of the fluorophore.

5.2.4 Response of Fluorophores 162 and 167 to Acids, Bases, and Anions

Since **167** showed the most interesting optical property, we decided to probe its response to acids, bases and small anions. We also compared its response to that of the "neutral" fluorophore **162** so we can separate the effects of the benzimidazole nucleus alone (in **162**) from those introduced by the donor–acceptor substitution and the resultant FMO spatial isolation (in **167**).

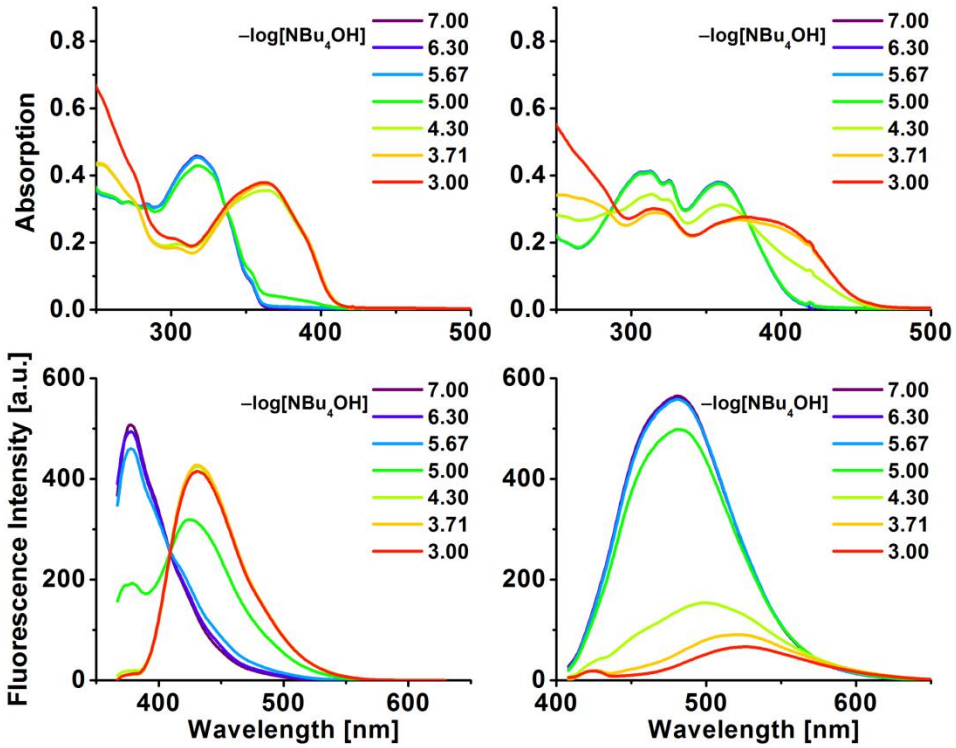

Figure 5.8 UV/Vis absorption (top) and emission (bottom) spectra for the titrations of THF solutions of fluorophores **162** (left two spectra) and **167** (right two spectra) with a concentrated aqueous solution of TBAOH. Excitation wavelengths for fluorescence emission titrations of **162** and **167** were 337 and 338 nm, respectively.

We titrated dilute solutions of the fluorophores with a concentrated aqueous solution of tetrabutylammonium hydroxide (TBAOH). In both fluorophores, red shifts in absorption (Figure 5.8, top; +45 nm for **162** and +43 nm for **167**) and emission (Figure 5.8, bottom; +54 nm for **162** and +43 nm for **167**) were observed, with clear isosbestic points suggesting simple interconversion between just two species: compounds **162** and **167** and their conjugate bases deprotonated at the benzimidazole ($pK_a \approx 12.8$).[207,208] These red shifts indicate that deprotonation destabilizes HOMO more than the LUMO;

the largely analogous responses of **162** and **167** are a consequence of the fact that both FMOs in both compounds have significant densities along the imidazole N–H bond being cleaved.

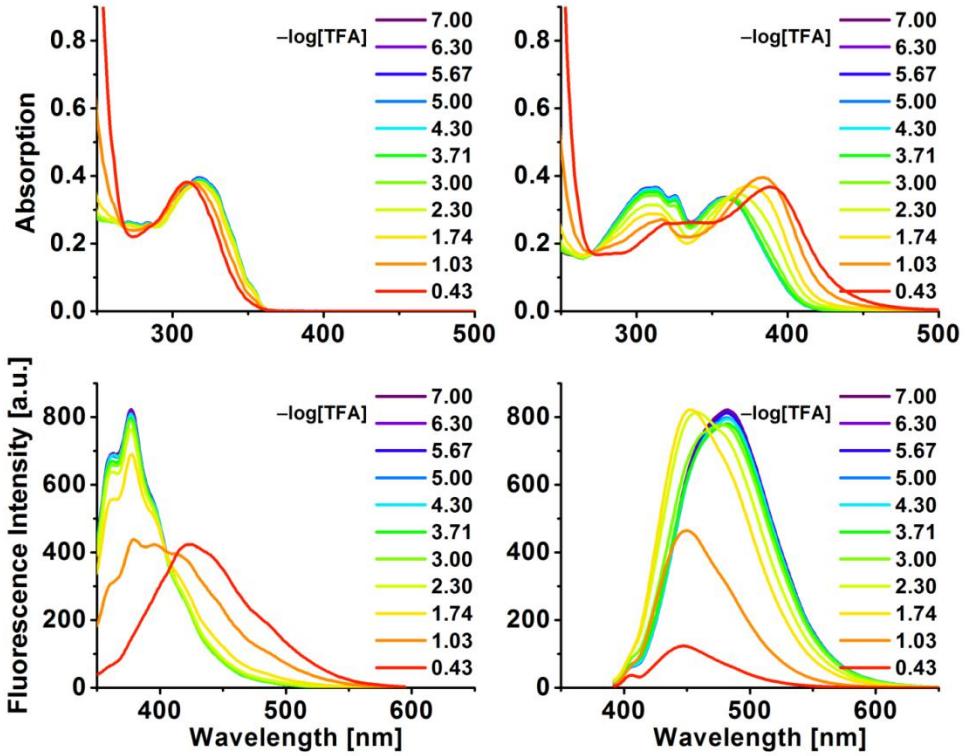

Figure 5.9 UV/Vis absorption (top) and emission (bottom) spectra for the titrations of THF solutions of fluorophores **162** (left two spectra) and **167** (right two spectra) with a concentrated solution of TFA in THF. Excitation wavelengths for fluorescence emission titrations of **162** and **167** were 313 and 362 nm, respectively.

Perhaps surprisingly, response of the prepared half-cruciform sensors to acids was more difficult to rationalize. Both **162** and **167** are largely unresponsive to trifluoroacetic acid (TFA) until –log[TFA] of approx. 2.30 is reached. At this point, **162** showed a minimal blue shift in absorption (Figure 5.9, top left; –7 nm) and a much larger red shift

and slight attenuation of its emission (Figure 5.9, bottom left; +47 nm). Since this compound can be protonated only at the benzimidazole ring, it would follow that this protonation preferentially stabilizes the LUMO. Compound **167**, on the other hand, responded by a red shift in absorption (Figure 5.9, top right; +29 nm) and a blue shift and significant attenuation of its emission (Figure 5.9, bottom right; –35 nm).

In compound **167**, there are three possible protonation sites: dimethylaniline, pyridine, and imidazole, with quite similar p*Ka* values for their conjugated acids of 5.15, 5.25, and 5.53, successively.[207,208] Based on our previous results with the benzobisoxazole cruciforms, the pyridine binding site is protonated before dimethyaniline.[152] Thus, the observed red-shift in the absorption spectrum can be rationalized by the stabilization of the LUMO (which is localized on the pyridine-bearing *y*-axis), resulting to a smaller HOMO–LUMO gap. The observed blue shift in the emission, however, is unexpected. It is known that in donor–acceptor chromophores, the electronic excitation is mostly accompanied by a charge density shift from the donor to the direction of acceptor substituents of the chromophore, *i.e.* increase in the dipole moment takes place.[209] Thus, it is possible that excitation of **167** led to a shift of the electron density from the dimethylaniline moiety to the nitrogen of the imidazole ring, in effect making it more basic than the pyridine ring. Since HOMO density is localized along the benzimidazole axis, its protonation stabilized the HOMO resulting in a larger HOMO–LUMO gap which caused the observed blue shift in emission. This is only a hypothesis at this point and additional work needs to be done to gain further insight on how these fluorophores respond to acidic analytes. For example, we can incorporate a

more basic pyridine nucleus, *e.g.* substituted with electron-donating methyl groups, to obtain a more predictable optical response to protonation.

Finally, we attempted to qualitatively assess whether half-cruciforms **162** and **167** can be used as fluorescent sensors for small inorganic and organic anions.[210–213] Dilute solutions of **162** and **167** in THF were exposed to an excess of TBA^+ salts of several representative anions. The resulting change in the emission of the solution upon addition of anions is shown in Figure 5.10. Both sensors minimally changed their fluorescence when exposed to weakly basic Cl^-, NO_3^-, and ClO_4^-, anions. However, more basic F^-, AcO^-, and $H_2PO_4^-$, anions turned ON the fluorescence of **162** and also significantly modulated the emission color of **167**. This response can be attributed to the interaction of the anions with the acidic hydrogen of the imidazole ring, *i.e.* hydrogen-bonding. On the other hand, the red shift in emission upon addition of F^- can be attributed to deprotonation—similar to the observed optical response of **167** when titrated with TBAOH.

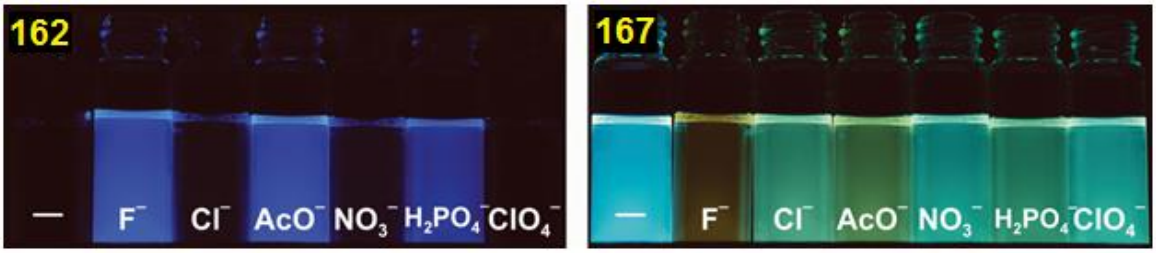

Figure 5.10 Changes in the emission color of benzimidazole sensors **162** (left) and **167** (right) upon exposure to anions. Anions were added in excess as their TBA^+ salts. Emission colors were recorded in THF, using a handheld UV lamp (λ_{exc} = 365 nm) as the excitation source.

5.3 Conclusions and Outlook

In conclusion, we have presented convenient two-step syntheses of several benzimidazole fluorophores starting from *o*-bromophenylenediamine, and shown that "half-cruciform" architecture can localize its FMOs provided that electron donor and acceptor groups are strategically positioned along the *x*- and/or *y*-axes. The optical response of the fluorophores to acids is moderate and somewhat difficult to rationalize, presumably on the account of (*a*) similar basicities of several possible protonation sites, and (*b*) incomplete spatial separation of FMOs within the molecules. On the other hand, their response to bases is much more dramatic, as all but two members of this class consistently shift their emission toward the red region.

Two major directions can be pursued for future work on this project: (*1*) modification of the substituents/core of the "half-cruciforms" to achieve desired properties for the fluorophores and (*2*) incorporation of these compounds into functional materials. For example, we can introduce polyethylene glycol units unto the central aromatic ring to make these fluorophores water soluble.[214] The benzimidazole unit can also be replaced with a different heterocyclic ring, such as benzothiazole, that can be used to sense other analytes including transition metals.[215] Lastly, tuning of the fluorophores' absorption and emission colors and intensities can be achieved by trying out different combinations of electron-acceptor and donor groups.

Since we observed that deprotonation of **162** resulted to the increase in its emission—this suggests that benzimidazolate anions of **162–170** could potentially be

used as building blocks for fluorescent and porous zeolitic imidazolate frameworks (ZIFs).[216,217] Thus, we can try to synthesize crystallographically ordered solid-state sensors from these fluorophores.

Finally, we can also explore the possibility of using these fluorophores as building blocks to generate self-assembled supramolecular systems for sensing similar to Kawai *et al.*'s ensemble[218] (Figure 5.11). Our half-cruciforms can coordinate with transition metals either through the benzimidazole core or via binding sites on the arms, *e.g.* pyridine units.

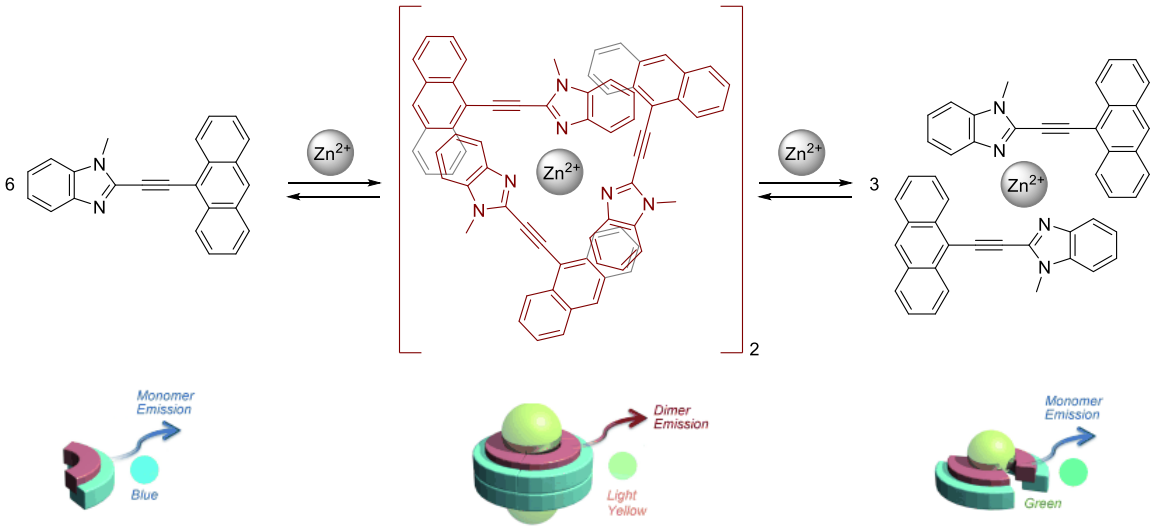

Figure 5.11 A selective supramolecular sensing system (for Zn^{2+}) generated from the self-assembly of 2-(anthracen-9-ylethynyl)-1-methylbenzimidazole in the presence of Zn^{2+}. The supramolecular ensemble gives off light-yellow emission at low concentrations of Zn^{2+} and green emission at high concentration.

5.4 Experimental Section

5.4.1 General Experimental Methods

All reactions were performed under nitrogen atmosphere in oven-dried glassware. Reagents were purchased from commercial suppliers and used without further purification. Solvents were used as received, except *N*,*N*-dimethylformamide, which was dried over activated alumina in an mBraun Solvent Purification System. Compounds 4-bromo-2,1,3-benzothiadiazole and 3-bromo-1,2-diaminobenzene were synthesized according to literature procedures.[219,220] Diisopropylamine was distilled over KOH pellets and degassed by a 15 min nitrogen purge prior to use. Microwave-assisted reactions were performed in a Biotage Initiator 2.0 microwave reactor, producing monochromatic microwave radiation with the frequency of 2.45 GHz. Mass spectral measurements were performed by the Mass Spectrometry Facility of the Department of Chemistry and Biochemistry at the University of Texas at Austin. NMR spectra were obtained on JEOL ECX-400, JEOL ECA-500, and Bruker Avance-800 MHz spectrometers, with working frequencies (for ^{1}H nuclei) of 400, 500, and 800 MHz, respectively. All ^{13}C NMR spectra were recorded with simultaneous decoupling of ^{1}H nuclei. ^{1}H NMR chemical shifts are reported in ppm units relative to the residual signal of the solvent ($CDCl_3$: 7.25 ppm, DMSO-d_6: 2.50 ppm, acetone-d_6: 2.05 ppm). NMR spectra were recorded at 25 °C for samples analyzed in $CDCl_3$ and acetone-d_6, while samples in DMSO-d_6 were analyzed at 90 °C with 1–3 drops of D_2O added to eliminate asymmetry induced by N–H tautomerization.[194] Infrared spectra were recorded on a Perkin-Elmer Spectrum 100 FT-IR spectrophotometer using Pike MIRacle Micrometer pressure clamp.

Microanalyses were conducted by Intertek USA, Inc. Melting points were measured in open capillary tubes using Mel-Temp Thermo Scientific apparatus, and are uncorrected. Column chromatography was carried out on silica gel 60, 32–63 mesh. Analytical TLC was performed on Merck aluminum-backed silica gel plates.

5.4.2 Synthesis of 7-Bromo-2-phenyl-1*H*-benzo[*d*]imidazole (**159**)

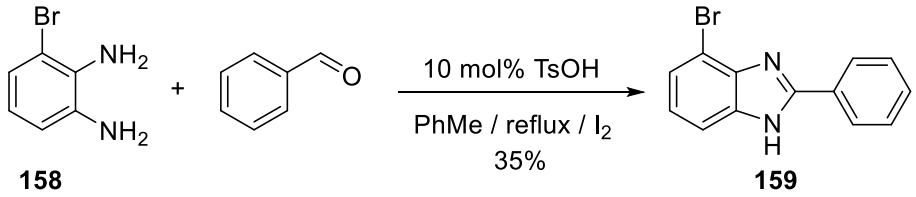

158 **159**

In a 250 mL round-bottom flask, compound **158** (2.12 g, 11.4 mmol) and benzaldehyde (1.16 mL, 11.4 mmol) were dissolved in PhMe (150 mL). *para*-Toluenesulfonic acid (0.22 g, 1.17 mmol) was added and the solution was sonicated for 20 min. After sonication, the solution was heated at reflux with a Dean-Stark trap for 12 h. After that time, I_2 (2.90 g, 11.4 mmol) was added, and the solution was kept at reflux for 24 h. After cooling, the solvent was removed and the brown oily residue was sonicated with CH_2Cl_2 until it formed a solid precipitate. The solution was filtered and washed with hexane to give compound **159** as a yellow solid (1.11 g, 35%).

159: yellow powder, mp 225–227 °C. IR (neat): 3061, 1621, 1457, 1311, 1029, 931, 750, 690 cm^{-1}. UV-Vis (AN): λ_{max} (log ε) = 206 (4.71), 242 (4.36), 248 (4.30), 300 (4.46) nm. ^{1}H NMR (acetone-d_6, 500 MHz): δ 8.24 (dd, J=8.3, 1.5 Hz, 2H), 7.55 (d, J=8.0 Hz, 1H), 7.50 (m, 3H), 7.39 (dd, J=8.0, 1.2 Hz, 1H), 7.12 (dd, J=8.0, 7.5 Hz, 1H) ppm. ^{13}C NMR

(acetone-d_6, 125 MHz): δ 152.7, 143.8, 136.3, 130.8, 130.4, 129.2, 125.5, 124.0, 113.2, 111.0 ppm. HRMS (ESI): Calcd for $C_{13}H_{10}BrN_2^+$: 273.0022. Found: 273.0020.

5.4.3 Synthesis of 4-(7-Bromo-1*H*-benzo[*d*]imidazol-2-yl)-*N*,*N*-dimethylbenzenamine (**160)**

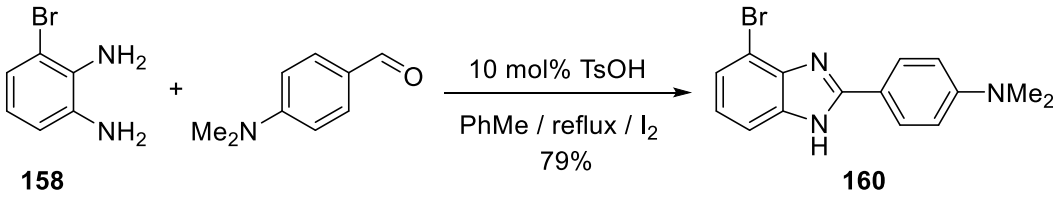

158 **160**

In a 250 mL round-bottom flask, compound **158** (1.12 g, 6.00 mmol) and 4-dimethylaminobenzaldehyde (895 mg, 6.00 mmol) were dissolved in PhMe (150 mL). *para*-Toluenesulfonic acid (196 mg, 1.03 mmol) was added, and the solution was sonicated for 20 min, during which time a precipitate formed. After sonication, the solution was heated at reflux with a Dean-Stark trap for 12 h. After that time, I_2 (1.52 g, 6mmol) was added and the solution was heated at reflux for 24 h. After cooling, the solution was filtered and the residue washed with hexane and Me_2CO to give a reddish brown solid that was identified as **160** (1.50 g, 79%). Further purification can be achieved by recrystallization in Me_2CO or EtOH.

160: red-brown powder, mp 161 °C, with decomposition. IR (neat): 3432, 1610, 1524, 1378, 1216, 816, 776, 641 cm^{-1}. UV-Vis (AN): λ_{max} (log ε) = 245 (4.46), 371 (4.64) nm. ^{1}H NMR (DMSO-d_6, 500 MHz): δ 8.08 (d, J=9.2 Hz, 2H), 7.65 (d, J=8.0 Hz, 1H), 7.63 (d, J=8.0 Hz, 1H), 7.32 (t, J=8.0 Hz, 1H), 6.89 (d, J=9.2 Hz, 2H), 3.05 (s, 6H) ppm. ^{13}C NMR (DMSO-d_6, 125 MHz): δ 153.8, 151.9, 133.4, 132.7, 130.4, 128.4, 126.9, 112.9,

112.2, 108.7, 105.7 ppm. HRMS (ESI): Calcd for $C_{15}H_{15}BrN_3^+$: 316.0444. Found: 316.0443.

5.4.4 Synthesis of 7-Bromo-2-(pyridine-4-yl)-1*H*-benzo[*d*]imidazole (**161**)

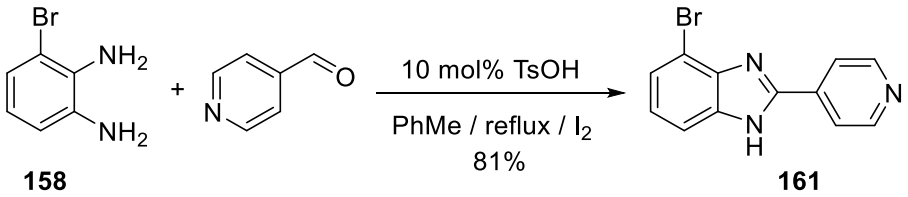

In a 250 mL round-bottom flask, compound **158** (2.51 g, 13.4 mmol) and 4-pyridinecarboxaldehyde (1.26 mL, 13.4 mmol) were dissolved in PhMe (150 mL). *para*-Toluenesulfonic acid (255 mg, 1.34 mmol) was added and the solution was sonicated for 20 min. After sonication, the solution was heated at reflux with a Dean-Stark trap for 12 h. After that time, I_2 (3.40 g, 13.4 mmol) was added into the solution. Immediate formation of a yellow-brown precipitate was observed. The mixture was kept at reflux for additional 24 h. After cooling, the solution was filtered and the residue washed with hexane and Me_2CO and to give a pale yellow solid (2.98 g, 81%). Further purification can be achieved by recrystallization from Me_2CO or EtOH.

161: pale yellow powder, mp 243 °C, with decomposition. IR (neat): 3071, 1638, 1503, 1224, 1151, 1032, 808, 743, 683 cm^{-1}. UV-Vis (AN): λ_{max} (log ε) = 202 (4.59), 245 (4.20), 313 (3.95), 350 (3.95) nm. ^{1}H NMR (DMSO-d_6, 500 MHz): δ 8.96 (d, J=6.3 Hz, 2H), 8.50 (d, J=6.9 Hz, 2H), 7.68 (d, J=8.0 Hz, 1H), 7.54 (d, J=7.5 Hz, 1H), 7.26 (dd, J=8.0, 7.5 Hz, 1H) ppm. ^{13}C NMR (DMSO-d_6, 125 MHz): δ 147.4, 144.2, 141.2, 138.3,

127.0, 126.4, 123.6, 114.4, 111.5 ppm. HRMS (ESI): Calcd for $C_{12}H_9BrN_3^+$: 273.9974. Found: 273.9974.

5.4.5 Synthesis of Half-Cruciform **162**

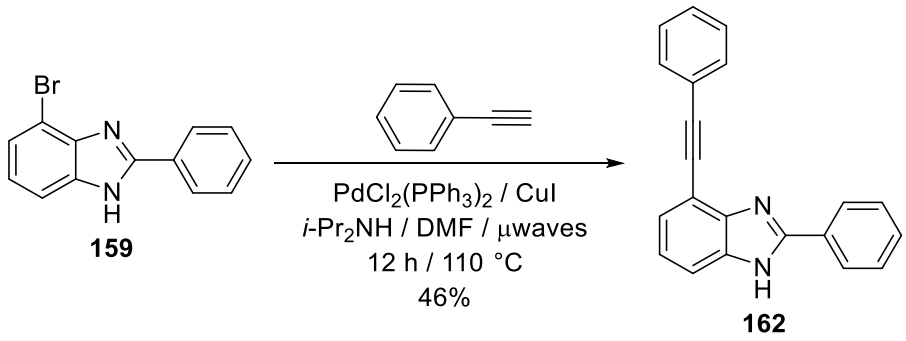

Phenylacetylene (450 mg, 4.40 mmol) was added to a thick-walled microwave pressure vial that contained a mixture of compound **159** (300 mg, 1.10 mmol), $PdCl_2(PPh_3)_2$ (60.0 mg, 0.09 mmol), CuI (20.0 mg, 0.11 mmol), *i*-Pr_2NH (5 mL), and DMF (5 mL). The vial was sealed and exposed to microwave irradiation for 12 h at 110 °C. After cooling, the reaction mixture was extracted with EA, washed with brine, and then dried over anhydrous $MgSO_4$. The product was isolated by column chromatography, eluting with a hexane/EA (7:3) mixture. The solvent was removed under reduced pressure, and the solid recrystallized from a mixture of THF and hexane to give pure compound **162** (150 mg, 46%).

162: white powder, mp 280 °C. IR (neat): 3052, 2324, 1473, 1459, 1418, 1395, 1253, 965, 973, 753, 707, 691 cm^{-1}. UV-Vis (THF): λ_{max} (log ε) = 213 (4.67), 233 (4.51), 247 (4.47), 261 (4.43), 272 (4.43), 283 (4.41), 318 (4.60) nm. ^1H NMR (DMSO-d_6 and 1 drop of D_2O, 500 MHz): δ 8.22 (br d, 2H), 7.64 (br d, 2H), 7.54 (m, 3H), 7.49 (m, 1H), 7.43

(m, 3H), 7.37 (d, *J*=7.5 Hz, 1H), 7.21 (dd, *J*=8.0 Hz, 7.5 Hz, 1H) ppm. ^{13}C NMR (DMSO-d_6 and 1 drop of D_2O, 200 MHz): δ 152.0, 144.4, 135.1, 131.6, 130.4, 129.8, 129.1, 128.9, 127.4, 126.8, 125.8, 122.9, 122.7, 112.9, 112.4, 109.6, 92.7, 87.7 ppm. HRMS (ESI/$[M+H]^+$): calcd for $C_{21}H_{15}N_2^+$ 295.1230, found 295.1230. Anal. Calcd. for $C_{21}H_{14}N_2 \cdot ¼THF$: C, 84.59; H, 5.16; N, 8.97. Found: C, 84.84; H, 3.95; N, 9.29.

5.4.6 Synthesis of Half-Cruciform **163**

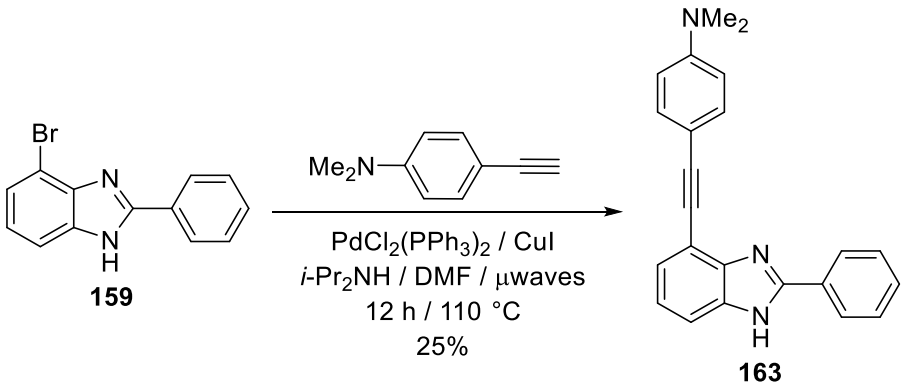

Anhydrous K_2CO_3 (831 mg, 6.01 mmol) was added to a solution of 2-(4-(*N*,*N*-dimethylamino)phenyl)trimethylsilylethyne (652 mg, 3.00 mmol) in a mixture of MeOH (5 mL) and THF (5 mL). After stirring for 30 min under nitrogen, the reaction mixture was filtered though Celite. The solvent was removed under reduced pressure to yield crude 4-ethynyl-*N*,*N*-dimethylaniline, which was used without purification in the next step. To minimize manipulations of this somewhat sensitive compound, we assumed a 95% yield for this reaction.[152]

The entire amount of 4-ethynyl-*N*,*N*-dimethylaniline (prepared as above-described) was added to a thick-walled microwave pressure vial that contained a mixture

of compound **159** (300 mg, 1.10 mmol), $PdCl_2(PPh_3)_2$ (60.0 mg, 0.09 mmol), CuI (20.0 mg, 0.11 mmol), *i*-Pr_2NH (5 mL), and DMF (5 mL). The vial was sealed and exposed to microwave irradiation for 12 h at 110 °C. After cooling, the reaction mixture was extracted with EA, washed with brine, and dried over anhydrous $MgSO_4$. The product was isolated by column chromatography, eluting with hexane/EA mixtures (60:40, 50:50, 20:80 and 0:100, successively). The solvent was removed under reduced pressure, and the solid was washed with EA (5 mL) and THF (3 mL) to give pure compound **163** (90.5 mg, 25%).

163: light green powder, mp 284 °C, with decomposition. IR (neat): 3091, 2206, 1607, 1588, 1524, 1457, 1386, 1363, 1186, 819, 747, 707 cm^{-1}. UV-Vis (THF): λ_{max} (log ε) = 253 (4.45), 293 (4.59), 317 (4.65), 351 (4.53) nm. ^1H NMR (DMSO-d_6 and 1 drop of D_2O, 500 MHz): δ 8.22 (br d, 2H), 7.51 (m, 5H), 7.41 (br s, 1H), 7.30 (d, *J*=7.5 Hz, 1H), 7.18 (dd, *J*=8.1 Hz, 7.4 Hz, 1H), 6.73 (d, *J*=9.2 Hz, 2H), 2.94 (s, 6H) ppm. ^{13}C NMR (DMSO-d_6 and 1 drop of D_2O, 200 MHz): δ 151.6, 150.1, 144.1, 135.1, 132.5, 130.1, 129.9, 128.9, 126.7, 125.2, 122.5, 113.9, 111.9, 111.4, 109.1, 94.2, 85.4, 39.5 ppm. HRMS (ESI/$[M+H]^+$): calcd for $C_{23}H_{20}N_3^+$ 338.1652, found 338.1650. Anal. Calcd. for $C_{23}H_{19}N_3 \cdot \frac{1}{3}$THF: C, 80.86; H, 6.04; N, 11.63. Found: C, 80.48; H, 5.46; N, 12.05.

5.4.7 Synthesis of Half-Cruciform **164**

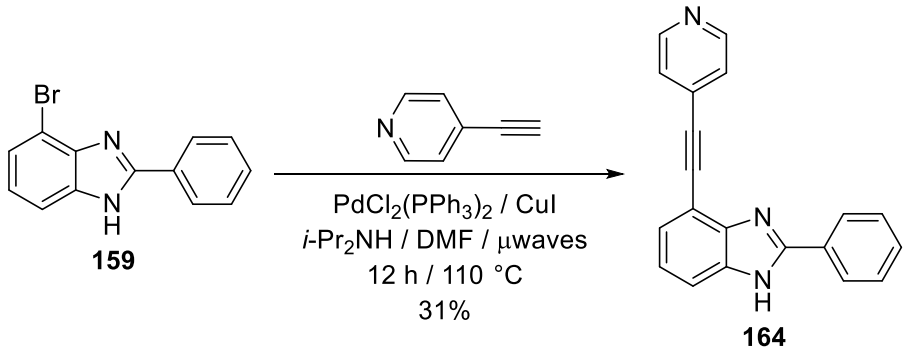

Anhydrous K_2CO_3 (1.00 g, 7.24 mmol) was added to a solution of 2-(4-(pyridyl)) trimethylsilylacetylene (630 mg, 3.59 mmol) in a mixture of MeOH (5 mL) and THF (5 mL). After being stirred for 30 min under nitrogen, the reaction mixture was filtered through Celite. The solvent was removed under reduced pressure to yield crude 4-ethynylpyridine, which was used without purification in the next step. To minimize manipulations of this somewhat sensitive compound, we assumed a 95% yield for this reaction.[152]

The entire amount of 4-ethynylpyridine (prepared as described above) was added to a thick-walled microwave pressure vial that contained a mixture of compound **159** (300 mg, 1.10 mmol), $PdCl_2(PPh_3)_2$ (60.0 mg, 0.09 mmol), CuI (20.0 mg, 0.11 mmol), *i*-Pr_2NH (5 mL), and DMF (5 mL). The vial was sealed and exposed to microwave irradiation for 12 h at 110 °C. After cooling, the reaction mixture was extracted with EA, washed with brine, and dried over anhydrous $MgSO_4$. The product was isolated by column chromatography, eluting first with pure EA, and then successively with EA/MeOH mixtures in 95:5 and 90:10 ratios. The solvent was removed under reduced

pressure, and the resulting solid was recrystallized from a mixture of THF and hexane to give pure compound **164** (102 mg, 31%).

164: white powder, mp 251 °C, with decomposition. IR (neat): 3085, 2224, 1598, 1456, 1415, 1270, 831, 793, 735, 697, 685, 648 cm^{-1}. UV-Vis (THF): λ_{max} (log ε) = 210 (4.66), 235 (4.48), 242 (4.48), 247 (4.46), 259 (4.34), 274 (4.30), 287 (4.36), 322 (4.57) nm. ^{1}H NMR (DMSO-d_6, 500 MHz): δ 12.86 (s, 1H), 8.63 (d, J=6.3 Hz, 2H), 8.22 (d, J=7.5 Hz, 2H), 7.65 (d, J=7.5 Hz, 1H), 7.53 (m, 5H), 7.43 (dd, J=7.5 Hz, J=1.2 Hz, 1H), 7.24 (dd, J=8.1 Hz, 7.5 Hz, 1H) ppm. ^{13}C NMR (DMSO-d_6 and 1 drop of D_2O, 200 MHz): δ 152.5, 150.2, 144.5, 135.2, 131.0, 130.8, 129.7, 129.2, 127.1, 126.5, 125.7, 122.8, 113.4, 111.7, 109.6, 92.2, 90.2 ppm. HRMS (ESI/$[M+H]^+$): calcd for $C_{20}H_{14}N_3^+$ 296.1182, found 296.1183. Anal. Calcd for $C_{20}H_{13}N_3 \cdot {}^1/_6$ THF: C, 80.76; H, 4.70; N, 13.67. Found: C, 80.76; H, 4.31; N, 13.88.

5.4.8 Synthesis of Half-Cruciform **165**

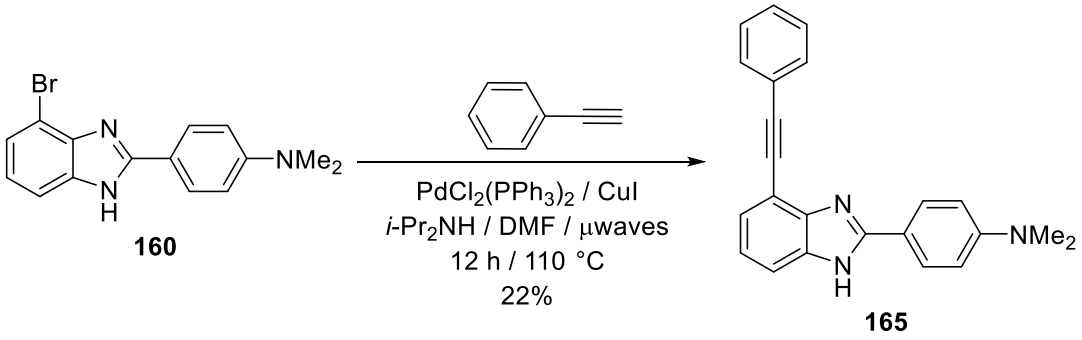

Phenylacetylene (387 mg, 3.79 mmol) was added to a thick-walled microwave pressure vial that contained a mixture of compound **160** (300 mg, 0.95 mmol), $PdCl_2(PPh_3)_2$ (60.0 mg, 0.09 mmol), CuI (20.0 mg, 0.11 mmol), *i*-Pr_2NH (5 mL), and

DMF (5 mL). The vial was sealed and exposed to microwave irradiation for 12 h at 110 °C. After cooling, the reaction mixture was extracted with EA, washed with brine, and dried over anhydrous $MgSO_4$. The product was isolated by column chomatography, eluting with a hexane/EA (70:30) mixture. The solvent was removed under reduced pressure, and the solid was recrystallized from a mixture of Et_2O, CH_2Cl_2, and hexane to give pure compound **165** (70 mg, 22%).

165: yellow powder, mp 247 °C. IR (neat): 3119, 2320, 1612, 1492, 1416, 1367, 1202, 956, 820, 753, 689, 668, 636, 601 cm^{-1}. UV-Vis (THF): λ_{max} (log ε) = 224 (4.59), 299 (4.48), 312 (4.45), 323 (4.46), 352 (4.57) nm. ^1H NMR ($CDCl_3$, 400 MHz): δ 7.96 (d, *J*=8.7 Hz, 2H), 7.68 (d, *J*=8.2 Hz, 1H), 7.58 (m, 2H), 7.40 (m, 4H), 7.20 (dd, *J*=8.2 Hz, 7.8 Hz, 1H), 6.74 (d, *J*=8.3 Hz, 2H), 3.03 (s, 6H) ppm. ^{13}C NMR ($CDCl_3$, 200 MHz): δ 162.2, 153.0, 151.8, 143.5, 131.8, 131.7, 128.5, 128.3, 126.2, 123.1, 122.5, 121.6, 116.0, 112.0, 93.5, 85.6, 40.2 ppm. HRMS (ESI): calcd for $C_{23}H_{20}N_3^+$ 338.1652, found 338.1654. Anal. Calcd for $C_{23}H_{19}N_3 \cdot ¼Et_2O$: C, 80.98; H, 6.09; N, 11.81. Found: C, 80.93; H, 5.48; N, 12.23.

5.4.9 Synthesis of Half-Cruciform **166**

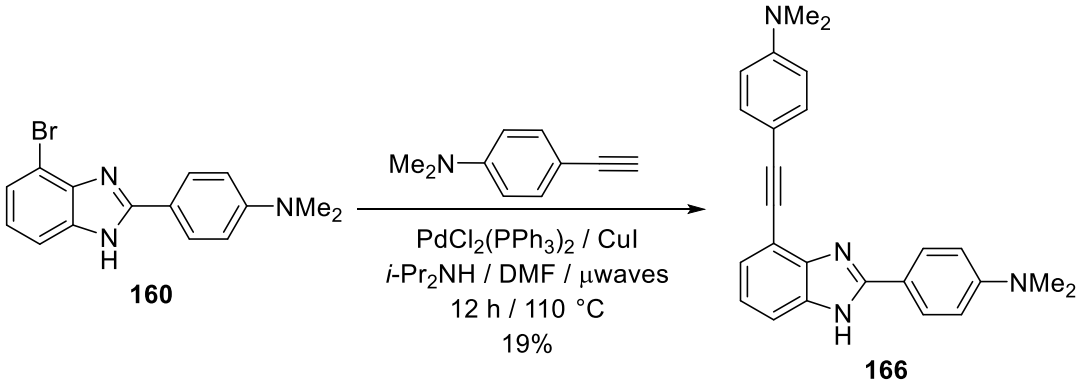

The entire amount of 4-ethynyl-*N*,*N*-dimethylaniline (prepared as in the synthesis of compound **163** described previously) was added to a thick-walled microwave pressure vial that contained a mixture of compound **160** (300 mg, 0.95 mmol), $PdCl_2(PPh_3)_2$ (60.0 mg, 0.09 mmol), CuI (20.0 mg, 0.11 mmol), *i*-Pr_2NH (5 mL), and DMF (5 mL). The vial was sealed and exposed to microwave irradiation for 12 h at 110 °C. After cooling, the reaction mixture was extracted with EA, washed with brine, and dried over anhydrous $MgSO_4$. The product was isolated by column chromatography, eluting with pure EA. The solvent was removed under reduced pressure, and the solid was recrystallized from a mixture of THF and hexane to give pure compound **166 (**67 mg, 19%).

166: yellow powder, mp 276 °C, with decomposition. IR (neat): 3046, 2209, 1609, 1517, 1482, 1443, 1415, 1366, 1247, 1183, 920, 821, 755 cm^{-1}. UV-Vis (THF): λ_{max} (log ε) = 220 (4.60), 292 (4.46), 339 (4.66), 353 (4.62) nm. ^1H NMR (DMSO-d_6 and 3 drops of D_2O, 500 MHz): δ 8.00 (d, *J*=8.1 Hz, 2H), 7.42 (m, 3H), 7.20 (d, *J*=7.5 Hz, 1H), 7.09 (dd, *J*=8.1 Hz, 7.5 Hz, 1H), 6.79 (d, *J*=9.2 Hz, 2H), 6.71 (d, *J*=8.6 Hz, 2H), 2.96 (s, 6H), 2.92 (s, 6H) ppm. ^{13}C NMR (DMSO-d_6 and 1 drop of D_2O, 200 MHz): δ 152.6, 151.4, 150.1, 144.4, 135.0, 132.5, 127.9, 124.7, 121.5, 118.1, 117.0, 113.0, 111.8, 110.7, 109.4, 106.6, 93.8, 85.8, 39.5 ppm. HRMS (ESI/$[M+H]^+$): calcd for $C_{25}H_{25}N_4^+$ 381.2074, found 381.2073. Anal. Calcd for $C_{25}H_{24}N_4 \cdot ½THF$: C, 77.85; H, 6.78; N, 13.45. Found: C, 77.45; H, 6.00; N, 13.96.

5.4.10 Synthesis of Half-Cruciform **167**

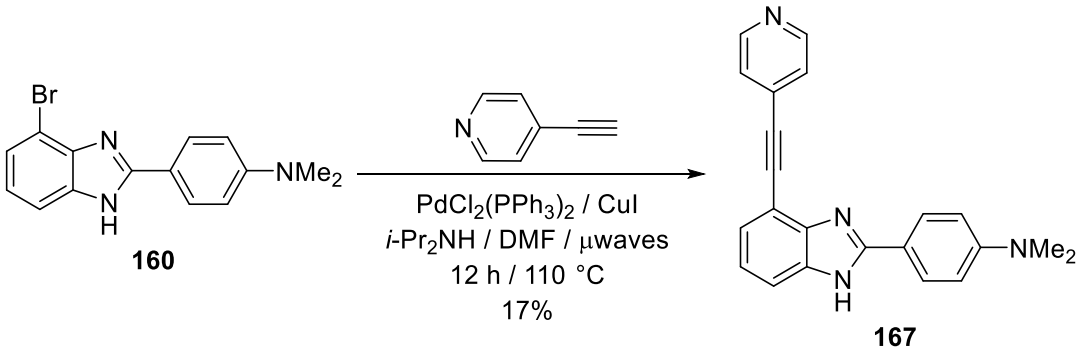

The entire amount of 4-ethynylpyridine (prepared as in the synthesis of compound **164** described previously) was added to a thick-walled microwave pressure vial that contained a mixture of compound **160** (300 mg, 0.95 mmol), $PdCl_2(PPh_3)_2$ (60.0 mg, 0.09 mmol), CuI (20.0 mg, 0.11 mmol), *i*-Pr_2NH (5 mL), and DMF (5 mL). The vial was sealed and exposed to microwave irradiation for 12 h at 110 °C. After cooling, the reaction mixture was extracted with EA, washed with brine, and dried over anhydrous $MgSO_4$. The product was isolated by column chromatography, eluting with pure EA. The solvent was removed under reduced pressure, and the solid was recrystallized from a mixture of THF and hexane to give pure compound **167** (55 mg, 17%).

167: yellow powder, mp 256 °C. IR (neat): 3419, 2227, 1609, 1500, 1413, 1365, 1352, 1205, 790, 739, 688, 608 cm^{-1}. UV-Vis (THF): λ_{max} (log ε) = 222 (4.65), 306 (4.56), 314 (4.56), 326 (4.53), 359 (4.53) nm. ^1H NMR (DMSO-d_6 and 1 drop of D_2O, 500 MHz): δ 8.62 (d, *J*=5.2 Hz, 2H), 8.02 (br s, 2H), 7.58 (br s, 3H), 7.35 (dd, *J*=8.0 Hz, 1.2 Hz, 1H), 7.16 (dd, *J*=8.1 Hz, 7.5 Hz, 1H), 6.81 (d, *J*=9.2 Hz, 2H), 2.97 (s, 6H) ppm. ^{13}C NMR (DMSO-d_6 and 1 drop of D_2O, 200 MHz): δ 153.5, 151.7, 150.0, 145.0, 135.1, 131.0,

128.2, 125.7, 125.5, 121.7, 116.6, 111.9, 111.5, 110.5, 92.5, 89.9, 39.5 ppm. HRMS (ESI/$[M+H]^+$): calcd for $C_{22}H_{19}N_4^+$ 339.1604, found 339.1606. Anal. Calcd. for $C_{22}H_{18}N_4 \cdot {}^1/_6$ THF C, 77.69; H, 5.56; N, 15.99. Found: C, 77.24; H, 5.09; N, 13.34.

5.4.11 Synthesis of Half-Cruciform **168**

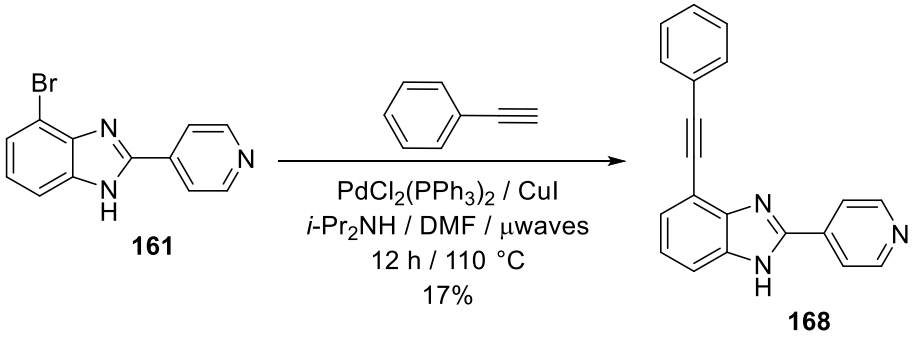

Phenylacetylene (418 mg, 4.09 mmol) was added to a thick-walled microwave pressure vial that contained a mixture of compound **161** (300 mg, 1.09 mmol), $PdCl_2(PPh_3)_2$ (60.0 mg, 0.09 mmol), CuI (20.0 mg, 0.11 mmol), *i*-Pr_2NH (5 mL), and DMF (5 mL). The vial was sealed and exposed to microwave irradiation for 12 h at 110 °C. After cooling, the reaction mixture was extracted with EA, washed with brine, and dried over anhydrous $MgSO_4$. The product was isolated by column chromatography, eluting first with pure EA, and then successively with EA/MeOH mixtures in 95:5 and 90:10 ratios. The solvent was removed under reduced pressure, and the solid was recrystallized in the mixture of THF, CH_2Cl_2 and hexane to give pure compound **168 (**58 mg, 17%).

168: white powder, mp 226 °C. IR (neat): 3076, 1609, 1437, 1250, 999, 829, 756, 736, 696, 630 cm^{-1}. UV-Vis (THF): λ_{max} (log ε) = 227 (4.45), 264 (4.46), 281 (4.36), 288

(4.34), 323 (4.46) nm. ^{1}H NMR (DMSO-d_6, 500 MHz): δ 13.14 (br s, 1H), 8.74 (d, J=6.3 Hz, 2H), 8.13 (br s, 2H), 7.63 (br s, 3H), 7.43 (m, 4H), 7.28 (dd, J=8.0 Hz, 7.5 Hz, 1H) ppm. ^{13}C NMR (DMSO-d_6 and 1 drop of D_2O, 200 MHz): δ 150.5, 149.6, 144.1, 136.9, 135.1, 131.7, 128.9, 127.4, 126.4, 123.7, 122.7, 120.8, 113.6, 112.9, 93.2, 87.2 ppm. HRMS (ESI/[M+H]$^+$): calcd for $C_{20}H_{14}N_3^+$ 296.1182, found 296.1185. Anal. Calcd for $C_{20}H_{13}N_3 \cdot {}^1/_5$THF: C, 80.65; H, 4.75; N, 13.57. Found: C, 80.41; H, 4.02; N, 13.97.

5.4.12 Synthesis of Half-Cruciform **169**

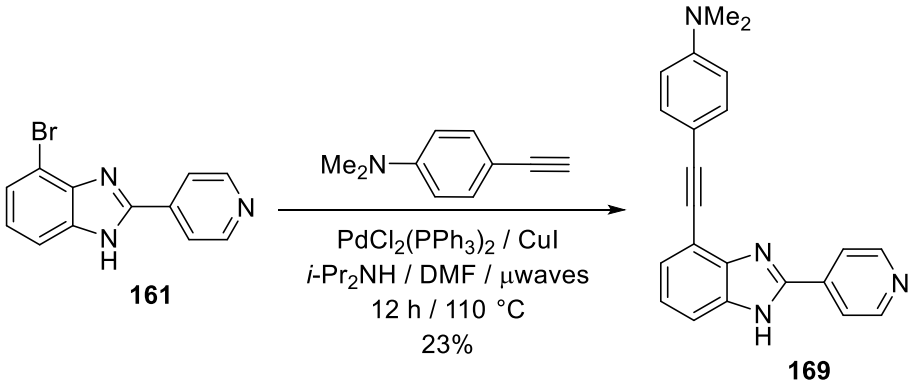

The entire amount of 4-ethynyl-*N*,*N*-dimethylaniline (prepared as in the synthesis of compound **163** described previously) was added to a thick-walled microwave pressure vial that contained a mixture of compound **161** (300 mg, 1.09 mmol), $PdCl_2(PPh_3)_2$ (60.0 mg, 0.09 mmol), CuI (20.0 mg, 0.11 mmol), *i*-Pr_2NH (5 mL), and DMF (5 mL). The vial was sealed and exposed to microwave irradiation for 12 h at 110 °C. After cooling, the reaction mixture was extracted with EA, washed with brine, and dried over anhydrous $MgSO_4$. The product was isolated by column chromatography, eluting first with pure EA, and then successively with EA/MeOH mixtures in 95:5 and 90:10 ratios. The solvent was

removed under reduced pressure, and the solid was recrystallized from a mixture of THF, MeOH and hexane to give pure compound **169** (85 mg, 23%).

169: yellow powder, mp 259 °C, with decomposition. IR (neat): 3098, 2215, 1608, 1524, 1445, 1363, 1186, 822, 795, 743, 701, 630 cm^{-1}. UV-Vis (THF): λ_{max} (log ε) = 265 (4.20), 294 (4.50), 315 (4.54), 357 (4.28) nm. ^{1}H NMR (DMSO-d_6 and 1 drop of D_2O, 500 MHz): δ 8.73 (d, J=6.3 Hz, 2H), 8.13 (br s, 2H), 7.60 (br s, 1H), 7.44 (d, J=8.6 Hz, 2H), 7.36 (d, J=8.0 Hz, 1H), 7.25 (dd, J=8.0 Hz, 7.5 Hz, 1H), 6.72 (d, J=9.2 Hz, 2H), 2.93 (s, 6H) ppm. ^{13}C NMR (DMSO-d_6 and 1 drop of D_2O, 200 MHz): δ 150.6, 150.4, 149.3, 143.9, 137.0, 135.2, 132.8, 125.9, 123.8, 120.8, 114.8, 112.1, 108.9, 95.1, 85.1, 39.5 ppm. HRMS (ESI/$[M+H]^+$): calcd for $C_{22}H_{19}N_4^+$ 339.1604, found 339.1605. Anal. Calcd for $C_{22}H_{18}N_4 \cdot ½THF$: C, 76.98; H, 5.92; N, 14.96. Found: C, 75.33; H, 5.35; N, 15.33.

5.4.13 Synthesis of Half-Cruciform **170**

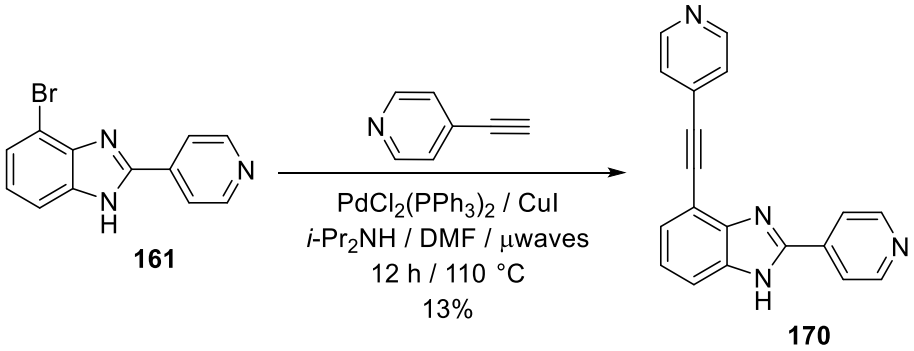

The entire amount of 4-ethynylpyridine (prepared as in the synthesis of compound **164** described previously) was added to a thick-walled microwave pressure vial that contained a mixture of compound **161** (300 mg, 1.09 mmol), $PdCl_2(PPh_3)_2$ (60.0 mg, 0.09

mmol), CuI (20.0 mg, 0.11 mmol), *i*-Pr_2NH (5 mL), and DMF (5 mL). The vial was sealed and exposed to microwave irradiation for 12 h at 110 °C. After cooling, the reaction mixture was extracted with EA, washed with brine, and dried over anhydrous $MgSO_4$. The product was isolated by column chromatography, eluting first with pure EA, and then successively with EA/MeOH mixtures in 95:5 and 90:10 ratios. The solvent was removed under reduced pressure, and the solid was recrystallized from a mixture of THF, MeOH, and hexane to give pure compound **170 (**41 mg, 13%).

170: off-white powder, mp 252 °C, with decomposition. IR (neat): 3067, 2227, 1601, 1438, 829, 792, 738, 698, 613 cm^{-1}. UV-Vis (THF): λ_{max} (log ε) = 262 (4.36), 277 (4.38), 289 (4.41), 327 (4.53) nm. ^1H NMR (DMSO-d_6, 500 MHz): δ 13.20 (br s, 1H), 8.75 (d, *J*=6.3 Hz, 2H), 8.64 (d, *J*=6.3 Hz, 2H), 8.13 (d, *J*=5.7 Hz, 2H), 7.72 (d, *J*=8.0 Hz, 1H), 7.56 (d, *J*=5.2 Hz, 2H), 7.49 (d, *J*=7.5 Hz, 1H), 7.31 (dd, *J*=8.0 Hz, 7.5 Hz, 1H) ppm. ^{13}C NMR (DMSO-d_6 and 1 drop of D_2O, 200 MHz): δ 150.7, 150.0, 149.8, 144.3, 136.8, 135.2, 130.7, 127.0, 125.7, 123.9, 120.8, 113.9, 112.3, 91.7, 90.4 ppm. HRMS (ESI/$[M+H]^+$): calcd for $C_{19}H_{13}N_4^+$ 297.1135, found 297.1136. Anal. Calcd for $C_{19}H_{12}N_4 \cdot \frac{1}{3}H_2O$: C, 75.48; H, 4.22; N, 18.53. Found: C, 75.19; H, 3.80; N, 18.22.

5.4.14 UV/Vis Absorption and Fluorescence Emission Spectra for the Titration of Half-Cruciforms **162–170** with TFA and *n*-Bu_4OH

UV-visible and fluorescence titrations were performed using Perkin-Elmer LAMBDA 25 UV/Vis Spectrometer and Perkin-Elmer Fluorescence Spectrometer LS-55,

respectively. Five stock solutions of TFA—0.1 mM, 0.001 M, 0.01 M, 0.1 M, 1 M, and 10 M and four stock solutions of 40% aq. TBAOH—0.1 mM, 0.001 M, 0.01 M, and 0.1 M were prepared in THF. In a quartz cuvette, 3 mL of 1×10^{-5} M solution of a given fluorophore in THF were titrated using the stock solutions of TFA, or 40% aq. TBAOH to give the indicated range of acid and base concentrations. The excitation wavelength used for fluorescence titration corresponds to the isosbestic point determined in the UV/Vis titration.

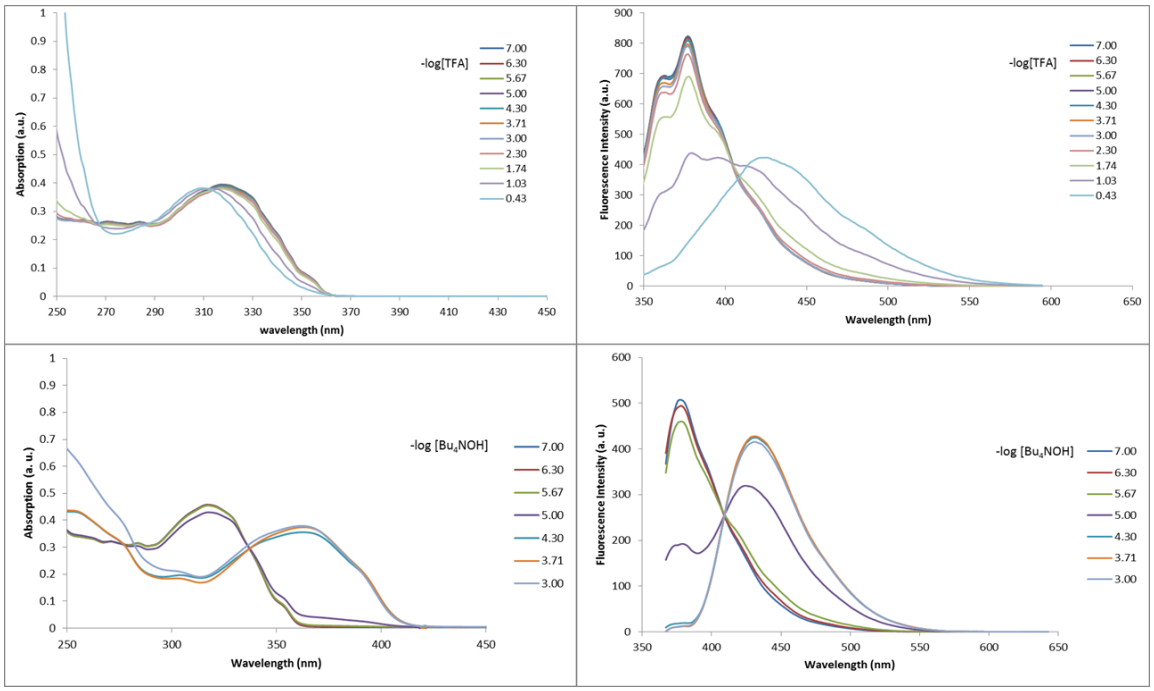

Figure 5.12 Absorption (left) and emission (right) spectra for the acid (top) and base (bottom) titration of **162**. For TFA titration, λ_{exc}=313 nm and for TBAOH titration, λ_{exc}=337 nm.

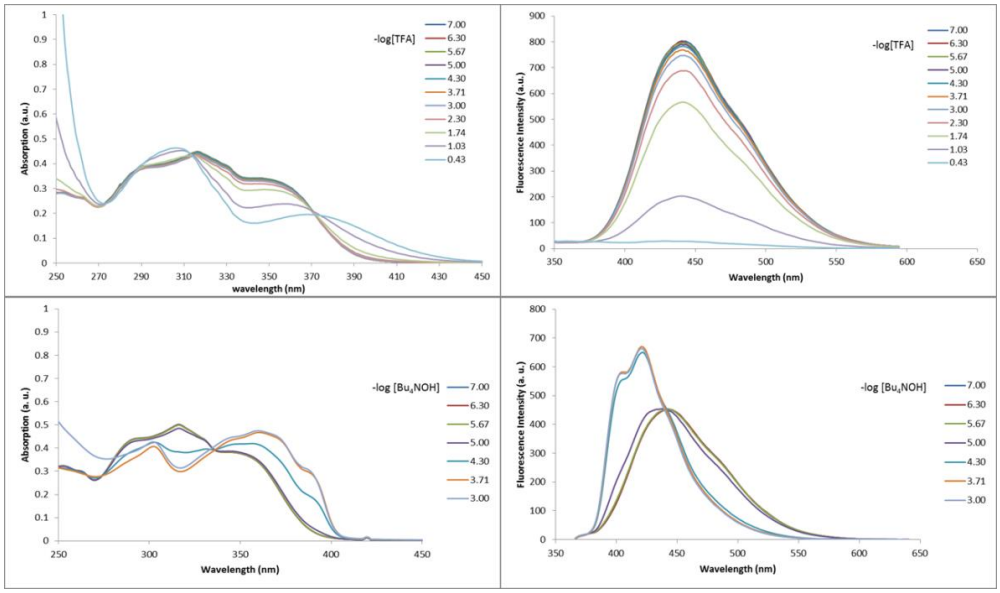

Figure 5.13 Absorption (left) and emission (right) spectra for the acid (top) and base (bottom) titration of **163**. For TFA titration, λ_{exc}=313 nm and for TBAOH titration, λ_{exc}=336 nm.

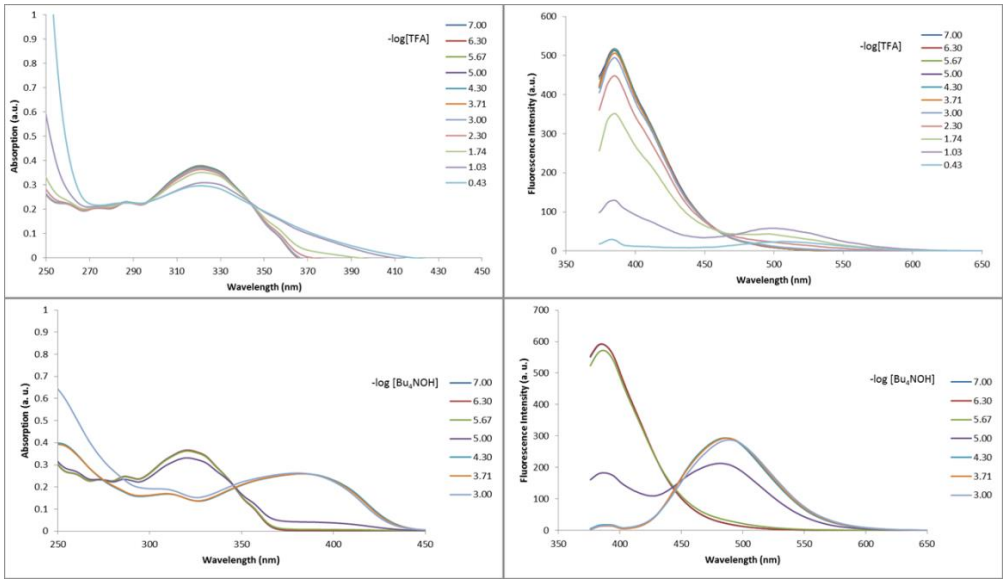

Figure 5.14 Absorption (left) and emission (right) spectra for the acid (top) and base (bottom) titration of **164**. For TFA titration, λ_{exc}=344 nm and for TBAOH titration, λ_{exc}=346 nm.

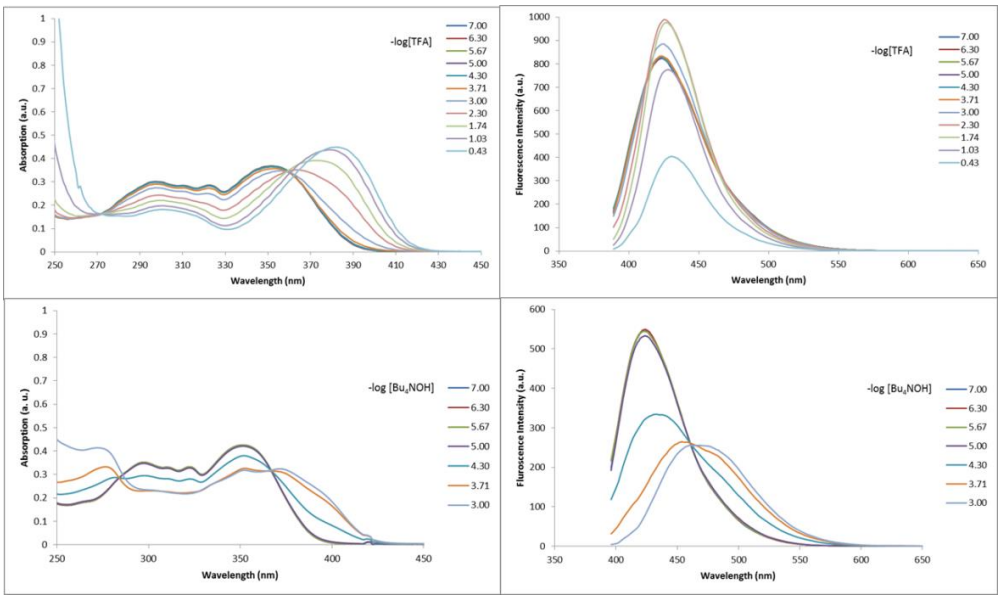

Figure 5.15 Absorption (left) and emission (right) spectra for the acid (top) and base (bottom) titration of **165**. For TFA titration, λ_{exc}=359 nm and for TBAOH titration, λ_{exc}=366 nm.

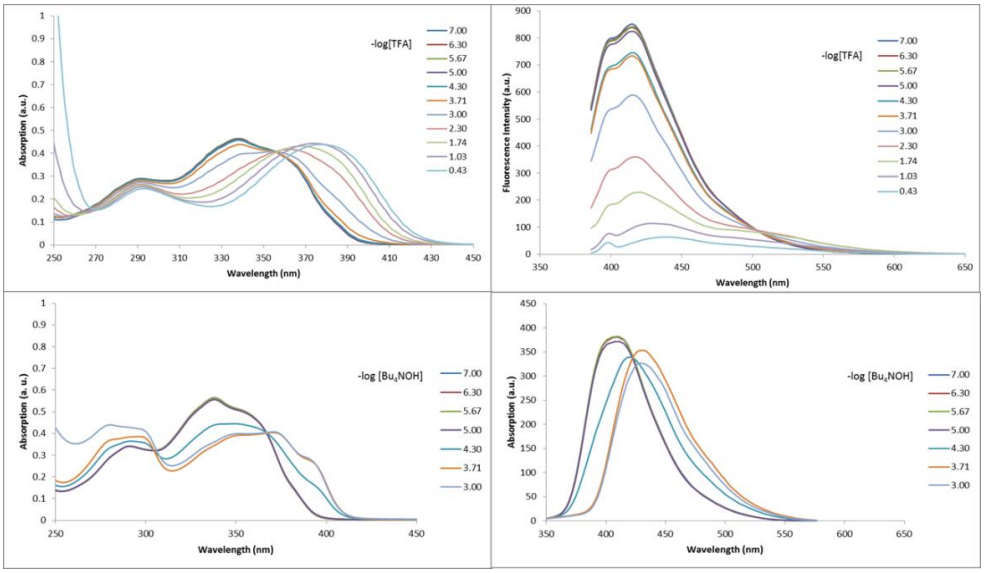

Figure 5.16 Absorption (left) and emission (right) spectra for the acid (top) and base (bottom) titration of **166**. For TFA titration, λ_{exc}=356 nm and for TBAOH titration, λ_{exc}=304 nm.

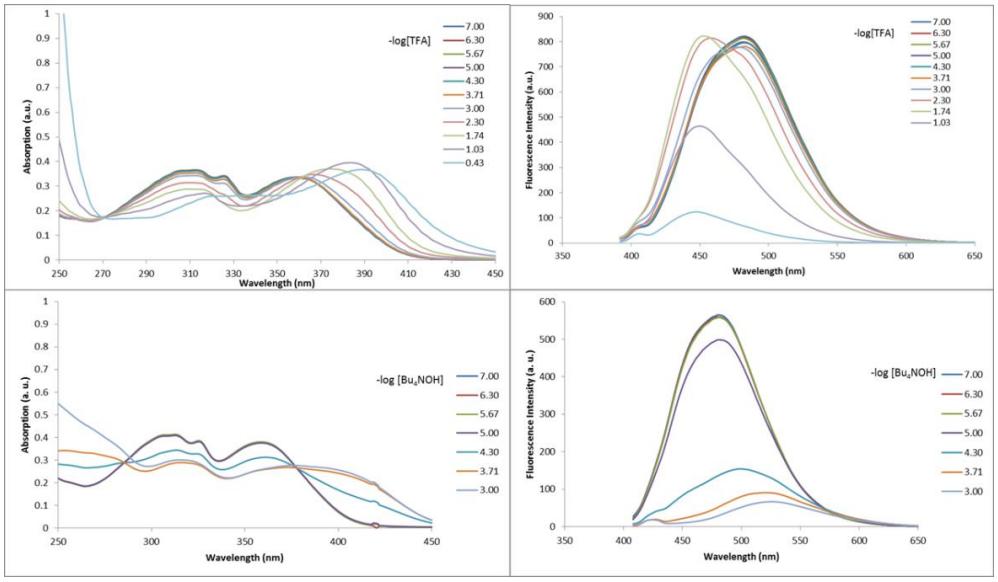

Figure 5.17 Absorption (left) and emission (right) spectra for the acid (top) and base (bottom) titration of **167**. For TFA titration, λ_{exc}=362 nm and for TBAOH titration, λ_{exc}=378 nm.

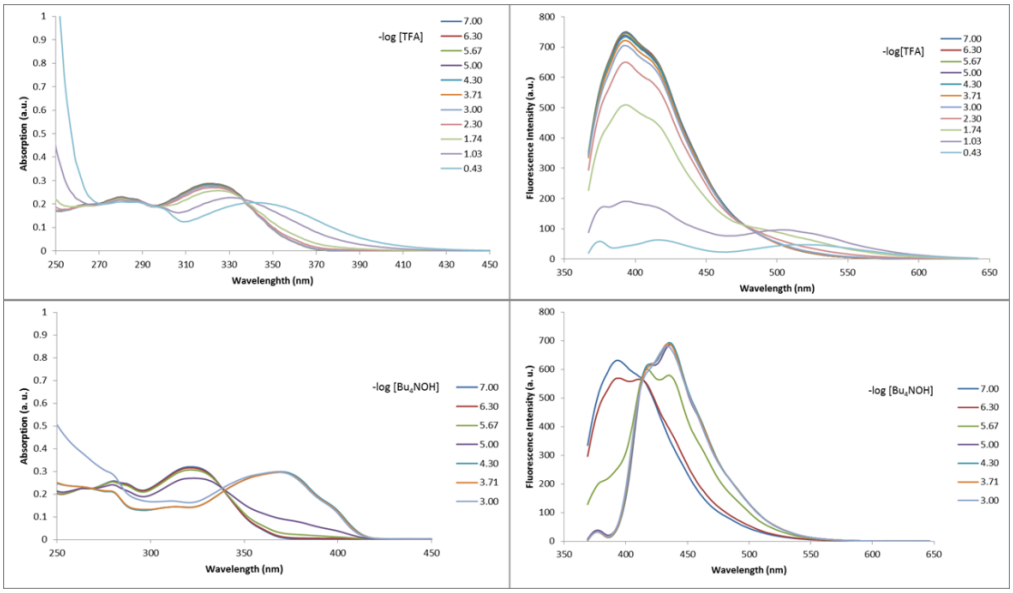

Figure 5.18 Absorption (left) and emission (right) spectra for the acid (top) and base (bottom) titration of **168**. For TFA titration, λ_{exc}=337 nm and for TBAOH titration, λ_{exc}=339 nm.

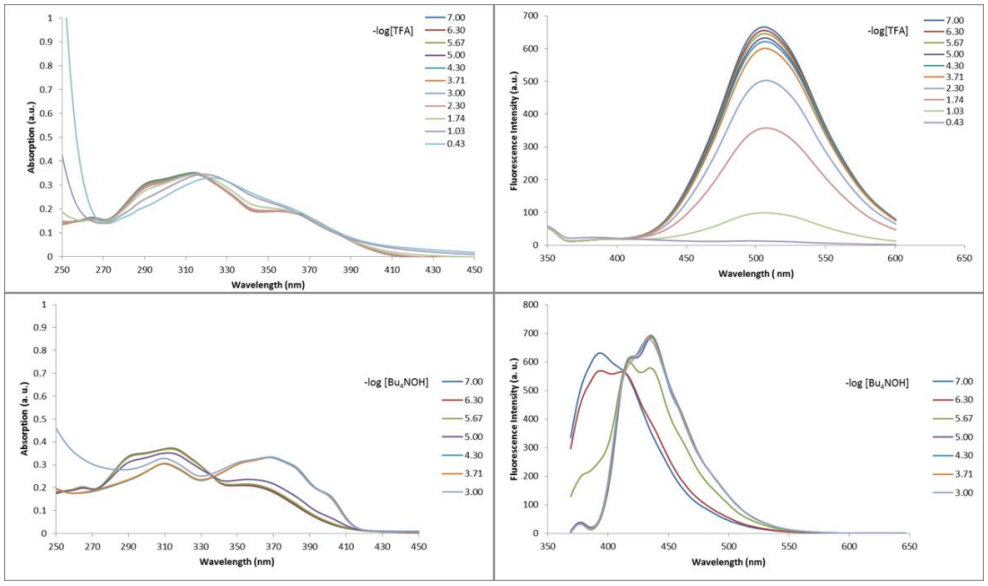

Figure 5.19 Absorption (left) and emission (right) spectra for the acid (top) and base (bottom) titration of **169**. For TFA titration, λ_{exc}=317 nm and for TBAOH titration, λ_{exc}=337 nm.

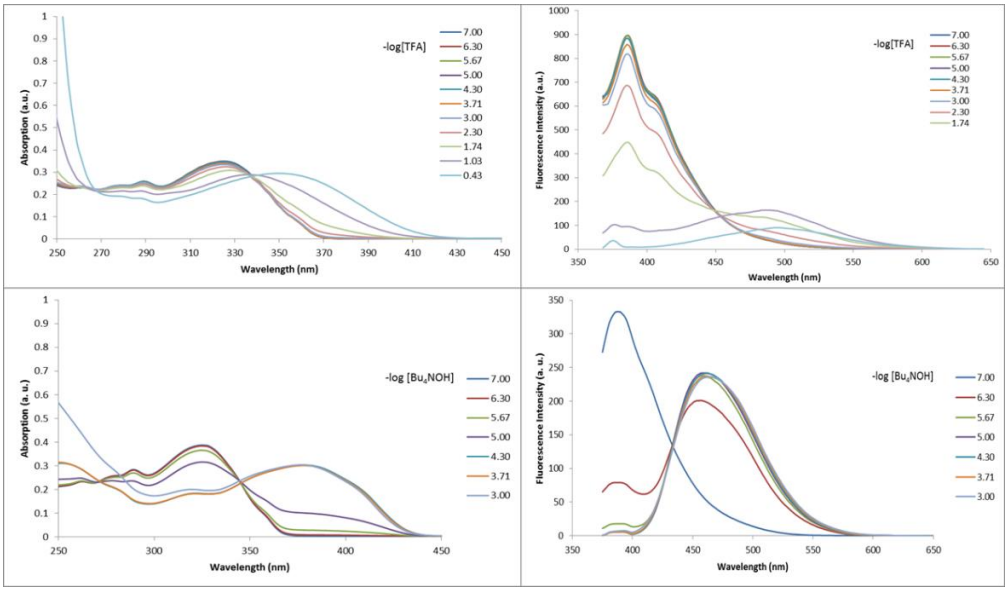

Figure 5.20 Absorption (left) and emission (right) spectra for the acid (top) and base (bottom) titration of **170**. For TFA titration, λ_{exc}=338 nm and for TBAOH titration, λ_{exc}=345 nm.

References

[1] Steed, J. W.; Turner, D. R.; Wallace, K. J. *Core Concepts in Supramolecular Chemistry and Nanochemistry*; John Wiley & Sons, Ltd: Hoboken, NJ, 2007.

[2] Steed, J. W.; Gale, P. A. *Supramolecular Chemistry: From Molecules to Nanomaterials*; Wiley: Chichester, 2012.

[3] Steed, J. W.; Atwood, J. L. *Supramolecular Chemistry*; 2nd ed.; John Wiley & Sons, Ltd.: Chichester, UK, 2009.

[4] "The Nobel Prize in Chemistry 1987". Nobelprize.org. Nobel Media AB 2014. Web. 4 Apr 2015. http://nobelprize.org/nobel_prizes/chemistry/laureates/1987/

[5] Lehn, J. M. *Chem. Soc. Rev.* **2007**, *36*, 151–160.

[6] Lehn, J. M. *Top. Curr. Chem.* **2012**, *322*, 1–32.

[7] Giuseppone, N.; Lehn, J. M. *Chem. Eur. J.* **2006**, *12*, 1715–1722.

[8] Giuseppone, N.; Lehn, J. M. *Angew. Chem. Int. Ed.* **2006**, *45*, 4619–4624.

[9] Ingerman, L. A.; Waters, M. L. *J. Org. Chem.* **2009**, *74*, 111–117.

[10] Li, J. W.; Nowak, P.; Otto, S. *J. Am. Chem. Soc.* **2013**, *135*, 9222–9239.

[11] Hafezi, N.; Lehn, J. M. *J. Am. Chem. Soc.* **2012**, *134*, 12861–12868.

[12] Corbett, P. T.; Leclaire, J.; Vial, L.; West, K. R.; Wietor, J. L.; Sanders, J. K. M.; Otto, S. *Chem. Rev.* **2006**, *106*, 3652–3711.

[13] Erlanson, D. A.; Hansen, S. K. *Curr. Opin. Chem. Biol.* **2004**, *8*, 399–406.

[14] Rode, B. M.; Fitz, D.; Jackschitz, T. in *Origin of Life: Chemical Approach*, Herdewijn, P.; Kisakürek, M. V. eds. Verlag Helvetica Chimica Acta:Wiley-VCH, Zürich/Weinheim, 2008.

[15] Jin, Y.; Yu, C.; Denman, R. J.; Zhang, W. *Chem. Soc. Rev.* **2013**, *42*, 6634–6654.

[16] Reek, J. N. H.; Otto, S. *Dynamic Combinatorial Chemistry*; Wiley-VCH: Weinheim, 2010.

[17] Ludlow, R. F.; Otto, S. *J. Am. Chem. Soc.* **2008**, *130*, 12218–12219.

[18] Lam, R. T. S.; Belenguer, A.; Roberts, S. L.; Naumann, C.; Jarrosson, T.; Otto, S.; Sanders, J. K. M. *Science* **2005**, *308*, 667–669.

[19] Hamieh, S.; Saggiomo, V.; Nowak, P.; Mattia, E.; Ludlow, R. F.; Otto, S. *Angew. Chem. Int. Ed.* **2013**, *52*, 12368–12372.

[20] Nitschke, J. R. *Acc. Chem. Res.* **2007**, *40*, 103–112.

[21] Zarra, S.; Wood, D. M.; Roberts, D. A.; Nitschke, J. R. *Chem. Soc. Rev.* **2015**, *44*, 419–432.

[22] Heinz, T.; Rudkevich, D. M.; Rebek, J. *Nature* **1998**, *394*, 764–766.

[23] Jiang, W.; Ajami, D.; Rebek, J. *J. Am. Chem. Soc.* **2012**, *134*, 8070–8073.

[24] Mal, P.; Breiner, B.; Rissanen, K.; Nitschke, J. R. *Science* **2009**, *324*, 1697–1699.

[25] Salles, A. G.; Zarra, S.; Turner, R. M.; Nitschke, J. R. *J. Am. Chem. Soc.* **2013**, *135*, 19143–19146.

[26] Miller, B. L. *Dynamic Combinatorial Chemistry in Drug Discovery, Bioorganic Chemistry, and Materials Science*; Wiley: Oxford, 2010.

[27] Osowska, K.; Miljanić, O. Š. *Synlett* **2011**, *12*, 1643–1648.

[28] Watson, J. D.; Crick, F. H. *Nature* **1953**, *171*, 737–738.

[29] Isaacs, L.; Park, S. K.; Liu, S. M.; Ko, Y. H.; Selvapalam, N.; Kim, Y.; Kim, H.; Zavalij, P. Y.; Kim, G. H.; Lee, H. S.; Kim, K. *J. Am. Chem. Soc.* **2005**, *127*, 18000–18001.

[30] Braekers, D.; Peters, C.; Bogdan, A.; Rudzevich, Y.; Bohmer, V.; Desreux, J. F. *J. Org. Chem.* **2008**, *73*, 701–706.

[31] Northrop, B. H.; Zheng, Y. R.; Chi, K. W.; Stang, P. J. *Acc. Chem. Res.* **2009**, *42*, 1554–1563.

[32] Saha, M. L.; Schmittel, M. *J. Am. Chem. Soc.* **2013**, *135*, 17743–17746.

[33] Castilla, A. M.; Ramsay, W. J.; Nitschke, J. R. *Acc. Chem. Res.* **2014**, *47*, 2063–2073.

[34] Jiang, W.; Schalley, C. A. *Proc. Natl. Acad. Sci. U. S. A.* **2009**, *106*, 10425–10429.

[35] Wu, J.; Leung, K. C.; Stoddart, J. F. *Proc. Natl. Acad. Sci. U. S. A.* **2007**, *104*, 17266–17271.

[36] Ji, Q.; Miljanić, O. Š. *J. Org. Chem.* **2013**, *78*, 12710–12716.

[37] Wu, A. X.; Isaacs, L. *J. Am. Chem. Soc.* **2003**, *125*, 4831–4835.

[38] Jiang, W.; Winkler, H. D. F.; Schalley, C. A. *J. Am. Chem. Soc.* **2008**, *130*, 13852–13853.

[39] Saha, M. L.; Schmittel, M. *Org. Biomol. Chem.* **2012**, *10*, 4651–4684.

[40] Ji, Q.; Lirag, R. C.; Miljanić, O. Š. *Chem. Soc. Rev.* **2014**, *43*, 1873–1884.

[41] Safont-Sempere, M. M.; Fernandez, G.; Wurthner, F. *Chem. Rev.* **2011**, *111*, 5784–5814.

[42] Masson, E.; Lu, X. Y.; Ling, X. X.; Patchell, D. L. *Org. Lett.* **2009**, *11*, 3798–3801.

[43] Gerasko, O. A.; Samsonenko, D. G.; Fedin, V. P. *Russ. Chem. Rev.* **2002**, *71*, 840–861.

[44] Hermans, T. M.; Frauenrath, H.; Stellacci, F. *Science* **2013**, *341*, 243–244.

[45] Sprung, M. M. *Chem. Rev.* **1940**, *26*, 297–338.

[46] Meyer, C. D.; Joiner, C. S.; Stoddart, J. F. *Chem. Soc. Rev.* **2007**, *36*, 1705–1723.

[47] Belowich, M. E.; Stoddart, J. F. *Chem. Soc. Rev.* **2012**, *41*, 2003–2024.

[48] Shriner, R. L.; Hermann, C. K. F.; Morrill, T. C.; Fuson, R. C. *The Systematic Identification of Organic Compounds*, Wiley: Hoboken, NJ; 2004.

[49] Tidwell, T. T. *Angew. Chem. Int. Ed.* **2008**, *47*, 1016–1020.

[50] Porai-Koshits, B. A.; Remizov, A. L., *Probl. Mekhanizma Org. Reaktsii, Akad. Nauk Ukr. SSR, Otdel Fiz Mat. I Khim. Nauk.* **1953**, 238; *Chem. Abstr.* **1956**, *50*, 16686.

[51] Layer, R. W. *Chem. Rev.* **1963**, *63*, 489–510.

[52] Seeman, J. I. *J. Chem. Educ.* **1986**, *63*, 42–48.

[53] Osowska, K.; Miljanić, O. Š. *J. Am. Chem. Soc.* **2011**, *133*, 724–727.

[54] Seeman, J. I. *Chem. Rev.* **1983**, *83*, 83–134.

[55] Osowska, K.; Miljanić, O. Š. *Angew. Chem. Int. Ed.* **2011**, *50*, 8345–8349.

[56] Kiss, A. A. *Advanced Distillation Technologies: Design, Control and Applications;* Wiley: Chichester, West Sussex, 2013.

[57] Hsu, C. W.; Miljanić, O. Š. *Angew. Chem. Int. Ed.* **2015**, *54*, 2219–2222.

[58] Cassidy, H. G. *Adsorption and Chromatography*; Interscience Publishers: New York, 1951.

[59] Lirag, R. C.; Osowska, K.; Miljanić, O. Š. *Org. Biomol. Chem.***2012**, *10*, 4847–4850.

[60] Tavare, N. S. *Industrial Crystallization: Process Simulation, Analysis and Design*, Plenum Press: New York; London, 1995.

[61] Kumar, D. K.; Steed, J. W. *Chem. Soc. Rev.* **2014**, *43*, 2080–2088.

[62] Bohnet, M. *Ullmann's Encyclopedia of Industrial Chemistry*, 6th ed.; Wiley-VCH: Weinheim, 2003.

[63] Mann, S. *Nature* **1988**, *332*, 119–124.

[64] Dirksen, J. A.; Ring, T. A. *Chem. Eng. Sci.* **1991**, *46*, 2389–2427.

[65] Kondepudi, D. K.; Asakura, K. *Acc. Chem. Res.* **2001**, *34*, 946–954.

[66] Klussmann, M.; Iwamura, H.; Mathew, S. P.; Wells, D. H.; Pandya, U.; Armstrong, A.; Blackmond, D. G. *Nature* **2006**, *441*, 621–623.

[67] Weissbuch, I.; Lahav, M. *Chem. Rev.* **2011**, *111*, 3236–3267.

[68] Beckmann, W. *Crystallization: Basic Concepts and Industrial Applications*, Wiley-VCH: Weinheim, 2013.

[69] National Research Council (U.S.). Committee on Prudent Practices for Handling Storage and Disposal of Chemicals in Laboratories. *Prudent Practices in the Laboratory: Handling and Disposal of Chemicals*, National Academy Press: Washington, D.C., 1995.

[70] Chen, J.; Sarma, B.; Evans, J. M. B.; Myerson, A. S. *Cryst. Growth Des.* **2011**, *11*, 887–895.

[71] Meyer, C. D.; Forgan, R. S.; Chichak, K. S.; Peters, A. J.; Tangchaivang, N.; Cave, G. W. V.; Khan, S. I.; Cantrill, S. J.; Stoddart, J. F. *Chem. Eur. J.* **2010**, *16*, 12570–12581.

[72] Acharyya, K.; Mukherjee, S.; Mukherjee, P. S. *J. Am. Chem. Soc.* **2013**, *135*, 554–557.

[73] Leclaire, J.; Husson, G.; Devaux, N.; Delorme, V.; Charles, L.; Ziarelli, F.; Desbois, P.; Chaumonnot, A.; Jacquin, M.; Fotiadu, F.; Buono, G. *J. Am. Chem. Soc.* **2010**, *132*, 3582–3593.

[74] Castilla, A. M.; Ramsay, W. J.; Nitschke, J. R. *Acc. Chem. Res.* **2014**, *47*, 2063–2073.

[75] Hutin, M.; Cramer, C. J.; Gagliardi, L.; Shahi, A. R. M.; Bernardinelli, G.; Cerny, R.; Nitschke, J. R. *J. Am. Chem. Soc.* **2007**, *129*, 8774–8780.

[76] Nongkunsarn, P.; Ramsden, C. A. *Tetrahedron* **1997**, *53*, 3805–3830.

[77] Saito, S.; Hatanaka, K.; Yamamoto, H. *Org. Lett.* **2000**, *2*, 1891–1894.

[78] Singh, H. B.; McWhinnie, W. R. *J. Chem. Soc. Dalton Trans.* **1985**, 821–825.

[79] Bennett, J. S.; Charles, K. L.; Miner, M. R.; Heuberger, C. F.; Spina, E. J.; Bartels, M. F.; Foreman, T. *Green Chem.* **2009**, *11*, 166–168.

[80] Nakajima, T.; Inada, T.; Igarashi, T.; Sekioka, T.; Shimizu, I. *Bull. Chem. Soc. Jpn.* **2006**, *79*, 1941–1949.

[81] Torregrosa, R.; Pastor, I. M.; Yus, M. *Tetrahedron* **2005**, *61*, 11148–11155.

[82] Miyazaki, D.; Nomura, K.; Yamashita, T.; Iwakura, I.; Ikeno, T.; Yamada, T. *Org. Lett.* **2003**, *5*, 3555–3558.

[83] Lirag, R. C.; Miljanić, O. Š. *Chem. Commun.* **2014**, *50*, 9401–9404.

[84] Vongvilai, P.; Ramström, O. *J. Am. Chem. Soc.* **2009**, *131*, 14419–14425.

[85] Wessjohann, L. A.; Rivera, D. G.; Leon, F. *Org. Lett.* **2007**, *9*, 4733–4736.

[86] Nitschke, J. R.; Lehn, J. M. *Proc. Natl. Acad. Sci. U.S.A.* **2003**, *100*, 11970–11974.

[87] Goral, V.; Nelen, M. I.; Eliseev, A. V.; Lehn, J. M. *Proc. Natl. Acad. Sci. U.S.A.* **2001**, *98*, 1347–1352.

[88] Leclaire, J.; Vial, L.; Otto, S.; Sanders, J. K. M. *Chem. Commun.* **2005**, 1959–1961.

[89] Rodriguez-Docampo, Z.; Otto, S. *Chem. Commun.* **2008**, 5301–5303.

[90] Sarma, R. J.; Otto, S.; Nitschke, J. R. *Chem. Eur. J.* **2007**, *13*, 9542–9546.

[91] Christinat, N.; Scopelliti, R.; Severin, K. *Angew. Chem. Int. Ed.* **2008**, *47*, 1848–1852.

[92] Içli, B.; Christinat, N.; Tönnemann, J.; Schüttler, C.; Scopelliti, R.; Severin, K. *J. Am. Chem. Soc.* **2009**, *131*, 3154–3155.

[93] Nagano, Y.; Orita, A.; Otera, J. *Tetrahedron* **2003**, *59*, 5569–5578.

[94] Orita, A.; Nagano, Y.; Nakazawa, K.; Otera, J. *Synlett* **2000**, *5*, 599–602.

[95] Nagano, Y.; Orita, A.; Otera, J. *Tetrahedron* **2002**, *58*, 8211–8217.

[96] Nagano, Y.; Orita, A.; Otera, J. *Bull. Chem. Soc. Jpn.* **2003**, *76*, 2183–2189.

[97] Chen, J. X.; Otera, J. *Angew. Chem. Int. Ed.* **1998**, *37*, 91–93.

[98] Chen, J. X.; Sakamoto, K.; Orita, A.; Otera, J. *Tetrahedron* **1998**, *54*, 8411–8420.

[99] Orita, A.; Nagano, Y.; Nakazawa, K.; Otera, J. *Adv. Synth. Catal.* **2002**, *344*, 548–555.

[100] Orrillo, A. G.; Escalante, A. M.; Furlan, R. L. E. *Chem. Commun.* **2008**, 5298–5300.

[101] Legrand, Y. M.; van der Lee, A.; Barboiu, M. *Inorg. Chem.* **2007**, *46*, 9540–9547.

[102] Okochi, K. D.; Han, G. S.; Aldridge, I. M.; Liu, Y. L.; Zhang, W. *Org. Lett.* **2013**, *15*, 4296–4299.

[103] Jin, Y. H.; Wang, Q.; Taynton, P.; Zhang, W. *Acc. Chem. Res.* **2014**, *47*, 1575–1586.

[104] Wilson, A.; Gasparini, G.; Matile, S. *Chem. Soc. Rev.* **2014**, *43*, 1948–1962.

[105] Barrell, M. J.; Campana, A. G.; von Delius, M.; Geertsema, E. M.; Leigh, D. A. *Angew. Chem. Int. Ed.* **2011**, *50*, 285–290.

[106] Deng, G. H.; Li, F. Y.; Yu, H. X.; Liu, F. Y.; Liu, C. Y.; Sun, W. X.; Jiang, H. F.; Chen, Y. M. *ACS Macro Lett.* **2012**, *1*, 275–279.

[107] Sakai, N.; Matile, S. *J. Am. Chem. Soc.* **2011**, *133*, 18542–18545.

[108] Teichert, J. F.; Mazunin, D.; Bode, J. W. *J. Am. Chem. Soc.* **2013**, *135*, 11314–11321.

[109] Piest, M.; Engbersen, J. F. J. *J. Controlled Release* **2011**, *155*, 331–340.

[110] Wollenberg, R. H.; Peries, R. *Tetrahedron Lett.* **1979**, 297–300.

[111] Myles, L.; Gathergood, N.; Connon, S. J. *Chem. Commun.* **2013**, *49*, 5316–5318.

[112] Pfaff, D.; Nemecek, G.; Podlech, J. *Beilstein J. Org. Chem.* **2013**, *9*, 1572–1577.

[113] Lee, A. S.-Y.; Yang, H.-C.; Su, F.-Y. *Tetrahedron Lett.* **2001**, *42*, 301–303.

[114] Zhang, J. M.; Wu, H. H.; Zhang, J. L. *Eur. J. Org. Chem.* **2013**, *2013*, 6263–6266.

[115] Andrus, M. B.; Harper, K. C.; Christiansen, M. A.; Binkley, M. A. *Tetrahedron Lett.* **2009**, *50*, 4541–4544.

[116] Alberti, M. N.; Orfanopoulos, M. *Org. Lett.* **2008**, *10*, 2465–2468.

[117] Vaccaro, W. D.; Sher, R.; Davis, H. R. *Biorg. Med. Chem.* **1998**, *6*, 1429–1437.

[118] Smith, B. M.; Kubczyk, T. M.; Graham, A. E. *Tetrahedron* **2012**, *68*, 7775–7781.

[119] Kumar, A.; Samuelson, A. G. *J. Organomet. Chem.* **2010**, *695*, 338–345.

[120] Bennett, J. S.; Charles, K. L.; Miner, M. R.; Heuberger, C. F.; Spina, E. J.; Bartels, M. F.; Foreman, T. *Green Chem.* **2009**, *11*, 166–168.

[121] Sarkar, A.; Yemul, O. S.; Bandgar, B. P.; Gaikwad, N. B.; Wadgaonkar, P. P. *Org. Prep. Proced. Int.* **1996**, *28*, 613–617.

[122] Gladding, J. A.; Bacci, J. P.; Shaw, S. A.; Smith, A. B. *Tetrahedron* **2011**, *67*, 6697–6706.

[123] Kim, E. J.; Ko, S. Y. *Biorg. Med. Chem.* **2005**, *13*, 4103–4112.

[124] Yamamoto, N.; Obora, Y.; Ishii, Y. *J. Org. Chem.* **2011**, *76*, 2937–2941.

[125] Kamijo, S.; Amaoka, Y.; Inoue, M. *Tetrahedron Lett.* **2011**, *52*, 4654–4657.

[126] Kuhakarn, C.; Panchan, W.; Chiampanichayakul, S.; Samakkanad, N.; Pohmakotr, M.; Reutrakul, V.; Jaipetch, T. *Synthesis* **2009**, 929–934.

[127] Schwaebel, T.; Lirag, R. C.; Davey, E. A.; Lim, J.; Bunz, U. H.; Miljanić, O. Š. *J. Vis. Exp.* **2013**, e50858.

[128] Cohen, Y.; Avram, L.; Frish, L. *Angew. Chem. Int. Ed.* **2005**, *44*, 520–554.

[129] Jiang, W.; Schafer, A.; Mohr, P. C.; Schalley, C. A. *J. Am. Chem. Soc.* **2010**, *132*, 2309–2320.

[130] Anzenbacher, P.; Lubal, P.; Bucek, P.; Palacios, M. a.; Kozelkova, M. E. *Chem. Soc. Rev.* **2010**, *39*, 3954–3979.

[131] Anslyn, E. V. *J. Org. Chem.* **2007**, *72*, 687–699.

[132] You, L.; Zha, D.; Anslyn, E. V. *Chem. Rev.* **2015**, *72*, 687–699.

[133] Cattrall, R. W. *Chemical Sensors*; Oxford University Press: Oxford ; New York, 1997.

[134] Hulanicki, A.; Glab, S.; Ingman, F. *Pure Appl. Chem.* **1991**, *63*, 1247–1250.

[135] Du, P. W.; Lippard, S. J. *Inorg. Chem.* **2010**, *49*, 10753–10755.

[136] Swinburne, A. N.; Paterson, M. J.; Beeby, A.; Steed, J. W. *Org Biomol Chem* **2010**, *8*, 1010–1016.

[137] Albert, K. J.; Lewis, N. S.; Schauer, C. L.; Sotzing, G. A.; Stitzel, S. E.; Vaid, T. P.; Walt, D. R. *Chem. Rev.* **2000**, *100*, 2595–2626.

[138] Gamsey, S.; Miller, A.; Olmstead, M. M.; Beavers, C. M.; Hirayama, L. C.; Pradhan, S.; Wessling, R. A.; Singaram, B. *J. Am. Chem. Soc.* **2007**, *129*, 1278–1286.

[139] Jose, D. A.; Elstner, M.; Schiller, A. *Chem. Eur. J.* **2013**, *19*, 14451–14457.

[140] Schiller, A.; Wessling, R. A.; Singaram, B. *Angew. Chem. Int. Ed.* **2007**, *46*, 6457–6459.

[141] Mosquera, J.; Zarra, S.; Nitschke, J. R. *Angew. Chem. Int. Ed.* **2014**, *53*, 1556–1559.

[142] Ghale, G.; Lanctot, A. G.; Kreissl, H. T.; Jacob, M. H.; Weingart, H.; Winterhalter, M.; Nau, W. M. *Angew. Chem. Int. Ed.* **2014**, *53*, 2762–2765.

[143] Ghosh, K.; Sarkar, A. R.; Samadder, A.; Khuda-Bukhsh, A. R. *Org. Lett.* **2012**, *14*, 4314–4317.

[144] Yuen, K. K. Y.; Jolliffe, K. A. *Chem. Commun.* **2013**, *49*, 4824–4826.

[145] Kumar, V.; Anslyn, E. V. *J. Am. Chem. Soc.* **2013**, *135*, 6338–6344.

[146] Leontiev, A. V.; Rudkevich, D. M. *J. Am. Chem. Soc.* **2005**, *127*, 14126–14127.

[147] Zhang, C.; Bailey, D. P.; Suslick, K. S. *J. Agric. Food. Chem.* **2006**, *54*, 4925–4931.

[148] Buryak, A.; Severin, K. *Angew. Chem. Int. Ed.* **2005**, *44*, 7935–7938.

[149] Palacios, M. A.; Wang, Z.; Montes, V. A.; Zyryanov, G. V.; Anzenbacher, P. *J. Am. Chem. Soc.* **2008**, *130*, 10307–10314.

[150] Lavigne, J. J.; Anslyn, E. V. *Angew. Chem. Int. Ed.* **2001**, *40*, 3119–3130.

[151] Rakow, N. A.; Suslick, K. S. *Nature* **2000**, *406*, 710–713.

[152] Lim, J.; Albright, T. A.; Martin, B. R.; Miljanić, O. S. *J. Org. Chem.* **2011**, *76*, 10207–10219.

[153] Lakowicz, J. R. *Principles of Fluorescence Spectroscopy*, 3rd ed.; Springer: New York, 2006.

[154] Bunz, U.; Schwaebel, T.; Trapp, O. *Chem. Sci.* **2013**, *4*, 273–281.

[155] Schwaebel, T.; Menning, S.; Bunz, U. H. F. *Chem. Sci.* **2014**, *5*, 1422–1422.

[156] Colour Contrast Analyser can be freely downloaded from: http://www.visionaustralia.org/digital-access-cca. Last accessed on June 25, 2015.

[157] Saeed, M. A.; Le, H. T. M.; Miljanić, O. Š. *Acc. Chem. Res.* **2014**, *47*, 2074–2083.

[158] Zucchero, A. J.; McGrier, P. L.; Bunz, U. H. F. *Acc. Chem. Res.* **2010**, *43*, 397–408.

[159] Miller, J. J.; Marsden, J. A.; Haley, M. M. *Synlett* **2004**, *1*, 165–168.

[160] Kang, H.; Evmenenko, G.; Dutta, P.; Clays, K.; Song, K.; Marks, T. J. *J. Am. Chem. Soc.* **2006**, *128*, 6194–6205.

[161] Hilger, A.; Gisselbrecht, J. P.; Tykwinski, R. R.; Boudon, C.; Schreiber, M.; Martin, R. E.; Luthi, H. P.; Gross, M.; Diederich, F. *J. Am. Chem. Soc.* **1997**, *119*, 2069–2078.

[162] Le, H. T. M.; El-Hamdi, N. S.; Miljanić, O. Š. *J. Org. Chem.*, **2015**, *80*, 5210–5217.

[163] Tlach, B. C.; Tomlinson, A. L.; Bhuwalka, A.; Jeffries-El, M. *J. Org. Chem.*, **2011**, *76*, 8670–8681.

[164] Tlach, B. C.; Tomlinson, A. L.; Ryno, A. G.; Knoble, D. D.; Drochner, D. L.; Krager, K. J.; Jeffries-EL, M. *J. Org. Chem.* **2013**, *78*, 6570–6581.

[165] Moonen, N. N. P.; Pomerantz, W. C.; Gist, R.; Boudon, C.; Gisselbrecht, J. P.; Kawai, T.; Kishioka, A.; Gross, M.; Irie, M.; Diederich, F. *Chem. Eur. J.* **2005**, *11*, 3325–3341.

[166] Marsden, J. A.; Miller, J. J.; Shirtcliff, L. D.; Haley, M. M. *J. Am. Chem. Soc.* **2005**, *127*, 2464–2476.

[167] Samori, S.; Tojo, S.; Fujitsuka, M.; Spitler, E. L.; Haley, M. M.; Majima, T. *J. Org. Chem.* **2007**, *72*, 2785–2793.

[168] Chase, D. T.; Young, B. S.; Haley, M. M. *J. Org. Chem.* **2011**, *76*, 4043–4051.

[169] Davey, E. A.; Zucchero, A. J.; Trapp, O.; Bunz, U. H. F. *J. Am. Chem. Soc.* **2011**, *133*, 7716–7718.

[170] Tolosa, J.; Zucchero, A. J.; Bunz, U. H. F. *J. Am. Chem. Soc.* **2008**, *130*, 6498–6506.

[171] Klare, J. E.; Tulevski, G. S.; Sugo, K.; Picciotto, A. d.; White, K. A.; Nuckolls, C. *J. Am. Chem. Soc*. **2003**, *125*, 6030–6031.

[172] Gaussian 09, Revision B.01: Frisch, M. J.; Trucks, G. W.; Schlegel, H. B.; Scuseria, G. E.; Robb, M. A.; Cheeseman, J. R.; Scalmani, G.;Barone, V.; Mennucci, B.; Petersson, G. A.; Nakatsuji, H.; Caricato, M.; Li, X.; Hratchian, H. P.; Izmaylov, A. F.;

Bloino, J.; Zheng, G.; Sonnenberg, J. L.; Hada, M.; Ehara, M.; Toyota, K.; Fukuda, R.; Hasegawa, J.; Ishida, M.; Nakajima, T.; Honda, Y.; Kitao, O.; Nakai, H.; Vreven, T.; Montgomery, J. A., Jr.; Peralta, J. E.; Ogliaro, F.; Bearpark, M.; Heyd, J. J.; Brothers, E.; Kudin, K. N.; Staroverov, V. N.; Keith, T.; Kobayashi, R.; Normand, J.; Raghavachari, K.; Rendell, A.; Burant, J. C.; Iyengar, S. S.; Tomasi, J.; Cossi, M.; Rega, N.; Millam, J. M.; Klene, M.; Knox, J. E.; Cross, J. B.; Bakken, V.; Adamo, C.; Jaramillo, J.; Gomperts, R.; Stratmann, R. E.; Yazyev, O.; Austin, A. J.; Cammi, R.; Pomelli, C.; Ochterski, J. W.; Martin, R. L.; Morokuma, K.; Zakrzewski, V. G.; Voth, G. A.; Salvador, P.; Dannenberg, J. J.; Dapprich, S.; Daniels, A. D.; Farkas, O.; Foresman, J. B.; Ortiz, J. V.; Cioslowski, J.; Fox, D. J. Gaussian, Inc., Wallingford, CT, 2010.

[173] Becke, A. D. *J. Chem. Phys.* **1993**, *98*, 5648–5652.

[174] Lee, C. T.; Yang, W. T.; Parr, R. G. *Phys Rev B* **1988**, *37*, 785–789.

[175] Lim, J.; Miljanić, O. Š. *Chem. Commun.* **2012**, *48*, 10301–10301.

[176] Lim, J.; Nam, D.; Miljanić, O. Š. *Chem. Sci.* **2012**, *3*, 559–563.

[177] Galbraith, E.; James, T. D. *Chem. Soc. Rev.* **2010**, *39*, 3831–3842.

[178] Nishiyabu, R.; Kubo, Y.; James, T. D.; Fossey, J. S. *Chem. Commun.* **2011**, *47*, 1106–1123.

[179] Guo, Z. Q.; Shin, I.; Yoon, J. *Chem. Commun.* **2012**, *48*, 5956–5967.

[180] Bull, S. D.; Davidson, M. G.; Van den Elsen, J. M. H.; Fossey, J. S.; Jenkins, A. T. A.; Jiang, Y. B.; Kubo, Y.; Marken, F.; Sakurai, K.; Zhao, J. Z.; James, T. D. *Acc. Chem. Res.* **2013**, *46*, 312–326.

[181] Cooper, C. R.; Spencer, N.; James, T. D. *Chem. Commun.* **1998**, 1365–1366.

[182] Yang, J. S.; Swager, T. M. *J. Am. Chem. Soc.* **1998**, *120*, 5321–5322.

[183] Comina, G.; Suska, A.; Filippini, D. *Lab Chip.* **2014**, *14*, 424–430.

[184] Wilson, J. N.; Bunz, U. H. F. *J. Am. Chem. Soc.* **2005**, *127*, 4124–4125.

[185] Lirag, R. C.; Le, H. T. M.; Miljanić, O. Š. *Chem. Commun.* **2013**, *49*, 4304–4306.

[186] Zucchero, A. J.; McGrier, P. L.; Bunz, U. H. F. *Acc. Chem. Res.* **2010**, *43*, 397–408.

[187] Molina, P.; Tárraga, A.; Otón, F. *Org. Biomol. Chem.* **2012**, *10*, 1711–1711.

[188] Benelhadj, K.; Massue, J.; Retailleau, P.; Ulrich, G.; Ziessel, R. *Org. Lett.* **2013,** *15*, 2918–2921.

[189] Hung, W.-Y.; Chi, L.-C.; Chen, W.-J.; Chen, Y.-M.; Chou, S.-H.; Wong, K.-T. *J. Mater. Chem.* **2010**, *20*, 10113–10119.

[190] Xue, Z. W.; Chen, M. L.; Chen, J. M.; Han, J. H.; Han, S. F. *RSC Adv.* **2014**, *4*, 374–378.

[191] Alvaro, M.; Garcia, H.; Palomares, E.; Achour, R.; Moussaif, A.; Zniber, R. *Chem. Phys. Lett.* **2001**, *350*, 240–246.

[192] Batista, R. M. F.; Oliveira, E.; Costa, S. P. G.; Lodeiro, C.; Raposo, M. M. M. *Tetrahedron* **2011**, *67*, 7106–7113.

[193] Moon, K. S.; Singh, N.; Lee, G. W.; Jang, D. O. *Tetrahedron* **2007**, *63*, 9106–9111.

[194] Abraham, Y.; Salman, H.; Suwinska, K.; Eichen, Y. *Chem. Commun.* **2011**, *47*, 6087–6089.

[195] Wilson, J. N.; Hardcastle, K. I.; Josowicz, M.; Bunz, U. H. F. *Tetrahedron* **2004**, *60*, 7157–7167.

[196] Zhang, H. C.; Guo, E. Q.; Zhang, Y. L.; Ren, P. H.; Yang, W. J. *Chem. Mater.* **2009**, *21*, 5125–5135.

[197] Lee, D. C.; Brownell, L. V.; Jang, K.; Han, S. J.; Robins, K. A. *Phys. Chem. Chem. Phys.* **2015**, *17*, 2457–2463.

[198] Zhou, N. Z.; Wang, L.; Thompson, D. W.; Zhao, Y. M. *Org. Lett.* **2008**, *10*, 3001–3004.

[199] Guo, Z. H.; Lei, T.; Jin, Z. X.; Wang, J. Y.; Pei, J. *Org. Lett.* **2013**, *15*, 3530–3533.

[200] Feng, K.; De Boni, L.; Misoguti, L.; Mendonca, C. R.; Meador, M.; Hsu, F. L.; Bu, X. R. *Chem. Commun.* **2004**, 1178–1180.

[201] Feng, X.; Hu, J. Y.; Tomiyasu, H.; Seto, N.; Redshaw, C.; Elsegood, M. R. J.; Yamato, T. *Org. Biomol. Chem.* **2013**, *11*, 8366–8374.

[202] Chen, S.; Read, F. S.; Ahmida, M.; Kaafarani, B. R.; Eichhorn, S. H. *Org. Lett.* **2013**, *15*, 558–561.

[203] Martínez–Martínez, V.; Lim, J.; Bañuelos, J.; López–Arbeloa, I.; Miljanić, O. Š. *Phys. Chem. Chem. Phys.* **2013**, *15*, 18023–18029.

[204] Alfonso, M.; Fernández, I.; Tárraga, A.; Molina, P. *Org. Lett.* **2015**, *17*, 2374–2377.

[205] Reichardt, C. *Chem. Rev.* **1994**, *94*, 2319–2358.

[206] Sauer, M.; Hofkens, J.; Enderlein, J. *Handbook of Fluorescence Spectroscopy and Imaging: From Single Molecules to Ensembles*, Wiley–VCH: Weinheim, 2011.

[207] Walba, H.; Isensee, R. W. *J. Org. Chem.* **1961**, *26*, 2789–2791.

[208] "Dissociation Constants of Organic Acids and Bases". Web. 23 June 2015. http://www.zirchrom.com/organic.htm

[209] Lohr, H. G.; Vogtle, F. *Acc. Chem. Res.* **1985**, *18*, 65–72.

[210] Carroll, C. N.; Naleway, J. J.; Haley, M. M.; Johnson, D. W. *Chem. Soc. Rev.* **2010**, *39*, 3875–3888.

[211] Martinez–Mañez, R.; Sancenon, F. *Chem. Rev.* **2003**, *103*, 4419–4476.

[212] Sessler, J. L.; Gale, P. A.; Cho, W. S. *Anion Receptor Chemistry*, RSC Publishing, Cambridge, 2006.

[213] Bayly, S. R.; Beer, P. D. *Top. Curr. Chem.* **2008**, *129*, 45–94.

[214] Seehafer, K.; Bender, M.; Schwaebel, S. T.; Bunz, U. H. F. *Macromolecules* **2014**, *47*, 7014–7020.

[215] Tanaka, K.; Kumagai, T.; Aoki, H.; Deguchi, M.; Iwata, S. *J. Org. Chem.* **2001**, *66*, 7328–7333.

[216] Wang, B.; Cote, A. P.; Furukawa, H.; O'Keeffe, M.; Yaghi, O. M. *Nature* **2008**, *453*, 207–211.

[217] Banerjee, R.; Phan, A.; Wang, B.; Knobler, C.; Furukawa, H.; O'Keeffe, M.; Yaghi, O. M. *Science* **2008**, *319*, 939–943.

[218] Ogawa, T.; Yuasa, J.; Kawai, T. *Angew. Chem. Int. Ed.* **2010**, *49*, 5110–5114.

[219] Peng, Q.; Xu, J.; Zheng, W. X. *J. Polym. Sci., Part A: Polym. Chem.* **2009**, *47*, 3399–3408.

[220] Pilgram, K.; Zupan, M.; Skiles, R. *J. Heterocycl. Chem.* **1970**, *7*, 629–633.